

# Geotechnical Reconnaissance and Engineering Effects of the December 29, 2020, M6.4 Petrinja, Croatia Earthquake, and Associated Seismic Sequence



**Lead Report Editors and GEER Team Leaders:** Ingrid Tomac, U.C. San Diego

Sonja Zlatović, Zagreb Univ. of Applied Sciences

**Authors (Leaders then Alphabetical):** Ingrid Tomac, Sonja Zlatović, Adda Athanasopoulos-Zekkos, Jelena Bleiziffer, Dubravko Domitrović, Tihomir Frangen, Verica Gjetvaj, Marin Govorčin, Igor Gukov, Marijan Herak, Petar Hrženjak, Dellena Kinikles, Ivan Kosović, Biljana Kovačević-Zelić, Bojan Matoš, Darko Matešić, Ivan Mihaljević, Zorana Mijic, Marta Miletić, Jack Montgomery, Jelena Parlov, Davor Pavelić, Ivica Pavičić, Dunja Perić, Nguyen Pham, Ivan Salković, Josip Terzić, Ingrid Tomac, Igor Vlahović, Zvonimir Vlahović, Helena Vučenović, Katerina Ziotopoulou, Petar Krešimir Žderić

Geotechnical Reconnaissance and Engineering Effects of the December 29, 2020, M6.4 Petrinja, Croatia Earthquake, and Associated Seismic Sequence

A report to the NSF-Sponsored Geotechnical Extreme Event Reconnaissance (GEER) Association<sub>1</sub>

## **GEER Team Members**

### **Local Team Members**

Jelena Bleiziffer  
Dubravko Domitrović  
Tihomir Frangen  
Verica Gjetvaj  
Marin Govorčič  
Igor Gukov  
Marijan Herak  
Petar Hržnejak  
Vedran Jagodnik  
Ivan Kalfatić  
Ivan Kosović  
Biljana Kovač  
Božica Marić  
Darko Matešić  
Bojan Matoš  
Ivan Mihaljević  
Evelina Oršulić  
Jelena Parlov  
Davor Pavelić  
Ivica Pavičić  
Goran Puž  
Anđelko Salković  
Ivan Salković  
Mirela Burečić Šafran  
Pero Šiša  
Josip Terzić  
Igor Vlahović  
Zvonimir Vlahović  
Helena Vučenović  
Sonja Zlatović  
Petar Krešimir Žderić

### **Virtual Team Members**

Adda Athanasopoulos-Zekkos  
Michael Grilliot  
Tara Hutchinson  
Nick Hudyma  
Dellena Kinikles  
Andrew Lyda  
Marta Miletić  
Zorana Mijč  
Monica Monteiro de Silva  
Jack Montgomery  
Dunja Perić  
Nguyen Pham  
Nicholas Sitar  
Ingrid Tomac (Local and  
Virtual)  
Mladen Vučetić  
Justin Wang  
Katerina Ziotopoulou

Report GEER-072: <https://doi.org/10.18118/G63T0S>  
August 3<sup>rd</sup>, 2021

## Acknowledgments

The work of the GEER Association is based in part on work supported by the National Science Foundation through the Geotechnical Engineering Program under US NSF Grant No. CMMI-1266418. Any opinions, findings, and conclusions, or recommendations expressed in this material are those of the authors and do not necessarily reflect the views of the NSF. The GEER Association is made possible by the vision and support of the past NSF Geotechnical Engineering Program Directors: Dr. Richard Frigaszy, the late Dr. Cliff Astill, and the current NSF Engineering for Civil Infrastructure Program Director, Dr. Giovanna Biscontin. GEER members donate their time, talent, and resources to collect time-sensitive field observations of the effects of extreme events.

In this report, results of many local volunteers are presented, supported by the colleagues based in the USA. Many Croatian geologists and geotechnical engineers worked on the inspection of the damages after the earthquake.

The editors of the report thank all the authors for their significant contributions in collecting perishable data in the field and preparing this report. Additionally, we would like to acknowledge non-authors for their support: Tomislav Ivšić, Mario Bačić, Marijan Car and Nicola Rossi from the University of Zagreb, Goran Malčić from the Zagreb University of Applied Sciences, as well as, Osman Dedić, Goran Dašič, Goran Grget and Marko Kaić from Geokon-Zagreb Ltd., Marko Veselčić and Danko Biondić from the Croatian Waters (Hrvatske Vode, Ltd.), Goran Puž and Darko Šošić from the Croatian Roads (Hrvatske Ceste, Ltd.) are warmly acknowledged for their support in inspecting the geotechnical damages in the the area and providing advice. Josip Atalić from the University of Zagreb is warmly acknowledged for organizing many volunteers through the Croatian Center for Earthquake Engineering.

Special thanks are due to Božica Marić, a honorary member of the Croatian Geotechnical Society, Misko Cubrinovski from the University of Canterbury, Eduardo Miranda from Stanford University, and Martin Sauter from University of Goettingen for their valuable support and advice.

We acknowledge Zagreb University of Applied Sciences as well as the University of Zagreb Faculty of Mining, Geology and Petroleum Engineering for donating and providing laboratory resources and personnel to the GEER team during the reconnaissance effort. We also acknowledge other institutions at the University of Zagreb: Faculty of Civil Engineering, Faculty of Geodesy, and Faculty of Science, and Croatian Geological Survey for supporting local GEER teams. We would like to acknowledge Croatian companies who donated resources and personnel, as well as provided the GEER team with professional reports and in-house collected perishable data: Gekon Ltd., Geotehnički Studio Ltd., Croatian Roads (Hrvatske Ceste), Croatian Waters (Hrvatske Vode), Metal Projekt Ltd., Moho Ltd., and Taus Ltd.. Finally, we would like to acknowledge the critical help of residents who provided access to private land to perform GEER reconnaissance activities.

## TABLE OF CONTENTS

### Acknowledgments

1. Introduction.....	6
2. Tectonic Setting.....	15
3. Geology, Geomorphology and Soil Characteristics .....	29
4. Recorded Ground Motions .....	39
5. Surface Deformations.....	47
6. Cover-Collapse Sinkholes.....	52
7. Liquefaction and Related Building Damage .....	100
8. Earthen Levee System .....	126
9. Infrastructure Damage .....	147
10. Complementary Geotechnical and Geophysical Investigation Works..	164

## 1.0 Introduction (Sonja Zlatović, Marta Miletić and Ingrid Tomac)

The December 2020 sequence of earthquakes in Croatia started on 28 December 2020 at 6:28 local time, with a magnitude M5.0 with epicenter near Petrinja. It was followed with a M4.7 at 7:49 and a M4.1 at 7:51, with a series of weaker aftershocks. On 29 December 2020 at 12:19, a M6.2 struck, which was felt in all parts of Croatia and neighboring countries. The sequence as shown in **Figure 1.1** continued for 36 days (Croatian Seismological Survey 2021). The main shock was felt throughout Croatia and the neighboring countries. Estimated accelerations are shown in **Figure 1.2** (USGS 2020).

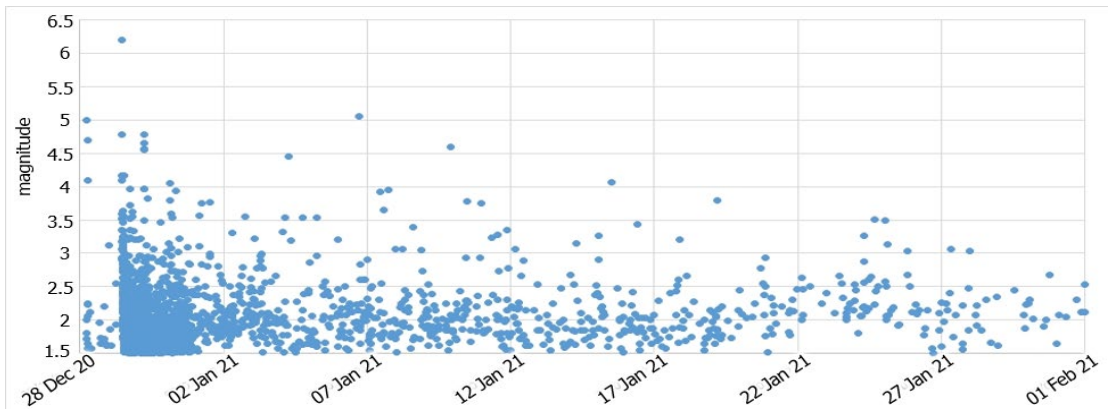


**Figure 1.1** Magnitudes of the earthquakes in the Petrinja area from 28 December 2020 to 01 February 2021. (Croatian Seismological Survey 2021).

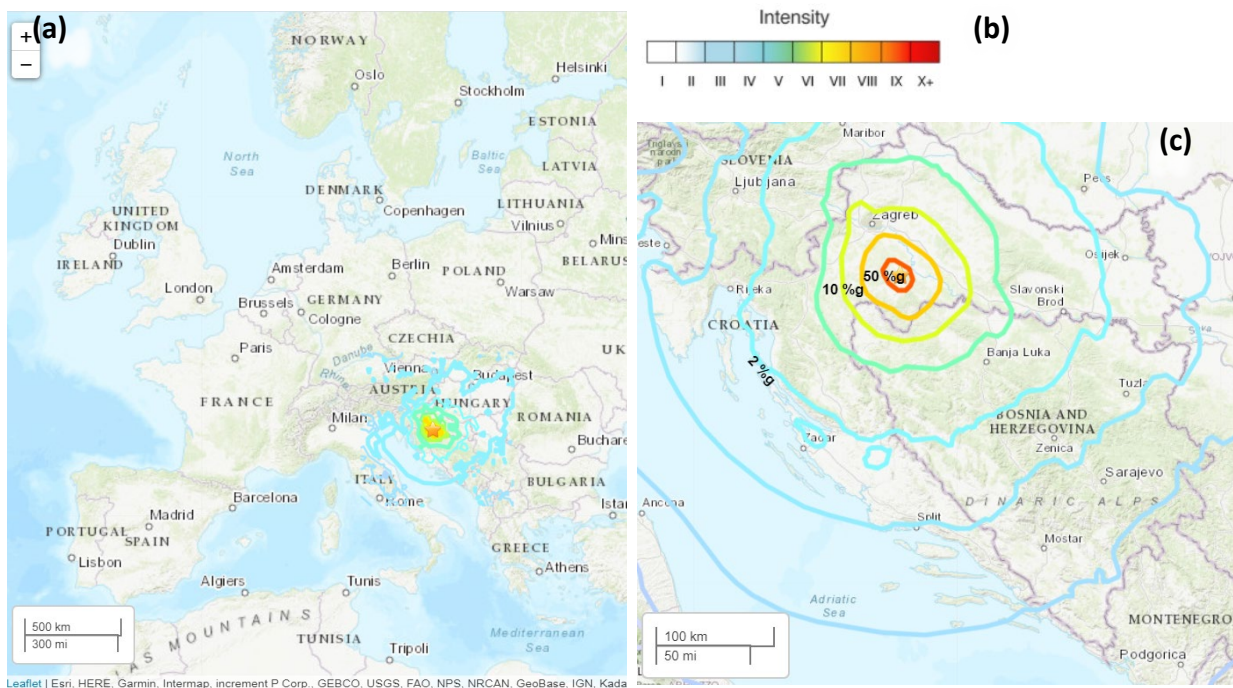


**Figure 1.2** (a) Shake map: epicenter and MMI contours. (b) Legend. (c) Estimated accelerations (USGS 2020).

Already the earthquakes in the morning of 28 December 2020 caused damages of some old houses in the area. Therefore, civil engineers, volunteers organized by the Croatian Center for Earthquake Engineering, started inspecting the buildings. This is how some of the engineers got hurt when the M6.2 struck next day. Luckily, weakened houses were already mostly abandoned. Additionally, this happened in the period between Christmas and New Year when schools were closed, with the partial lockdown due to the COVID-19 pandemic. However, seven citizens lost their lives. Immediately after the earthquake, volunteers from all over the country started bringing water, food, clothes, toys etc., taking down the damaged chimneys, repairing roofs and helping in all necessary ways. Organized support intensified, both from the civilians and from civil engineers. Many campers were brought, and many mobile houses and prefabricated houses. The epicenters of the earthquake sequence are shown in **Figure 1.3** with a section of the geologic map covering the area most affected by the earthquake. Some of the most important locations are indicated in the map. Sisak, which has been developing since Roman times (Siscia), is city of the headquarters of the Sisak-Moslavina County. Petrinja was administrative center for a long time, famous for its meat industry. Glina has an important wood industry. However, in most of the area affected by the earthquake citizens live from agriculture. The area, although very beautiful and pleasant, is one of the least developed areas of Croatia.

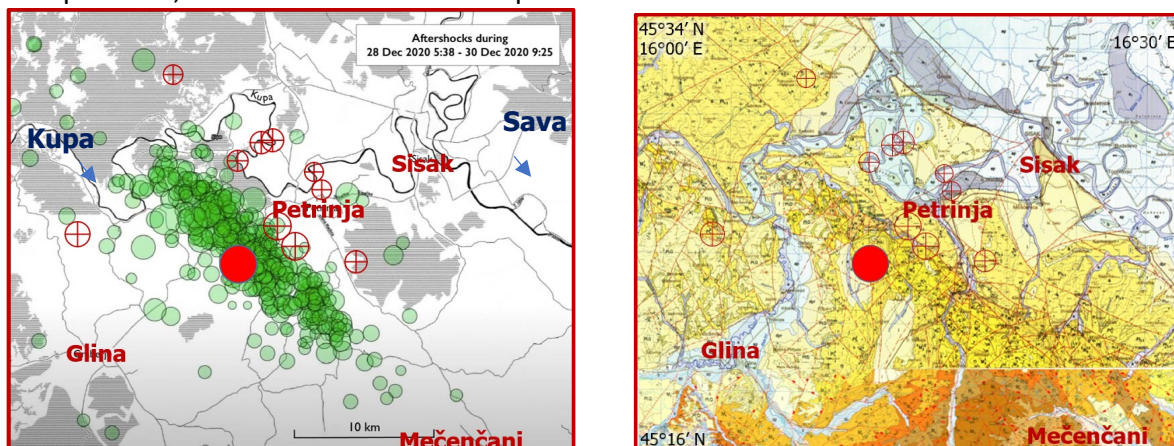


**Figure 1.3 (left)** The full red circle shows the epicenter of the main shock; the green circles show the epicenters of the earthquakes in the area from 28 December 2020 at 5:38 to 30 December 2020 at 9:25. (Croatian Seismological Survey). Red circles show the epicenters for earthquakes with magnitudes above M2.5 from 28 December 2020 to the end of April 2021 (USGS). **(right)** Corresponding sections of the geologic maps (Pikija 1987, Šikić 2014). Names of some of the main locations discussed in the report are indicated.

Geology of the area is presented in more details in Chapter 3. The area affected by the earthquake is the mostly flat valley of the meandering rivers Kupa and Sava with their tributaries, with mostly soft layers and a high ground water table. The underlying limestone is visible in rare locations. The levees erected to protect the cities, villages and the fields from the high waters of the Sava and Kupa rivers, were inspected by the geotechnical engineers who later joined the GEER team. Mostly built in or since the 1950s from the local clays, in several stretches, the levees got longitudinal cracks. In some cases, cracks crossed the levee crest, in some cases connection of two levees failed. Measured depth of the cracks is up to 2 m.

Along the toes of the levees sandy ejecta, were often found. Croatian Waters, the institution in charge of flood protection in Croatia, immediately repaired some of the damages, and built secondary levees where necessary. Descriptions of levee damages are presented in Chapter 8. Although liquefaction was observed in the past in Croatia, the sand boiling was a surprise (**Figures 1.4-1.6**). Sand ejecta were found in a series of yards and around family houses in Petrinja, Glina, some villages and in many fields (**Figure 1.7**).



**Figure 1.4** Levee south from Stara Drenčina, along the Kupa river. Sand ejecta are visible in front, levee on the left, settlement of the levee in the distance, and secondary levee (white box barrier) on the right side of the photograph (45.4609N, 16.3362E).



**Figure 1.5** Sand boiling observed during the main shock in Sisak – a snapshot from the video recorded by Daniel Pavlič (45.4735N, 16.3926E) at the distance of 15km from the epicenter and under the levee along the Sava river.



**Figure 1.6** A crack in Brest Pokupski which opened through several yards and houses, ejecting water and sandy soil in time of the main shock (**left** 45.4553N, 16.2628E; **right** 45.4539N, 16.2611E; photos by Igor Gukov).



**Figure 1.7** A 15 m long crack with sand ejecta at the football playground in Letovanić (45.5057N,16.1979E).

An overview of the liquefaction damage is given in Chapter 7: air photos were used to recognize some of the locations in Petrinja and Sisak. Some illustrative examples (Petrinja, Glina, Stari Brod) are shown in more details. The Croatian volunteers, geologists and geotechnical engineers, detected sand boils at 85 locations, lateral spreading at 8 and subsidence at 6 (Pollak et al. 2021).

The most prominent, surprising, and relatively rare geotechnical earthquake effect includes the collapse of numerous sinkholes in the time frame of three months after the main shock. Ninety-one new sinkholes collapsed within a 4km<sup>2</sup> area surrounding Borojevići and Mečenčani villages between Petrinja and Hrvatska Kostajnica. Sinkhole diameters vary from 1 m to 25 m, with a maximum depth of 11.7 m. Cover-collapse sinkholes occurred in the past but very sparsely and were considered rare events. Residents refer to historical sinkhole events through jokes, such as saying, “I wish your field turned into a pond”. The GEER team registered 136 sinkholes, 91 which opened after the 29 December, and 45 old ones, as well as three potential sinkholes, as shown in Chapter 6, together with an overview of the geological and hydrogeological characteristics of the area, and details of the most interesting sinkholes. The geotechnical and geophysical investigations consisted of 61 nanometrics ambient noise readings, four geotechnical boreholes, two Multichannel Analysis of Surface Waves (MASW) profiles, and one compound electrical resistivity tomography (ERT) profile performed by the joint effort of the US and local GEER teams in the period between March 15 and March 26. The comprehensive database of lidar images of around 60 sinkholes is available as open-source in DesignSafe Data Depot. The most interesting sinkholes are presented in detail in Chapter 6, with the results of geotechnical and geophysical investigation. Chapter 10 describes details of the extent of complementary investigation works. **Figures 1.8 - 1.10** show some characteristic examples. Although not included as part of this GEER report, the Croatian company Terra Compacta in cooperation with the University of Zagreb, Faculty of Mining, Geology and Petroleum Engineering, performed geophysical investigations in the area, in order to find a safe location for the temporary container settlement for the villagers of Mečenčani and Borojevići, and to inspect the roads. The Croatian companies Karst and Geotehnički studio performed borings in order to inspect safety of some houses, however, still uncertainty remains.



**Figure 1.8** The largest (diameter of 26m) of the sinkholes which opened a week after the main earthquake in Mečenčani (45.2833N, 16.4259E; 26 February 2021).



**Figure 1.9** (a) One of the previously known sinkholes with pond containing spring (45.286953N, 16.426297E). (b, c) a sinkhole which opened under an unoccupied house two days after the main earthquake (45.283, 16.4295) photographed on 4 January and 15 February 2021.



**Figure 1.10** Deformed ground surface in the previously flat field as a potential sinkhole near Borojevići (45.2963N,16.4140E) on 19 March 2021.

Some landslides were affected or initiated in the area. **Figure 1.11** shows sliding in Hađer, at the distance of around 8km from the epicenter. The Croatian volunteers, geotechnical engineers and geologists, detected 36 slides and 4 rockfalls Pollak et al. (2021). The data will be presented on the pages of the Croatian Geologic Survey ([www.hgi-cgs.hr](http://www.hgi-cgs.hr)).



**Figure 1.11** Sliding in Hađer on the top of a hill, (a) in three directions (45.3795N, 16.1200E; Bačić & Terzić 2021). Ground is recognized by the farmer as exceptionally soft (b) consequent gap opening (45.3793N,16.12016E). (c) An existing landslide situation worsened in the earthquake (45.3798N,16.1198E).

Damages on infrastructure - several bridges and roads are presented in Chapter 9. **Figure 1.12** shows Brest bridge near Petrinja after the earthquake. **Figure 1.13** shows building damage.



**Figure 1.12** Bridge Brest after the earthquake (45.4481N,16.2600 E).

The tectonic setting of the area is given in Chapter 2, and an overview of geology and soil characteristics is given in Chapter 3. Additional perishable data are given in following chapters. This was the largest earthquake to occur in Croatia since the advent of modern seismic instrumentation, and the important earthquake which happened in the area in the year 1909 in Pokupsko, or Pokuplje, in the river Kupa valley. Andrija Mohorovičić, the Croatian meteorologist and seismologist on this occasion corresponded with many prominent seismologists, compared data from 36 seismic stations and proved the existence of the crust-mantle boundary later named Mohorovičić discontinuity, or Moho (Herak & Herak 2010). Some recorded ground motions are presented in Chapter 4. Interferometric Synthetic Aperture Radar (InSAR) was used to analyze the ground surface deformations induced by the 29 December 2020 earthquake, as shown in Chapter 5. Croatian State Geodetic Administration (Državna geodetska uprava) published precise geodetic measurements of the fixed points of geodetic basis at their web pages (State Geodetic Administration 2021). Chapter 10 gives complementary geotechnical and geophysical investigation works.



(a)



(b)

**Figure 1.13** Photos of the damaged buildings after an earthquake rocked (a) Sisak, and (b) Petrinja, Croatia (Source: Miranda et al., 2021), Coordinates of the photo (a) 45.476794, 16.368347, and (b) 45.441082, 16.277061).

### **Socio-economic and COVID-19 pandemic impacts**

The 6.4 magnitude Petrinja, Croatia earthquake occurred on December 29, 2020. The importance of this time is multifold: The quake happened right between Christmas and New Year's Eve, while children were out of school due to the winter break and families were gathered at home. In addition, the nationwide lockdown, mitigation measures, and travel restrictions due to the COVID-19 pandemic were in place at the time of the earthquake, which made the emergency response even more challenging than usual. Lastly, the 6.4 Petrinja, Croatia earthquake occurred only nine months after the devastating March 22, 2020 earthquake of magnitude 5.3 Mw, which hit Croatia's capital Zagreb 50 km northwest of the Petrinja earthquake epicenter. Thus, the event had a severe psychological impact on people due to overlapping extreme events. The city of Sisak mainly developed after the 2nd World War as a modern industrial city with rich cultural life. In contrast, the town of Petrinja, due to its administrative role, has a distinctive old city center, with most of the residents living in family houses. Many of the homes in the area were built by their owners. After the war in the 1990s, the damaged houses were repaired or rebuilt by the state. Some single-story residences were later added with an extra floor by their owners. Consequently, there has been no extensive geotechnical investigation even though liquefaction occurred in the area a century ago.

A series of Croatian structural engineers who were inspecting the buildings contributed to the report. The structural engineers together with architects and other civil engineers, as volunteers, were invited and organized by the Croatian Center for Earthquake Engineering, HCPI. The citizens were invited to report on the damages, and the group of volunteers performed the preliminary inspection of the buildings. Total number of reported damages and an overview of the estimates is given in **Figure 1.14** for the 8 January and **Figure 1.15** for the 21 May 2021.

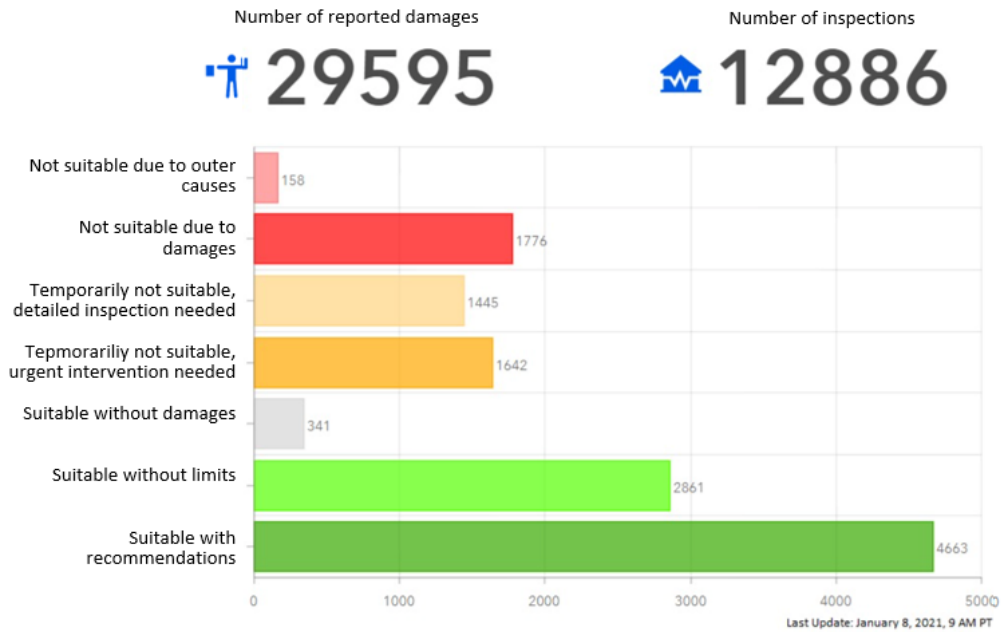


**Figure 1.14** Results of the damage estimates on buildings after the earthquake near Petrinja in the year 2020 on the 8 January 2021, 11 days after the main shock (HCPI, 2021).

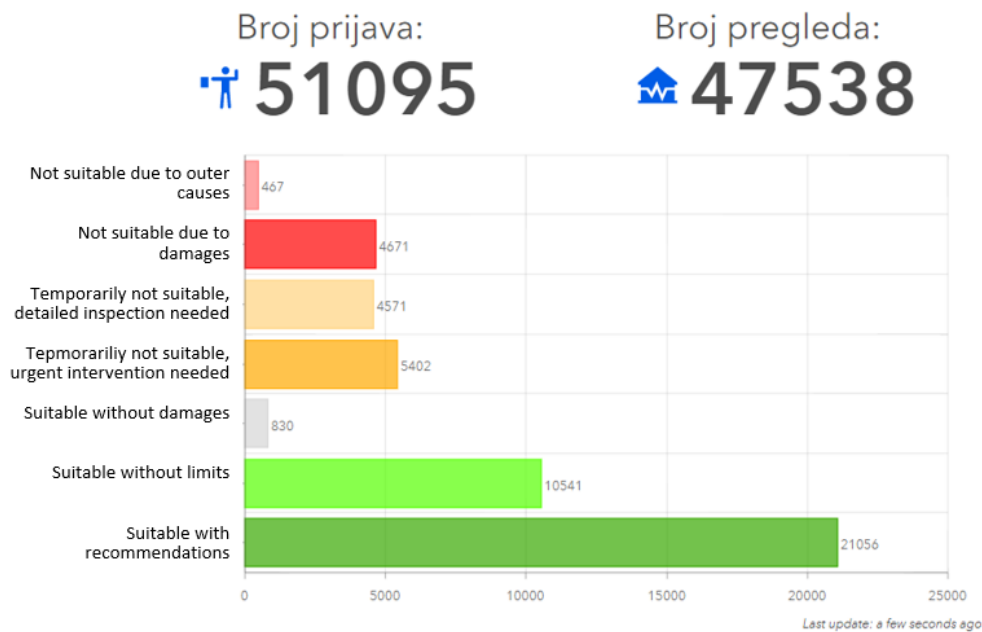


**Figure 1.15** Results of the damage estimates on buildings after the earthquake near Petrinja in the year 2020 on the 20 May 2021 (HCPI, 2021).

## Scope of USA-Croatia GEER Reconnaissance

A starting point to the present report was the preliminary hybrid reconnaissance report jointly prepared by Earthquake Engineering Research Institute (EERI) - Learning From Earthquakes (LFE) Program and the Structural Extreme Events Reconnaissance (StEER) Network, where several members of the Geotechnical Extreme Events Reconnaissance Association (GEER) team also participated. A preliminary list of locations with liquefaction, landslide, lateral spreading, sinkholes, and damage to levees was prepared as part of the joint EERI's LFE and StEER reconnaissance report, which was then subsequently expanded as part of this investigation (Miranda et al., 2021).

### List of Figures taken from the EERI'S LFE and StEER report:

- Figure 6.2. Soil properties in the area from the thermal electric power plant in Sisak, Čret (45.4538, 16.4145) (source: Conex, Zagreb).
- Figure 2.17. Map of publicly reported seismic stations (source: Google Earth). The epicenter of the December 29, 2020 earthquake is shown with a red star.
- Figure 4.6. Collapsed URM buildings in downtown Petrinja (a) before the earthquake (Source: Google Earth) and (b) after the earthquake (source: Nenad Bijelić).
- Figure 4.42. Building #2: (a) front view and (b) back view (source: Croatia Week 2021, Jan 5).

Immediately after the December 29 earthquake, a joint GEER team formed between the Croatian scientists and engineers (local team) and the GEER sponsored by the U.S. National Science Foundation (NSF). The local reconnaissance team, media, volunteers, and Croatian state-owned companies Croatian Waters – Hrvatske Vode Ltd. Croatian Roads – Hrvatske Ceste Ltd. conducted field observations and collected liquefaction and infrastructure damage data right after the main event. The second GEER team consisted of one US-based researcher and local team members who visited the affected region between March 15 and 26, 2021, to perform additional geotechnical investigations. The GEER team organized geotechnical investigation works mainly around Mečenčani and Borojevići. A substantial number of sinkholes appeared in the two months following the mainshock, from January until mid-March 2021.

## Survey Regions and Methods

The local and the U.S. GEER teams performed ground-level surveys and detailed inspections throughout the affected region (Petrinja, Siska, Glina). During the U.S. GEER team visit in March 2021, the field investigations followed: four geotechnical boreholes, in-situ soil classification, and index tests, two Multichannel Analysis of Surface Waves (MASW) profiles in Mečenčani and Borojevići, and two in Petrinja on-field liquefaction site and 65 Horizontal-to-vertical Spectral Ratio seismic method (HVSr) measurements, 61 HVSr in Mečenčani and Borojevići and four HVSr in Petrinja near MASW's. In addition, the GEER team analyzed the ground surface deformations induced by the main event with the Interferometric Synthetic Aperture Radar (InSAR).

## References

- Bačić, M., Terzić, . (2021) *Geotehnički problemi nakon potresa 29.12.2020*. Croatian Geotechnical Society,  
[https://drive.google.com/file/d/1u\\_R04UovDpBsDyNplZ5s7BfQxZ790fVg/view](https://drive.google.com/file/d/1u_R04UovDpBsDyNplZ5s7BfQxZ790fVg/view)  
Croatian Seismological Survey, 2020, Preliminarni rezultati serije potresa kod Petrinje od 28. prosinca 2020. do 28. siječnja 2021.  
[https://www.pmf.unizg.hr/geof/seizmoloska\\_sluzba/mjesec\\_dana\\_od\\_glavnog\\_petrinjskog\\_potresa](https://www.pmf.unizg.hr/geof/seizmoloska_sluzba/mjesec_dana_od_glavnog_petrinjskog_potresa), Accessed 30 April 2021
- Croatian Seismological Survey (2021) Potresi kod Petrinje za 28. i 29. prosinac 2020. godine, Department of Geophysics, Faculty of Science, University of Zagreb, published 2 February 2021  
[https://www.pmf.unizg.hr/geof/seizmoloska\\_sluzba/potresi\\_kod\\_petrinje?@=1m6am#news\\_118053](https://www.pmf.unizg.hr/geof/seizmoloska_sluzba/potresi_kod_petrinje?@=1m6am#news_118053)
- HCPI (2021) Rezultati procjena oštećenja građevina nakon potresa kod Petrinje 2020. Available at <https://www.hcpi.hr/>
- Herak, Davorka; Herak Marijan 2010 The Kupa Valley (Croatia) Earthquake of 8 October 1909--100 Years Later. January 2010 Seismological Research Letters 81(1):30-36. DOI: 10.1785/gssrl.81.1.30
- Miranda, E., Brzev, S., Bijelić, N., Arbanas, Ž., Bartolac, M., Jagodnik, V., Lazarević, D., Mihalić Arbanas, S., Zlatović, S., Acosta, A., Archbold, A., Bantis, J., Borozan, J., Božulić, I., Blagojević, N., Cruz, C., Dávalos, H., Fischer, E., Gunay, S., Hadzima-Nyarko, M., Heresi, P., Lignos, D., Lin, T., Marinković, M., Messina, A., Miranda, S., Poulos, A., Scagliotti, G., Tomac, I., Tomić, I., Ziotopoulou, K., Žugić, Ž., Robertson, I. (2021). StEER-EERI: Petrinja, Croatia December 29, 2020, Mw 6.4 Earthquake Joint Reconnaissance Report (JRR). Available at: DOI: 10.17603/ds2-1w0y-5080 (Accessed: 8 May 2021).
- Pikija, M. (1987). Osnovna geološka karta SFRJ 1:100.000, List Sisak L33–93. – Geološki zavod, Zagreb (1975–1986); Savezni geološki institut, Beograd. Available at request at <https://www.hgi-cgs.hr/osnovna-geoloska-karta-republike-hrvatske-1100-000/>
- Pollak et al. (2021) *The preliminary inventory of coseismic ground failures related to December 2020 – January 2021 Petrinja earthquake series*. Geol. Croat., doi: 10.4154/gc.2021.08
- Državna geodetska uprava (2021) *Izvešće analiza rezultata preciznih geodetskih mjerenja o pomicanju Zemljine kore na potresom pogođenom području*, Zagreb, February 2021,  
<https://dgu.gov.hr/UserDocsImages/dokumenti/VIJESTI/potres/Izvie%C5%A1%C4%87e%20GNSS%20mjerjenja%20-SM%C5%BD.pdf>
- Šikić, K. (2014): Osnovna geološka karta SFRJ 1:100.000, List Bosanski Novi L33-105. – Fond stručne dokumentacije Instituta za geološka istraživanja, Zagreb. (manuskript) Available at request at <https://www.hgi-cgs.hr/osnovna-geoloska-karta-republike-hrvatske-1100-000/>
- USGS (2020) *M 6.4 - 2 km WSW of Petrinja, Croatia*. Available at <https://earthquake.usgs.gov/earthquakes/eventpage/us6000d3zh/executive>. Published 29 December 2020. Accessed 30 April 2021

## 2. Tectonic Setting (Dunja Perić, Bojan Matoš, Marijan Herak)

### 2.1 Introduction

On December 29, 2020, at approximately 12:20 pm CET (11:20 am UTC) an earthquake of magnitude 6.4  $M_w$  (6.2  $M_L$ ) occurred in central Croatia. U.S. Geological Survey (USGS 2020b) located the hypocenter at a depth of 10 km, approximately at 45.422° N and 16.255°E while the Croatian Seismological Survey of the University of Zagreb located the hypocenter at 45.4002N and 16.2187E, 3 km southwest of Petrinja and 12 km southwest of Sisak, at a depth of 11.5km. (Croatian Seismological Survey 2020) The information suggests that a rupture occurred within the central portion of the shallow Pokupsko–Petrinja strike-slip fault in the transition zone of the Adria Microplate and Eurasian plate. The maximum intensity of the earthquake was VIII (severe) on Modified Mercalli Intensity (MMI) scale and VIII (heavily damaging) to IX (destructive) on European Macro-seismic Scale (EMS). The earthquake was preceded by several foreshocks, the strongest of which had a magnitude of 5.2  $M_w$ , and followed by series of aftershocks, the strongest of which had a magnitude of 4.9  $M_w$  ((Croatian Seismological Survey 2021; USGS 2020b; Markušić et al 2021).

While Petrinja was the most affected city, severe damage also occurred in Sisak, Dvor, Glina, Topusko, Strašnik, Majska Poljana, Gora etc. Damage also occurred in Zagreb and Zaprešić, located approximately 50 km and 60 km, respectively, to the north northwest of the epicenter. The earthquake caused seven fatalities, 26 persons were injured, and several hundred people had to be displaced (Pušić et al., 2021). The earthquake was felt throughout Croatia and in large parts of Slovenia, Austria, Bosnia and Herzegovina, Serbia, Hungary, Slovakia and Italy, and some parts of Montenegro, Germany, and the Czech Republic.

### 2.2 Regional Tectonic Setting

Croatia is located in a highly active Alpine–Mediterranean seismic region. While the convergent boundary region between the African and Eurasian plates primarily governs the tectonics of the Circum-Mediterranean, the tectonics of Croatia is controlled by the Adria Microplate – Eurasian Plate collision at the rate of 3.5–5 mm/yr that resulted in the formation of the Alps, Dinarides, Albanides, and Helenides (**Figure 2.1**).



**Figure 2.1** Tectonic plates in Alpine–Mediterranean region (after Handy et al., 2015).

The complexity of this region is reflected in microplates and regional-scale structures that promote tectonic motions along the regional scale crustal faults (**Figure 2.2**). The collision between Adriatic and Eurasian plates presently remains the subject of many investigations (D'Agostino et al., 2008; Schmid et al., 2008; Ustaszewski et al., 2010; Ivančić et al 2018).

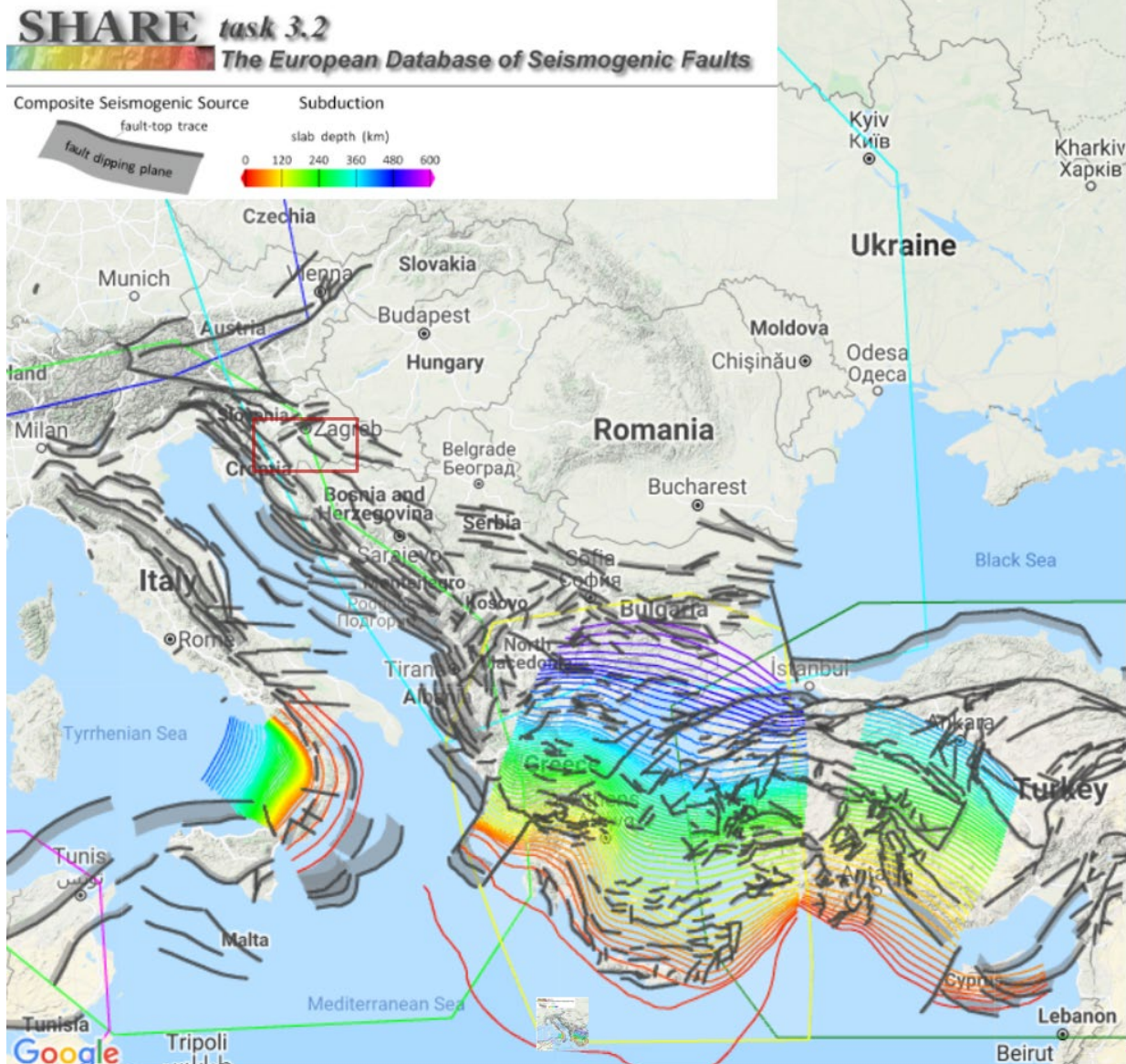


**Figure 2.2** Section of the map of the seismogenic faults in Europe (Basili et al., 2013). Red frame show area shown in Figure 2.9.

The major tectonic units that govern the seismicity of Croatia (**Figure 2.3**) are the Pannonian Basin to the north, the Eastern Alps, the Dinarides, and Adria Microplate–Eurasian Plate transition zone (Schmidt et al. 2008). The interaction between these tectonic units controls the earthquakes in the upper crust that are distributed along active faults in the region (Stanko et al. 2020). While most of the recent earthquakes occurred in the coastal area due to the ongoing collision between Adria Microplate and the Eurasian Plate in the domain of the Dinarides, the seismicity of the Pannonian Basin to the north is characterized by far-field stress transfer, i.e., intra-plate events. The seismogenic faults in the SE part of the coastal area (Dalmatia) are predominately reverse faults, striking along the coastline, i.e., perpendicularly to the average tectonic stress direction. More to the NW along the coast, transpression and strike-slip are the dominant regimes. The



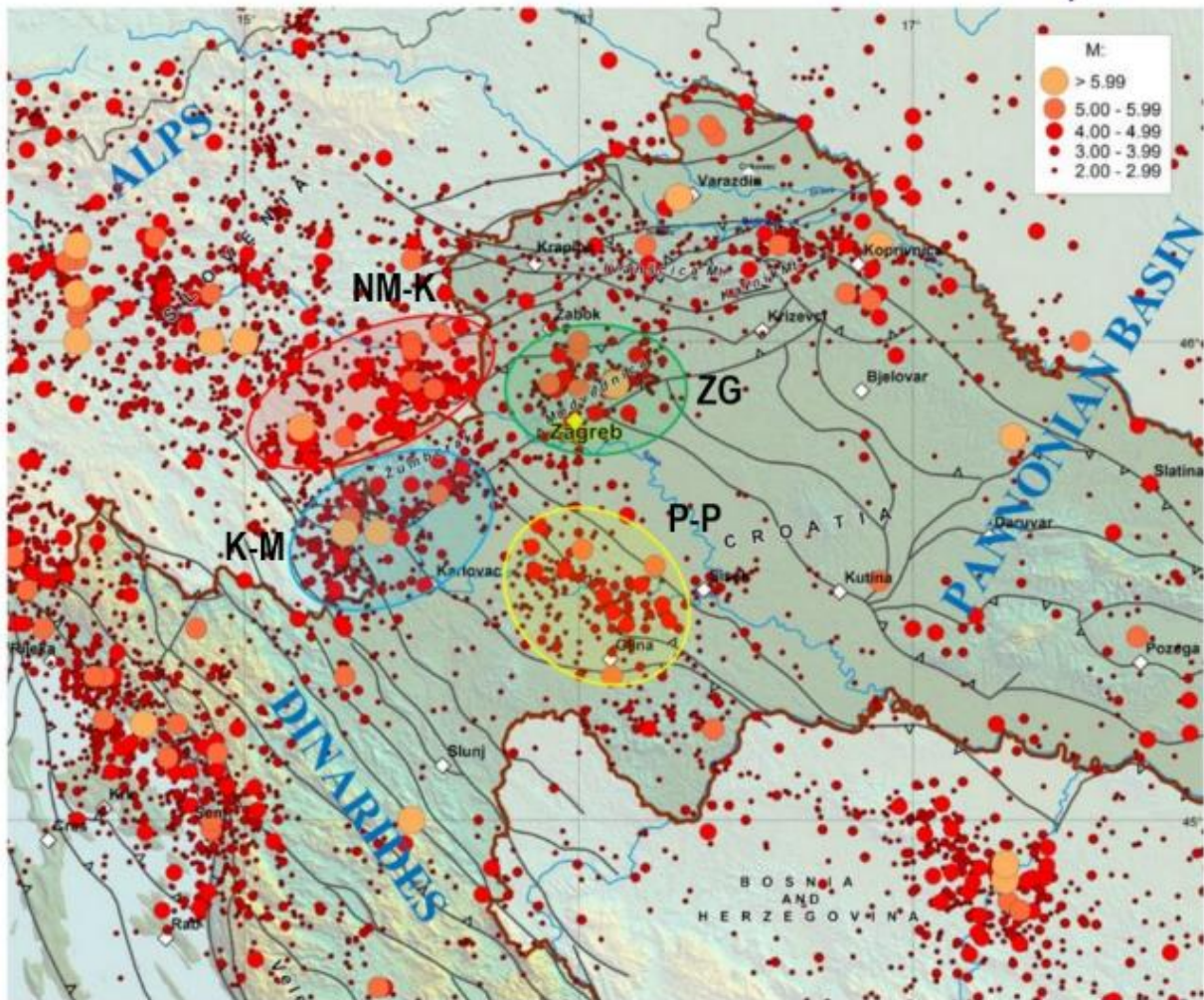


**Figure 2.4** Spatial distribution of earthquake locations in the investigated area (373BC–2019, according to the Croatian Earthquake Catalogue (CEC), the updated version first described in Herak et al. 1996. Seismic zones are marked as: ZG (Zagreb) – green, NM-K (Novo Mesto–Krško) – red, K-M (Karlovac–Metlika) – blue, and P-P (Pokupsko–Petrinja) – yellow. Faults are marked with black lines (Ivančić et al., 2006, Ivančić et al., 2018), (adapted from Stanko et al., 2020).

### October 8, 1909 Earthquake

On October 8, 1909, an earthquake occurred in Pokuplje ( $M_s = 5.8$ ), with the epicenter located about 29 km south of Zagreb (Herak and Herak, 2010). This is the strongest known earthquake that occurred in Pokupsko–Petrinja zone before December 29, 2020. A number of seismographs, which were installed in Europe before this earthquake, provided invaluable data for Andrija Mohorovičić, a Croatian geophysicist. Based on the recorded seismograms, he determined that seismic waves reflect and refract upon striking a boundary between different materials in the Earth’s interior, and longitudinal and transverse elastic waves propagate through rocks with different velocities. Mohorovičić concluded that the properties of rocks within the Earth must abruptly change at a depth of about 54 km, at the discontinuity, which separates the Earth’s crust

from its mantle, and is now known as the Mohorovičić discontinuity or simply the Moho. It is presently known that the thickness of the crust is 5–9 km below the ocean floor and 25–70 km below the continents.

Subsequent studies of the Earth's interior confirmed the existence of the discontinuity under all continents and oceans. Mohorovičić's theories were visionary at the time and were fully understood much later based on detailed observations of the effects of earthquakes on buildings and locating earthquake epicenters. The Kupa valley earthquake is cited in seismological literature predominantly in the context of the discovery of the Moho. Thus, the earthquake that occurred in Pokuplje on October 8, 1909, has been instrumental in geophysics for more than 100 years, and it has potentially a significant impact on the understanding of the December 29, 2020, Petrinja earthquake. More about Mohorovičić's contributions to seismology may be found by consulting translations into English of the original papers (Mohorovičić, 1910a,b; 1992; 2009), or in Herak and Herak (2007, 2010).

#### March 22, 2020 Earthquake

At approximately 6:24 am CET (5:24 am UTC) on March 22, 2020, an earthquake of magnitude 5.3  $M_w$  with the hypocenter at a depth of 10 km struck Zagreb (**Figure 2.5**) (USGS 2020a). According to the Croatian Seismological Survey of the University of Zagreb (2020a), the earthquake had a magnitude of 5.5  $M_L$ , and its epicenter was located 7 km north of the city in the northern suburbs of Zagreb. USGS ShakeMap depicted in Figure 2.5 (USGS 2020b) estimates PGA in the range of 0.2 g, which, along with the intensity of VII (MMI) is consistent with the observed levels of damage. The earthquake was felt throughout Croatia, in Slovenia, Bosnia and Herzegovina, Hungary and Serbia.

The focal mechanism of the earthquake was reverse faulting on a west-southwest–east-northeast trending fault (Tomljenović, 2020). Herak (2020) found that the rupture plane had a strike of 75° and dip angle of 45° to the south-southeast while USGS (USGS 2020b) reported a strike of 74°, but dip angle of 51°. According to Herak (2020), the axis of maximum tectonic pressure (P) was horizontal (with a plunge angle of 0° in the NNW–SSE direction), while the axis of maximum tension (T) was almost vertical with a plunge angle of 86°. The moment tensor solution for the March 22, 2020 earthquake (USGS 2020a) is shown in **Figure 2.6**.

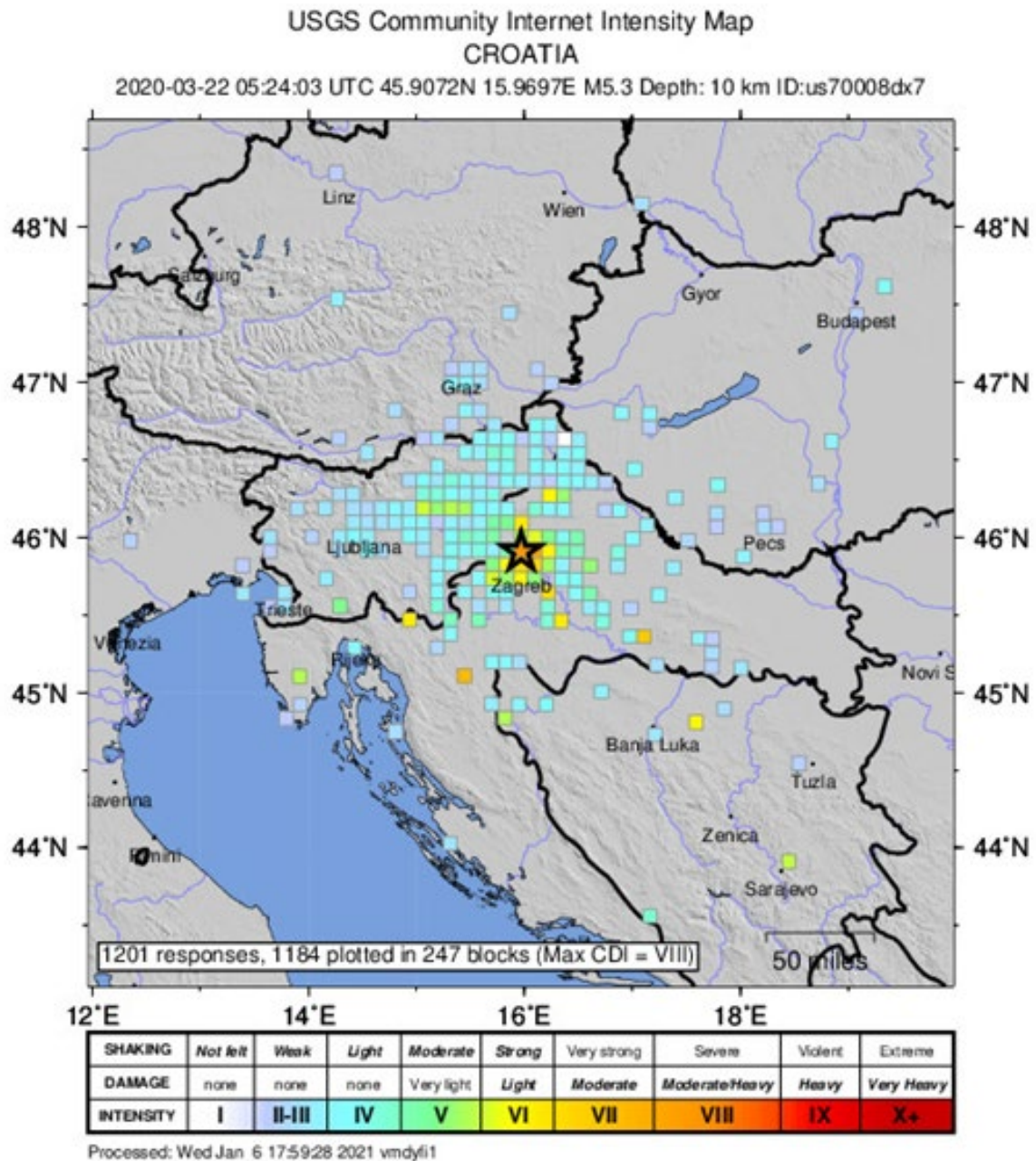


**Figure 2.5** Intensity map estimated from ShakeMap of March 22, 2020 earthquake (source: USGS 2020a).

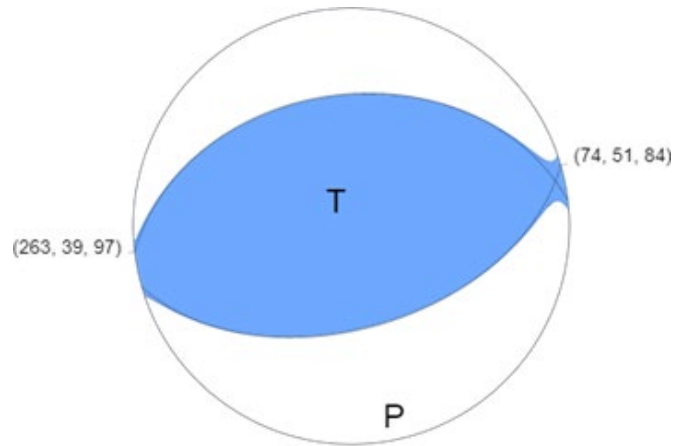


**Figure 2.6** Moment tensor solution for the March 22, 2020 earthquake (source: USGS 2020a).

#### December 29, 2020 Earthquake

On December 29, 2020, at 12:20 pm (ETC), an earthquake of magnitude of  $M_w = 6.4$  occurred near Petrinja, Croatia (**Figure 2.7**) (USGS 2020b). This is one of the two strongest earthquakes instrumentally recorded in Croatia. The earthquake was felt across Croatia and in neighboring countries. The earthquake was preceded by two sizeable foreshocks having magnitudes of 4.7 and 5.2 on December 28, 2020 (USGS 2020b). While most of the aftershocks have occurred within the Petrinja Fault zones, some of them occurred within the nearby Jastrebarsko and North Medvednica Fault. Nevertheless, due to the proximity of the Jastrebarsko and North Medvednica faults to the epicenter of the March 22, 2020, Zagreb earthquake, the aftershocks that occurred along these faults can be associated with the Zagreb earthquake.

Based on geological maps, field data, field prospecting, and available seismological and preliminary satellite data, the December 29, 2020 earthquake activated the fault system in the wider Sisak, Petrinja, and Glina area. The main fault is highlighted in **Figures 2.8** and **2.9**. The fault consists of multiple segments with strike-slip movement.

A large amount of released energy during the movement of fault blocks caused the ruptures in the rock to manifest on the surface of the terrain along with ground shaking. The various coseismic features resulting from the earthquake were open surface cracks, , fluid spills, gravitational slides, sand boils induced by liquefaction in Kupa and Sava river valleys, opening of cover-collapse sinkholes, deformation on the surface of the terrain, and deformation of the linear infrastructural objects.

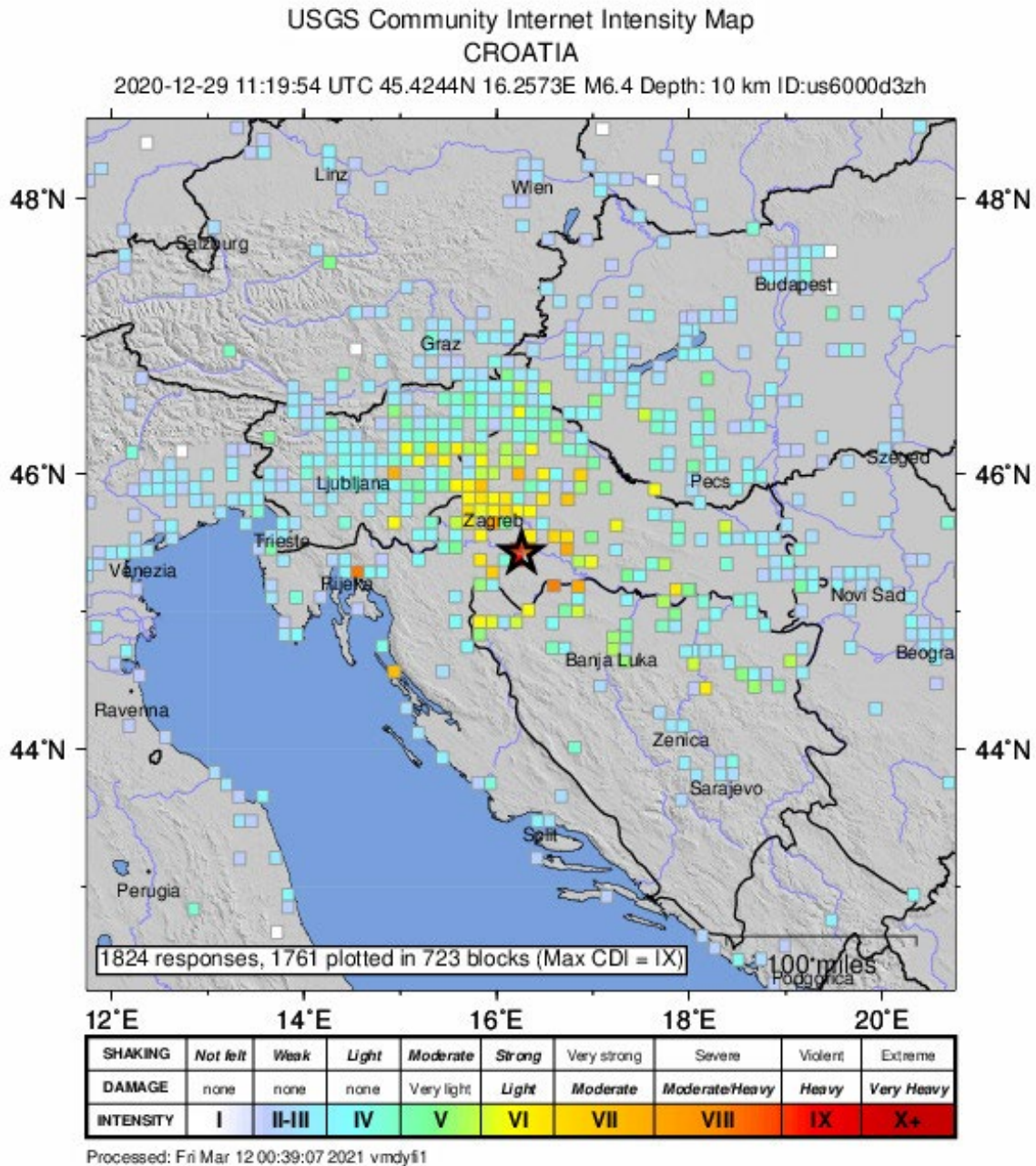


**Figure 2.7** Intensity map estimated from ShakeMap of December 29, 2020 earthquake (USGS 2020).

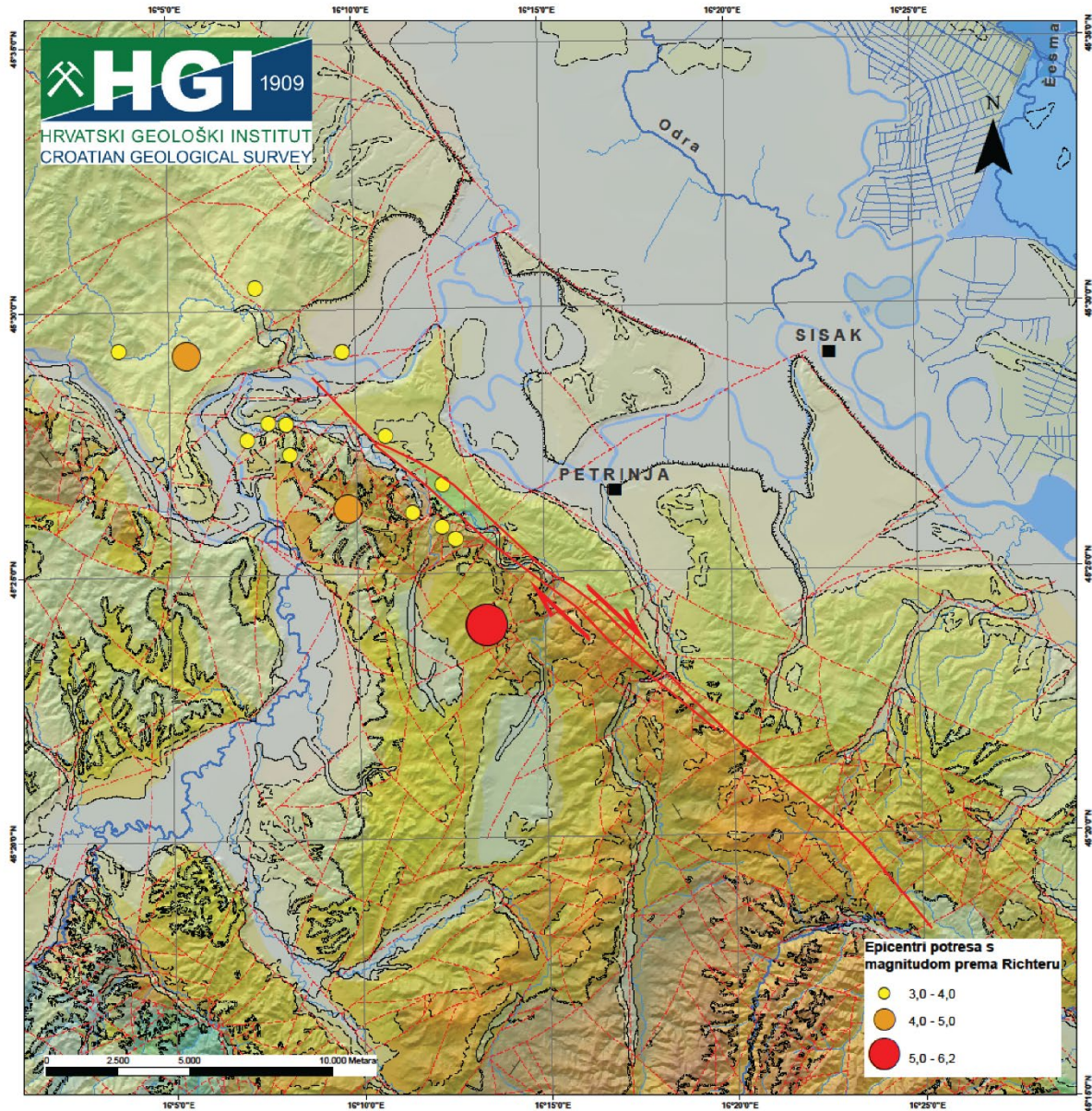
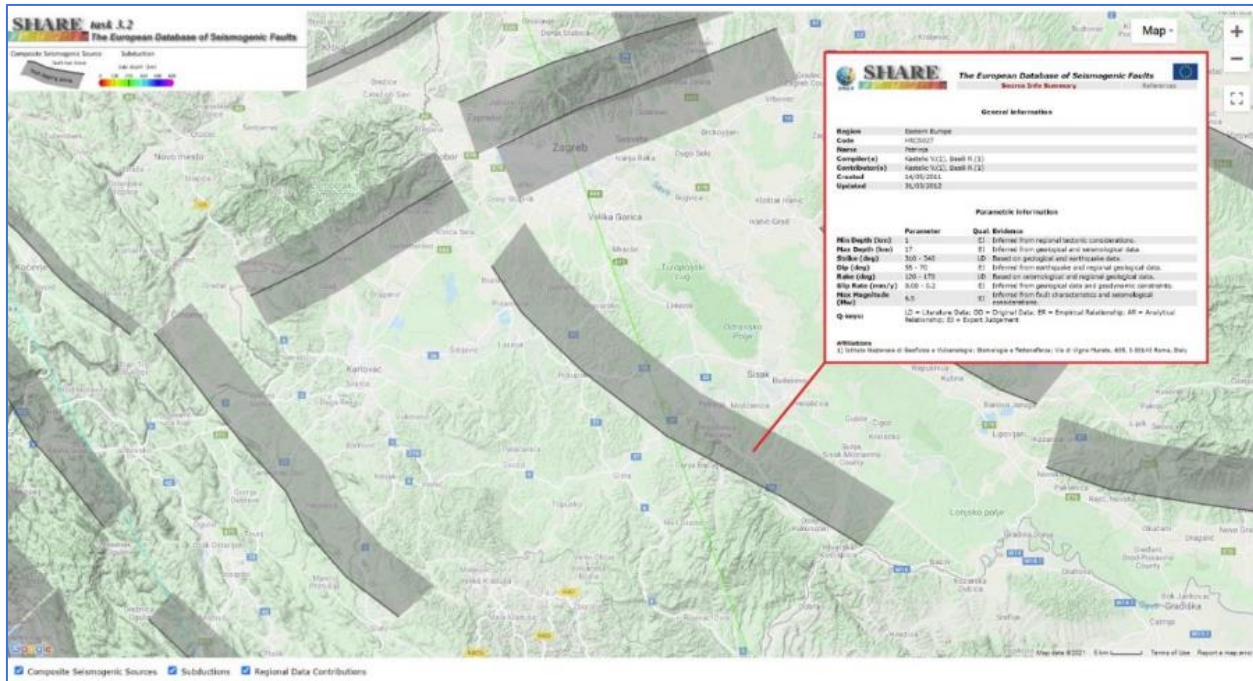


**Figure 2.8** Excerpt from a geological map of a wider epicentral area: the fault (fault zone), which is preliminarily considered to be the cause of the main Petrinja earthquake and the series of weaker earthquakes, is marked in red. Prepared by Pavle Ferić on the geologic map by Pikija 1987 (Vukovski 2021)



## The European Database of Seismogenic Faults



Source Info Summary

References

### General information

<b>Region</b>	Eastern Europe
<b>Code</b>	HRCS027
<b>Name</b>	Petrinja
<b>Compiler(s)</b>	Kastelic V.(1), Basili R.(1)
<b>Contributor(s)</b>	Kastelic V.(1), Basili R.(1)
<b>Created</b>	14/05/2011
<b>Updated</b>	31/03/2012

### Parametric information

	Parameter	Qual.	Evidence
<b>Min Depth (km)</b>	1	EJ	Inferred from regional tectonic considerations.
<b>Max Depth (km)</b>	17	EJ	Inferred from geological and seismological data.
<b>Strike (deg)</b>	310 - 340	LD	Based on geological and earthquake data.
<b>Dip (deg)</b>	55 - 70	EJ	Inferred from earthquake and regional geological data.
<b>Rake (deg)</b>	120 - 170	LD	Based on seismological and regional geological data.
<b>Slip Rate (mm/y)</b>	0.08 - 0.2	EJ	Inferred from geological data and geodynamic constraints.
<b>Max Magnitude (Mw)</b>	6.5	EJ	Inferred from fault characteristics and seismological considerations.

**Q-keys:** LD = Literature Data; OD = Original Data; ER = Empirical Relationship; AR = Analytical Relationship; EJ = Expert Judgement

### Affiliations

1) Istituto Nazionale di Geofisica e Vulcanologia; Sismologia e Tettonofisica; Via di Vigna Murata, 605, I-00143 Roma, Italy

**Figure 2.9** Basic characteristics of the Petrinja Fault shown in The European Database of Seismogenic Faults (Basilli, et al 2013)

The moment tensor of December 29, 2020, Petrinja earthquake is shown in **Figure 2.10**. It indicates a strike-slip fault focal mechanism. One nodal plane corresponds to left-lateral movement with a slight thrust component on a fault striking in the NE–SW direction. The other nodal plane indicates right-lateral movement on a fault striking NW–SE and dipping sub vertically to the southwest. It is because NW–SE direction of the Petrinja fault that Fault Plane 2 is likely defining the causative fault.

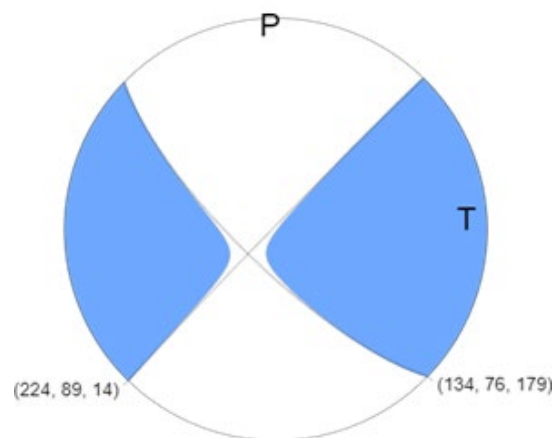


**Figure 2.10** Moment tensor solution for the December 29, 2020 earthquake (source: USGS 2020b).

### References

- Basili R., Kastelic V., Demircioglu M. B., Garcia Moreno D., Nemser E. S., Petricca P., Sboras S. P., Besana-Ostman G. M., Cabral J., Camelbeeck T., Caputo R., Danciu L., Domac H., Fonseca J., García-Mayordomo J., Giardini D., Glavatovic B., Gulen L., Ince Y., Pavlides S., Sesetyan K., Tarabusi G., Tiberti M. M., Utkucu M., Valensise G., Vanneste K., Vilanova S., Wössner J. (2013). The European Database of Seismogenic Faults (EDSF) compiled in the framework of the Project SHARE [Online]. Available at: <http://diss.rm.ingv.it/share-edsf/>. (Accessed: 9 May 2021).
- Croatian Seismological Survey (2020) *Obavijesti o potresima kod Petrinje*. University of Zagreb, Faculty of Science, Department of Geophysics, Seismological Survey, available at [https://www.pmf.unizg.hr/geof/seizmoloska\\_sluzba/izvjesca\\_o\\_potresima?@=1m692](https://www.pmf.unizg.hr/geof/seizmoloska_sluzba/izvjesca_o_potresima?@=1m692). Published 29 December 2020, Accessed 30 April 2021
- Croatian Seismological Survey (2021a) *Potresi kod Petrinje za 28. i 29. prosinac 2020. godine*. University of Zagreb, Faculty of Science, Department of Geophysics, Seismological Survey, available at [https://www.pmf.unizg.hr/geof/seizmoloska\\_sluzba/potresi\\_kod\\_petrinje?@=1m6am#news\\_118053](https://www.pmf.unizg.hr/geof/seizmoloska_sluzba/potresi_kod_petrinje?@=1m6am#news_118053), edited 2 January 2021, Accessed 30 April 2021.

- Croatian Seismological Survey (2021b) *Potresi kod Petrinje*, University of Zagreb, Faculty of Science, Department of Geophysics, Seismological Survey, available at [https://www.pmf.unizg.hr/geof/seizmoloska\\_sluzba/potresi\\_kod\\_petrinje](https://www.pmf.unizg.hr/geof/seizmoloska_sluzba/potresi_kod_petrinje). Accessed 30 April 2021
- D'Agostino, N., Avallone, A., Cheloni, D., D'Anastasio, E., Mantenuto, S. & Selvaggi, G. (2008). 'Active tectonics of the Adriatic region from GPS and earthquake slip vector'. *Journal of Geophysical Research – Solid Earth*, 113 (B12413), pp. 1-19. doi:10.1029/2008JB005860.
- Handy, M.R., Ustaszewski, K. & Kissling, E. (2015). 'Reconstructing the Alps–Carpathians–Dinarides as a key to understanding switches in subduction polarity, slab gaps and surface motion'. *Int J Earth Sci (Geol Rundsch)*, 104, pp. 1–26. Available at: <https://doi.org/10.1007/s00531-014-1060-3>. (Accessed: 8 May 2021).
- Hantken v. Prudnik, M. (1882). Das Erdbeben von Agram im Jahre 1880. Mittheilungen aus dem Jahrbuche der Kon. Ungarischen Geologischen Anstalt, Budapest, Gebruder Legrady.
- Herak, D. and Herak, M. (2006). Veliki zagrebački potres 1880., *Meridijani*, 109, 24-33.
- Herak, M., Herak D., Markušić, S. (1996). 'Revision of the earthquake catalogue and seismicity of Croatia, 1908–1992'. *Terra Nova*, 8(1), pp. 86-94. Available at: <https://doi.org/10.1111/j.1365-3121.1996.tb00728.x>. (Accessed: 8 May 2021).
- Herak D. and Herak M. (2007). 'Andrija Mohorovičić (1857–1936) - on the occasion of the 150th anniversary of his birth'. *Seismol. Res. Lett.*, 78, pp. 671–674.
- Herak D. and Herak M. (2010). 'The Kupa Valley (Croatia) earthquake of 8 October 1909 - 100 years later'. *Seismol. Res. Lett.*, 81, pp. 30–36.
- Ivančić, I., Herak, D., Markušić, S., Sović, I. & Herak, M. (2006). 'Seismicity of Croatia in the period 2002–2005'. *Geofizika*, 23(2), pp. 87-103.
- Ivančić, I., Herak, D., Herak, M., Allegretti, I., Fiket, T., Kuk, K., Markušić, S., Prevolnik, S., Sović, I., Dasović, I. & Stipčević J. (2018). 'Seismicity of Croatia in the period 2006–2015'. *Geofizika*, 35, pp. 69–98. doi:10.15233/gfz.2018.35.2.
- Markušić, S.; Stanko, D.; Penava, D.; Ivančić, I.; Bjelotomić Oršulić, O.; Korbar, T.; Sarhosis, V. (2021) Destructive M6.2 Petrinja Earthquake (Croatia) in 2020—Preliminary Multidisciplinary Research. *Remote Sens.* 2021, 13, 1095. <https://doi.org/10.3390/rs13061095>
- Mohorovičić A. (1910a). 'Das Beben vom 8. X. 1909 (Earthquake of 8 October 1909)'. *Jahrbuch des meteorologischen Observatoriums in Zagreb (Agram) für das Jahr 1909*, pp. 1-63 (in German).
- Mohorovičić A. (1910b). 'Potres od 8. X. 1909 (Earthquake of 8 October 1909)'. *Godišnje izvješće Zagrebačkog meteorološkog opservatorija za godinu 1909*, pp. 1-56 (in Croatian).
- Mohorovičić A. (1992). 'Earthquake of 8 October 1909 (translation into English)'. *Geofizika*, 9 (1), pp. 3-55. Available at: <http://geofizika-journal.gfz.hr/vol09.htm>.
- Mohorovičić, A. (2009). 'Effects of earthquakes on buildings (translation into English)'. *Geofizika*, 26, pp. 1-65. Available at: <http://geofizika-journal.gfz.hr/vol26.htm>.
- Pikija, M. (1987). Osnovna geološka karta SFRJ 1:100.000, List Sisak L33–93. – Geološki zavod, Zagreb (1975–1986); Savezni geološki institut, Beograd. Geologic map available on request at <https://www.hgi-cgs.hr/osnovna-geoloska-karta-republike-hrvatske-1100-000/>.
- Pušić, M., Šarčević, T., Dešković, M., Jutarnji.hr, Hina, Krnić, I., Žabec, K., Toma, I., Karakaš Jakubin, H., Patković, N. (2020). 'Snažan potres magnitude 6,2 pogodio Petrinju, raste broj

- žrtava, mnogo je ozlijeđenih (Strong earthquake of magnitude 6.2 hit Petrinja, number of victims is increasing, lots of injured)'. *Jutarnji list*, 29 December. Available at: <https://www.jutarnji.hr/video/news/snazan-potres-magnitude-6-2-pogodio-petrinju-raste-broj- zrtava-mnogo-je-ozlijedenih-15039620> (Accessed: 9 May 2021).
- Schmid, S.M., Bernoulli, D., Fügenschuh, B., Matenco, L., Schefer, S., Schuster, R., Tischler, M. & Ustaszewski, K. (2008). 'The Alpine–Carpathian–Dinaridic orogenic system: correlation and evolution of tectonic units'. *Swiss Journal of Geosciences*, 101, pp. 139–183.
- Stanko, D., Markušić, S., Korbar, T., & Ivančić, J. (2020). 'Estimation of the High-Frequency Attenuation Parameter Kappa for the Zagreb (Croatia) Seismic Stations'. *Applied Sciences*, 10(24), p. 8974. Available at: <https://doi.org/10.3390/app10248974>. (Accessed: 8 May 2021).
- The European Database of Seismogenic Faults (2021). SHARE task 3.2 [Online]. Available at: [http://diss.rm.ingv.it/share-edsf/sharedata/SHARE\\_WP3.2\\_Map.html](http://diss.rm.ingv.it/share-edsf/sharedata/SHARE_WP3.2_Map.html) (Accessed: 9 May 2021).
- Tomljenović, B. (2020). *Osvrt na potres u Zagrebu 2020. godine. Autor teksta je prof. dr. sc. Bruno Tomljenović.* (in Croatian). Sveučilište u Zagrebu, Rudarsko Geolosko Naftni Fakultet. Available at: <https://www.rgn.unizg.hr/hr/izdvojeno/2587-osvrt-na-potres-u-zagrebu-2020-godine-autor-teksta-je-prof-dr-sc-bruno-tomljenovic> (Accessed: 9 May 2021).
- Torbar, J. (1882). Izvješće o zagrebačkom potresu 9. studenoga 1880. Djela Jugoslavenske akademije znanosti i umjetnosti, knjiga I, JAZU, Zagreb.
- USGS (2020a) *M 5.3 - 2km WSW of Kasina, Croatia*. Available at <https://earthquake.usgs.gov/earthquakes/eventpage/us70008dx7/executive> (Accessed 22 March 2020)
- USGS (2020b). '*M 6.4 – 3 km WSW of Petrinja, Croatia*'. Available at: <https://earthquake.usgs.gov/earthquakes/eventpage/us6000d3zh/executive> (Accessed: 29 December 2020).
- Ustaszewski, K., Kounov, A., Schmid, S.M., Schaltegger, U., Krenn, E., Frank, W., Fügenschuh, B. (2010). 'Evolution of the Adria–Europe plate boundary in the northern Dinarides: from continent–continent collision to back-arc extension'. *Tectonics*, 29 (TC66017), pp. 1-34. Available at: <http://dx.doi.org/10.1029/2010TC002668>. (Accessed: 8 May 2021).
- Vukovski, M. (2021) *Potres u Petrinji – preliminarno izvješće* Croatian Geologic Survey. Available at <https://www.hgi-cgs.hr/potres-u-petrinji-preliminarno-izvjesce/> Accessed 8 May 2021.

### 3 Geology, Geomorphology and Soil Characteristics (Dunja Perić, Ingrid Tomac)

#### 3.1 Geology and Geomorphology

A wide zone of convergence between Eurasian and African plates during Late Cretaceous and Cenozoic time occurred in the overall compression setting, in which extensional basins have developed since Oligocene in association with subduction zones, thus consuming oceanic and attenuating subduction zones. The Pannonian or Carpathian Basin, which is located in the SE part of Central Europe, is an integral part of the Alpine orogenic system. The basin is of Miocene through Quaternary age, and it is surrounded by the Carpathian, Alpine, and Dinaric mountains (**Figure 3.1**). The basin is of extensional origin, and its formation was accompanied by intensive magmatism during the Middle Miocene rifting climax within its Croatian part.

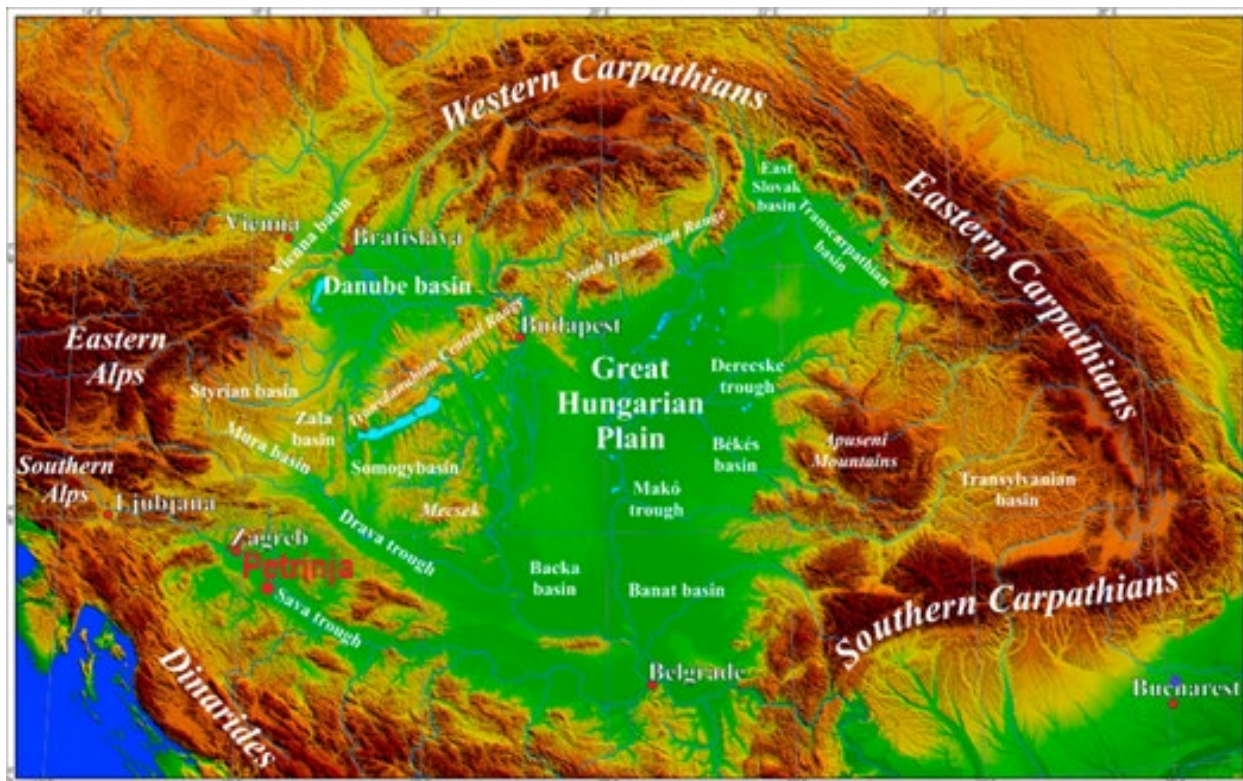


**Figure 3.1** Digital terrain model of the Pannonian basin (adapted from Horváth et al., 2015).

The geomorphological term Pannonian Plain is more widely used to denote roughly the region of the Pannonian basin, although the former typically denotes only the lowlands, the plain that remained after the Pliocene Epoch Pannonian Sea dried out. Pannonian Basin is a geomorphological sub-system of the Alps–Himalaya system, a sediment-filled-back-arc basin, which spread apart during the Miocene. Most of the plain consists of the Great Hungarian Plain to the south and southeast and Little Hungarian Plain to the northwest that is divided by Transdanubian mountains (**Figure 3.1**).

The Pannonian Basin forms a topographically discrete unit set in the European landscape, surrounded by the Carpathian Mountains, Dinarides, and the Alps. The basin extends roughly between Vienna in the northwest, Košice in the northeast, Zagreb in the southwest, Novi Sad in the south, and Satu Mare in the east. The rivers Danube and Tisza divide the basin roughly in half.

Petrinja is located near the southwestern edge of the Pannonian Basin, where the basin meets Dinarides (**Figure 3.1**). In addition, Petrinja is also located in the vicinity of the South Marginal Fault (SMF) of the Pannonian basin (**Figure 3.2**). The active tectonics of the Pokupsko–Petrinja–Sisak region is driven by the continuous movement of the Adria Microplate to the north. Consequently, strain occurs at the contact of Dinarides and the Pannonian basin in the upper part of the Earth's crust. Individual faults are activated and reactivated as strain reaches critical levels. A sudden movement of the blocks of the crust causes the release of energy, thus resulting in the occurrence of earthquakes.

Petrinja is located about 14 km southwest of Sisak while the epicenter of the December 29, 2020 earthquake was located 3 km southwest of Petrinja. A basic geological map of the Sisak unit is shown in **Figure 3.3**. Tectonically, this entire region belongs to the southwestern part of the Pannonian Basin. According to Pikija (1987) the oldest recognized rocks on the surface of this region are sedimentary and igneous rocks of Upper Cretaceous (Senonian) age. The most widespread sedimentary rocks are pelagic limestones of the “scaglia” type, the prevailing igneous rocks are tuffaceous rocks and spilites. Late Cretaceous events resulted in uplift while clastic deposition occurred during Paleocene and Eocene. Coarse-grained clastic rocks formed during the Helvetian after a long emersion.

The area most affected by the earthquake is covered by two Basic Geological Maps on a 1:100,000 scale: the Sisak sheet (**Figure 3.3**) and the Bosanski Novi sheet (**Figure 3.4**). In this brief review, only the rocks from the area surrounding the Petrinja area are described. According to Pikija (1987), the oldest rocks within the region are Upper Cretaceous sedimentary and igneous rocks. The most common sedimentary rocks are micritic and clayey limestones similar to "Scaglia limestone" and the most frequent igneous rocks are spilites and tuffitic rocks. Late Cretaceous tectonic movements resulted in uplift and formation of source areas for most clastic rocks deposited during Paleocene and Eocene. Deposition in Eocene was followed by a relatively long emergence phase during which Sava depression started to form. Middle Miocene sedimentation started by an accumulation of coarse-grained clastic rocks.

Marine transgression in the Badenian occurred throughout this entire region. While terrigenous clastic rocks were locally deposited in the basal part, the rest is characterized by the facial diversity of deposits. During the Sarmatian period, clastites are dominant rocks within the Sava depression, while carbonates and clastic rocks predominated in other areas. During Pannonian and Pontian (late Miocene) limestones, calcareous marls, marls, sands, and sandstones were deposited. Pliocene lacustrine deposits are represented by clays, sands, gravels and coal beds. Loess, marsh loess and alluvial sediments were deposited during the Pleistocene, while deposition in Holocene is dominated by slope, deluvial deposits, alluvial, and marsh deposits. The map shown in **Figure 3.3** indicates that the top soil layers near Petrinja are of Quaternary age, including 1)

flood deposits (silts and sands; ap), 2) terrace deposits (silts, sands, and gravels; a1), 3) deluvium–proluvium deposits (silts, sands, gravels, blocks; dpr), and 4) loess (l).

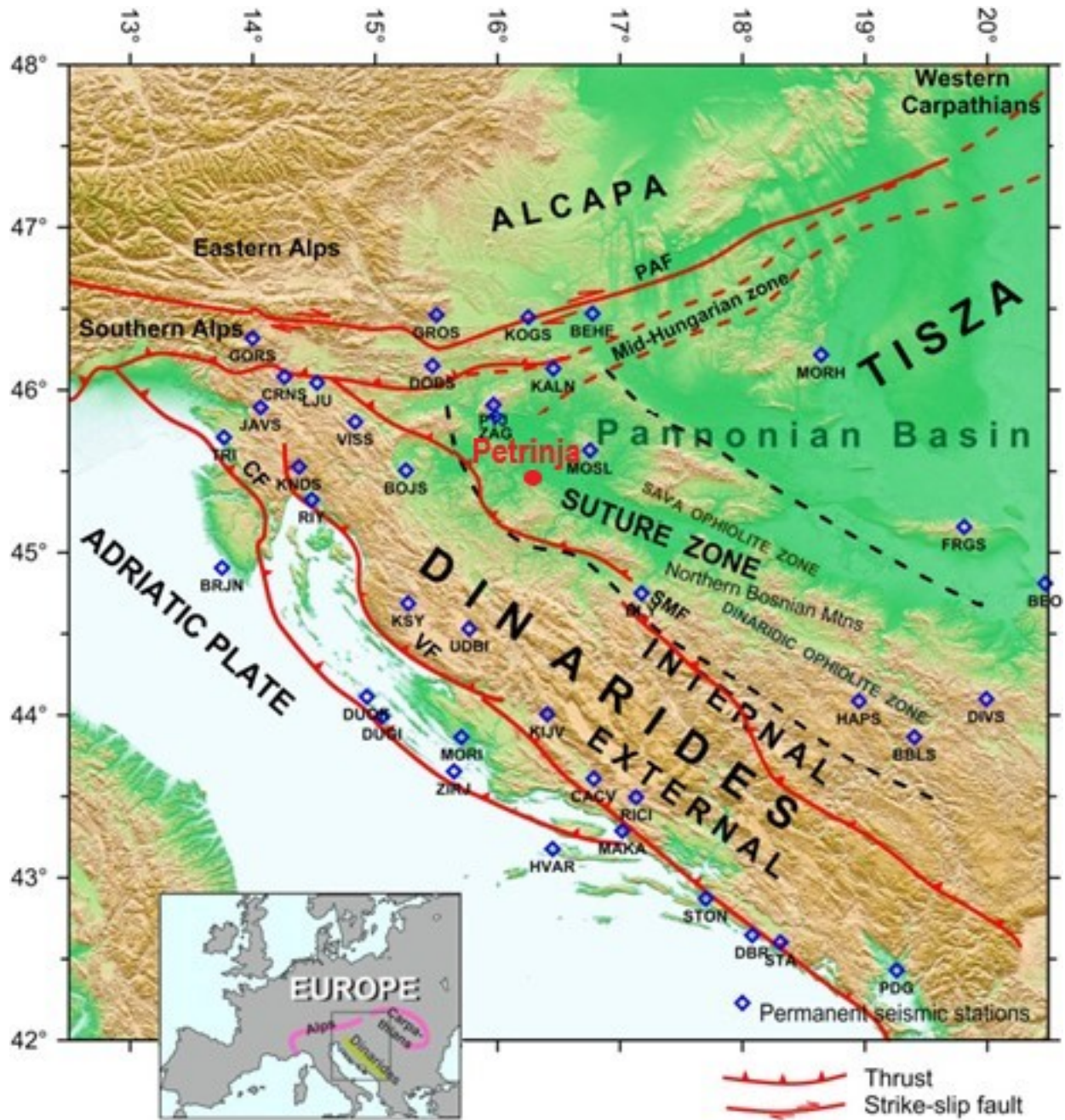


**Figure 3.2** Topographic and tectonic map of the Pannonian–Dinaridic region with border part of the Alcapa (Alpine–Carpathian tectonic unit) with positions of the seismic stations. The main tectonic units and faults are superimposed on the topographic map (PAF – Periadriatic fault, CF – Čičarija fault, VF – Velebit fault, SMF – South marginal fault of the Pannonian basin). The borders of the suture zone after Šumanovac (2010), (adapted from Šumanovac et al., 2017).

Two rivers, the Sava and Kupa rivers, have formed alluvial deposits at depths up to 50 m within the affected area. The interchanging layers of loose sands and loose gravels are underlain by 1 to 5 m thick clay with up to 26% organic content. Medium to stiff clay of low to high plasticity is located below the alluvial deposits. Heavy industrial buildings located in this area are typically founded on floating drilled shafts due to generally soft soils while one to two-story commercial and residential buildings are founded on shallow foundations. The groundwater level in the city of Sisak is about 4 to 5 m deep, but it can vary seasonally and even reach the ground level. It is strongly affected by the water level in the nearby Kupa and Sava rivers. Further details of a typical geotechnical profile and soil characteristics in this region are provided in Section 3.2 of this report.

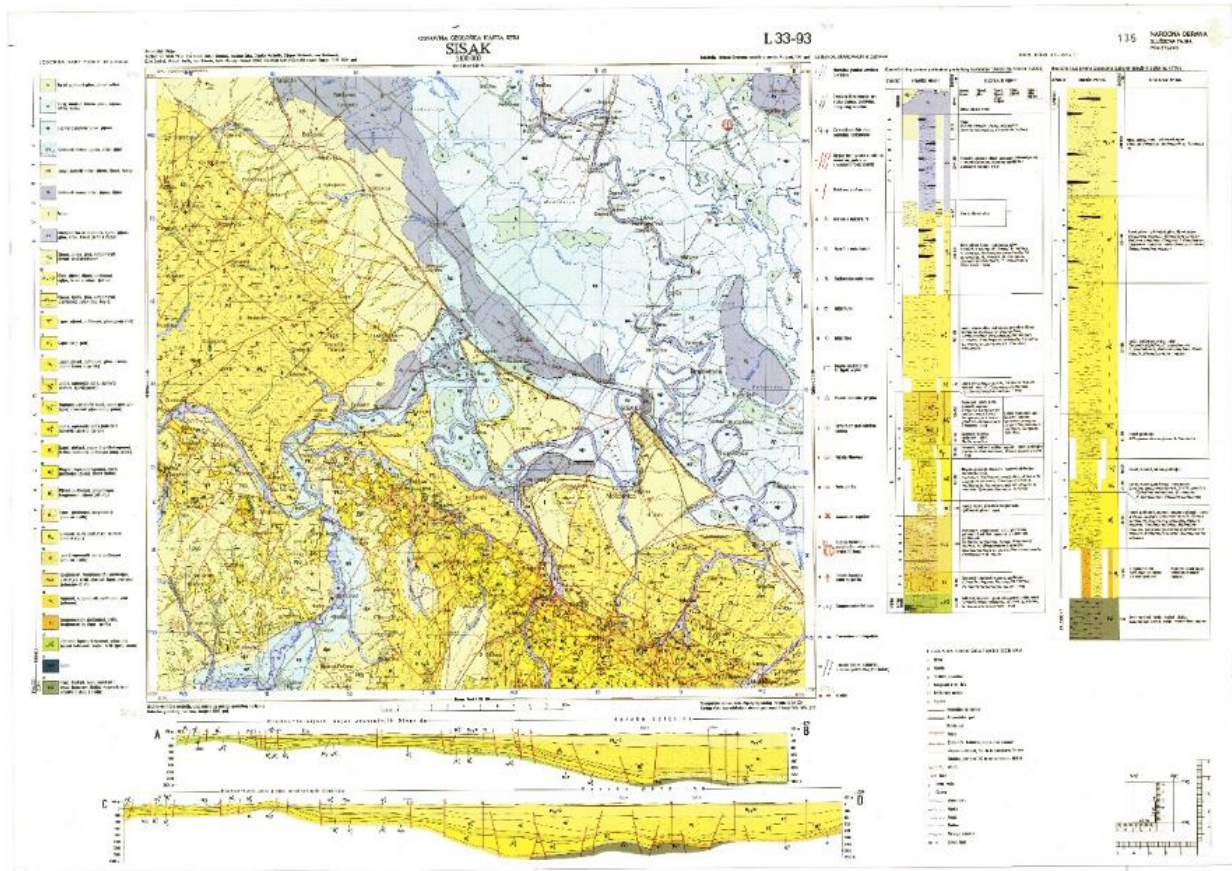


Figure 3.3 Basic geological map Sisak sheet 1:100,000 (Pikija 1987).

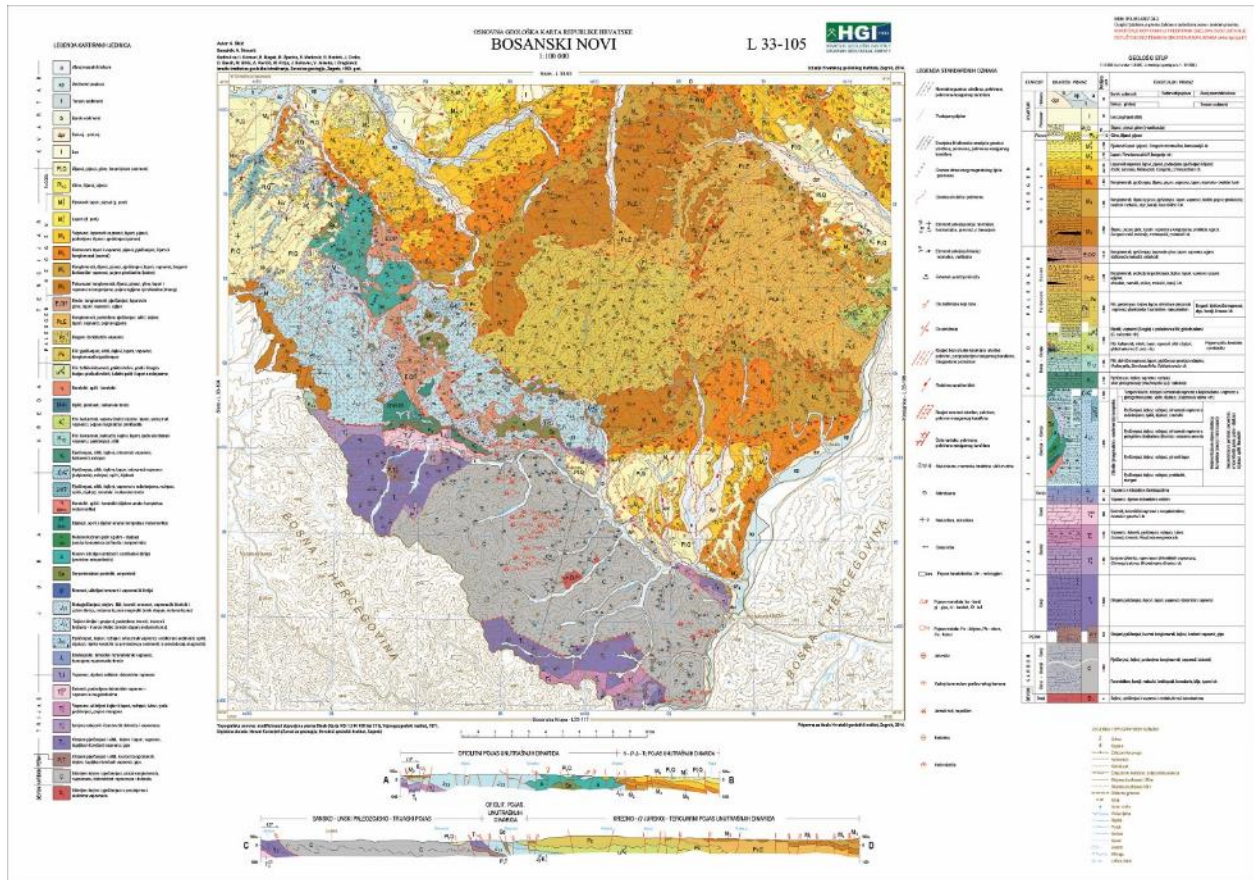


Figure 3.4 Basic geological map Bosanski Novi sheet 1:100,000 (Šikić, 2014).

### 3.2 Geotechnical Soil Characteristics

Several available geotechnical reports from locations in the sedimentary basin show layers of loose sand, that can have high liquefaction potential. For example, in Braće Hanžeka street nr. 23 in Petrinja, two 6 m deep borehole logs show SFs (silty sand, loose, wet, brown) at 5.7 and 6.0 m depth, with ground water registered at the top of the sand layer (Tomac, 2009). In Sisak, within the perimeter of thermal powerplant Čret heavy buildings and chimneys are founded on floating large diameter piles, 10-15 m deep (Figure 3.5). The pump station is founded on a 33.5 m deep diaphragm wall in the stiff clay layer under alluvial layers, showing small settlements. Primary consolidation for 12 m deep pile raft system took more than 15 years,  $w = 6.7$  cm. Secondary consolidation was 1-2 cm. Calculated settlement values were slightly exceeded in the majority of cases. Reasons for the discrepancy between predicted and actual behavior is maybe because of seasonal water table changing up to 10 m, or machine vibrations in the power plant area that might cause some negative friction on piles. The location of the power plant is on alluvial deposits between rivers Sava and Kupa in the vicinity of town Sisak. The area is known for its weak soils that can reach depths of 50 m – composed of loose sand and gravel layers intermixed with soft and medium clays and organic material (Marić, 2005; Marić et al., 2007). A comprehensive geotechnical investigation performed in the past includes deep boreholes which also show various sand layers shown in Figure 3.6. Average SPT blow counts, collected from 31 deep





**Figure 3.6** Soil cores taken from the area near the thermal powerplant in Sisak, Čret (45.4538, 16.4145) (Marić, 2005).

On the location of the Čret thermal powerplant, the soil water level varies from 5.5 to 6.5 m below ground surface and strongly depends on the river Sava water level. Six borehole logs indicate strong soil layer heterogeneity that is typical for alluvial deposits. A surficial (I) fill layer is up to 3 m thick and is composed of brown fine sand and gravel; below is a 0.5 - 2.6 m thick brown (II) clay

(CL-CH) layer, with soft consistency, very silty ( $w_0 = 26.3 - 28.6\%$ ,  $w_L = 16.2 - 63.2\%$ ,  $w_P = 12.4 - 26.0\%$ ,  $I_P = 9.5 - 44.4\%$ ,  $g = 18.6 - 19.5 \text{ kN/m}^3$ ,  $g_d = 14.6 - 15.4 \text{ kN/m}^3$ ,  $q_u = 18 - 195 \text{ kPa}$ ,  $c' = 20 - 50 \text{ kPa}$ ,  $f' = 24 - 28^\circ$ ). Below the clay layer is (III) 3.5 - 13 m thick sand, with various classifications: SFs, SFc, SP, SU, typically as fine sands, light-brown color. The SPT results are  $N_{\text{SPT}}=5-16$ , indicating loose to medium compacted sands. Granulometry shows particle sizes ranges: sand 59 - 99%, silt 6 - 38% and clay 1 - 6%. The next detected layer is also (IV) sand (SFs, SP), 2.1 - 14.5 m thick, fine, poorly graded, with clay and silt, sometimes with gravel, loose to medium dense, with  $N_{\text{SPT}}=5 - 16$ . Below is a layer of (V) gravel (GW, GP, GFs) 1.8 - 11.0 m thick. However, at the same depths, some boreholes demonstrated thinner or thicker layers of sand (SP), somewhere even 7.0 m thick. Gravel granulometry shows particle size ranges: gravels 19 - 88%, sands 12 - 81% and silt 0 - 2%. The bottom layer is (VI) clay (CL-CH), with varied plasticity in different boreholes, stiff to very stiff, of blue-grey color. Clay strata are detected at depths 22.5 - 28.0 m from the surface, while some 30 m boreholes did not display the bottom clay layer, but only sand. Clay properties are as follows:  $w_0 = 18.2 - 30.7\%$ ,  $w_L = 21.8 - 63.5\%$ ,  $w_P = 17.1 - 23.5\%$ ,  $I_P = 0.1 - 40.9\%$ ,  $\gamma = 15.6 - 20.4 \text{ kN/m}^3$ ,  $\gamma_d = 15.2 - 17.4 \text{ kN/m}^3$ ,  $q_u = 81 - 366 \text{ kPa}$ ,  $c' = 6 - 64 \text{ kPa}$ ,  $\phi' = 13 - 31^\circ$ . **Figure 3.7** shows CPTU tests performed within a perimeter of the thermal powerplant.

Oprema: **GEOTECH**

Klasa: **CPT3**

Kalibracijski kod:

Nulto čitanje prije sondiranja

Nulto čitanje poslije sondiranja

$q_c$	$f_c$	$u$
HZ	KQ	KF
0	0	100
-11.42	0	100

Datum:

12.02.2008

Posao:

**Sisak**

Datoteka:

12040102.CPT

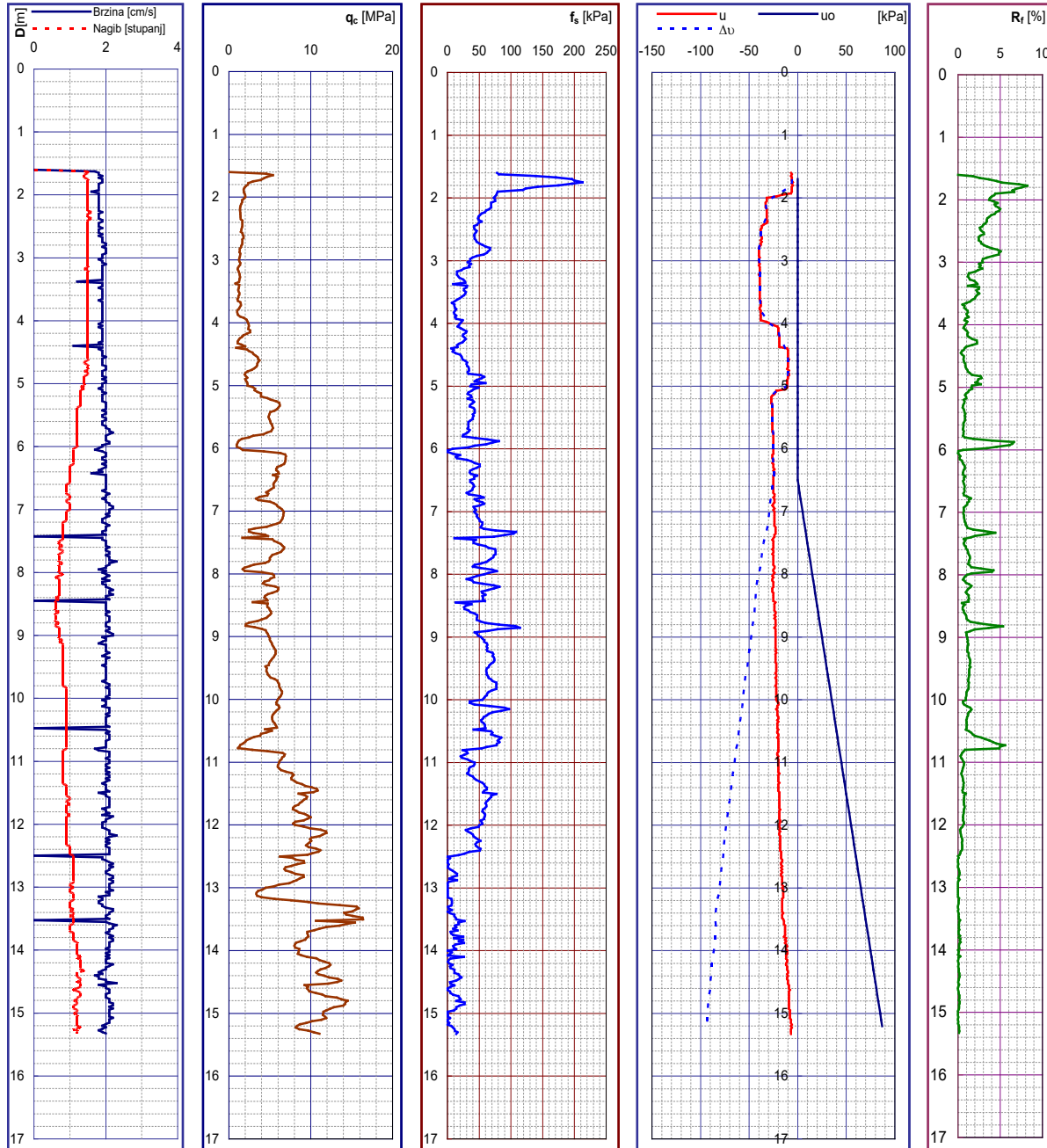


**Figure 3.7** CPTU from thermal powerplant in Sisak, "Blok 3" Čret, (45.4538, 16.4145) (Marić, 2005).

## References

- Horváth, F., Musitz, B., Balázs, A., Végh, A., Uhrin, A., Nádor, A. Koroknai, B., Pap, N., Tóth, T., Wórum, G. (2015). 'Evolution of the Pannonian basin and its geothermal resources.' *Geothermics*, 53, pp. 328–352.
- Marić, B. (2005). *TE Sisak, Kombi-elektrana, BLOK 3, Sisak. Geotehnički Izveštaj, broj.pr. 09-05 (Combi-Power Plant Geotechnical Report) 02/2005*. Zagreb: Conex Ltd.
- Marić, B., Tomac, I., Puljak, S. and Lovrenčić, D. (2007). *Settlement measurements in the area of the town of Sisak over a period of 30 years*. Proceedings of the 6th Austrian Geotechnik Tagung, "Vienna - Terzaghi Lecture". Vienna, Austria, 18-19 January 2007. VOEBU, Wien.
- Pikija, M. (1987) Osnovna geološka karta SFRJ 1:100.000, List Sisak L33–93. – Geološki zavod, Zagreb (1975–1986); Savezni geološki institut, Beograd. Geologic map available on request at <https://www.hgi-cgs.hr/osnovna-geoloska-karta-republike-hrvatske-1100-000/>.
- Šikić, K. (2014) Osnovna geološka karta SFRJ 1:100.000, List Bosanski Novi L33-105. – Fond stručne dokumentacije Instituta za geološka istraživanja, Zagreb. (manuskript) Geologic map available on request at <https://www.hgi-cgs.hr/osnovna-geoloska-karta-republike-hrvatske-1100-000/>.
- Šumanovac, F. (2010). 'Lithosphere structure at the contact of the Adriatic microplate and the Pannonian segment based on the gravity modelling'. *Tectonophysics*, 485(1–4), pp. 94–106. Available at: <https://doi.org/10.1016/j.tecto.2009.12.005>.
- Šumanovac, F., Markušić, S., Engelsfeld, T., Jurković, K., Orešković, J. (2017). 'Shallow and deep lithosphere slabs beneath the Dinarides from teleseismic tomography as the result of the Adriatic lithosphere downwelling'. *Tectonophysics*, 712–713, pp. 523–541. Available at: <https://doi.org/10.1016/j.tecto.2017.06.018>.
- Tomac, I. (2019). *Family House, Ul. Braće Hanžeka, Petrinja, k.č. 254, k.o. Petrinja. Geotechnical Report nr. 02/2009*. Zagreb: Projekt Adrion Ltd.

#### 4. Recorded Ground Motions (Dunja Perić, Marijan Herak)

USGS ShakeMap depicted in **Figure 2.7** (USGS 2020) estimates PGA of approximately 0.4 g in the epicentral region and corresponding MMI of VIII while the Croatian Seismological Survey of the University of Zagreb reported intensity of VIII–IX on the EMS98 scale. Miranda et al. (2021) provided a list of 15 seismic stations located within the distance of 250 km of the epicenter in their Table 2.3. The information provided includes station name, coordinates, distance from the epicenter, and directions and magnitudes of PGA (Peak Ground Acceleration) and PGV (Peak Ground Velocity). The maximum recorded PGA was 24.7 cm/s<sup>2</sup> corresponding to 0.0252 g while the maximum PGV was 2.25 cm/s. Both PGA and PGV were recorded at the Črešnjevec (CRES), station of the Seismic Network of Slovenia, in the North-South direction. The source-to-site distance of the CRES station was 70.55 km, thus placing it the closest to the rupture out of a total of 15 stations considered in that report.

The Croatian Seismograph Network (code CR, DOI: 10.7914/SN/CR; **Figure 4.1**) recorded both the foreshock and the mainshock, as well as the subsequent aftershock activity (still ongoing). In the first two months, over 4300 aftershocks could have been reliably located.

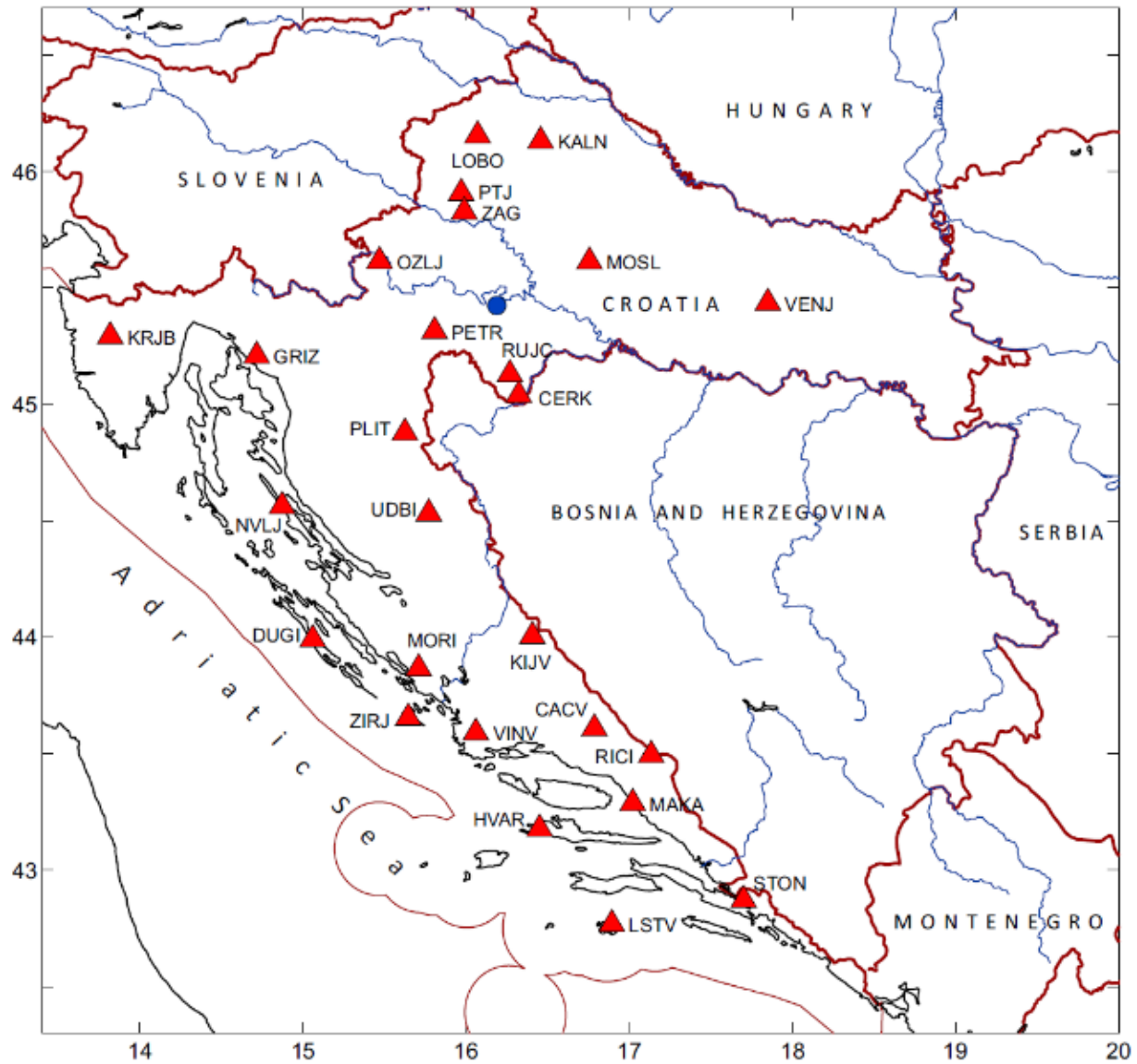


**Figure 4.1** Subset of stations of the Croatian Seismograph Network (code CR, DOI: 10.7914/SN/CR) managed by the Seismological Survey and the Andrija Mohorovičić Geophysical Institute, Faculty of Science, University of Zagreb. The epicenter of the mainshock is shown as a blue circle.

Seismogram examples for the foreshock, the mainshock, and the largest aftershock as recorded by selected broad-band stations of the Croatian Seismograph Network are shown in **Figures 4.2, 4.3, 4.4, 4.5, and 4.6.**

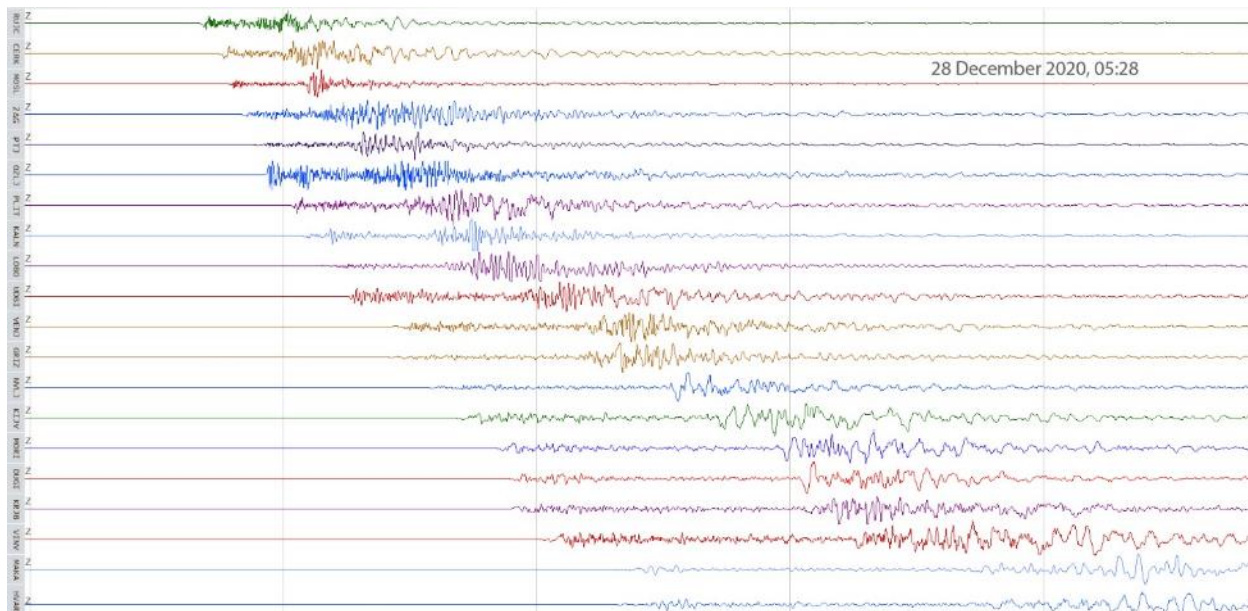


**Figure 4.2** Vertical component broad-band seismograms of the foreshock of December 28, 2020, recorded on selected stations of the CR network. Vertical grey lines are 30 seconds apart.

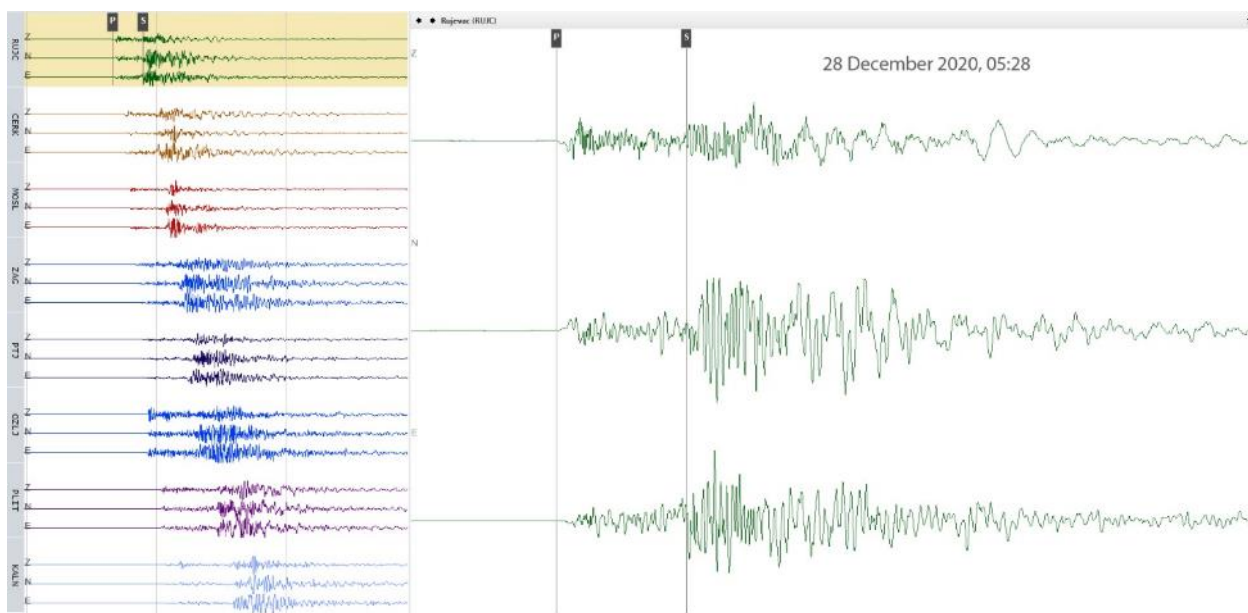


**Figure 4.3** *Left panel:* 3-component broad-band seismograms of the foreshock of December 28, 2020, recorded on eight selected stations of the CR network. Vertical grey lines are 30 seconds apart. *Right panel:* Zoom-in into the seismogram of the station RUJC, the closest one to the epicenter (station PETR in Fig. 1 was installed later).

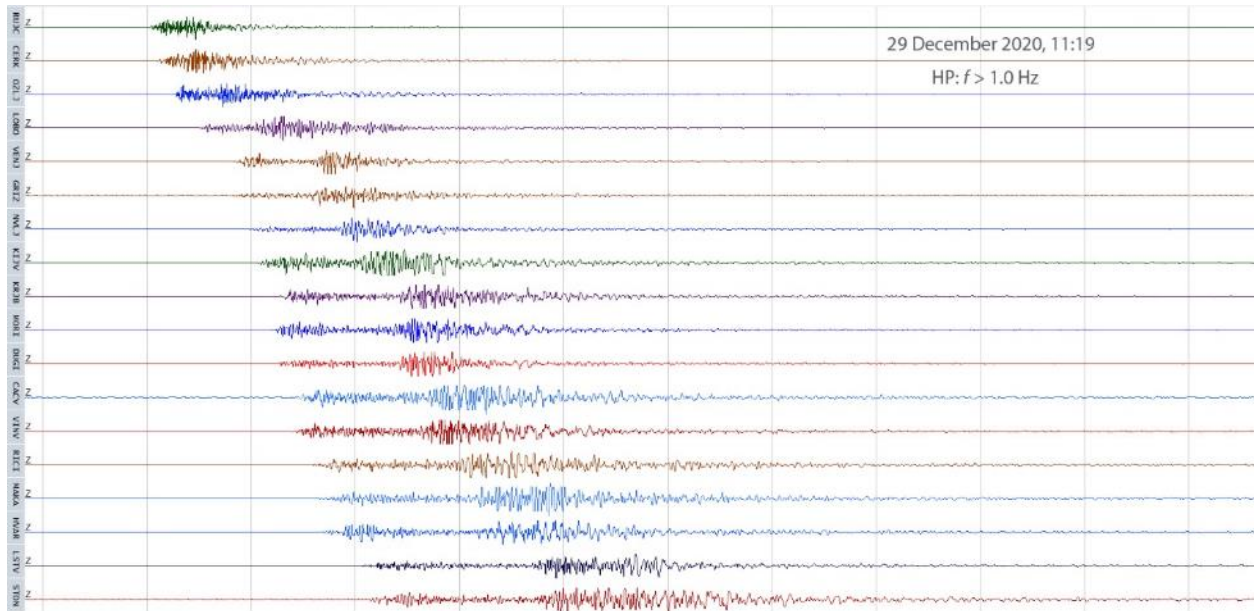


**Figure 4.4** Vertical component broad-band seismograms of the mainshock of December 29, 2020, recorded on selected stations of the CR network. Vertical grey lines are 30 seconds apart. The seismograms are filtered with a high-pass filter with a corner frequency of 1.0 Hz.

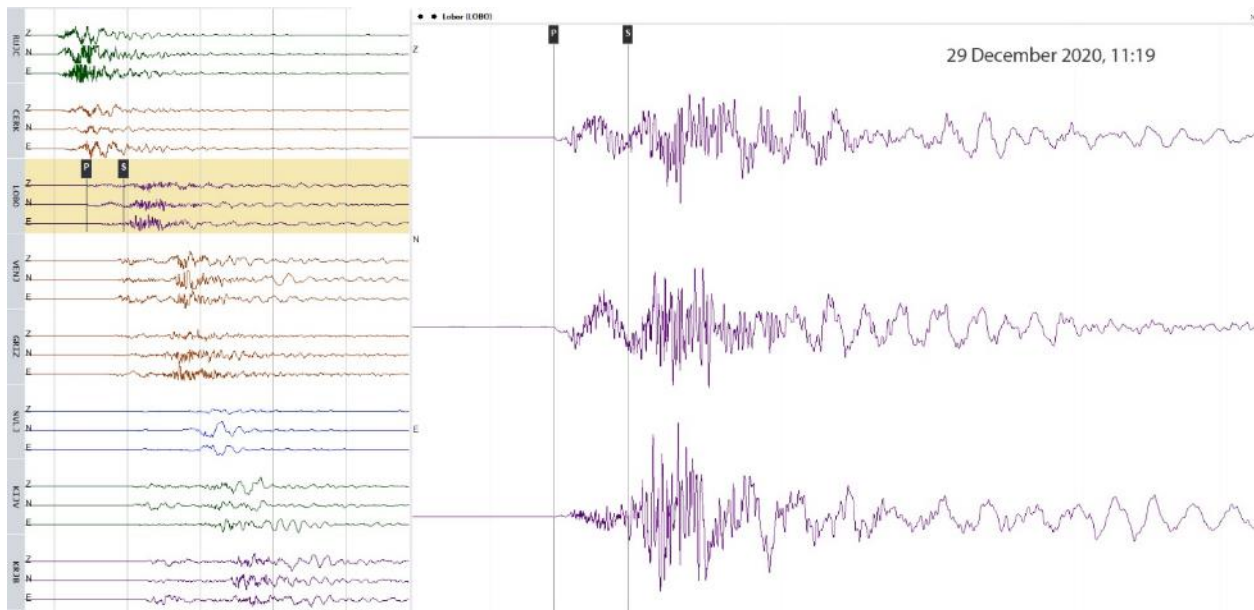


**Figure 4.5** Left panel: 3-component broad-band seismograms of the mainshock of December 29, 2020, recorded on eight selected stations of the CR network. Vertical grey lines are 30 seconds apart. Right panel: Zoom in into the seismogram of the station LOBO.

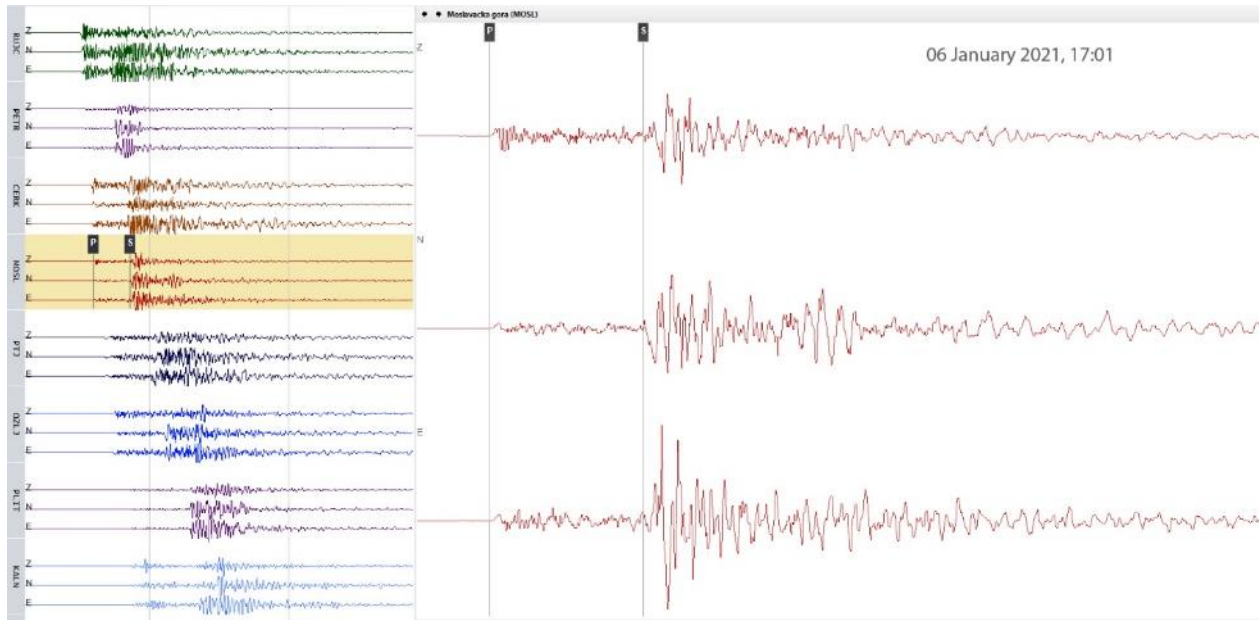


**Figure 4.6** *Left panel:* 3-component broad-band seismograms of the largest aftershock of January 6, 2021, recorded on eight selected stations of the CR network. Vertical grey lines are 30 seconds apart. *Right panel:* Zoom in into the seismogram of the station MOSL.

Information about the location of the six strong-motion stations located in Zagreb is provided in **Table 4.1** while **Table 4.2** provides the preliminary information based on the recordings from these stations. As shown in Table 4.2 the maximum PGA of 243.16 cm/s<sup>2</sup> (0.248 g) and PGV of 9.59 cm/s were recorded at the QKAS station, which is not the closest to the epicenter. The PGD (Peak Ground Displacement) of 4.214 cm was recorded at QARH station.

**Table 4.1** Basic information about stations of accelerogram grid in the city of Zagreb (adapted from Prevolnik, 2021).

Station	Latitude [°N]	Longitude [°E]	Elevation above sea level [km]	Distance from epicenter $R_{epi}$ [km]
QARH	45.777	15.993	0.100	45.462
QZAG	45.827	15.987	0.179	50.775
QKAS	45.914	16.103	0.264	57.795
QUHS	45.808	15.999	0.115	48.503
QGAJ	45.811	15.879	0.122	52.754
QPTJ	45.907	15.968	0.994	59.654

**Table 4.2** Corrected values:  $PGA_{corr}$ ,  $PGV_{corr}$ , and  $PGD_{corr}$  (adapted from Prevolnik, 2021).

Station	Recorded component	$PGA_{corr}$ [cm/s <sup>2</sup> ]	$PGV_{corr}$ [cm/s]	$PGD_{corr}$ [cm]
QARH	Z	45.482	2.160	0.859
	N	93.358	7.792	2.768
	E	79.973	8.490	4.214
QZAG	Z	57.450	2.664	0.796
	N	97.696	5.240	1.791
	E	106.458	6.399	2.954
QKAS	Z	122.490	3.574	0.664
	N	243.165	9.586	1.021
	E	162.763	6.072	0.937
QUHS	Z	42.681	2.427	0.862
	N	124.275	5.960	2.309
	E	95.777	6.234	2.870
QGAI	Z	36.999	1.743	0.500
	N	112.538	6.728	1.372
	E	127.554	7.483	2.508
QPTJ	Z	19.697	1.244	0.549
	N	38.826	1.776	0.797
	E	27.842	2.340	1.247

Based on the values shown in **Table 4.2** it can be concluded that values of  $PGA_{corr}$  recorded at four stations (QUHS, QARH, QGAJ, and QZAG) are comparable and approximately equal to 0.05 g for vertical and 0.1 g for horizontal components. These are expected values for the earthquake of the given magnitude and epicentral distance. Three stations (QUHS, QARH, and QGAJ) are located at comparable epicentral distances with similar relevant soils, which are of type C according to EUROCODE-8, the European standard EN 1998 Design of structures for Design of structures for earthquake earthquake resistance. For the fourth station (QZAG) it is reasonable to assume that soil type B is relevant (Prevolnik, 2021). This explains why there is no significant difference among the ground motions recorded at these four stations. Nevertheless, the values recorded at the two most distant stations (QKAS and QPTJ), which are located at similar epicentral distances, are significantly different from those recorded at the stations QUHS, QARH, QGAJ, and QZAG. The maximum values of  $PGA_{corr}$ , including vertical (0.12 g) and horizontal components (0.25 g) were recorded at station QKAS. These values are roughly two times larger than those recorded at stations QARH, QUHS, QZAG i QGAJ. The smallest values of  $PGA_{corr}$  for both, vertical (0.02 g) and horizontal (0.04 g) components were recorded at station QPTJ. Prevolnik (2021) reported that the corresponding soil is of type A according to EUROCODE-8, for which amplification is not expected. Prevolnik (2021) stated that this pattern of recorded values of ground motions has most likely been caused by local soils and topography.

Finally, it also can be noted that the horizontal component of  $PGA_{corr}$  in the north direction (N) is roughly two times larger than the vertical component. This could be explained by the geographic location of the stations relative to the fault and distribution of energy related to the focal mechanism (Prevolnik 2021). **Figure 4.6** depicts the location of six stations in Zagreb along with the location of the epicenter. In addition, Figure 2.17 from Miranda et al. (2021) shows the location of all stations, including the previously mentioned 15 stations and additional six stations located in Zagreb.



**Figure 4.6** Epicenters of Petrinja earthquake denoted by red circles and accelerometers in Zagreb denoted by red triangles (Source: Prevolnik, 2021).

## References

- International Federation of Digital Seismograph Networks (2021) CR: Croatian Seismograph Network. Available at: DOI: 10.7914/SN/CR. (Accessed: 9 May 2021).
- Miranda, E., Brzev, S., Bijelić, N., Arbanas, Ž., Bartolac, M., Jagodnik, V., Lazarević, D., Mihalić Arbanas, S., Zlatović, S., Acosta, A., Archbold, A., Bantis, J., Borozan, J., Božulić, I., Blagojević, N., Cruz, C., Dávalos, H., Fischer, E., Gunay, S., Hadzima-Nyarko, M., Heresi, P., Lignos, D., Lin, T., Marinković, M., Messina, A., Miranda, S., Poulos, A., Scagliotti, G., Tomac, I., Tomić, I., Ziotopoulou, K., Žugić, Ž., Robertson, I. (2021). *StEER-EERI: Petrinja, Croatia December 29, 2020, Mw 6.4 Earthquake Joint Reconnaissance Report (JRR)*. Available at: DOI: 10.17603/ds2-1w0y-5080 (Accessed: 8 May 2021).
- Prevolnik S. (2021) Analiza akcelograma Petrinjskih potresa (Accelerogram analysis of Petrinja earthquakes) [Online]. University of Zagreb, Faculty of Science, Department of Geophysics

Available at:

[https://www.pmf.unizg.hr/geof/seizmosloska\\_sluzba/potresi\\_kod\\_petrinje\\_2020](https://www.pmf.unizg.hr/geof/seizmosloska_sluzba/potresi_kod_petrinje_2020)

(Published 2 January 2021. Accessed: 6 March 2021).

USGS (2020). '*M 6.4 – 3 km WSW of Petrinja, Croatia*'. Available at:

<https://earthquake.usgs.gov/earthquakes/eventpage/us6000d3zh/executive> (Accessed: 29

December 2020).

## 5 Surface Deformations (Marin Govorčin, Dellena Kinikles)

### 5.1 Surface Deformations

Interferometric Synthetic Aperture Radar (InSAR) was used to analyze the ground surface deformations induced by the Dec. 29, 2020  $M_w$  6.4 Petrinja Earthquake. The technique measures ground surface displacements by comparing radar imagery generated from satellite Synthetic Aperture Radar (SAR) acquisitions. Based on the phase information of received back-scattered radar signals in repeated SAR acquisitions over the same area, it is possible to extract ground surface displacements in the radar line-of-sight. In this analysis, the pre-seismic SAR acquisitions were combined with post-seismic acquisitions to generate the maps of coseismic ground displacements associated with the  $M_w$  6.4 Petrinja earthquake.

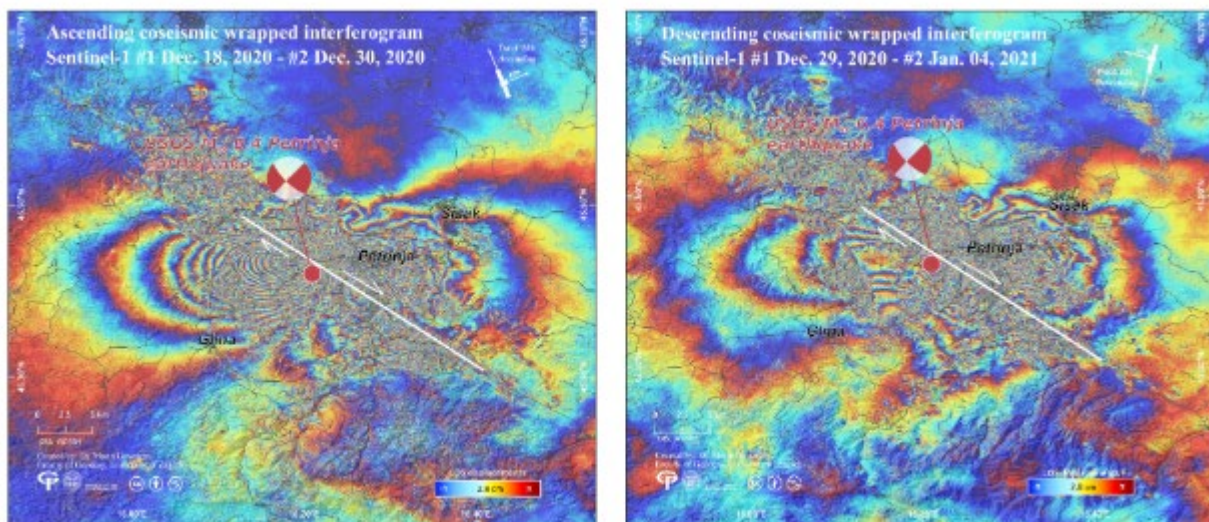


**Figure 5.1.** Coseismic wrapped interferograms calculated with the data acquired from Sentinel-1 a) ascending and b) descending track. Interferograms show ground displacements wrapped in  $2\pi$  modulo (a fringe) in the satellite's line-of-sight direction depicted with white arrows in the right upper image corner. One-color cycle ("fringe") represents half of the satellite's wavelength movement of 2.8 cm. The white line marks a potential location, length, and orientation of the activated Petrinja fault. The focal mechanism solution and epicenter location of  $M_w$  6.4 Petrinja earthquake is shown as red beachball and circle, respectively (adapted from USGS, 2020).

We used Sentinel-1 images acquired on Dec. 18 and Dec. 30 from the ascending orbit track 146 and the images acquired on Dec. 29 and Jan. 04 from the descending orbit track 124 to form an ascending and descending track coseismic interferogram, respectively (**Figure 5.1 a,b**). Coseismic ground deformations can be observed in the form of interferometric fringes (color cycles; red-yellow-green-blue-red), where one fringe represents a ground motion of 2.8 cm (the half of satellite wavelength). A total number of "fringes" multiplied by 2.8 cm gives a maximum ground displacement. The interferograms show a classic strike-slip "butterfly" deformation pattern

forming two deformation lobes on each side of the fault (Fialko et al., 2005). The observed deformation pattern points to an NW-SE-oriented fault situated between Petrinja and town Glina. However, the exact surface fault trace cannot be observed in the interferograms due to a high level of decorrelation in the fault's near-field. We suspect that this is due to the shaking of a ground highly saturated with water. The potential location of the Petrinja fault trace is depicted as white and black lines centered in the middle of a ground deformation pattern in **Figure 5.1 a,b**, and **Figure 5.2 a,b**, respectively. The ascending track interferogram shows around 15 fringes west and 11 fringes east of the decorrelation zone corresponding to a maximum displacement of around 40 cm towards the satellite (in NW-direction) and about 31 cm away from the satellite (in SE-direction), respectively. The descending track interferogram shows around six fringes west and ten fringes east, corresponding to a maximum displacement of 18 cm away from the satellite (in NW-direction) and 28 cm towards the satellite (in SE-direction) respectively. Coseismic ground deformations are shown in **Figure 5.2**, as unwrapped interferograms obtained after the unwrapping process, i.e., calculation of absolute interferometric phase values. We consider the observed ground deformation to be almost completely associated with the  $M_w$  6.4 Petrinja earthquake, due to a short period between Sentinel-1 acquisitions and the earthquake. Both interferograms point to a right-lateral motion consistent with a published USGS moment tensor solution.

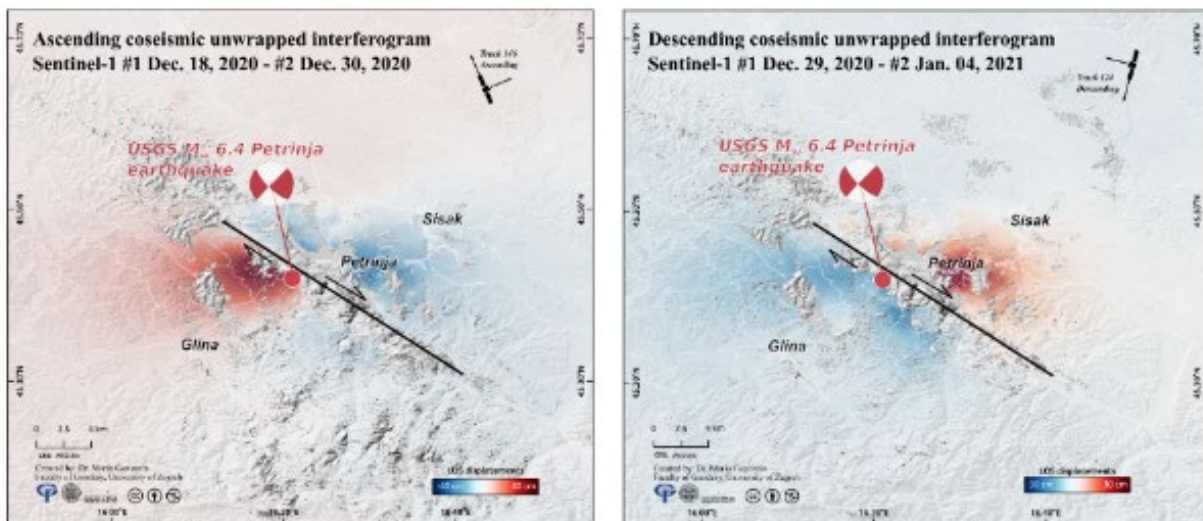


**Figure 5.2.** Coseismic unwrapped interferograms calculated with the data acquired from Sentinel-1 a) ascending and b) descending track. Unwrapped interferograms show ground movement in the satellite line-of-sight shown in the upper right image corner. Highly decorrelated areas are masked out from the interferograms. The black line marks a potential location, length, and orientation of the activated Petrinja fault. The focal mechanism solution and epicenter location of  $M_w$  6.4 Petrinja earthquake is shown as red beachball and circle, respectively (source USGS, 2020).

## 5.2. Surface deformations during past earthquakes strike-slip faults worldwide

One of the most prominent right-lateral strike-slip faults globally is the San Andreas fault (Pacific Plate and North American Plate) which is over 800 miles long and at least 10 miles deep into the Earth's crust (Schulz & Wallace, 2016). The land characteristics of the fault movement appear as long straight escarpments, narrow ridges, and small undrained ponds (Schulz & Wallace 2016). San Andreas' largest recorded strike-slip movements were recorded in the 1906 earthquake (Mw= 7.9) and had an offset of 21 feet (Bray et al., 1994). Recent geological surveys of topography in California between Cajon Pass and the Salton Sea displayed similar terranes on opposite sides of the fault, showing a potential of over 150 miles of strike-slip movement along the San Andreas fault (Schulz et al., 2016). Wells and Coppersmith (1994) conducted an empirical analysis of 69 field cases of surface fault rupture, finding that the magnitude of the quake and fault type movement exhibited surface displacements of 1 centimeter to at most 10 meters (in Bray et al., 1994). From this field case study, further geotechnical analysis on earthquake fault propagation through soil found that three parameters affect ground deformation: type of fault movement, the inclination of the fault plane, and nature of overlying soil deposit (Bray et al., 1994). In Bray et al. (1994), strike-slip faults tend to follow an almost vertical orientation of the underlying bedrock fault and may spread or "flower" near the ground surface. The movement centralizes above the bedrock, and after the failure occurs, differential displacement localizes to distinct failure planes (Bray et al., 1994). If the soil is ductile, the fault movement will be more significant (Bray et al., 1994). Compared to the normal and reverse faults, strike-slip faulting produces the least amount of subsidiary fault movement and secondary deformation in bedrock due to the differential movement diminishing as the fault propagates up toward the ground surface (Bray et al., 1994). Several physical experiments explained better strike-slip earthquake movements: Tchalenko (1970) comparing Riedel experiment direct shear box of plastic clay with strike-slip fault zones, and Emmons (1969) strike-slip faulting in the sand (after Bray et al., 1994). Field observations and experimental data indicate that both stress characteristics and kinematic constraints control the behavior of the soil above the bedrock fault movement (Bray et al., 1994). In 1972 Managua earthquake (Mw=6.4) a left-lateral strike-slip fault occurred with approximately 3 inches of slip (Rojahn, 1973). The city is on a relatively flat alluvial plain with thick volcanic ash-laden mudflows and thinner bed deposits. Boring reports showed the soil ranges from poorly to well consolidated, with low densities and high porosities (Rojahn, 1973). A massive underground concrete bank vault (that was stronger than the sand and gravel around it) deflected the rupture out of its normal alignment (Bray et al., 1994). The 2002 Denali seismic event was a right-lateral strike-slip earthquake (Mw=7.9) with several smaller aftershocks occurring seconds afterward (Eberhart-Phillips et al., 2003). The event ruptured three faults (Susitna glacier Fault, Denali Fault, and Totschunda Fault), and horizontal slip deformations were at an average of 5.3 meters (Eberhart-Phillips et al., 2003). Geotechnical reconnaissance was performed after the quake, and 35 soil samples were tested from areas (Slana, Nabesna, Tok, Gerstle, Delta, Fielding, and Susitna River) affected by liquefaction (Kayen et al., 2004). The depths of samples ranged from 0 to 2.4 meters and characterized the soils from poorly graded to well-graded sand and gravel, with some silty sand (Kayen et al., 2004). The 2001 Kokoxili earthquake (Mw = 7.8) in the northeastern edge of the Tibet plateau recorded the first-time observation of simultaneous events of pure strike-slip and normal faulting (Klinger et al., 2005). The rupture front propagated faster near the surface

resulting in tension cracks opening ahead of the shear dislocation and then later disrupted by a propagating strike-slip offset (Klinger et al., 2005). Breaks occurred in alluvial areas of summer floods of seasonal streams using field observations and high-resolution satellite images (Klinger et al., 2005). The 2010 Darwin (Mw=7.1) right-lateral strike-slip earthquake resulted in 4.6 meters of displacement and an average of approximately 2.3 meters across the entire rupture on the Greendale Fault (Cubrinovski et al., 2010). The most severe damages were liquefaction, and historical studies showed that the areas affected were previously river flood plains, lagoon, and estuaries (Cubrinovski et al., 2010). Before this event, the Greendale Fault had not ruptured since the Last Glaciation (Cubrinovski et al., 2010).

## References

- Bray, D. J., Seed, R. B., Cluff, L.S., Seed, B. H. (1994). *Earthquake fault rupture propagation through soil*. Journal of Geotechnical Engineering, 120(3), p.543–561.
- Cubrinovski, M., Russell A. G., Allen, J., Ashford, S., Bowman, E., Bradley, B., Cox, B., Hutchinson, T., Kavazanjian, E., Orense, R., Pender, M., Quigley, M., & Wotherspoon, L. (2010). *Geotechnical Reconnaissance of the 2010 Darfield (Canterbury) Earthquake*. Bulletin of the New Zealand Society for Earthquake Engineering, 43 (4), p.243–320. Available at: <https://doi.org/10.5459/bnzsee.43.4.243-320> (Accessed: 8 May 2021)
- Eberhart-Phillips, D., Haeussler, P. J., Freymueller, J. T., Frankel, A. D., Rubin, C. M., Crow, P., Ratchkovski, N. A., Anderson, G., Carver, G. A., Crone, A. J., Dawson, T. E., Fletcher, H., Hansen, R., Harp, E. L., Harris, R. A., Hill, D. P., Hreinsdóttir, S., Jibson, R. W., Jones, L. M., Kayen, R., Keefer, D. K., Larsen, C. F., Moran, S. C., Personius, S. F., Plafker, G., Sherrod, B., Sieh, K., Sitar, N., Wallace, W. K. (2003). *The 2002 Denali Fault Earthquake, Alaska: A Large Magnitude, Slip-Partitioned Event*. Science, 300(5622), p1113–18. Available at: <https://doi.org/10.1126/science.1082703> (Accessed: 8 May 2021)
- Emmons, R. C. (1969). "Strike-slip rupture patterns in sand models." Tectonophysics, 7(1), 71-87.
- Fialko, Y., Sandwell, D., Simons, M., Rosen, P. (2005). *Three-dimensional deformation caused by the Bam, Iran, earthquake and the origin of shallow slip deficit*. Nature, 435, p295–299.
- Kayen, R., Thompson, E., Minasian, D., Moss, R. E. S., Collins, B. D., Sitar, N., Dreger, D. and Carver, G. (2004). *Geotechnical Reconnaissance of the 2002 Denali Fault, Alaska, Earthquake*. Earthquake Spectra, 20(3), p639–667. Available at: <https://doi.org/10.1193/1.1778389> (Accessed: 8 May 2021)
- Klinger, Y., Xu, X., Tapponnier, P., Van der Woerd, J., Lasserre, C. and King, G. (2005). *High-Resolution Satellite Imagery Mapping for the Surface Rupture and Slip Distribution of the Mw ~7.8, 14 November 2001 Kokoxili Earthquake, Kunlun Fault, Northern Tibet, China*. Bulletin of the Seismological Society of America, 95(5), p1970–1987.
- Rojahn, C. (1973). *Managua, Nicaragua Earthquake of December 23, 1972*. Earthquake Engineering Research Institute Conference Proceedings Vol.1 Supported in part by the National Science Foundation; Cosponsored by Ministry of Public Works of Nicaragua, American Concrete Institute, American Iron and Steel Institute, American Society of Civil Engineers, Association of Engineering Geologists, Seismological Society of America, Structural Engineers Association of California, November 29-30, 1973, San Francisco, California. Oakland: Earthquake Engineering Research Institute.

- Schulz, S. S., Wallace, R. E. (2016). *The San Andreas Fault* [Online]. U.S Department of the Interior: U.S. Geological Surveys. Available at: <https://pubs.usgs.gov/gip/earthq3/safaultgip.html> (Accessed: 8 May 2021)
- Tchalenko, J. S. (1970). "Similarities between shear zones of different magnitudes." *Geol. Soc. Am. Bull.*, 81(Jun.), 1625-1640
- USGS (2020) M 6.4 - 2 km WSW of Petrinja, Croatia. Available at <https://earthquake.usgs.gov/earthquakes/eventpage/us6000d3zh/executive>. Published 29 December 2020.
- Wells, D., and Coppersmith, K. (1994). "New empirical relationships among magnitude, rupture length, rupture width, rupture area and surface displacements." *Seism. Soc. Am. Bull.*, 84(4)

## 6 Cover-Collapse Sinkholes (Ingrid Tomac, Igor Vlahović, Jelena Parlov, Bojan Matoš, Darko Matešić, Ivan Kosović, Ivica Pavičić, Tihomir Frangen, Josip Terzić, Davor Pavelić, Nguyen Pham)

### 6.1 Geological Setting

GEER reconnaissance team registered 91 cover-collapse sinkholes that opened because of the Petrinja earthquake of December 29, 2020, and numerous aftershocks. Sinkholes appeared within the small 4 km<sup>2</sup> area surrounding Mečenčani and Borojevići villages located 20–25 km SE of the epicentral area during only three months. Although the proposed trace of Petrinja fault as a seismogenic source stretches very close, Mečenčani and Borojevići are outside of the most active fault segment: epicenters of only a few low-magnitude earthquakes were near the sinkhole area (**Figure 6.1**). Cover-collapse sinkholes found in Mečenčani and Borojevići formed due to the particular combination of heavily karstified limestones covered by relatively thick clayey soil. Therefore, in the approximately 1.000 km<sup>2</sup> large area affected by the Petrinja earthquake sequence, only a small area of roughly 4 km<sup>2</sup> is prone to cover-collapse sinkholes (**Figures 6.2 and 6.3**). Subhorizontal Badenian deposits (M<sub>4</sub>) are composed of alternating highly porous Lithothamnium limestones and calcarenites that are very susceptible to karstification. Karst phenomena form, for example, sinkholes/dolines visible on outcrops in the neighboring hilly area SW of Mečenčani and Borojevići. A 4–15 m thick sequence of Holocene deluvial–proluvial deposits (dpr) built of clays with interlayers lenses of gravel and sand in lateral and vertical alternations covers the heavily karstified carbonate bedrock.

During wet periods high water pressure from underlying highly permeable confined karst aquifer caused both gradual underground erosion of non-cohesive fine-grained cover soil (suffosion) or successive failures of cohesive soil (see Gutiérrez and Cooper, 2013). Continuous removal of eroded sediment caused by groundwater flow through karstified systems in underlying carbonates creates and gradually expands cavernous space. Unlike subsidence that slowly creates depressions with gentle slopes by suffosion in non-cohesive deposits, the collapse of cover cohesive soil deposits is sudden, usually occurring within minutes or hours. Cover-collapse structures usually have steep or even overhanging margins – as most of the studied in the vicinity of Mečenčani and Borojevići – and occur mostly in more competent rocks. The collapse of cover deposits is more common during periods of heavy rainfall, as water significantly increases the total weight of soil and at the same time reduces soil strength and arching stability.

Mečenčani and Borojevići areas are naturally prone to cover-collapse sinkholes. Therefore, in addition to 91 recently opened sinkholes, a total of 45 **fossil cover-collapse sinkholes** formed before the 2020–2021 Petrinja earthquake series were registered by the GEER team (**Figures 6.2 to 6.5**). Several of these sinkholes were filled up years ago by local farmers and did not reactivate during the studied earthquake series, except for subtle subsidence recorded in a few of them (mostly around 10 cm). Eight out of ten largest sinkholes found in the area are fossil ones, having the largest diameter between 10 and 18 m (including major springs in the area, Davidovića vrelo and Pašino vrelo located close to the Sunja river).

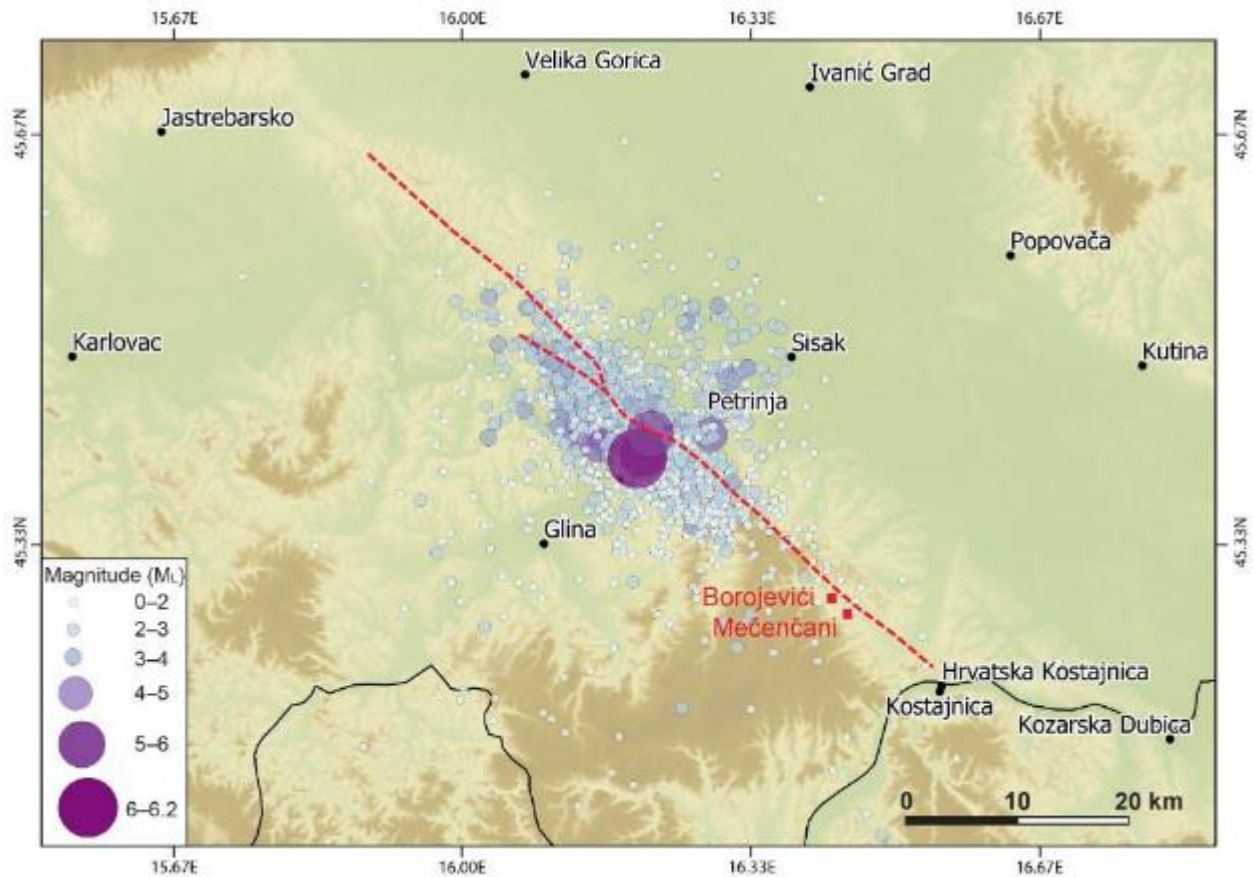


**Figure 6.1** Map of the preliminary position of earthquake epicenters in the Petrinja area from December 28, 2020, to January 28, 2021, with approximate fault position estimated with InSAR analysis (Chapter 5) and Borojevići and Mečenčani villages. Note that only a few epicenters of low-magnitude earthquakes are around this area characterized by numerous cover-collapse sinkholes. Map of earthquake epicenters by the Croatian Seismologic Survey (2021)

Fossil sinkholes are generally morphologically very similar to recent ones, including common very steep to sub-vertical walls. However, besides testimonies of local farmers, three major characteristics enabled their recognition:

- (1) Lack of freshly opened collapsed margins and irregular cover of fresh soil and grass at their bottoms.
- (2) Common old trees are growing, including sometimes old garbage found at their bottoms.
- (3) In the case of sinkholes filled with water, fossil sinkholes are characterized by abundant fresh-water macrophytic vegetation, while newly formed sinkholes have no fresh-water plants.

Numerous earthquakes significantly accelerated natural processes in the area: according to local people, a new cover-collapse sinkhole would be opened in the area once every few years. The changes in stress states caused by the 2020–2021 Petrinja Earthquake Sequence resulted in the opening of as many as 91 cover-collapse sinkholes within only three months. We speculate that

high groundwater levels additionally fostered such an intense sinkhole collapsing during Petrinja Earthquake Sequence during the studied period.

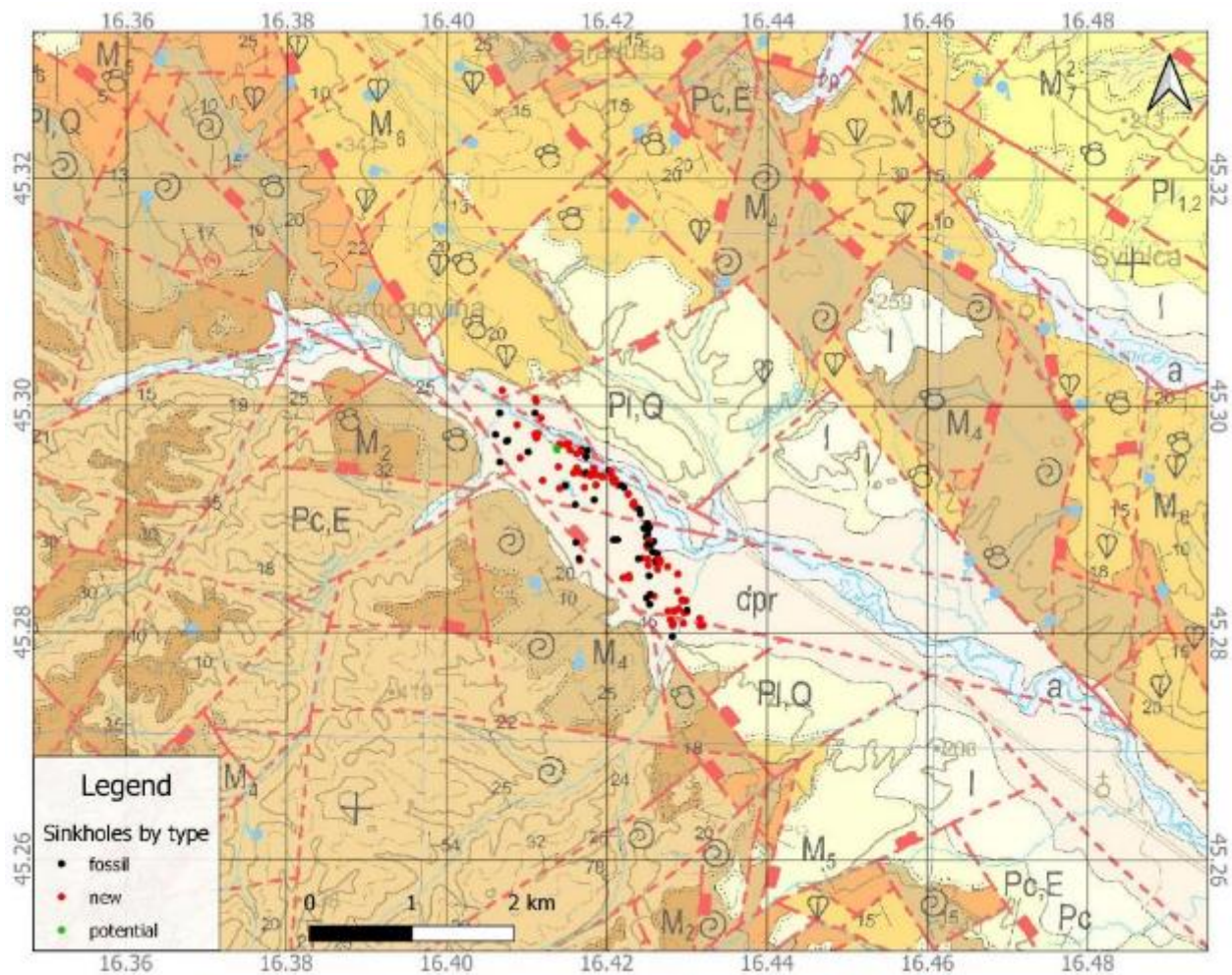


**Figure 6.2.** Detail of the Basic geological map of the Republic of Croatia 1:100,000, Bosanski Novi sheet (Šikić, 2014) with the position of studied cover-collapse sinkholes. Note that all sinkholes are in the small area where deluvial–proluvial deposits (dpr) cover Middle Miocene limestones and calcarenites (M<sub>4</sub>, Badenian).

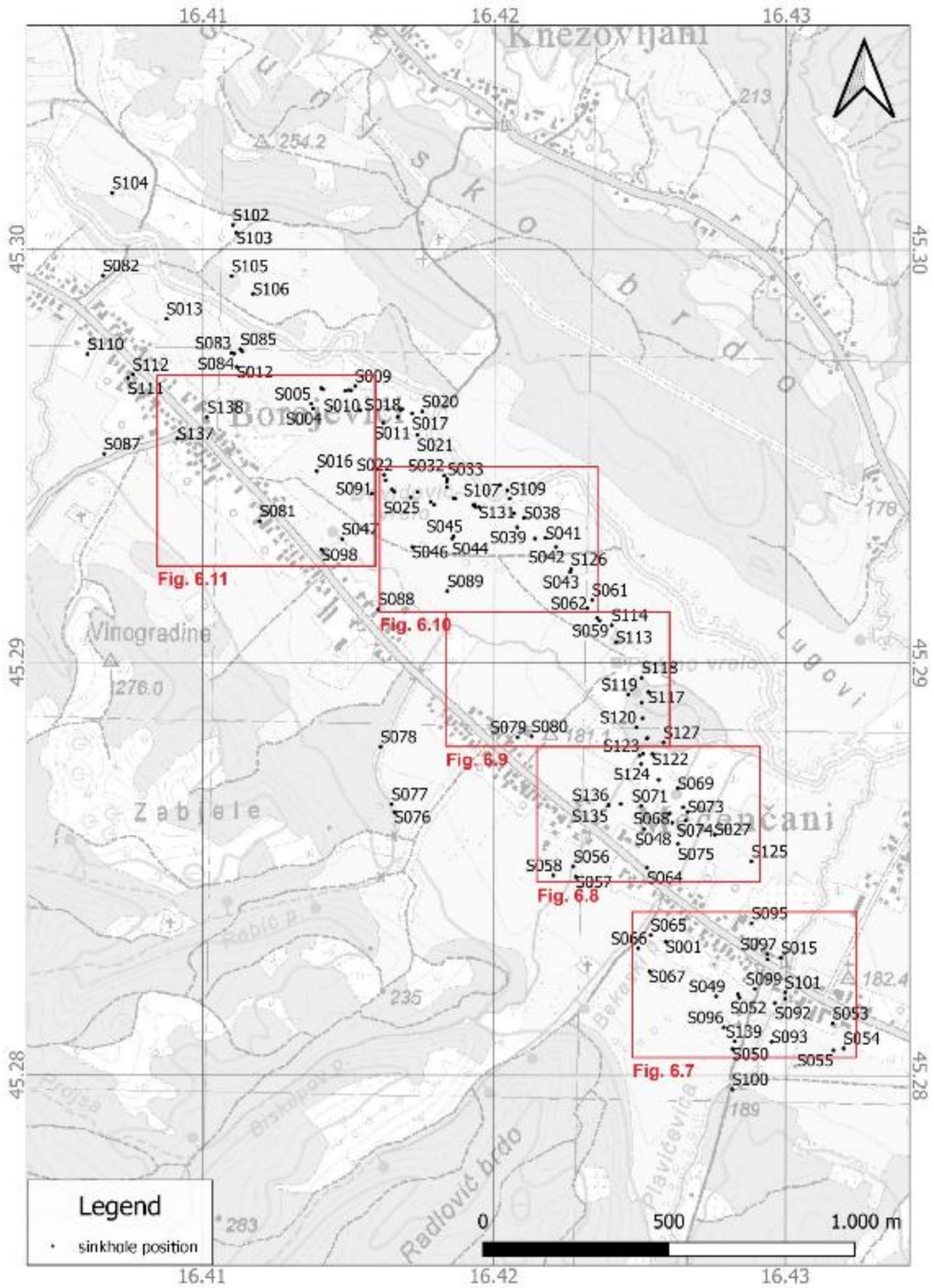


**Figure 6.3** Position of cover-collapse sinkholes in Borojevići and Mečenčani on the topographic map with positions of areal photogrammetry shown in **Figures 6.7 to 6.11**.



**Figure 6.4** Sinkhole S069, with the largest diameter of 16.8 m, is a fossil cover-collapse sinkhole representing a freshwater spring (45.28696N, 16.42630E).

## 6.2 Spatio-Temporal Dynamics of Earthquake-Induced Cover-Collapse Sinkholes in Mečenčani–Borojevići area

Local and virtual reconnaissance teams recovered and assembled spatio-temporal data from drone imaging, field observations, and critical consideration of multiple interviews with residents and police. Although residents provided new sinkholes positions, information about their opening time was often inaccurate and confusing. During the first month after the major earthquake, drones flew exclusively by the Croatian Mountain Rescue Service (HGSS), followed by four drone campaigns by the GEER team members. Three drone flights were by the Croatian Geological Survey on January 29, March 4, and March 31, and one by the Faculty of Mining, Geology and Petroleum Engineering on February 18 and 19.

**Figure 6.5** shows spatio-temporal positions of sinkholes sorted into time windows of appearance and sizes. The GEER team could not obtain better resolution data than the time windows presented in **Figure 6.5**. Grey-colored circles represent fossil sinkholes, which are pre-existing cover-collapse sinkholes. A more significant number of fossil sinkholes characterize the area between two villages, including Pašino vrelo (vrelo meaning spring in Croatian). Pašino vrelo has been turned into a commercial well and serves as a drinking water source for Hrvatska Kostajnica. Fewer but relatively larger and deeper sinkholes and fewer of them per area collapsed in the eastern part around Mečenčani than in the north of Borojevići. The biggest sinkhole, 25x23 m in

diameter and 11.7 m deep, is in Mečenčani and the second-largest new sinkhole, 10.8x9.8 m in diameter and 3.6 m deep.

A total of 136 cover-collapse sinkholes (45 fossil and 91 newly opened), as well as three potential sinkholes were observed and documented. Lengths, widths, and depths were measured directly on-site for each sinkhole, and lidar point clouds were collected for 63 sinkholes and are curated in NHERI NSF DesignSafe Data Depot. The majority of sinkholes appeared dry during the reconnaissance, while some also had standing water. Depths of sinkholes and time of appearance are shown in **Figure 6.6**. Areal images of drone flights acquired by the Croatian Geological Survey show parts of the area in **Figures 6.7 to 6.11**. The GEER team identified the fossil in black circles and new, in white circles, cover-collapse sinkholes. The largest sinkhole is shown in **Figure 6.7** as S001, Pašino vrelo pumping station is in Figure 6.6 between S113 and S118.

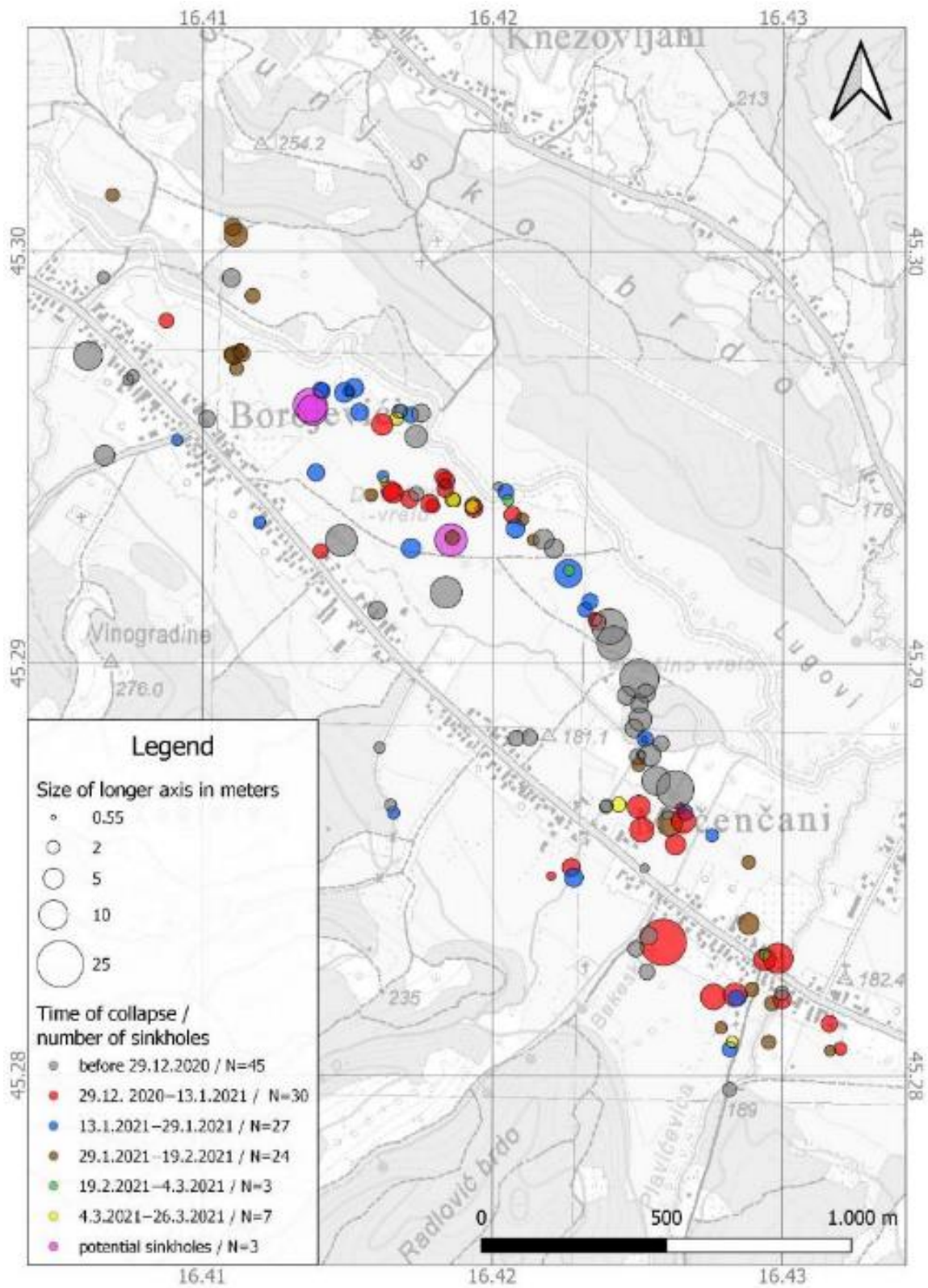


**Figure 6.5** Spatio-temporal map of sinkholes in Borojevići and Mečenčani and their longer diameter on the topographic map.

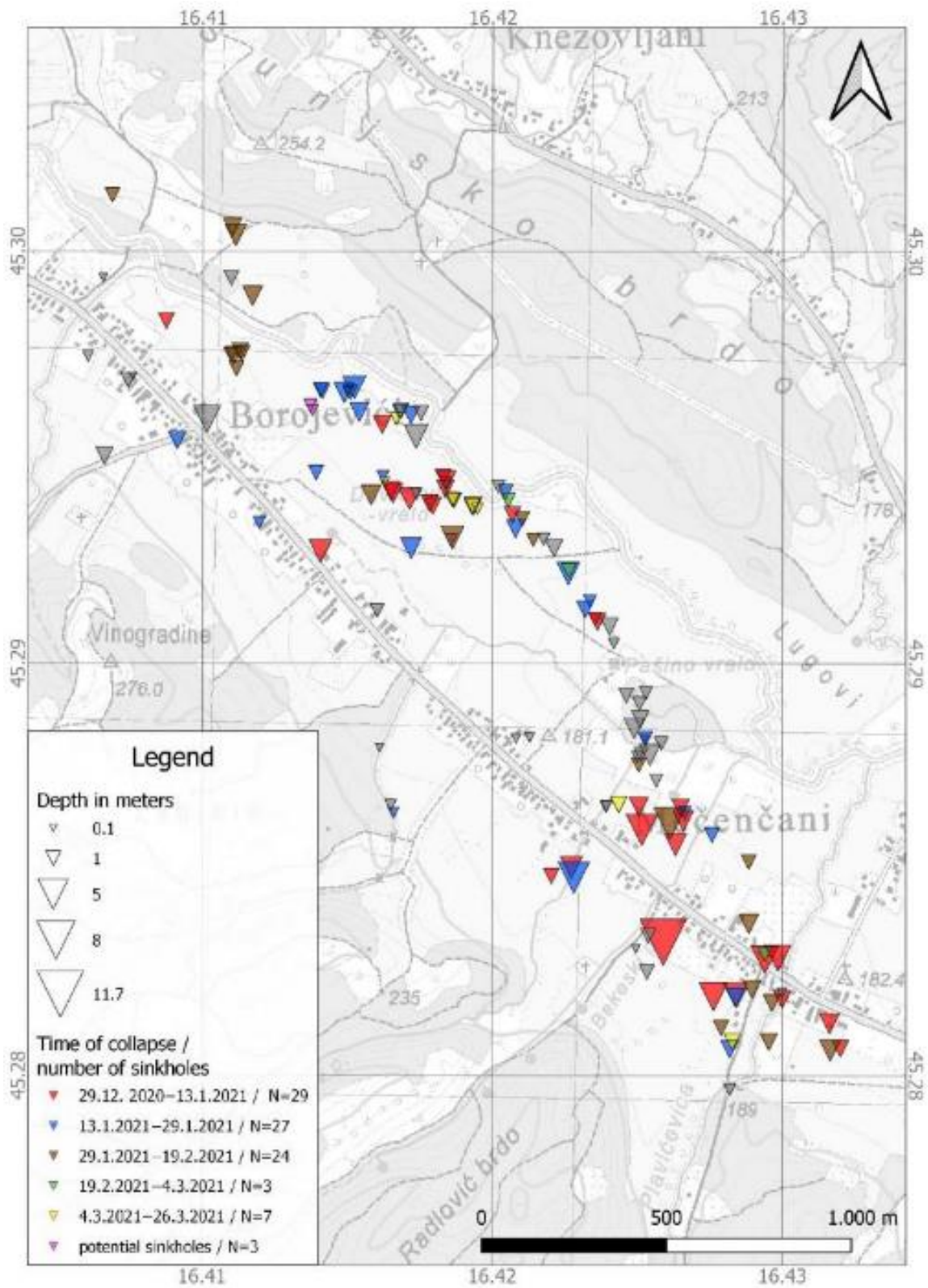


**Figure 6.6** Spatio-temporal map of sinkholes in Borojevići and Mečenčani area and their depths on the topographic map.



**Figure 6.7** Areal image of cover-collapse sinkholes in Mečenčani village (white – new sinkholes opened after M6.4 earthquake, black – fossil sinkholes opened before the Petrinja earthquake sequence). Image by Croatian Geological Survey.



**Figure 6.8** Areal image of sinkholes north of Mečenčani village (white – new sinkholes opened after M6.4 earthquake, black – fossil sinkholes opened before the Petrinja earthquake sequence). Image by Croatian Geological Survey.



**Figure 6.9** Areal image of sinkholes between Borojevići and Mečenčani villages (white – new sinkholes opened after M6.4 earthquake, black – fossil sinkholes opened before the Petrinja earthquake sequence). Image by Croatian Geological Survey.

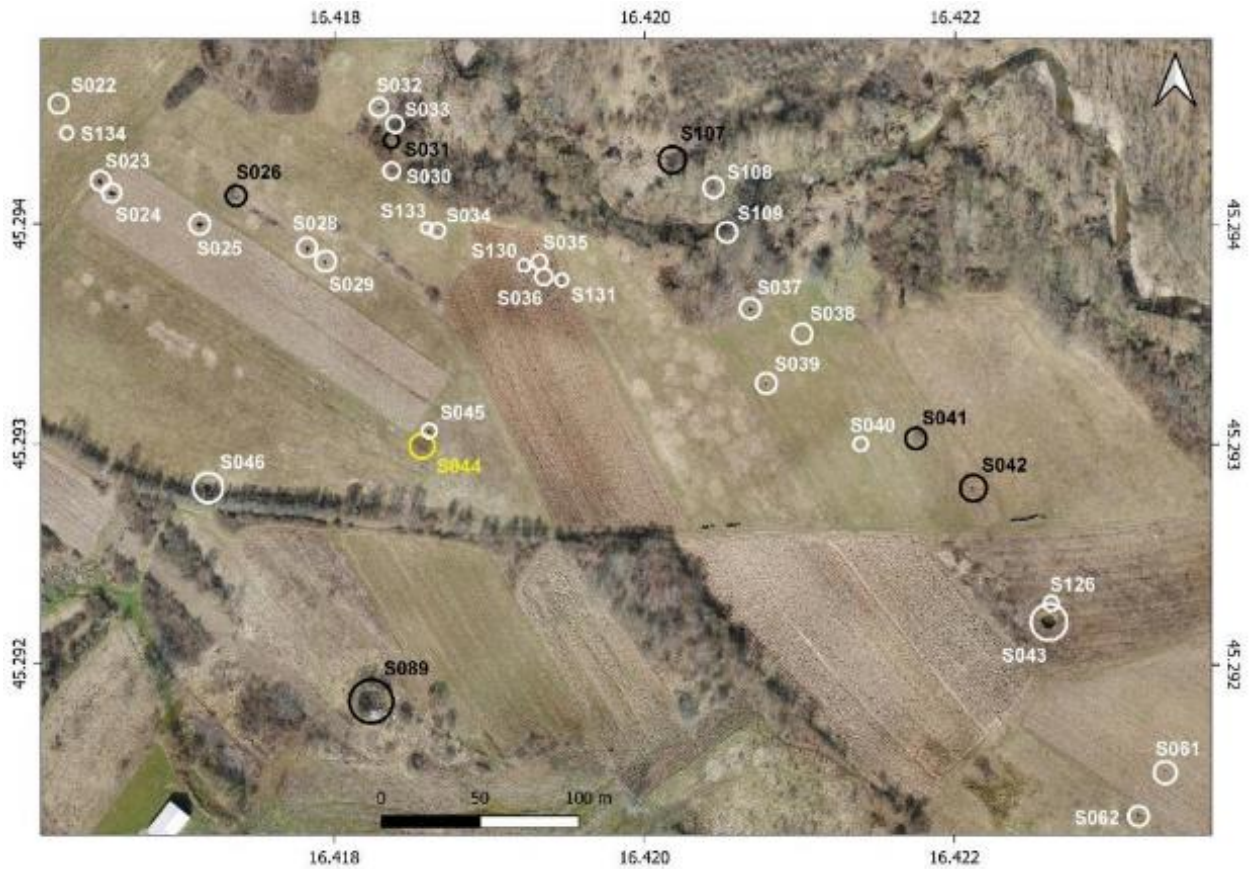


**Figure 6.10** Areal image of sinkholes north of Borojevići village (white – new sinkholes opened after M6.4 earthquake, black – fossil sinkholes opened before the Petrinja earthquake sequence, yellow – potential locations of new cover-collapse sinkholes). Image by Croatian Geological Survey.



**Figure 6.11** Areal image of sinkholes north of Borojevići village (white – new sinkholes opened after M6.4 earthquake, black – fossil sinkholes opened before the Petrinja earthquake sequence, yellow – potential locations of new cover-collapse sinkholes). Image by Croatian Geological Survey.

### 6.3 Hydrogeological characteristics of the Mečenčani and Borojevići area

The Sunja river valley in Mečenčani and Borojevići represents a flat area covered with Quaternary deposits of sand, silt, and clay on average 10 m thick. The material has low permeability but contains a certain amount of water and forms an unconfined aquifer from which it is possible to exploit a smaller amount of water. For this reason, most households use water from shallow dug wells with an average depth of about 8 meters (**Figure 6.12**). The fluctuation of groundwater level in the alluvial aquifer during dry and wet periods is about 2 m. The alluvial aquifer is underlain by a well-permeable confined karst aquifer in which the water pressure during wet periods becomes

subartesian to artesian. The groundwater level fluctuation in the karst aquifer is slightly less than in the alluvial aquifer, except near the Pašino vrelo pumping station, where both aquifers are strongly influenced by the well operation regime, i.e., the amount of pumping rate, which is 38 l/s on average.

These two aquifers are hydraulically connected, and pressure changes in one aquifer cause changes in hydraulic conditions in the other. They form a single aquifer system (**Figure 6.13**). The recharge of the karst aquifer is almost exclusively done through precipitation falling on the nearby hills where the Badenian Lithothamnium limestones and calcarenites crop out. Discharge of the karst aquifer takes place in the spring of Pašino vrelo. Next to the spring couple of deep wells were made, from which water is pumped for the public water supply. The spring of Pašino vrelo is a fossil cover-collapse sinkhole, which at its bottom has a direct connection with the karstified carbonate aquifer. Close to the Pašino vrelo spring, several other springs with a similar origin also play the role of discharge points.

The earthquake of December 29, 2020, occurred during a period of high waters. The water level in the alluvial aquifer was very close to the surface, and in the karst aquifer, artesian conditions prevailed. The piezometric level was about ten centimeters above the surface (**Table 6.1**).



**Figure 6.12** a) Typical shallow well in an alluvial aquifer (depth 8 m, shallow well 3 in **Table 6.1**; 45.28154N, 16.43189E), b) Piezometer in a karst aquifer (depth 150 m; 45.29028N, 16.41797E).

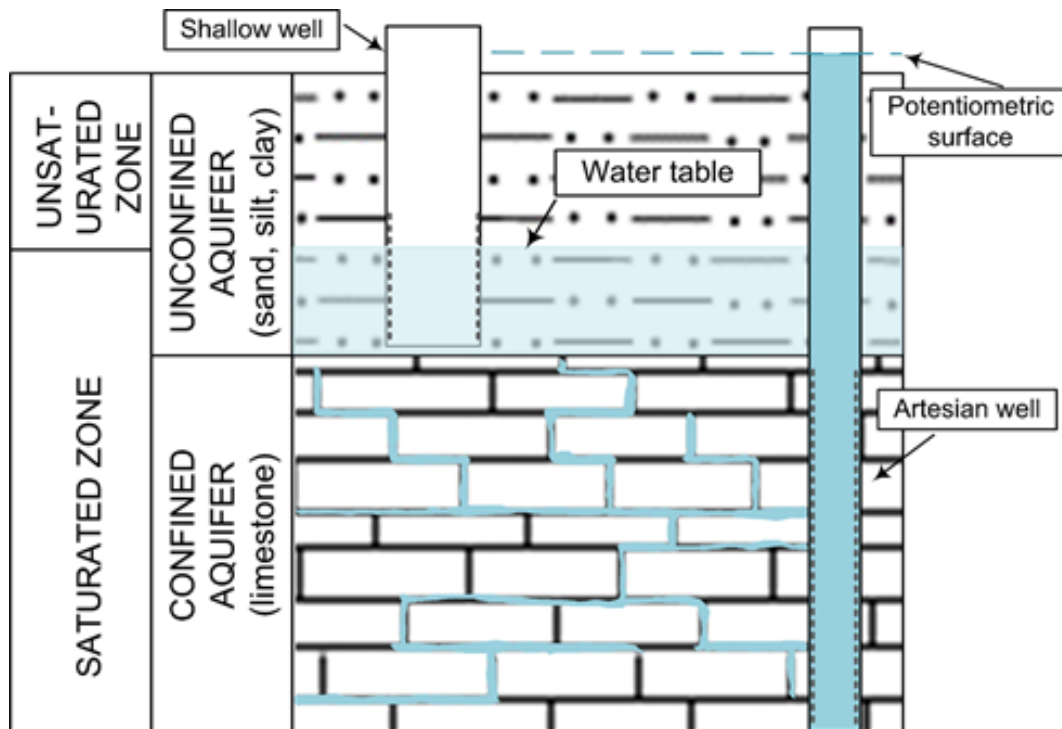


**Figure 6.13** A conceptual model of hydrological condition in aquifer system during the earthquake (Mečenčani, Croatia).

**Table 6.1** Position of three piezometers and three shallow wells located within the study area with their depths, terrain elevation, and groundwater level measured on February 9, 2021. All piezometers, including the shallowest one, penetrated the confined carbonate aquifer. Still, artesian pressure was recorded only in Piezometer 3 since the other two are close to the operating pumping site.

SITE	Latitude N	Longitude E	Depth (m)	Terrain elev. (m a.s.l.)	Water level February 9, 2021 (m a.s.l.)
Piezometer 1	45.29028	16.41797	150.0	183.5	183.59
Piezometer 2	45.28965	16.42395	28.0	178.6	175.65
Piezometer 3	45.28980	16.42342	10.0	178.9	176.08
Shallow well 1	45.29558	16.41006	14.0	191.4	185.98
Shallow well 2	45.28868	16.41876	10.0	185.5	184.63
Shallow well 3	45.28154	16.43189	8.0	183.4	179.95

## 6.4 Geotechnical and Geophysical Investigation Works

GEER team performed geotechnical and geophysical investigations in the zone impacted by numerous sinkhole collapses. Chapter 10 describes details of the extent of complementary investigation works. Local companies performed compound electrical resistivity tomography (ERT), Multichannel Analysis of Surface Waves (MASW), and borehole drilling. At the same time, the geotechnical laboratory at the University of Zagreb, Faculty of Mining, Geology and Petroleum Engineering conducted laboratory index testing of soil samples, and GEER team members analyzed data during March 2021. Two nanometric sensors for measuring horizontal to vertical spectral ratio were brought to the site by the GEER team from Natural Hazards Engineering Research Infrastructure (NHERI) RAPID facility at the University of Washington, Seattle, USA. An overview of complementary investigation works is shown in **Figure 6.14** on a geological map of the area. The GEER team performed 51 nanometric readings of ambient noise, five geotechnical boreholes, two MASW profiles, and one compound electrical resistivity tomography (ERT) profile. **Figure 6.14** shows the global positioning of nanometric and boreholes, while a detailed description of soil properties on specific sites is in Chapter 10.

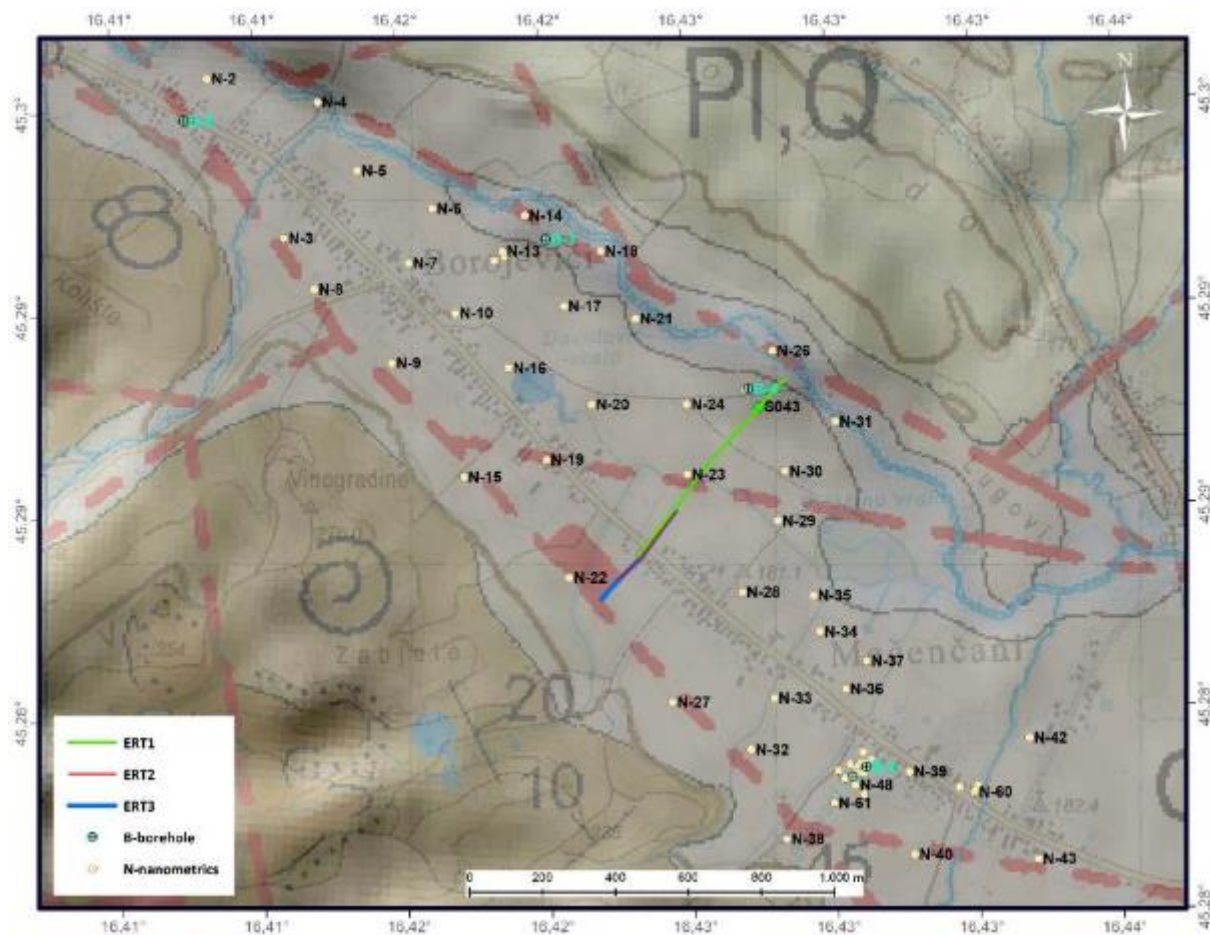


**Figure 6.14** Overview of complementary investigation works on the geologic map (Basic geological map of the Republic of Croatia, Bosanski Novi sheet 1:100,000 – Šikić 2014).

Three electrical resistivity tomography (ERT) profiles were recorded by GEER team members from the Croatian Geological Survey (**Figures 6.14 and 6.15**). The POLARES 2.0 system with Wenner–Schlumberger array recorded all profiles, while interpretation and 2D visualization utilized Res2Dinvx64 software. ERT-1 profile was oriented 43–223°, 630 m long with 10 m distance between electrodes, and crosses perpendicularly from the Sunja river through the area between Mečenčani and Borojevići towards the hill at SW. The electrical resistivity profile detected a couple of predominately fossil sinkholes. To obtain a better resolution, two additional profiles with the same orientation, ERT-2 and ERT-3, were recorded with a distance of 5 m between the electrodes and lengths of 235 and 315 m.

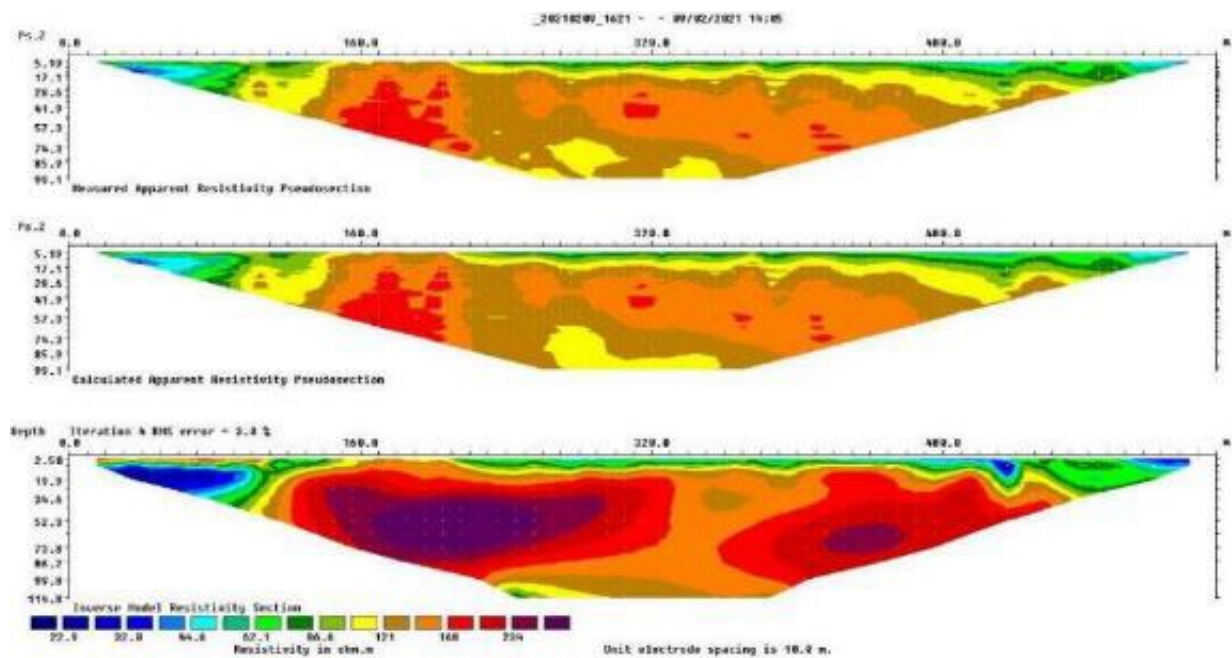


**Figure 6.15** Electrical resistivity tomography (ERT) profiles recorded in the area between Mečenčani and Borojevići (left side of profiles NE, right side SW). For the position of profiles, see Figure 11.

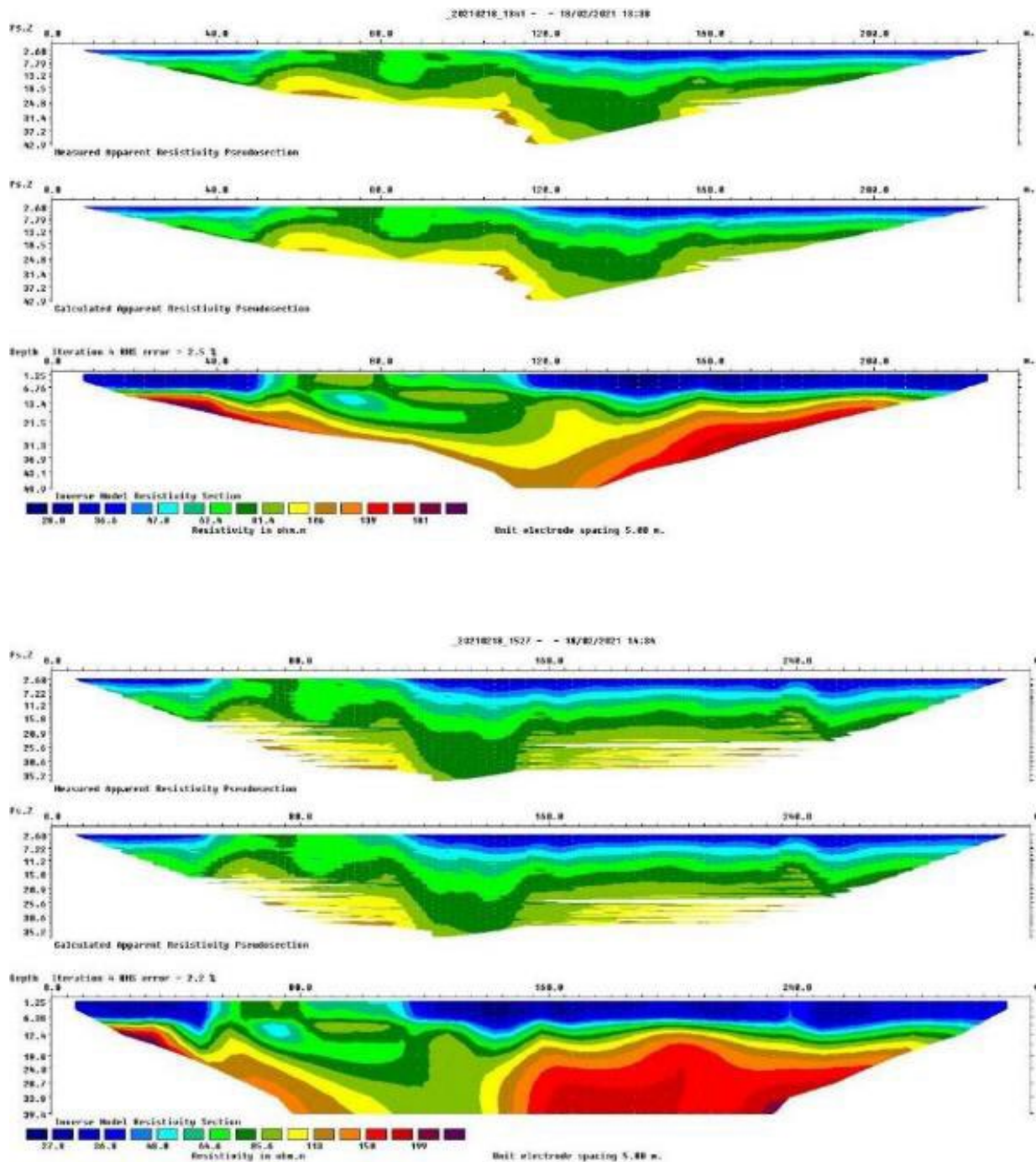


**Figure 6.15 (cont.)** Electrical resistivity tomography (ERT) profiles recorded in the area between Mečenčani and Borojevići (left side of profiles NE, right side SW). For the position of profiles, see Figure 11.

An HVSR analysis is shown in **Figure 6.16** that sorts approximate depths of karstic bedrock with colors. Although the research performed at this stage is a unique process described in Chapter 10, it should be noted that the fundamental resonant frequency  $f_0$  determination was challenging

for some positions. Therefore, the analysis accuracy may be low. However, a few reliable results yielded representative data of the cover layer's relatively low thicknesses, which we detected for positions in proximity and along the Sunja river. We detected karst at deeper levels in the area between Mečenčani and Borojevići, and thicker cover in these locations could explain the absence of new sinkholes. Geotechnical boreholes near Sunja river were performed until shallow depths because the manual drilling equipment had difficulties penetrating through the alluvial deposits of clayey gravel with up to 15 cm grain sizes. The actual depth of the karst was not detected, unlike the B-1 in Borojevići, where the karst depth correlates with the N-1 nanometric result.

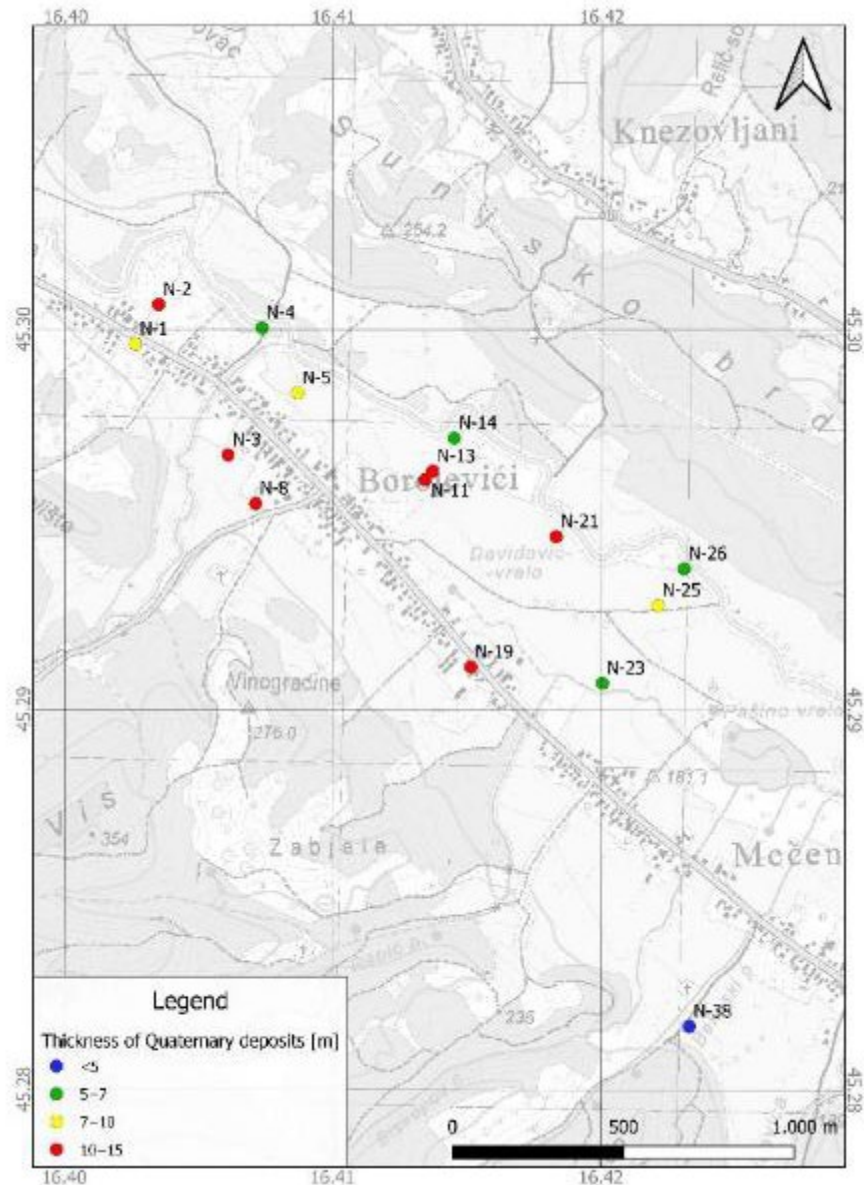


**Figure 6.16** Estimated karst depths from HVSR measurement and analysis on a topographic map.

## 6.5. Detailed Description of Characteristic Sinkholes

This section shows lidar imagery, analysis, and conclusions from geotechnical and geophysical investigation works. The overview presents selected sinkholes, such as the largest sinkhole S001, sinkholes that collapsed in the vicinity of buildings and agricultural facilities, and smaller grouped sinkholes in Borojevići and near the Sunja river as well as fossil sinkholes. A comprehensive database of lidar images of around 60 sinkholes is available as open-source in DesignSafe Data Depot.

### *General Characterization of Sinkhole S001*

The largest sinkhole, S001 (**Figure 6.17**) collapsed in Mečenčani between the January 4, 2021 afternoon and 13:00 h of January 5, more than 30 hours before the main aftershock, which took place at 18:01 on January 6 (M 4.9). The first subtle subsidence of the area was noticed by land-owners on January 4 afternoon. Two major foreshocks on December 28 (M 5.2 and M 4.7) and the main earthquake of December 29, 2020 (M 6.4) preceded a week before the S001 collapse. The surface soil collapsed at once into S001, forming a sinkhole about 15 m in diameter, followed by minor adjustments and collapses of walls, which remained sub-vertical. **Figure 6.18** shows snapshots from the video recorded on January 6, where the walls are collapsing with an unstable, brittle clay block of approximately 2–3 m, and S001 is widening (Vidić, 2021. Available at: <https://www.youtube.com/watch?v=br-ocSaXIDgwww>).



**Figure 6.17** A giant sinkhole (S001) in the Mečenčani. The photograph was taken on March 15, 2021, during lidar imaging (45.283243N, 16.425887E).

GEER team did lidar imaging on March 15 and March 23. The GEER team recorded an MASW profile in the vicinity of S001, two boreholes B-1 and B-2, eight nanometric sensors (N-51 to N-58) were measuring ambient noise for approximately 25–30 minutes positioned closely around S001 and seven nanometric in the vicinity (N-44 to N-49). **Figure 6.19** shows a schematic of data collection and positions of geotechnical and geophysical investigation works. The GEEER team was measuring water levels in geotechnical boreholes during drilling, 3 hours and three days after the drilling. Water depth was also measured in a well on the same compound approximately 5 m away from S001. The water level in S001 was measured on February 15, 2021, as 2.5 m below the ground surface, and it is relatively stable since its opening. The maximum depth of the sinkhole measured from the ground surface to the bottom of the deposited collapsed material using custom-built weight was 11.7 m.



a) The collapse of the edge of a larger unstable clay block.



b) Upper portions of the block are falling.



c) Large block collapse.



d) Material sinks under the water

**Figure 6.18.** S001 brittle wall collapse sequence on January 6, 2021 (45.2833444N, 16.4259639E) (Vidić, 2021. Available atČ <https://www.youtube.com/watch?v=br-ocSaXIDgwww>).

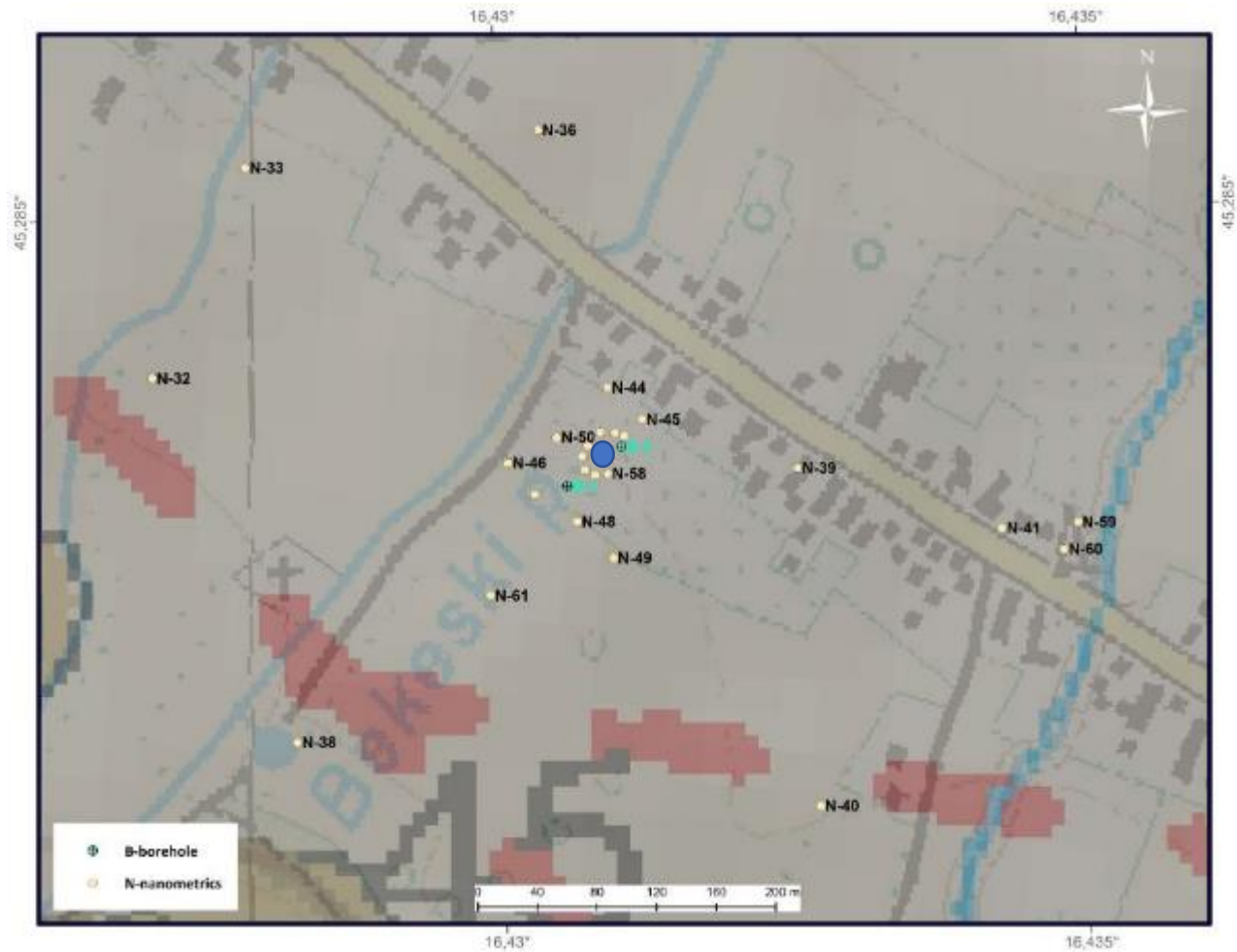


**Figure 6.19** Positions of geotechnical and geophysical investigation works around S001 on the topographic map background.

### ***Morphological and Spatial Characteristics of S001***

S001 is characterized by vertical walls in brown clay, with sparse 30–60 cm thick lenses of round grain gravel. **Figure 6.20** shows a photograph taken by the lidar imaging positions and a sample scan. The bundle links 13 setups with 35 links with the bundled error 8 mm. **Figure 6.21** shows the top view where the longest axis diameter is about 24.55 m, and the largest diameter at the bottom of the scan is 21.865 m (**Figure 6.22**). The water depth is 2.507 m from the upper edge of the sinkhole, as shown in **Figure 6.23**. **Figure 6.24** shows an example of sinkhole volume calculation from terrestrial lidar point cloud data. However, due to the relatively high water level, the GEER team could not obtain information about the sinkhole contours under the water.

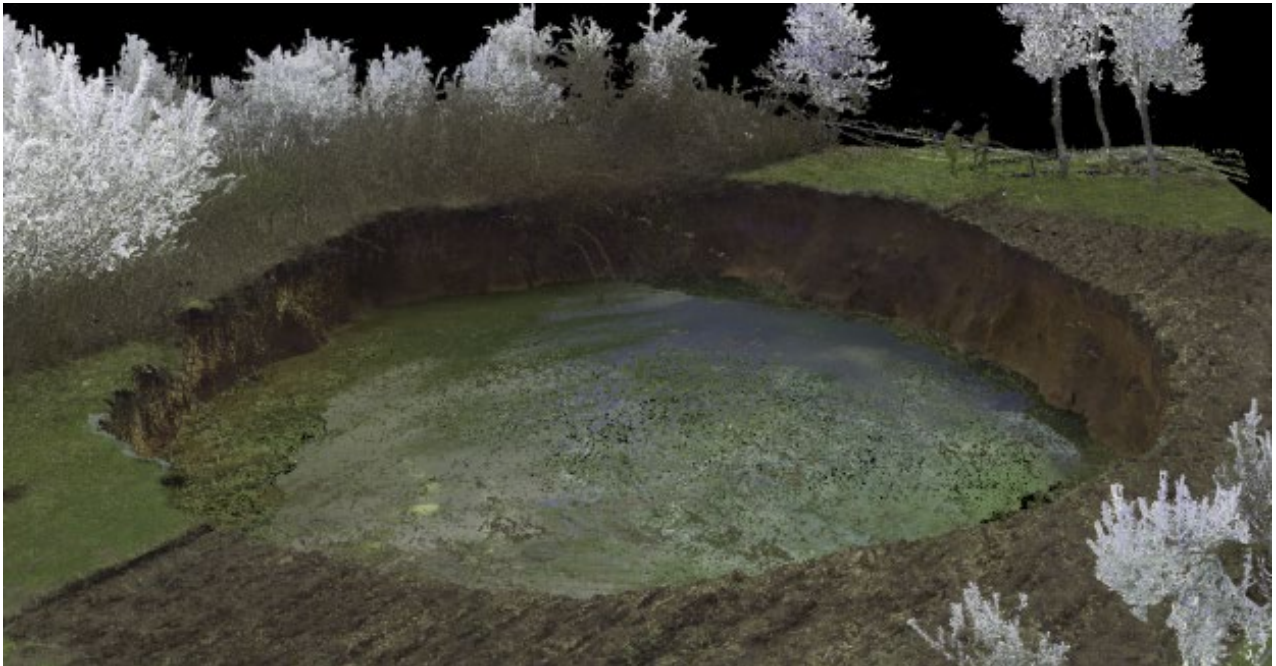
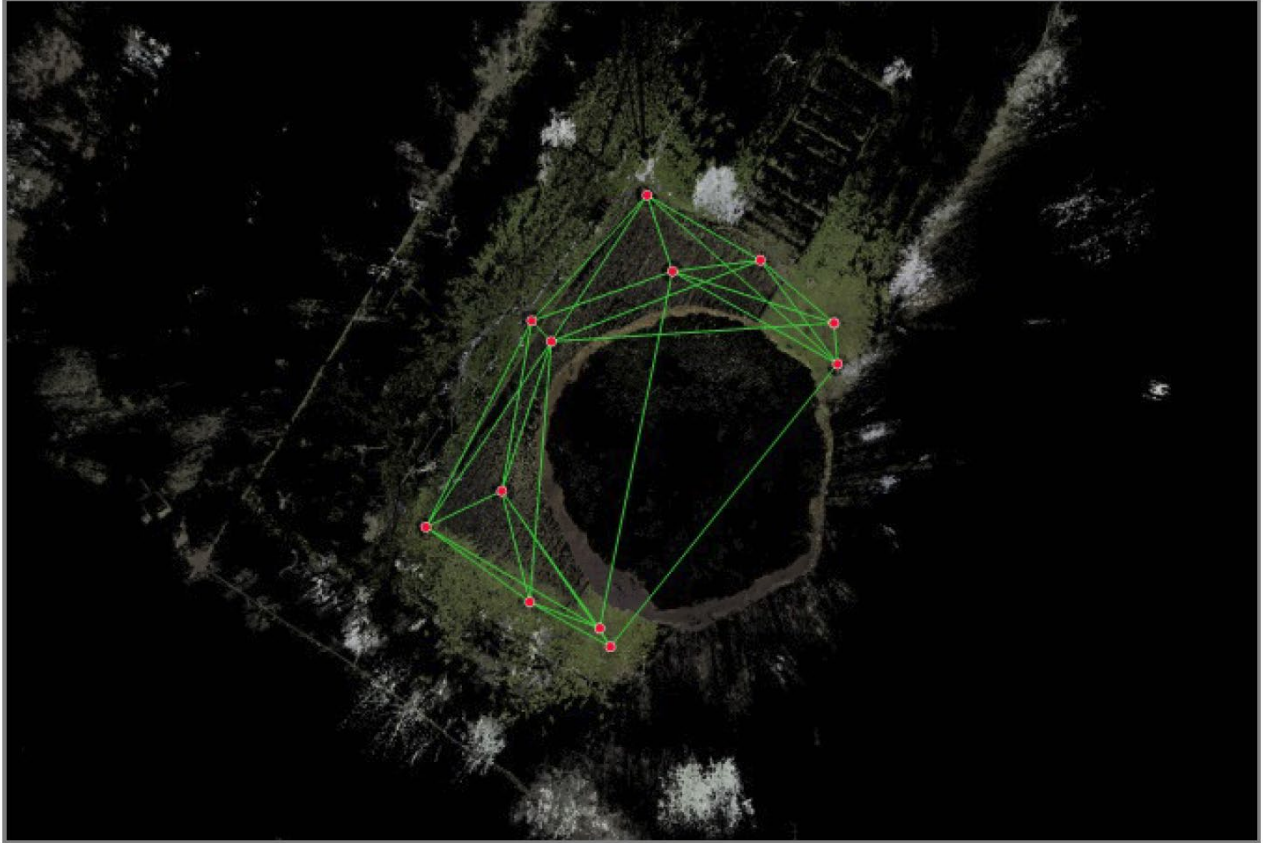


**Figure 6.20** Lidar bundle with 13 setups and 35 links around S001 (45.2833444N, 16.4259639E).

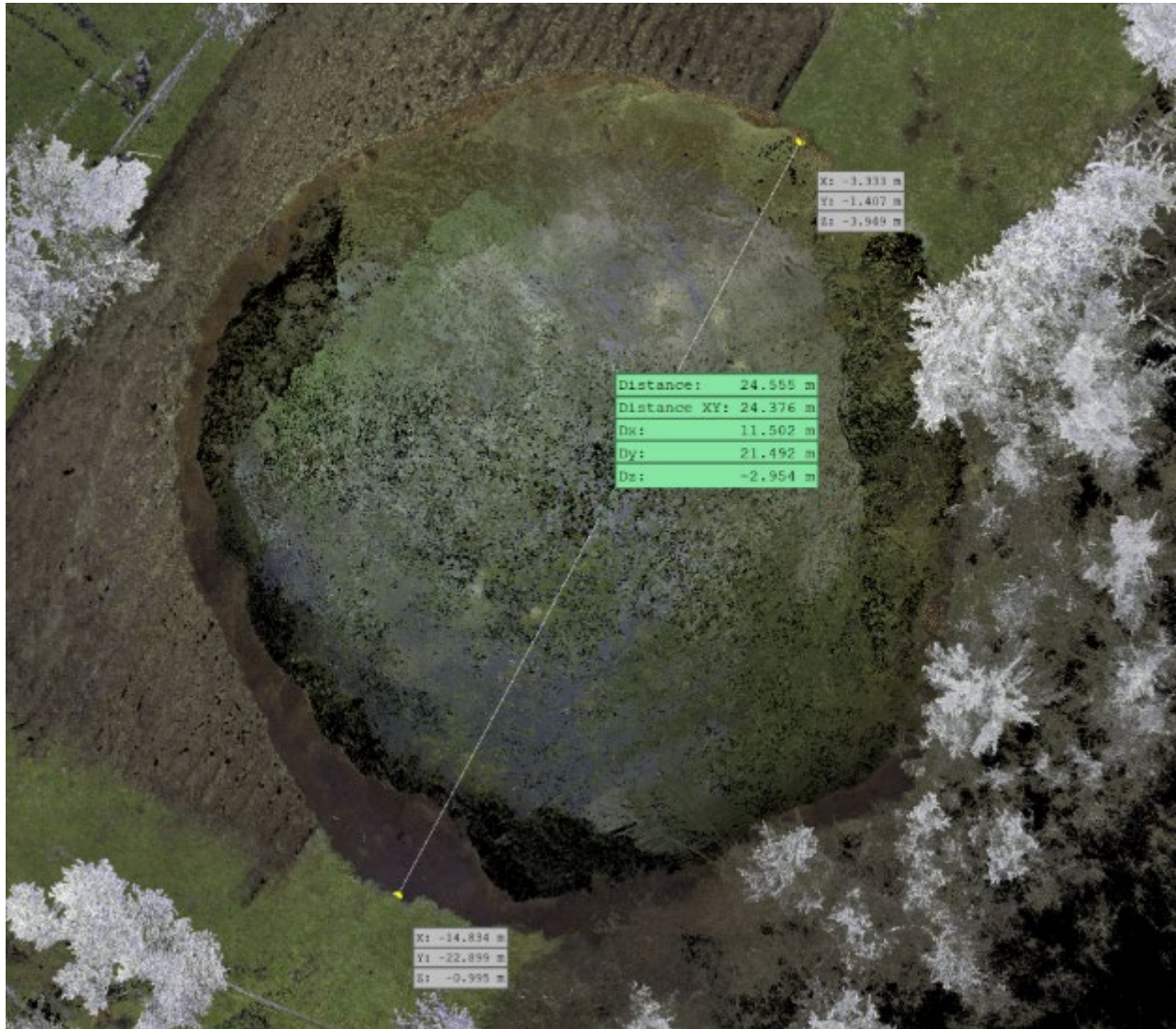
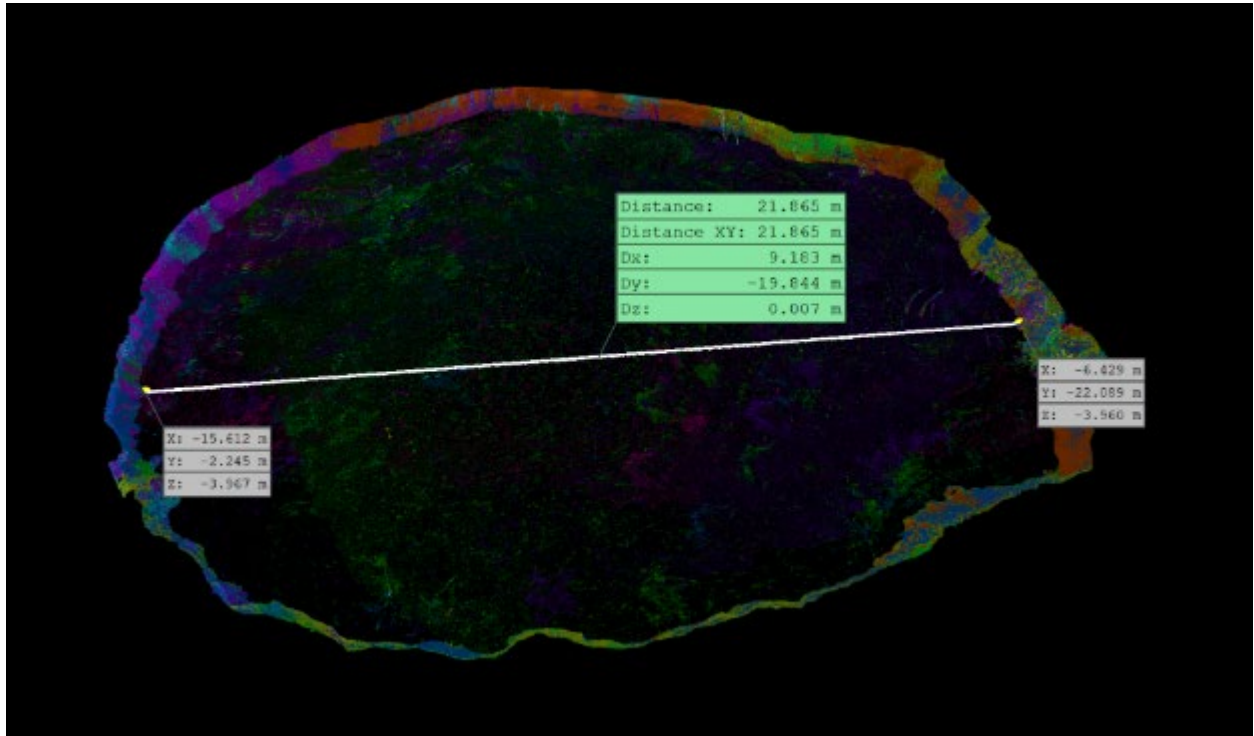


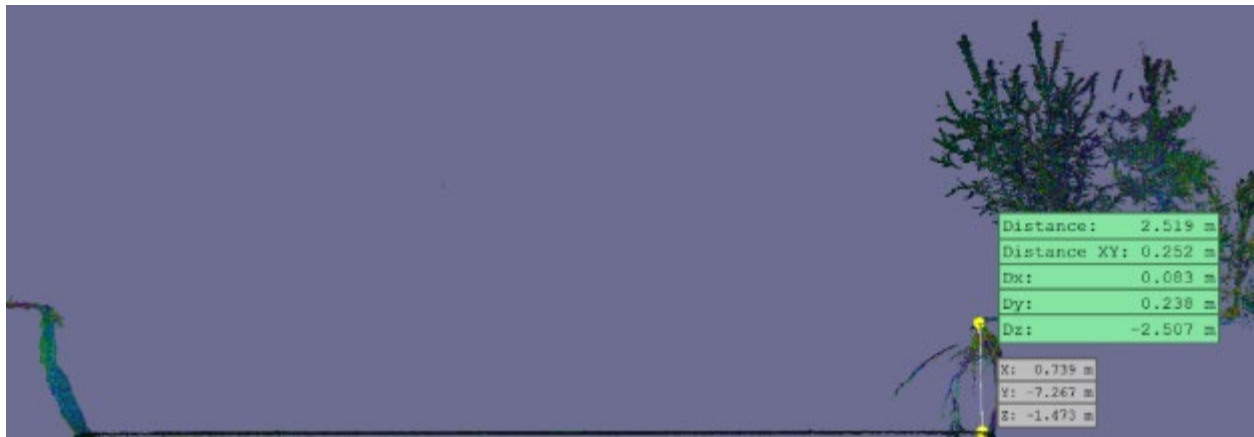
Figure 6.21 Top view diameter of S001 from lidar scan (45.2833444N, 16.4259639E).



**Figure 6.22** Diameter at the lidar scan on the bottom level of S001 (45.2833444N, 16.4259639E).



(a)



(b)

**Figure 6.23** Y-axis cross-section scans with dimensions of S001 (45.2833444N, 16.4259639E).

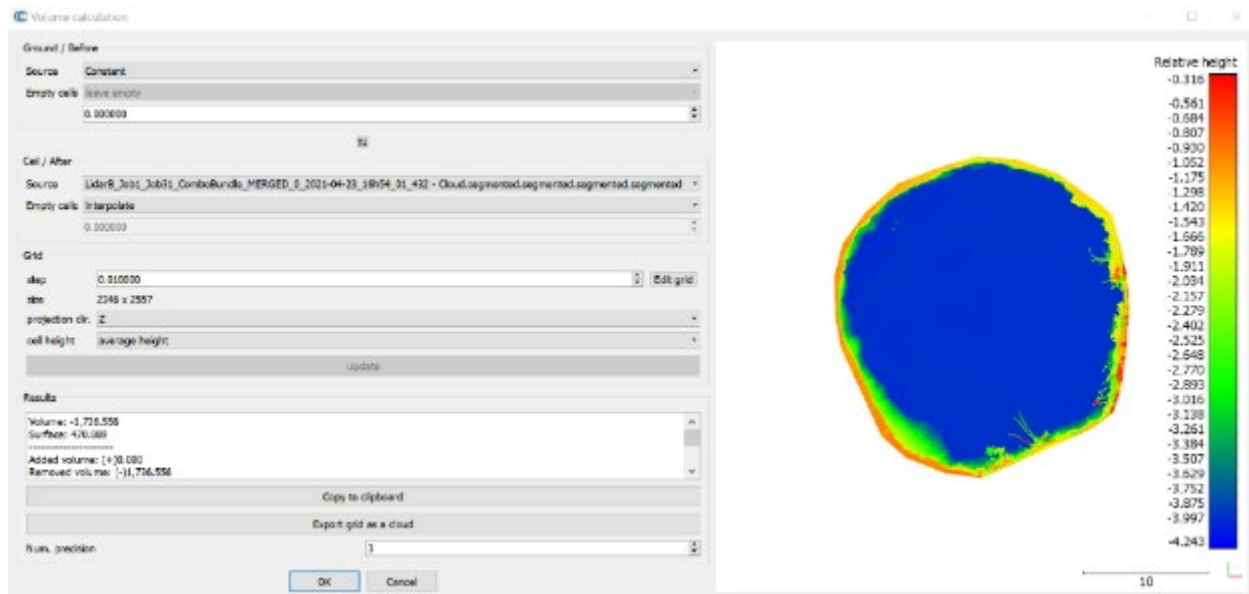


**Figure 6.24** Volume calculations of S001 (45.2833444N, 16.4259639E).

### ***Geotechnical and Geophysical Investigation Results of Soil around S001***

Insight into two geotechnical boreholes reveals that soil consists of 0.5 of fill, 3.5 of sandy lean, and fat clay that is firm to stiff, containing sparse traces of limestone particles up to 20 mm in diameter, with sharp edges (**Figure 6.25**). Limestone particles are distinct and white. Below is stiff to very stiff clay, interlayered by very moist clay with gravel. Boreholes were drilled without heavy machinery and stopped where the equipment could not penetrate stiffer layers at approximately 8,0 m depth. Lower layers are in B-1 gray lean marly clay, with low plasticity and high stiffness. Bedrock or cobbles appeared below 8 m, where also the Standard Penetration Test equipment bounced off without penetration.

Multichannel Analysis of Surface Waves (MASW) has been performed just along the edge of S001. **Figure 6.26** shows a two-dimensional interpretation of the MASW profile near S001, where lower shear wave velocities of 180–220 m/s occur until 5–6 m depth, under which are slightly higher velocities 300–400 m/s between 6 and 10 m. Relatively uniform strata down to 25 m are shown in green and yellow colors, which has heterogeneous 400–500 m/s velocities. It can be concluded that the compact rock layer appears below 25 m, which is geologically characterized as karst. Comparing to MASW profiles, indeed, shear wave velocities increase at that depth. Detailed presentation of investigation works is in Chapter 10.

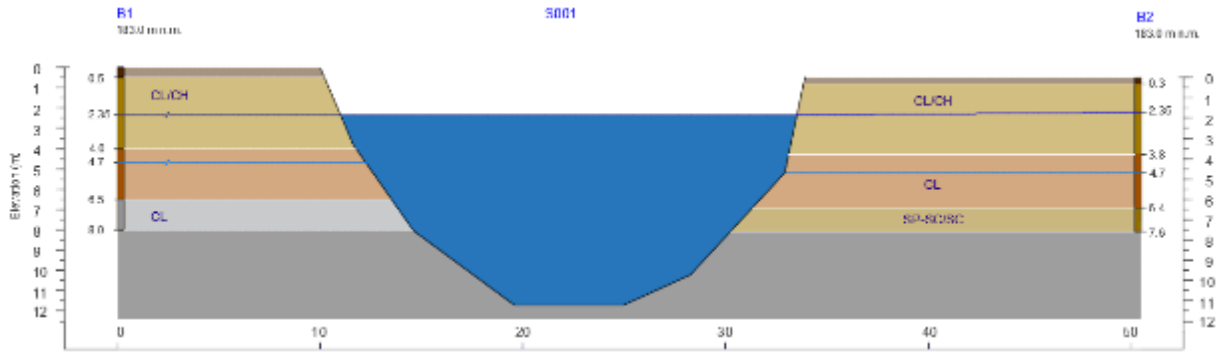


Figure 6.25 Soil profile around S001, dimensions are given in mm (45.2833444N, 16.4259639E).

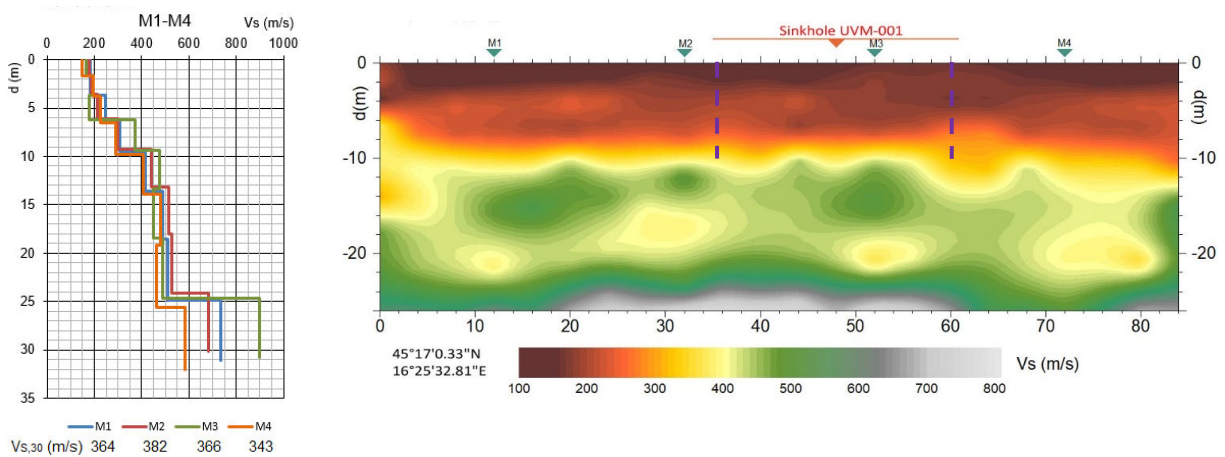


Figure 6.26 MASW profile with a sketch of S001 to the depth of 11.2 m (45.2833444N, 16.4259639E).

Horizontal-to-Vertical Spectral Ratio (HVSr) analysis obtained curves which are not showing a distinct peak to get  $f_0$  frequency. A potential rock stratum was approximately determined using the shear wave velocity obtained from MASW and expression using the quarter-wavelength equation:

$$H = v_{s,avg} / (4 \cdot f_0)$$

where  $H$  is the thickness of the sediment above the bedrock,  $v_{s,avg}$  is the average shear wave velocity over the sediment, and  $f_0$  is the fundamental resonant frequency. **Table 6.2** gives an overview of estimated depths, and **Table 6.3** shows HVSr analysis results for each. The analysis indicates HVSr uncertainties when handling weathered karst mixed with stiff clays and clay mixed with larger granite gravel cobbles that were found in boreholes as lenses within clays at different heights. Granite cobbles were detected in the broader area as well, even sometimes on the ground surface. The density of weathered karst is  $2290 \text{ kg/m}^3$  and  $2062 \text{ kg/m}^3$ , which indicates a significant presence of voids in intact rock. Despite the challenges presented here, HVSr shows two material horizons at 4–5 m north from S001 and 10–12 m depth south from S001, which

correlates with boreholes and MASW data. Additional seven nanometric measurements also indicate clay cover depths from 5.4 m to 9.8 m, where N-50 between S001 and S065 suggests the interface depth at  $H=5.4$  m.

**Table 6.2** Calculated depths of karstic formation around the sinkholes.

Nanometrics Name	Longitude	Latitude	$f_0$	$V_{s,avg}$ (m/s)	$H$ (m)
N-50	45.2834833N	16.4255583E	12	220	4.6
N-51	45.2834861N	16.4261361E	12.4	220	4.4
N-52	45.2835056N	16.4260583E	12.1	220	4.5
N-53	45.2835111N	16.4259306E	5.64	220	9.8
N-54	45.2834333N	16.4258250E			
N-55	45.2833667N	16.4257750E	5.45	220	10.1
N-56	45.2832833N	16.4257944E	4.55	220	12.1
N-57	45.2832528N	16.4258806E	4.96	220	11.1
N-58	45.2832583N	16.4259917E	5	220	11.0

**Table 6.3** HVRS analysis for nanometric surrounding S001.

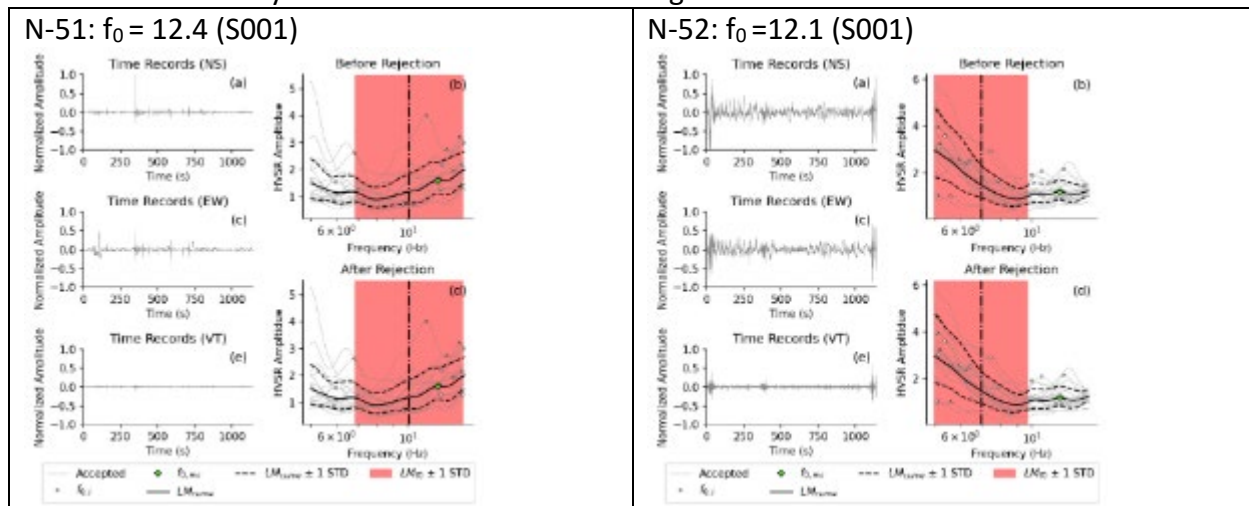
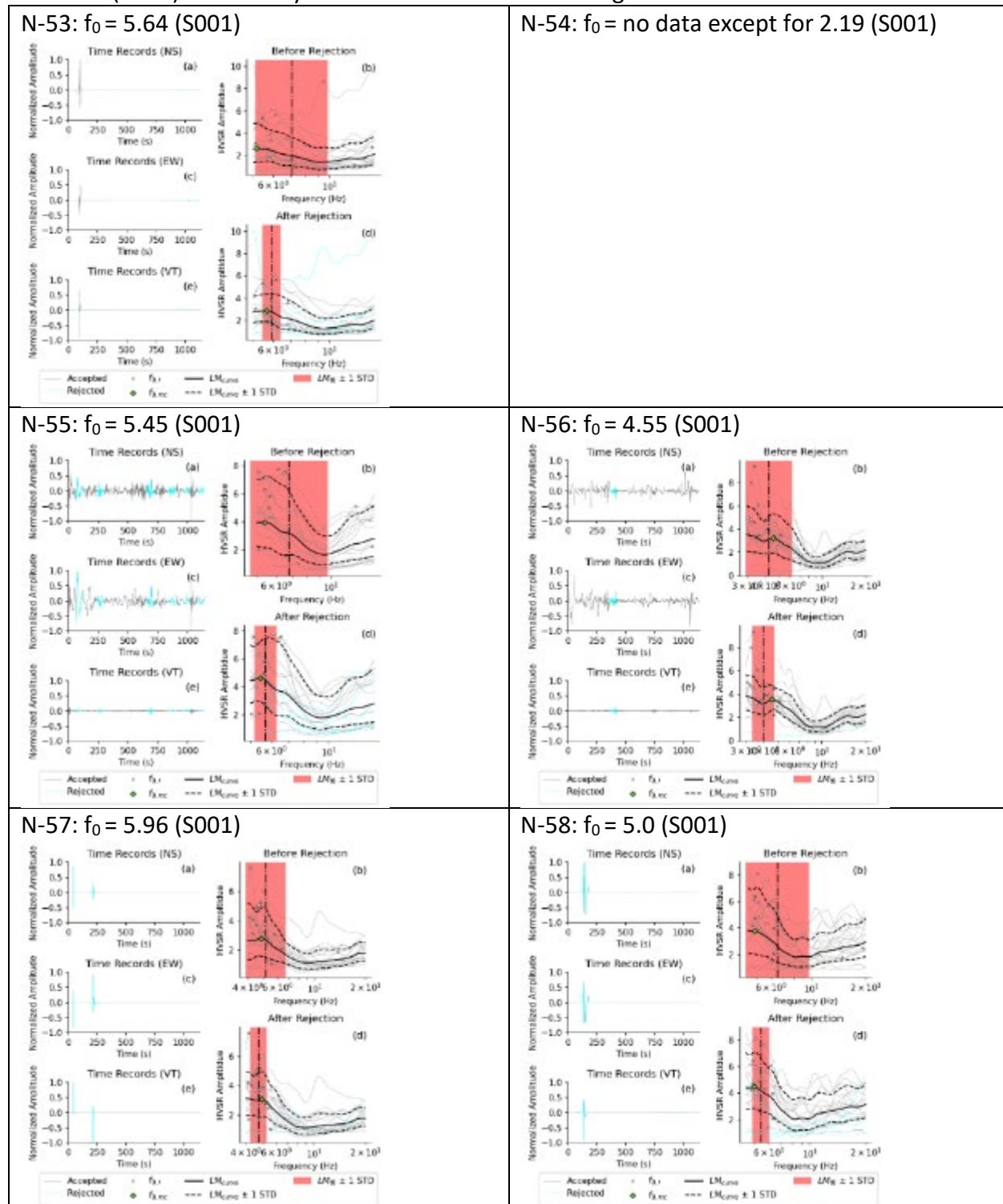


**Table 6.3 (cont.) HVRS analysis for nanometric surrounding S001.**



### **Groundwater Levels near S001**

Detected groundwater levels in boreholes B-1 and B-2 are shown in **Table 6.4**. Groundwater rises from ~-5.0 to ~-2.2 m from the ground surface with different dynamics. Additionally, the well water levels placed ~5 m from S001 were consistent at ~-5.0 m. The groundwater level rise in boreholes may occur due to flow from adjacent saturated soil or artesian pressure in the subsurface karstic formation. Since piezometers are not installed at the site, the groundwater pressure is not measured now.

**Table 6.4** Measured levels of groundwater at different times and locations near S001

<b>Description</b>	<b>G.W.L. (m below ground level)</b>	<b>Date</b>	<b>Time</b>
Private Well	-5	3/23/2021	NPV*
BH B-1	-4.7	3/23/2021	10:30:00 AM (PPV**)
BH B-1	-2.25	3/23/2021	15:30 PM (NPV*)
BH B-1	-1.8	3/26/2021	NPV*
BH B-2	-5.2	3/23/2021	PPV**
BH B-2	-2.4	3/26/2021	NPV*

\*NPV is the groundwater level.

\*\*PPV is the groundwater level first appearance.

We estimated the degree of saturation using phase relationships for samples in B-1 and B-2. The specific gravity measurements were unreliable and yielded too low values in the lab, so we assumed an average value of  $G_s=2.75$  instead. Results indicate unsaturated zone in B-1 at 2.0–2.3 depth at  $S_r=0.82$ , and saturated zone at 4.0–4.3 at  $S_r=1.0$ , 6.0–6.3 at  $S_r=0.96$ . Results relate to the behavior of the groundwater in B-1, which was detected at 4.7 m depth and rose to 2.25 m in three hours. In B-2, unsaturated zone was detected at 1.0–1.3 at  $S_r=0.56$ , 4.0–4.3 at  $S_r=0.6$  and 5.0–5.3 at  $S_r=0.62$ . Groundwater depth was stable at 5.2 m depth during March 23 and did not rise as in B-1 after a few hours, despite the proximity of both boreholes. Three days later, the groundwater indeed rose to 2.4 m below the ground surface in B-2.

### **6.5.6 Examples of Sinkholes Near Buildings**

The GEER reconnaissance team recorded a total of 6 sinkholes that collapsed very close to buildings and greenhouses, including S001. Sinkhole S015 is the second-largest sinkhole in the backyard in Mečenčani, and the family house was tagged as non-livable. Another sinkhole, S014 collapsed under an old brick house. Three sinkholes, S053, S054, and S055, were relatively smaller in diameter but caused distress to a family that has greenhouses. The following section shows each sinkhole and lidar data.

#### **Sinkhole S015**

S015 collapsed on December 29, 2020, with the first subsidence noticed six hours after the main shock, followed by the opening of two cover-collapse structures (each about 1.5 m in diameter

and cca. 1 m deep) within the next three hours and further collapse and formation of united sinkhole until the morning of December 30. **Figure 6.27** shows a lidar bundle scan near a house, where **Figures 6.28** and **6.29** show measurements from point cloud data.



**Figure 6.27** The lidar scan of S015 (45.282859N, 16.429841E).



Figure 6.28 Top and bottom diameters from the lidar scan of S015 (45.282859N, 16.429841E).

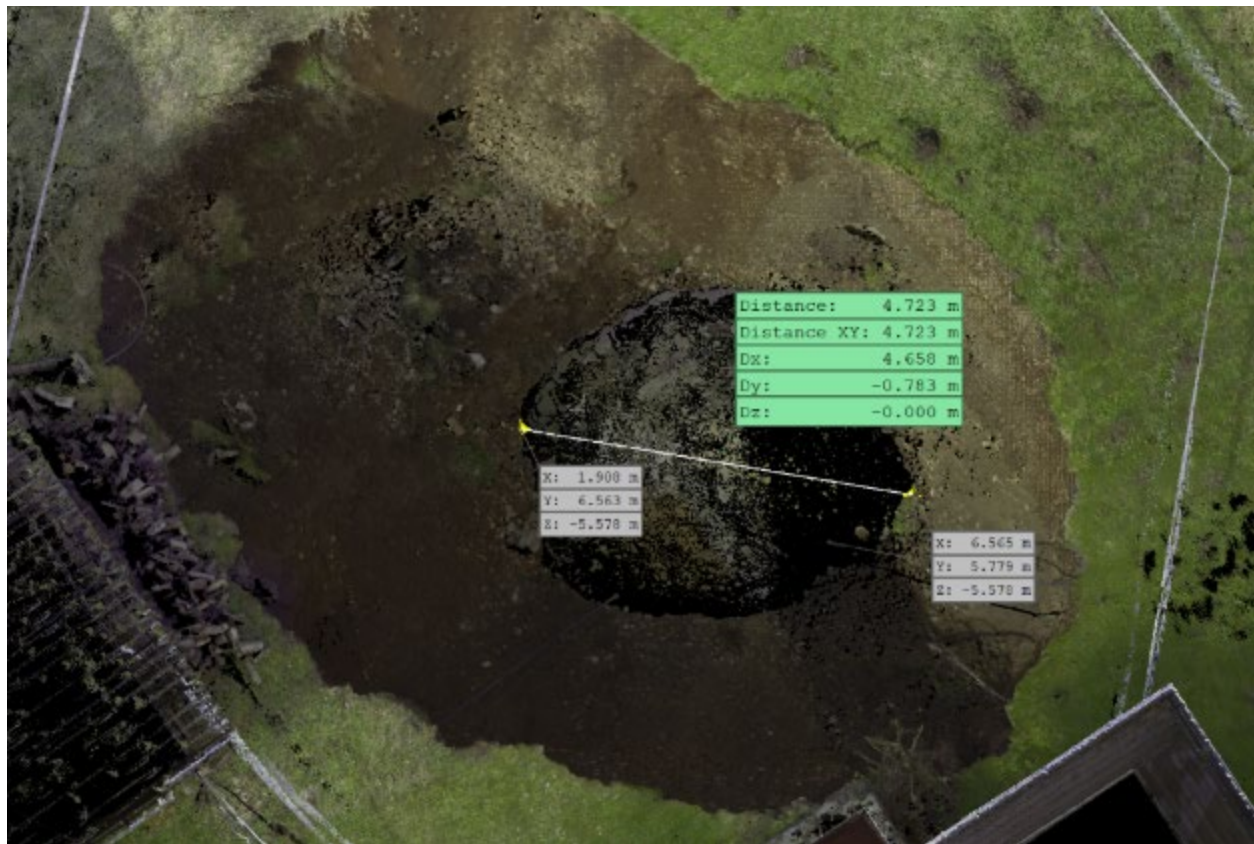
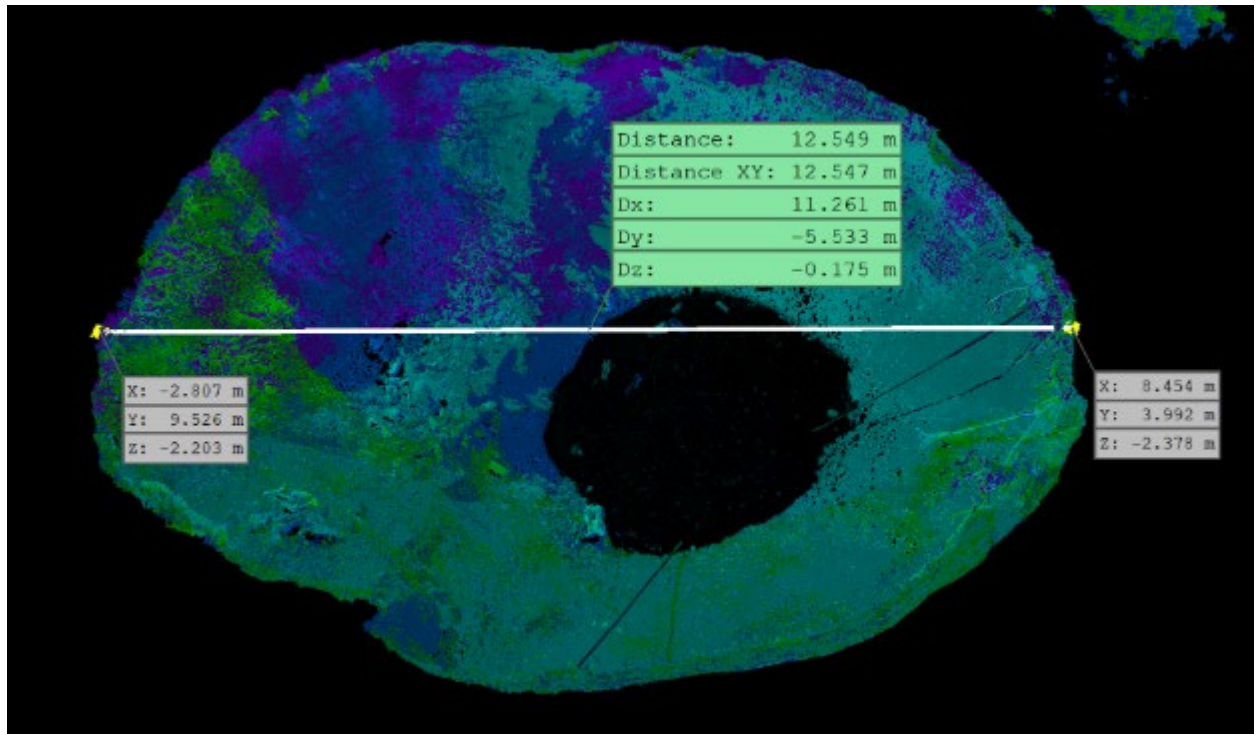
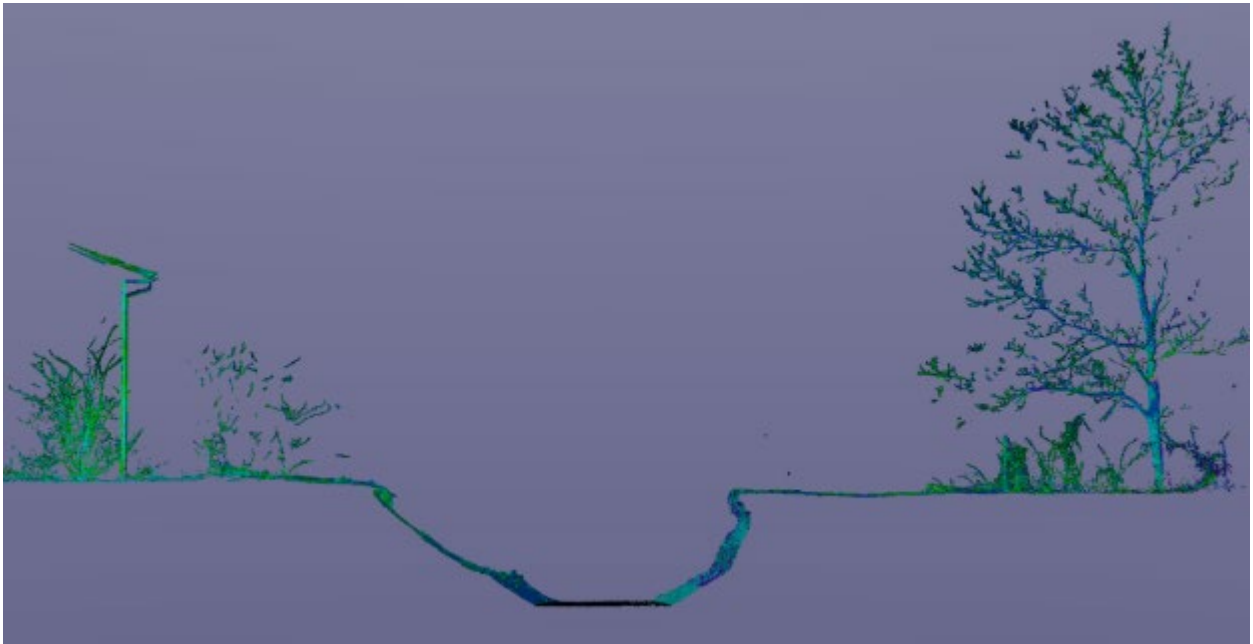
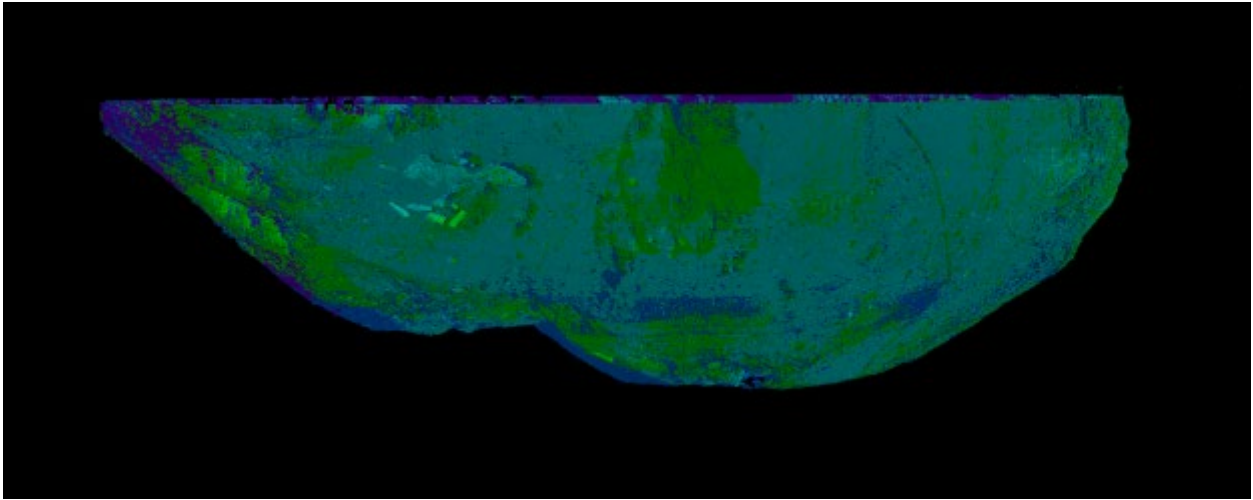
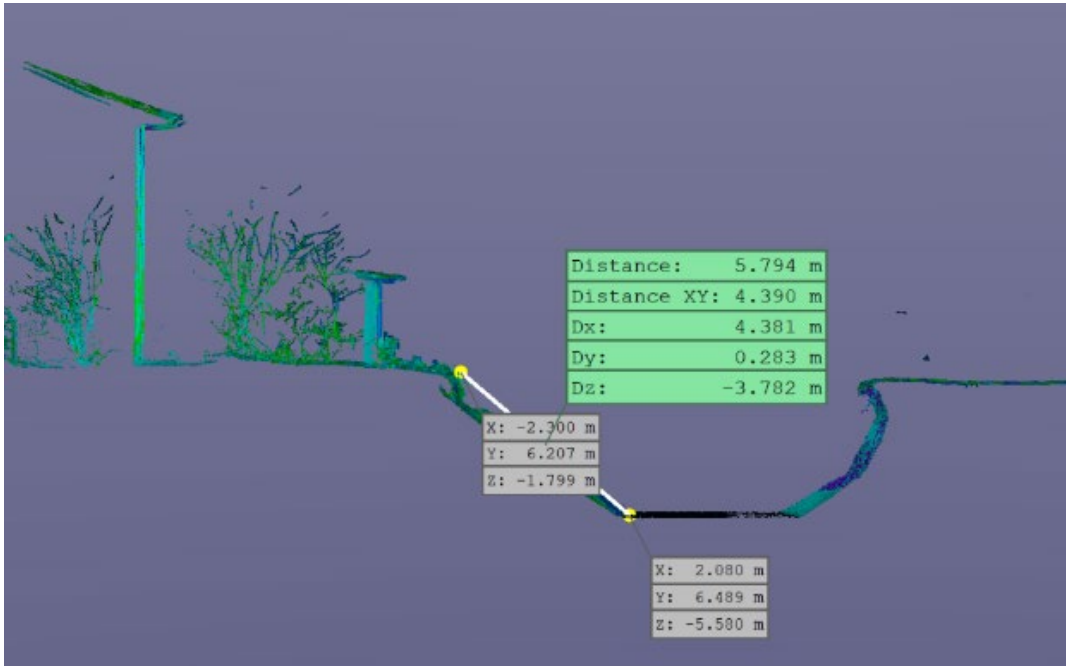


Figure 6.28 (cont.) Top and bottom diameters from the lidar scan of S015 (45.282859N, 16.429841E).



**Figure 6.29** Below surface cross-sections from the lidar scan of S015 (45.282859N, 16.429841E).



**Figure 6.29 (cont.)** Below surface cross-sections from the lidar scan of S015 (45.282859N, 16.429841E).

### ***Sinkhole S014***

Sinkhole S014 collapsed on December 31, 2020, near a brick wall family house, as shown in **Figures 6.30** and **6.31**, and is full of water. S014 caused floor slab and house walls failure, whose materials then fell into the sinkhole.



**Figure 6.30** Street view of the house and S014 position (45.282822N, 16.429389E).



**Figure 6.31** S014 images (45.282822N, 16.429389E).

***Sinkholes S053, S054 and S055***

Sinkholes S053, S054, and S055 have a relatively small diameter, as shown in **Figures 6.32 to 6.38**. Three sinkholes collapsed within an agricultural family compound in Mečenčani. S053 was just next to the family house wall, as shown in **Figure 6.32**. S054 and S055 collapsed near greenhouses.



**Figure 6.32** S053 bundle image (45.281270N, 16.431618E).

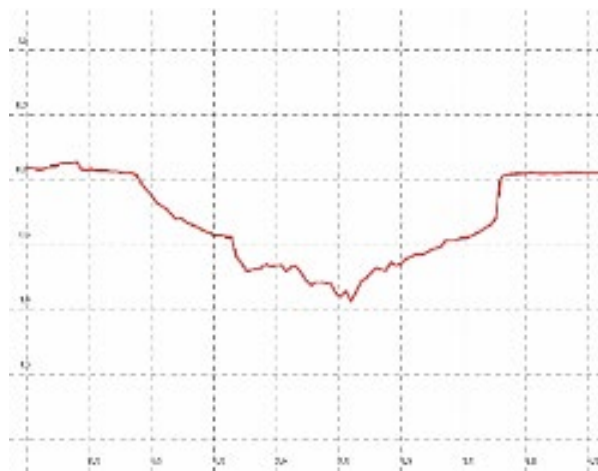
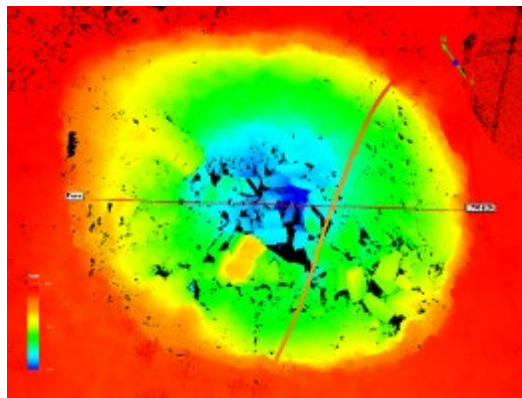


**Figure 6.33** S053 Surface level measurement and cross-sectional profile (45.281270N, 16.431618E).

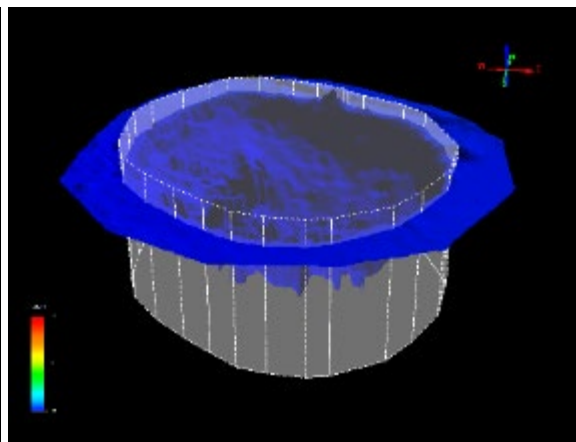
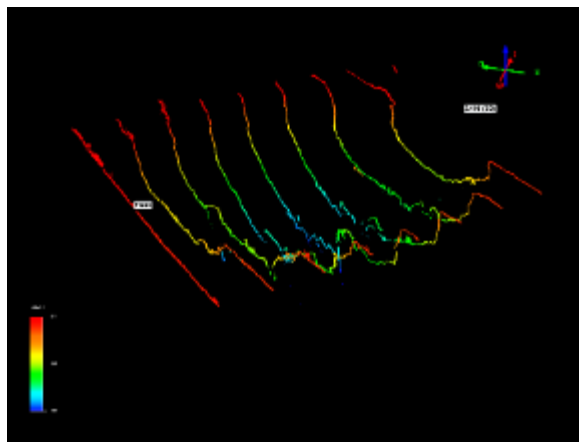


**Figure 6.34** S053 Cross sections and volume estimate  $V=2.98 \text{ m}^3$  (45.281270N, 16.431618E).



Figure 6.35 S054 lidar scan bundle view (45.280665N, 16.431996E).

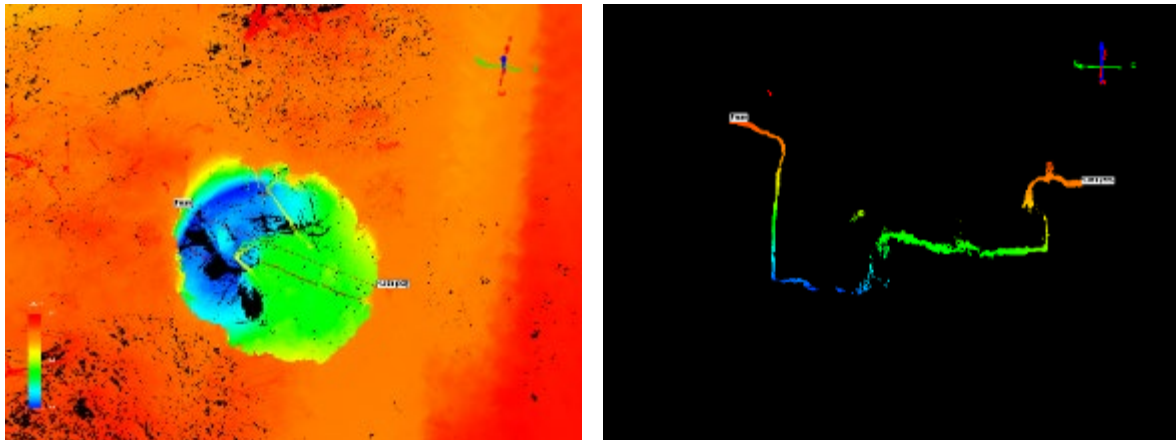
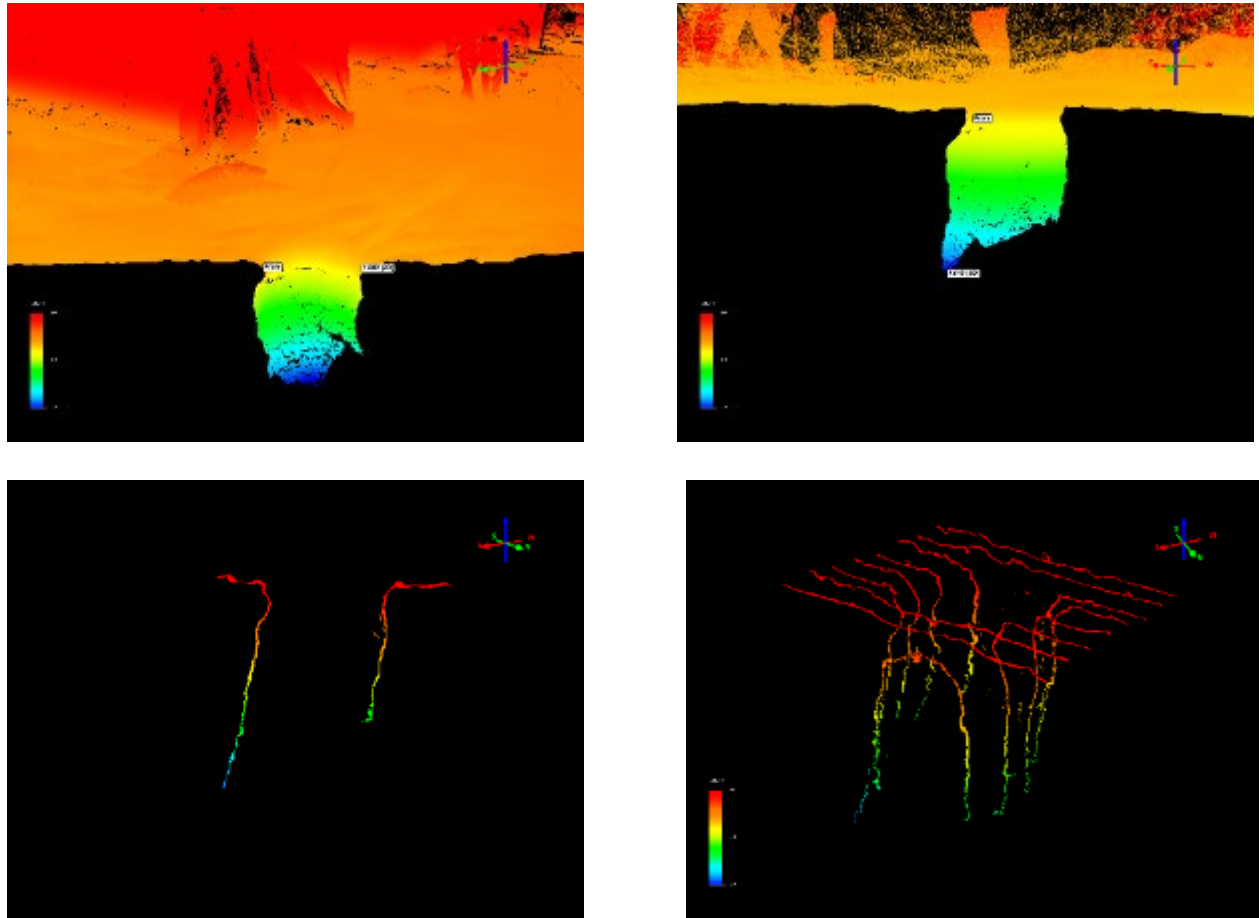


Figure 6.36 S054 plan view and cross section (45.280665N, 16.431996E).



Figure 6.37 S055 lidar scan bundle view (45.280618N, 16.431644E).



**Figure 6.38** S055 cross sections (45.280618N, 16.431644E).

### ***Sinkholes in Borojevići Area***

Numerous sinkholes collapsed in Borojevići, where many are near and along the Sunja river. Sinkholes in this particular area are generally shallower and have a smaller diameter. **Figures 6.39** to **6.45** show a few typical examples of lidar scans and measurements. It was possible to bundle scans of two or three sinkholes into one in several locations, which provided a good idea about the qualitative spatial variability of sinkhole characteristics. Sinkholes were either similar or very different next to each other. In some locations, new sinkholes opened near fossil sinkholes. Such variability depicts the heterogeneity and unpredictability of underlying karstic formations in these locations.

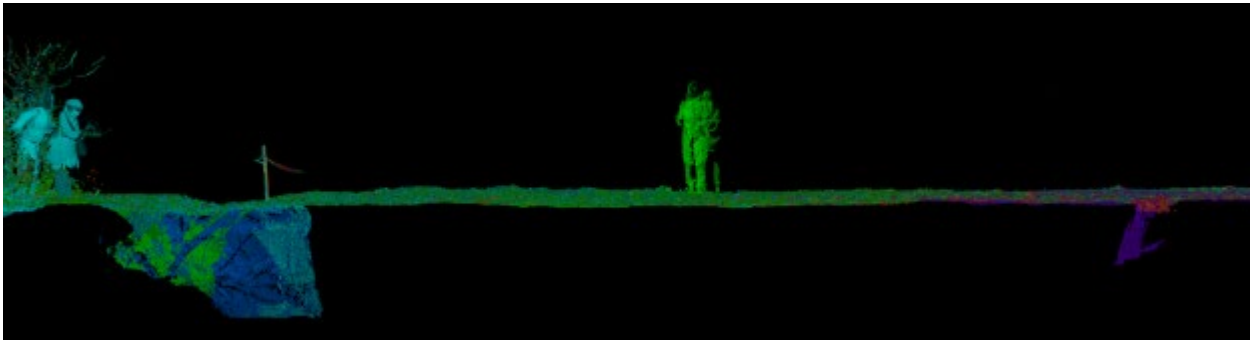


**Figure 6.39** Cross-sections of the lidar bundle with two adjacent sinkholes, S007 (45.296599N, 16.415005E) and S008 (45.296589N, 16.415085E).



**Figure 6.40** Cross-section of the lidar bundle with two adjacent sinkholes, S023 (45.294192N, 16.416487E) and S024 (45.294139N, 16.416563E).

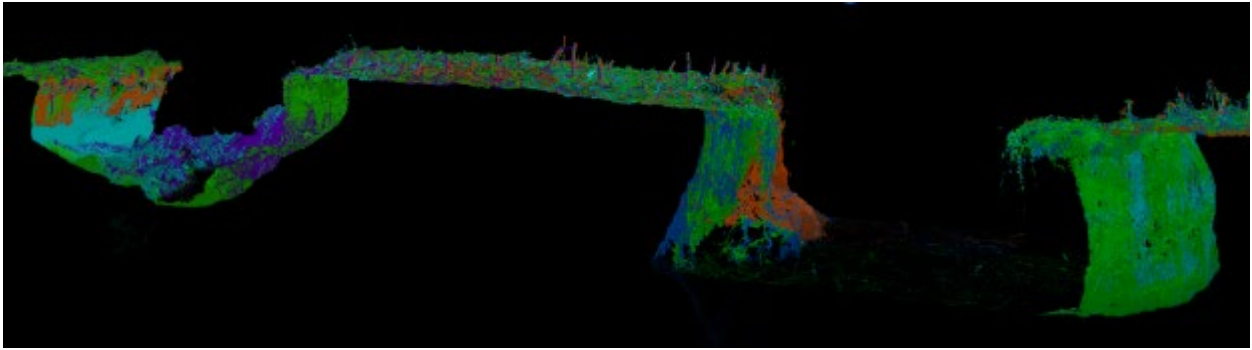


**Figure 6.41** Cross-section of the lidar bundle with two adjacent sinkholes, S023 (45.294192N, 16.416487E) and S024 (45.294139N, 16.416563E).

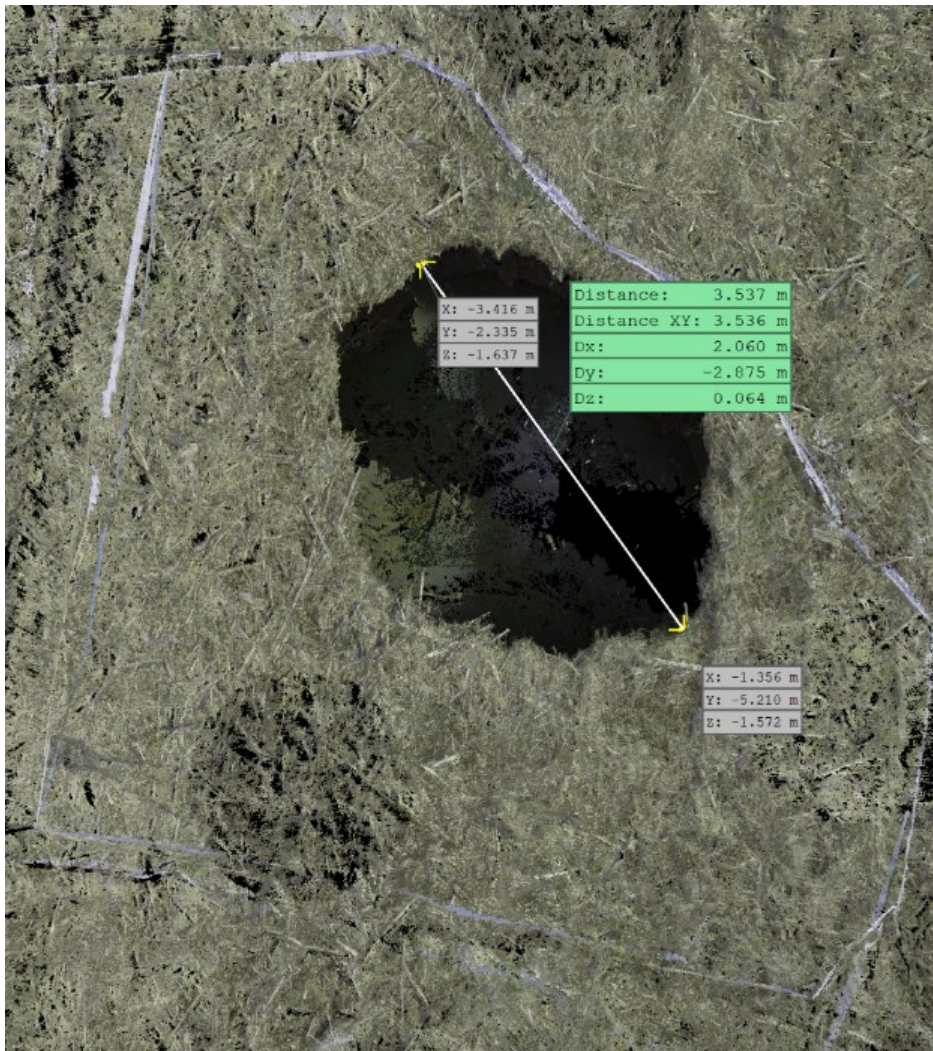


**Figure 6.42** The lidar scan of the sinkhole S025 (45.293997N, 16.417133E).

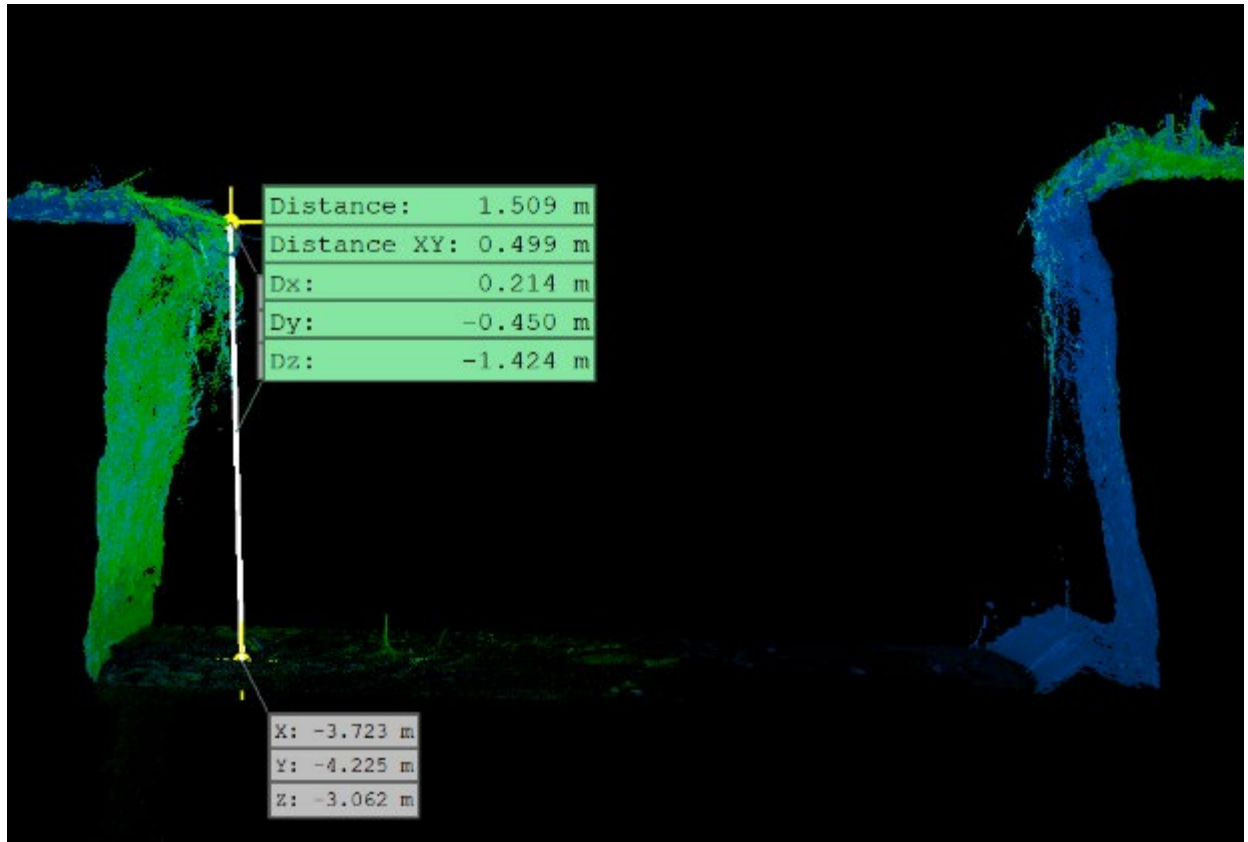


**Figure 6.43** The lidar scan with the cross-section of the sinkhole S025 (45.293997N, 16.417133E).



**Figure 6.44** The lidar plan view of the sinkhole S043 (45.292195N, 16.422607E).



**Figure 6.45** The lidar scan with the cross-section of the sinkhole S043 (45.292195N, 16.422607E).

## 6.6. Concluding Remarks and Future Work

The GEER reconnaissance team recorded a total of 139 sinkholes surrounding Borojevići and Mečenčani. Although naturally prone to the formation of cover-collapse sinkholes, the area exhibited unusual activity during the Petrinja M6.4 earthquake in December 2020 and aftershocks. The collapsed activity ceased approximately three months after the main shock but is expected to continue in the future with much lower frequency. None of the sinkholes, to our knowledge, synchronously opened at the time of an earthquake, and the time-lag of collapses of several hours or days following the major earthquakes is typical for this site. The area of approximately 4 km<sup>2</sup> is in the alluvial valley between karstic hillslopes and the Sunja river. Repeatability and regularity of cover-collapse sinkholes appearance exist to some extent. For example, relatively smaller, shallower, and closer to each other are sinkholes north of Borojevići and closer to Sunja. More sparsely spatially located, deeper and larger sinkholes collapsed around Mečenčani. Sinkholes are characterized with a few specific features found in almost all cases: vertical or even over hanged sidewalls, and collapsed materials are clays and clayey gravels, which are most likely not overconsolidated, but phase relationship-based calculations using geotechnical indices of samples near S001 sinkhole indicate unsaturated zone. Therefore, we conclude that soil failure is a brittle failure. What remains unknown is the mechanism of collapse, the undefined role of time and seismic load, as well as hydrology and seismicity-related pore pressure fluctuations as possible triggers.

Finally, to put the sinkhole's collapse unusual coseismic activity in context, the GEER virtual team performed a focused literature review on sinkhole occurrence related to earthquakes, given as follows. The 2012 Varzeghan–Ahar earthquake in Iran provided an example of sinkholes opening in response to earthquakes. Two sinkholes were recorded, the first on a riverbed with a diameter of approximately 2 m. The other about 10 m in diameter, but it was noted that cracks developed nearly 15 m from the site. As written in the paper by Memarian and Mahdaviifar (2012), “*the area is underlain by a wide variety of sedimentary and volcanic rocks and unconsolidated sedimentary deposits*”, diverse in their composition and degree of consolidation, and among which alluvium has been identified. Agreeably, Singh et al. (1997) concluded that “*earthquakes [...] increase the frequency of the occurrence of sinkholes*”. By explaining the increase of pore pressure during the rainy season, Singh et al. are laying the groundwork to understand why there would be 15–20 reported sinkholes every year in the Tohoku district of Japan between 1974 and 1987, “except in 1978 when an earthquake of 7.4 magnitude caused 219 sinkholes”. Caramanna et al. (2008) have found that in Southern Italy, “*another group of collapses in plain areas is characterized by thick alluvial or pyroclastic cover over deep-buried bedrock with an upward migration of the phenomenon*,” finding the commonality of alluvium near the sinkhole site again. Between the Molise, Basilicata, and Calabria regions of Italy, Caramanna et al. (2008) report that due to soil liquefaction, sinkholes are often isolated and collapse as quickly as 24 hours after a high magnitude earthquake, but rarely beyond 30 days.

In contrast to the previous reports of sinkholes opening after earthquake activity, Chiaro et al. (2015) have studied sinkhole formation since 2013, pointing out earthquakes as a factor that may increase and more severe sinkhole development. They specifically cite the Gorkha earthquake of

2015, during which “muddy water” was observed near the event site. Though they did not observe any sinkhole formation because of this earthquake, Chiaro et al. (2015) warned that sinkholes should be anticipated in the future since the water build-up betrays the erosion occurring in the subsoil. These articles clarify that earthquakes can cause sinkhole formation, but certain conditions (soil composition, erosion, pore pressure, water presence) significantly increase the likelihood of sinkhole development.

## References

- Caramanna, Ciotoli G. and Nisio S. (2008) *A review of natural sinkhole phenomena in Italian plain areas*. *Natural Hazards*, (45), p145–172. Available at: DOI: <https://doi.org/10.1007/s11069-007-9165-7>. (Accessed: 8 May 2021)
- Chiaro, G., Kiyota, T., Pokhrel, M. R., Goda, K., Katagiri, T. Sharma, K. (2015). *Reconnaissance report on geotechnical and structural damage caused by the 2015 Gorkha Earthquake, Nepal*. *Soils and Foundations*, 55(5), p.1030-1043. Available at: DOI: <https://doi.org/10.1016/j.sandf.2015.09.006>
- Croatian Seismologic Survey (2021). *Preliminary results of the Petrinja earthquake series between December 28 2020 and January 28, 2021*. In *Croatian: Preliminarni rezultati serije potresa kod Petrinje od 28. prosinca 2020 do 28. siječnja 2021*. University of Zagreb, Faculty of Science, Department of Geophysics. [Online]. Available at: [http://www.pmf.unizg.hr/geof/seizmoloska\\_sluzba/mjesec\\_dana\\_od\\_glavnog\\_petrinjskog\\_potresa#](http://www.pmf.unizg.hr/geof/seizmoloska_sluzba/mjesec_dana_od_glavnog_petrinjskog_potresa#) (Accessed: 8 May 2021)
- Gutiérrez F. and Cooper, A.H. (2013). *Surface morphology of gypsum karst*. In: Shroder, J. *Treatise on Geomorphology*. *Karst Geomorphology* (6), p425–437. Available at: <http://www.speleogenesis.info/directory/karstbase/publication.php?id=13244>. (Accessed: 8 May 2021)
- Memarian P. and MahdaviFar M. (2012). *Distribution and characteristics of landslides induced by the Varzeghan-Ahar earthquake doublet (Mw=6.4 and Mw=6.3) in 2012 in Azerbaijan Sharghi, northwest of Iran*. In: *Proceedings of the IPL Symposium*. Kyoto, Japan 20-23 November 2012. International Consortium of Landslides.
- Singh, K. B. and Dhar, B. B. (1997). *Sinkhole subsidence due to mining*. *Geotechnical and Geological Engineering* (15) p327-341
- Šikić, K. (2014). *Osnovna geološka karta SFRJ 1:100.000, List Bosanski Novi L33-105*. – Fond stručne dokumentacije Instituta za geološka istraživanja, Zagreb. (manuskript) Geologic map available on request at <https://www.hgi-cgs.hr/osnovna-geoloska-karta-republike-hrvatske-1100-000/>. (Accessed: 8 March 2021)
- Vidić M. (2021). *Look how a whole is widening in Mečenčani! Suffusion and karstification of limestone*. In *Croatian: Pogledajte kako se širi rupa u Mečenčanima! Sufozija i okršavanje vapnenačke stijene* [Online video] 9 January 2001. Dnevno.hr. Available at: <https://www.youtube.com/watch?v=br-ocSaXIDg> (Accessed: 15 April 2021)

## 7 Liquefaction and Related Building Damage (Sonja Zlatović, Katerina Ziotopoulou, Jack Montgomery, Zorana Mijic, Verica Gjetvaj)

The December 29, 2020, Petrinja earthquake caused widespread liquefaction with extensive surface manifestations. Most of the surface manifestations of liquefaction were observed in the predominantly flat valleys surrounding the Kupa and Sava rivers and their tributaries. These locations were close to the epicenters of the main shock and aftershocks (**Figure 7.1**). Both the Kupa and Sava rivers have been meandering, producing alluvial deposits (**Figure 7.1**) with up to 50-m depths, primarily layers of soft clay, silt, and sand. Liquefaction effects were identified in many streets in Petrinja, Glina, Stari Brod, some villages and surrounding fields. Liquefaction was also present along several stretches of levees, as discussed in Chapter 8.

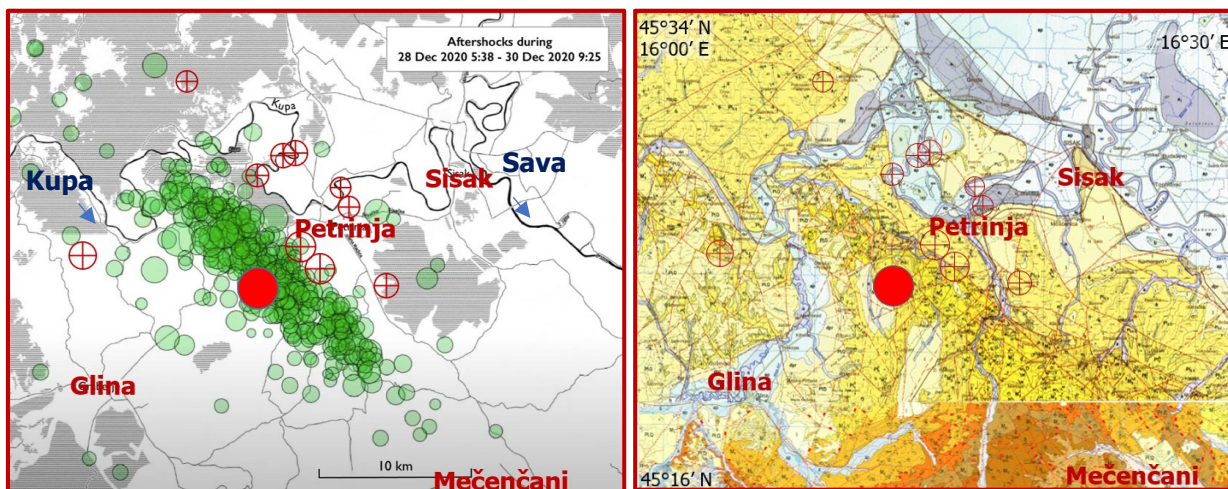


**Figure 7.1** Full red circle shows the location of the main shock  $M_w$  6.4, green circles indicate earthquakes from December 29, 2020, to December 30, 2020, at 9:25 a.m. (Croatian Seismologic Survey 2020), and red circles show aftershocks with magnitudes above 2.5 (USGS Earthquake Catalog). On the right is the appropriate section of the geologic maps Sisak (Pikija 1987) and Bosanski Novi (Šikić 2014). The locations of the most damaged cities and villages mentioned in the text are shown on both figures.

The city of Sisak developed mainly after the 2<sup>nd</sup> World War as a modern industrial city with rich cultural life, while the town of Petrinja, due to its administrative role, has a distinctive old city center, with most of the residents living in family houses. Most of the family houses in the broader area affected by the earthquake are founded on shallow foundations and have no basements. This is due to the groundwater table being very high in the area. Many of the houses in the area were built by their owners. After the war in the 1990s, the damaged houses were repaired or rebuilt by the state. Some single-story residences had an extra story added by their owners. Consequently, there had been no extensive geotechnical investigations even though liquefaction occurred in the area a century ago (discussed in Section 7.2). Pre-earthquake geotechnical investigations were performed for the Sisak Refinery, Sisak Thermal Power Plant, and a series of buildings in areas where no liquefaction occurred due to this earthquake.

## 7.1. Geological Information

The region where liquefaction was observed is underlain by Quaternary alluvial deposits (**Figure 7.2**). The primary geologic units in the affected areas are Holocene floodplain (ap) and terrace deposits (a<sub>1</sub>) near the active river channels along with deluvium-proluvium (dpr). Only few locations with liquefaction effects were identified in the Pleistocene and Pliocene deposits (Pl<sub>2,3</sub> and Pl<sub>Q</sub>); however, all of them were located near the contact with the Holocene deposits near Glina and Petrinja. Given the scale and date of the geologic map, the locations of these contacts are approximate; hence, and it is likely that these observations occurred within the Holocene sediments.

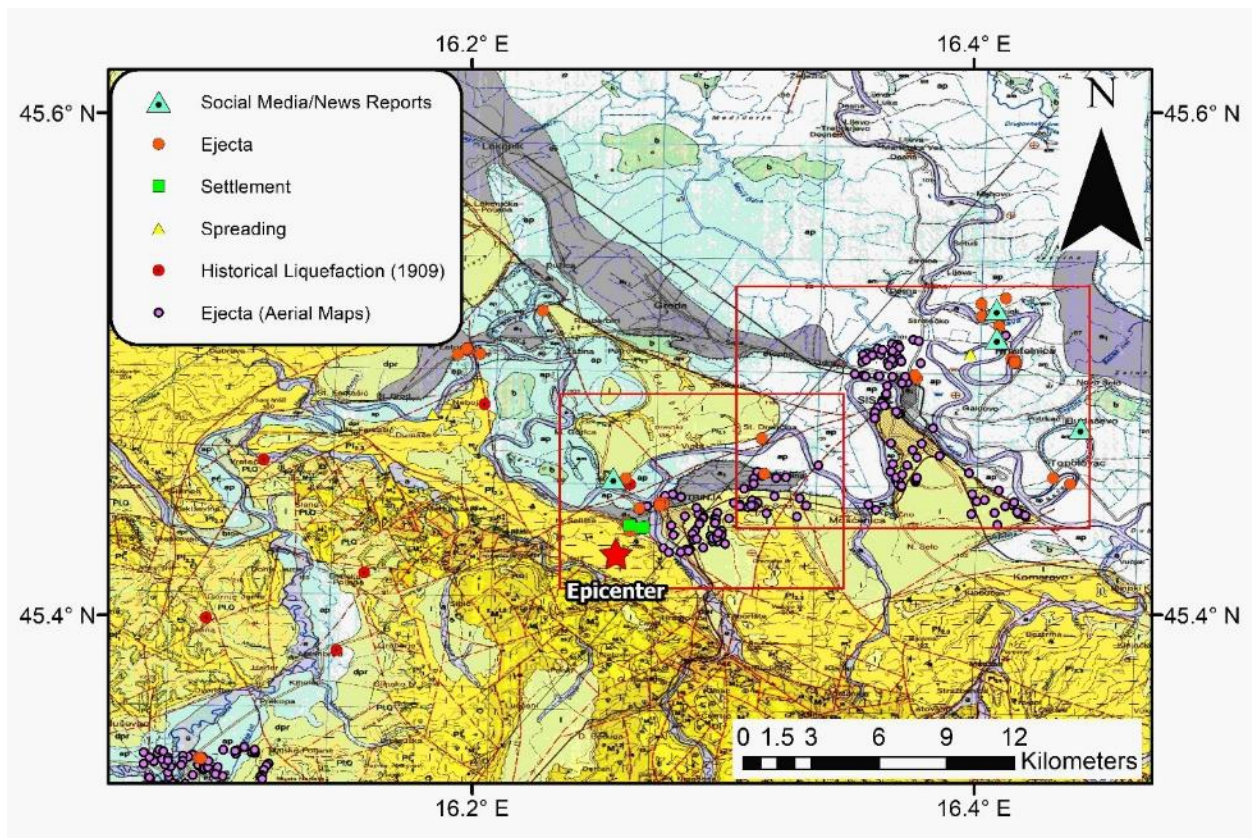


**Figure 7.2.** Geologic map of the study area showing locations of liquefaction observations. The red boxes indicate the extent of the focused maps of Petrinja and Sisak. Historical observations from the 1909 earthquake were mapped based on the LIQUEFACT GIS database (Lai et al. 2018). The translated legend of the geologic map from Pikija (1987) is shown in **Figure 7.3**.



**Figure 7.3.** Legend for geologic maps from Pikija (1987). Translated from Croatian.

**Moreover, Figure 7.4** shows the geologic units in the Petrinja region along with the liquefaction observations and historical reports of liquefaction (discussed in a subsequent section). The epicenter of the earthquake was located approximately 2 km west of Petrinja (**Figure 7.4**). Many of the locations where ejecta were observed occurred along with the contact between the terrace sediments ( $a_1$ ) and the flood sediments (ap) or within the area mapped as diluvium-proluvium (dpr).

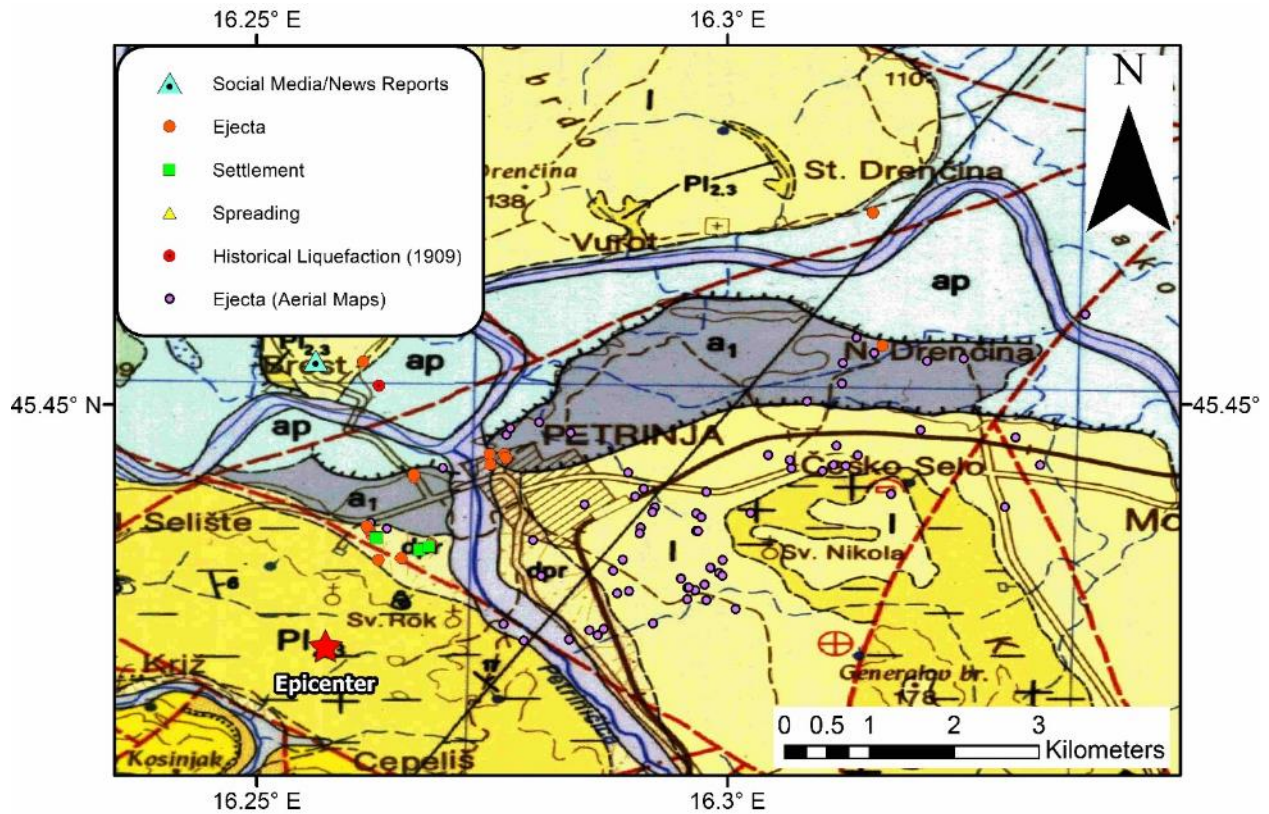


**Figure 7.4.** Geologic map of the Petrinja region showing locations of liquefaction observations. A single observation from the 1909 earthquake was in this region (Lai et al. 2018). The translated legend of the geologic map from Pikija (1987) is shown in **Figure 7.3**.

Finally, **Figure 7.5** shows the geologic units in the Sisak region along with the liquefaction observations and historical reports of liquefaction (discussed in subsequent sections). All of the locations where ejecta were observed occurred within the flood sediments (ap). All of the observations were relatively close to the active river channels.

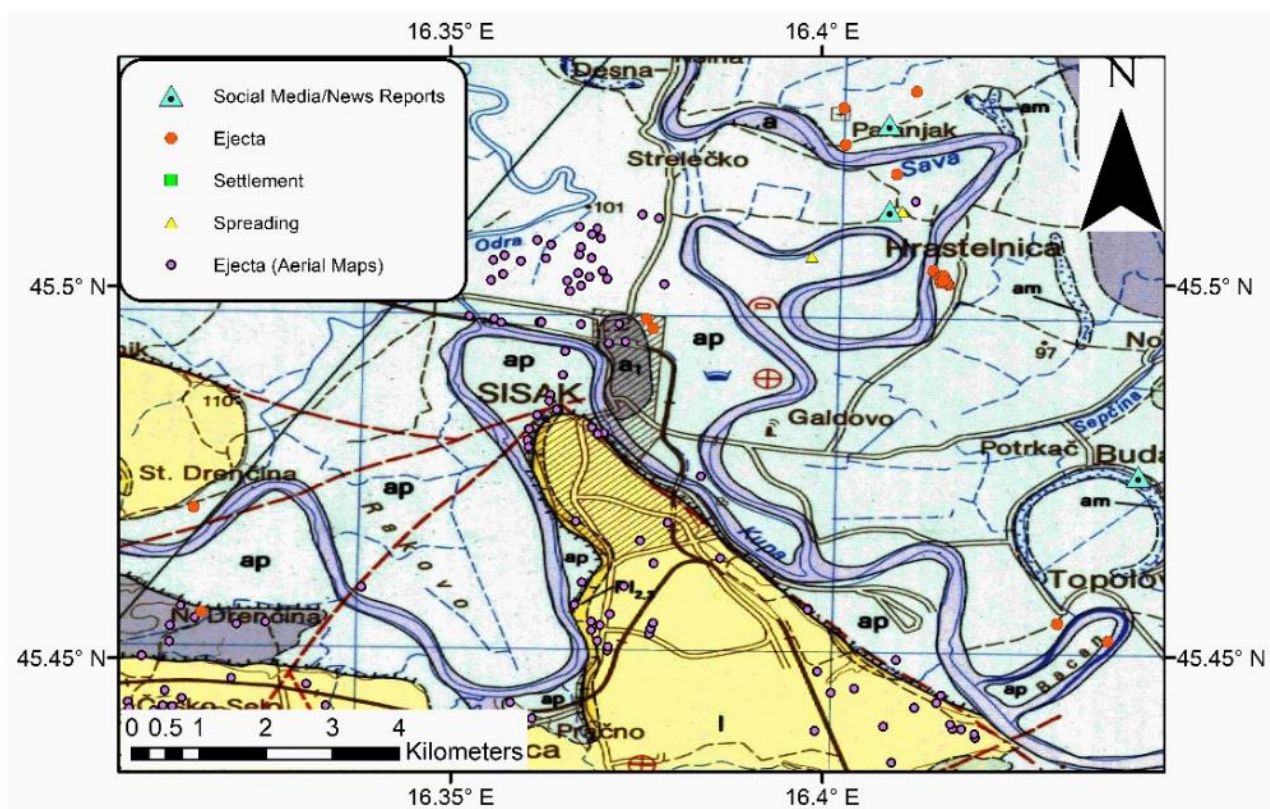


**Figure 7.5.** Geologic map of the Sisak region showing locations of liquefaction observations. No observations from the 1909 earthquake were mapped in this region. The translated legend of the geologic map from Pikija (1987) is shown in **Figure 7.3**.

## 7.2 Historical Observations

Croatia is a country with rather high seismic activity and several occurrences of liquefaction during earthquakes have been documented over the years, e.g., Dubrovnik 1667, Virovitica 1757, Zagreb 1880, and during the Dubrovnik and Montenegro earthquake of 1979 (Veinović 2007). The historical evidence also confirms that liquefaction is not a new hazard for the areas surrounding the Kupa and Sava rivers. In 1880, six cases of water gushing from the earth alongside the formation of sand boils were during the November 9 Zagreb earthquake (Torbar, 1882, after Veinović et al. 2007). The 1909 Kupa valley earthquake also produced cases of liquefaction. The areas where such phenomena have been observed are close to the Krško-Brežice field in Slovenia and in the valley of the Sava River (Veinović et al. 2007; Herak et al. 2009; Herak and Herak 2010). Brežice also lies by the Sava River northwest of Zagreb. **Figure 7.6** illustrates the epicenters of earthquakes at the Krško-Brežice field and in its close surroundings from 567 to 2007 AD, as well as the locations where liquefaction-related effects were observed during the Zagreb (blue dots) and Kupa Valley (yellow dots) earthquakes (Smolar et al. 2019). Smolar et al. (2019) performed a liquefaction assessment study in the Brežice Hydroelectric Power Plant (Slovenia), close to the Sava River, and found a stratigraphy similar to the ones in the areas affected by the Petrinja earthquake: a top layer up to 5-m thick, consisting of the recent deposit of very loose silts and

sands (ML, SM, SP), likely liquefiable, overlying a medium dense to dense Quaternary gravel, beneath which there are over-consolidated, uncemented Miocene silts and marls. The LiqueFACT project (Lai et al. 2018) further indicates that 13 liquefaction cases have been observed in Croatia during three earthquakes while the microzonation and liquefaction hazard mapping of Veinović et al. (2007) clearly indicates that some areas around rivers in Croatia have a high liquefaction potential.

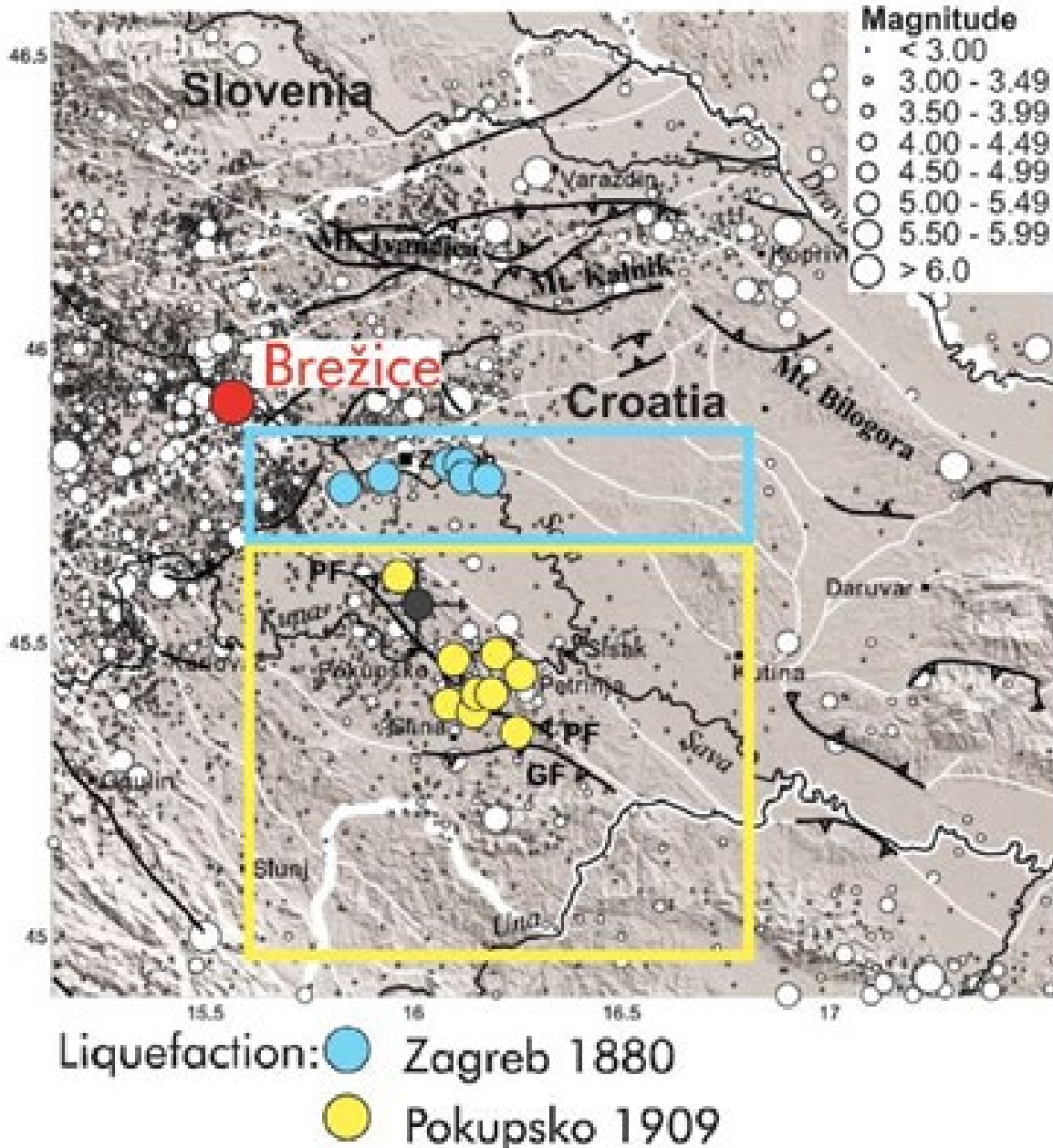


**Figure 7.6** Epicenters of earthquakes at the Krško-Brežice field and in its close surroundings from 567 to 2007 AD, alongside with the locations where liquefaction-related effects were observed during the Zagreb (blue dots) and Kupa Valley (yellow dots) earthquakes (Veinović et al. 2007, Herak and Herak 2010) (after Smolar et al. 2019).

### 7.3 Liquefaction Observations following the December 29 2020 Petrinja Earthquake

Liquefaction observations were documented using reports from residents, observations from field visits, social media reports, and mapping using aerial and satellite images of affected regions. Post-earthquake digital orthophotographs for Drenčina, Glina, Mošćenica, Petrinja, and Sisak were developed by the Faculty of Geodesy at the University of Zagreb, while the corresponding aerial photographs were acquired by the Croatian Mountain Rescue Service (HGSS) (© OpenStreetMap contributors). High-resolution satellite imagery was available in Google Earth for regions around Petrinja and Sisak. The orthophotographs were visually inspected for traces of liquefaction ejecta. Evidence of ejecta was mapped manually with points recorded (shown as purple circles in **Figures 7.2, 7.4, 7.5, 7.7, 7.8, and 7.9**). An example of one of the sites where ejecta was mapped is shown in **Figure 7.10**. The mapped locations near Petrinja and Sisak are shown in **Figures 7.7 and 7.8**, respectively. Locations with liquefaction observations near Glina are shown in **Figure 7.9**. Importantly, the absence of ejecta away from Drenčina, Glina, Mošćenica, Petrinja, and Sisak and near the Kupa, Sava, and Odra rivers is not necessarily due to any mitigating effects but due to the limited coverage of aerial photographs. The locations of ejecta marked by triangles colored in cyan in **Figures 7.2, 7.4, 7.5, 7.7, and 7.8**, are approximate as they are based on news and social media reports (Buljan 2021, Jakubin 2020, Kovač 2021, Milotić and Uremović 2021, Šarčević 2021).

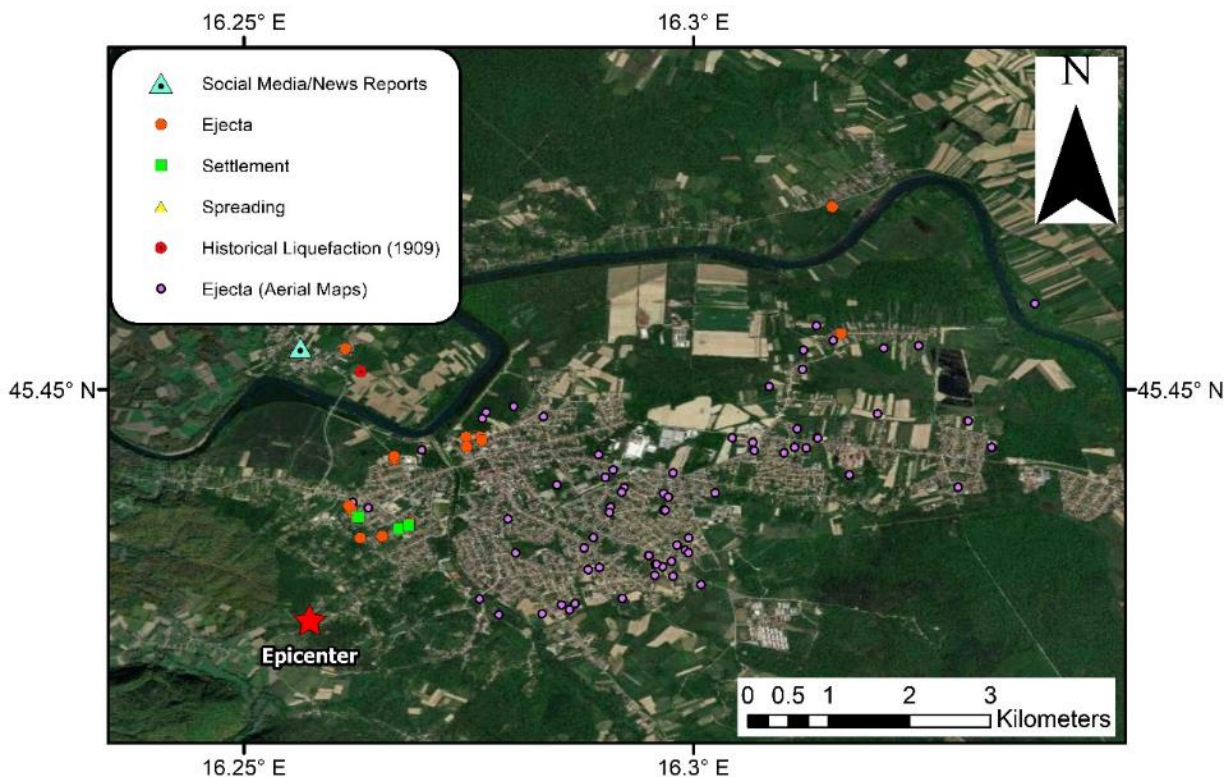


**Figure 7.7** Satellite map of the Petrinja region showing locations of liquefaction observations.

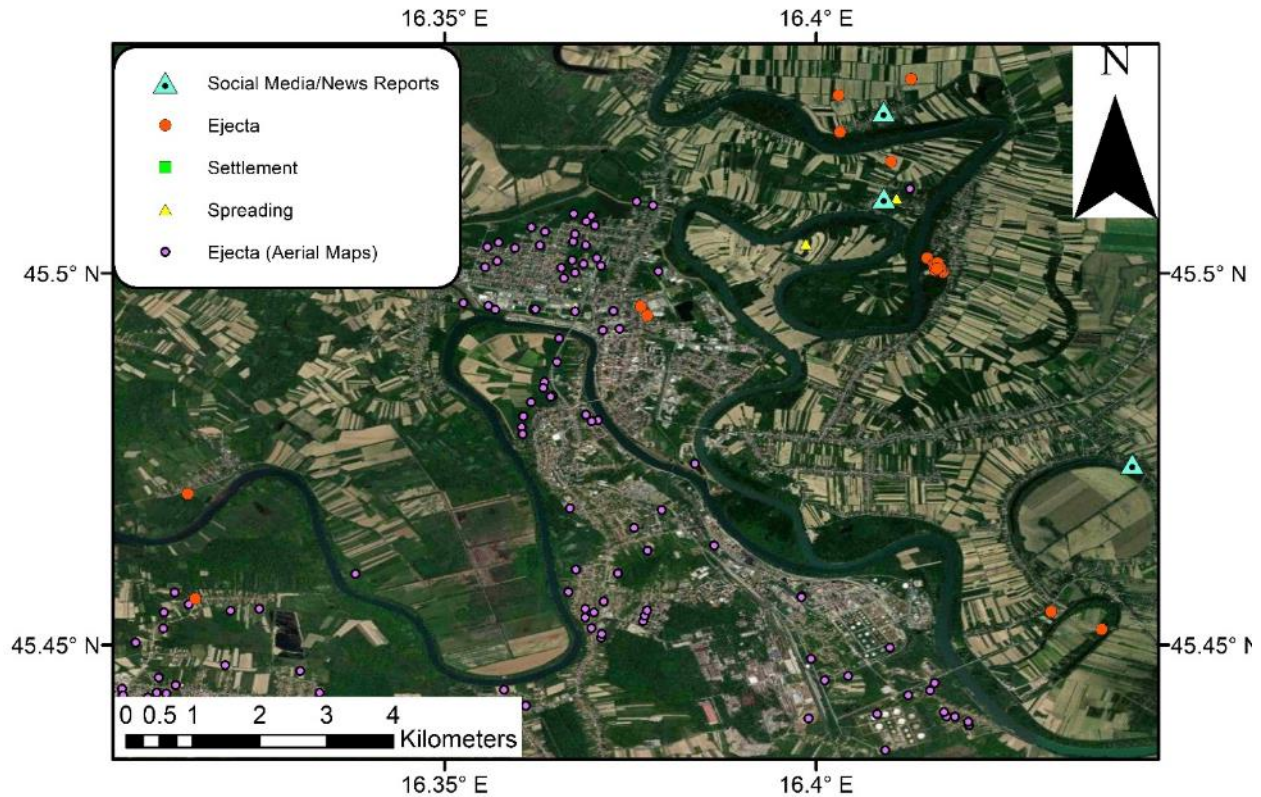


**Figure 7.8** Satellite map of the Sisak region showing locations of liquefaction observations.

Direct observations of liquefaction effects were made at more than 70 sites along the Kupa, Glina, and Sava rivers (**Figure 7.2**). These locations were mapped based on direct observations during reconnaissance trips by field team members and local collaborators and reports from residents. Many of the liquefaction observations occurred in open fields, such as agricultural fields (e.g., **Figure 7.11**) or sports fields (e.g., **Figure 7.12**), located near rivers. Damage to levees is discussed in Chapter 8. The field team noted that the groundwater table was near the ground surface in many of these locations. Many of the sites had multiple locations where ejecta were observed, indicating extensive liquefaction of the loose alluvial sediments underlying these locations (**Figure 7.11**). Differential settlements were observed at some residential structures in Petrinja (**Figure 7.7**), while lateral displacements were observed at two locations, Bok Palanječki (northeast of Sisak, **Figure 7.8**) and Stari Brod (northwest of Petrinja, **Figure 7.2**), as discussed in Section 7.5.1. Additional lateral spreading and cracking of levees is discussed in Chapter 8.

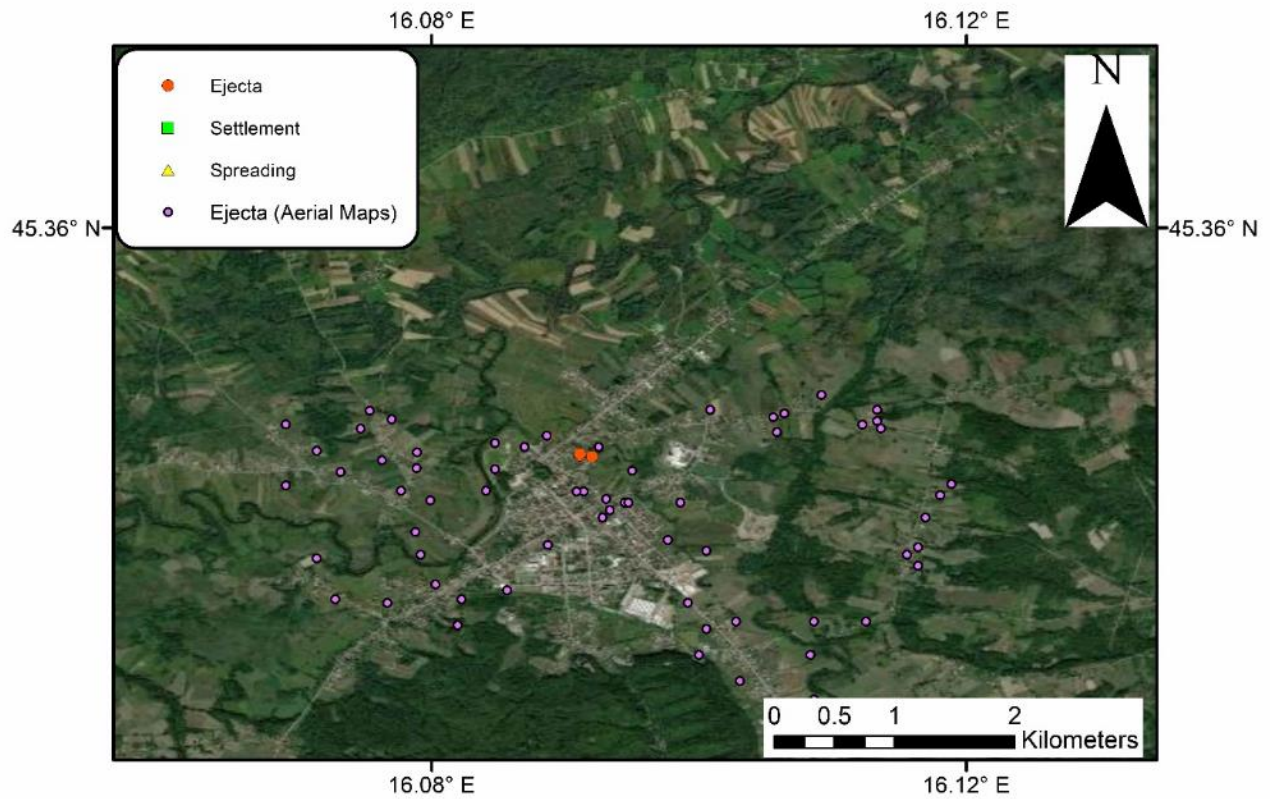


**Figure 7.9** Satellite map of the Glina region showing locations of liquefaction observations mapped from aerial imagery and by the field team.



**Figure 7.10** Linear pattern of sand boils at a field north of Glina (45.343889N, 16.084722E).



**Figure 7.11** Ejecta in an agricultural field near Hrastelnica (45.5009N, 16.4166E).



**Figure 7.12** Ejecta in a football field near Letovanić (45.506095N, 16.198165E).

One common observation in both the aerial and field images was the linear pattern of sand boils emerging from surface cracks (e.g., **Figures 7.10 - 7.13**). For the locations shown in **Figures 7.10-7.13**, no ejecta were observed without cracks. Ejecta were also commonly observed within water wells in residential areas that penetrate through the overlying non-liquefiable soil layers to the sandy liquefiable soils below. **Figure 7.14** shows a nearby water well that was partially filled with sand following the earthquake, as well as the road settlement in Drenačka Street, Petrinja, without the presence of ejecta. This non-liquefiable crust found in this region may partially explain the lack of significant damage associated with liquefaction.



**Figure 7.13** Linear patterns of ejecta located along cracks in Petrinja (left; 45.444714N, 16.274728E) and Hrastelnica (45.500594N, 16.416287E).



**Figure 7.14** Liquefaction under the Drenačka Street in Petrinja (45.4560936N,16.3173009E) and sand in the well nearby (45.4562236N, 16.3164433E).

## 7.5 Selected Case Histories of Liquefaction Effects

Liquefaction occurred in many locations across the Kupa and Sava river valleys and tributaries, as previously discussed. This section presents some additional details on selected illustrative

locations where damage was observed (lateral spreading or settlement) and locations where in-situ data (dynamic penetrometer soundings) were collected. Additional spreading and cracking of levees is discussed in Chapter 8.

### 7.5.1 Lateral Spreading

Lateral spreading is shown for two locations in Figure 7.2. Additional spreading and cracking of levees is discussed in Chapter 8. In Bok Palanječki, cracking and lateral offsets were observed on both sides of the river (**Figure 7.15**). Vertical offsets of approximately 30 cm and lateral offsets of approximately 10 cm were observed for the driveway of one of the residences in Bok Palanječki (**Figure 7.16**). Cracks were observed in the fields too, but no damage to the structures in this area was noted.



**Figure 7.15** Post-earthquake satellite imagery (01/27/2021) near Bok Palanječki (45.510N, 16.409E). The yellow triangles indicate locations where cracking was observed.



**Figure 7.16** Cracks in the driveway of one of the residences in Bok Palanječki (45.510058N, 16.410803E).

In the village of Stari Brod (approximately 10 km from the epicenter of the main shock), liquefaction and lateral spreading were identified around a series of houses along the Kupa River. The residents noticed water with sand and mud coming out from the ground around houses, in their yards, and the fields. Like other locations in the region, many water wells were filled with liquefied sand and became unusable. Liquefaction was noted at 83, 97, 98, 99, 99B, 110, and 110A Ižišće Street (Bostjančić, 2021), and their positions are shown in **Figure 7.17**.



**Figure 7.17** Location of the liquefaction ejecta by the Kupa River in the Ižišća Street in Stari Brod. (45.480N, 16.182E; [Google Maps](#)). Numbers show street numbers where liquefaction was observed. Cracks and sliding due to lateral spreading is shown in the area bordered by the white rectangle and enlarged in **Figure 7.24**.

**Figure 7.18a** shows a crack in the yard of the house at 97 Ižišća Street that propagated through the neighboring yards, on the western side, while **Figure 7.18b** shows a crack on the eastern, river side. Both cracks are parallel with the riverbank. The property also had sand ejecta (**Figure 7.18c**). The house is slightly inclined towards the river suggesting the land is sliding towards the river. The house itself was not severely damaged, although some damages are to be repaired and further settlement due to liquefaction could be expected. **Figure 7.18d** shows the crack between the terrace and the house.

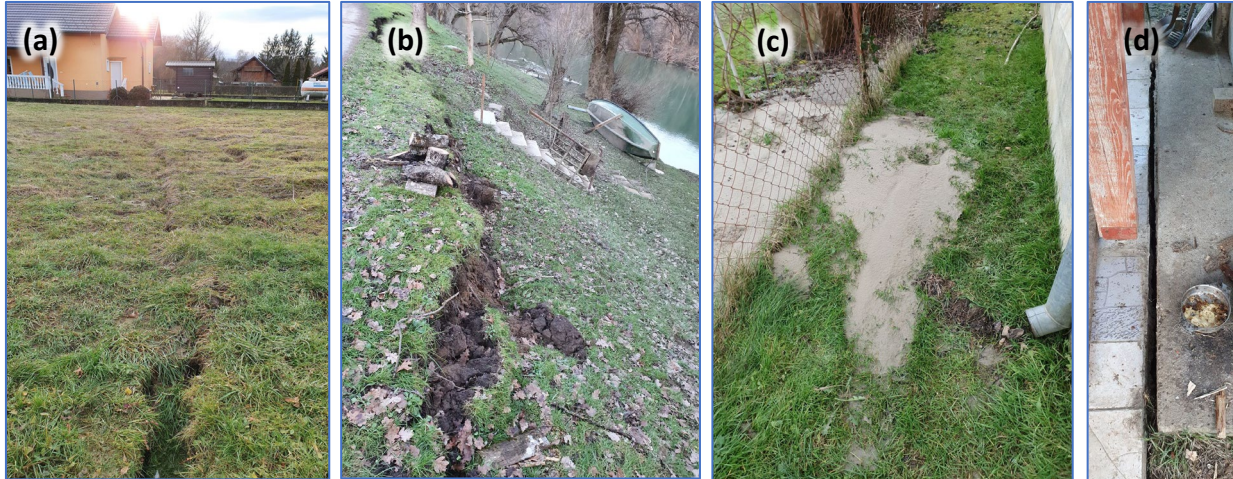


**Figure 7.18** (a) Crack in the yard west from the house, (b) crack along the riverbank, (c) sand ejecta around the house, and (d) crack due to settlement of the terrace, at 97 Ižišća Street, Stari Brod (45.4801N, 16.1841E) (Taus 2021e). The cracks are parallel with the riverbank.

The 98 Ižišća Street property contained the same ground crack observed in the western yard of the house at 97 Ižišća Street (further referred to as the “western” crack). The house at 98 Ižišća Street was damaged and in danger due to differential settlement and possible sliding. The crack in the yard and the crack along the riverbank that progressed from 97 Ižišća Street– both parallel with the riverbank – as well as sand ejecta are shown in **Figure 7.19**. Therefore, it may be concluded that the sliding was caused or contributed to by liquefaction of underlying sandy layers.

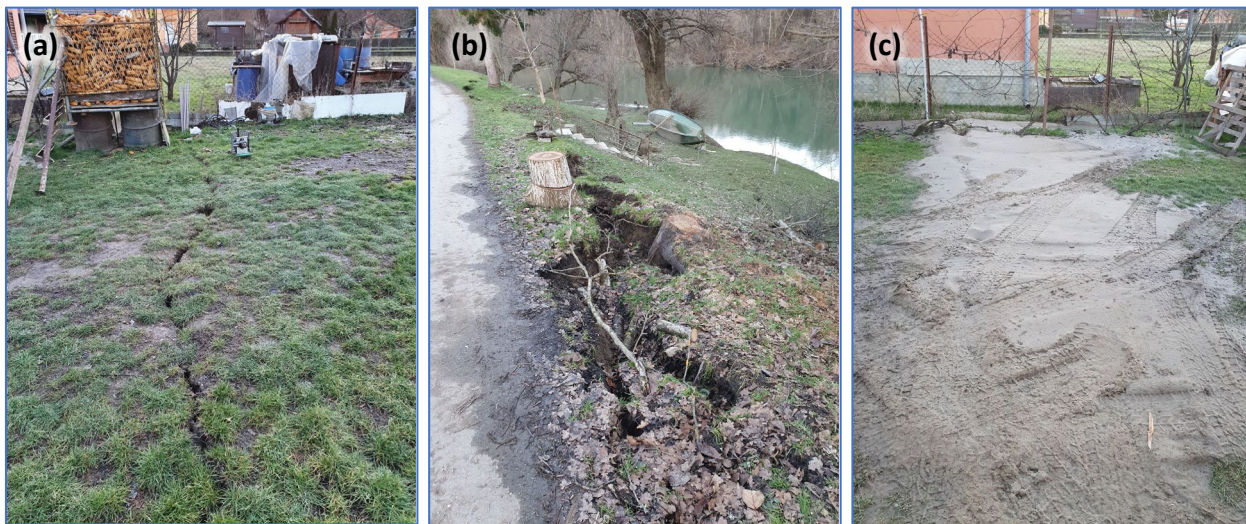


**Figure 7.19** (a) Crack in the yard west from the house, (b) crack along the bank, and (c) sand ejecta around the house at 98 Ižišća Street, Stari Brod (45.480158N, 16.184210E) (Taus 2021f). The cracks are parallel with the riverbank.

Furthermore, the neighboring 99 Ižišća Street property had the same “western” crack that now passed through the house causing severe damage and the same crack on the bank side that originated at 97 Ižišća Street. **Figure 7.20** gives a southeastern view of the house and the water

well at the property. During the earthquake, sand was ejected upward through the well and onto the surrounding ground, as visible in **Figure 7.20a**. The well remained filled with sand up to the 6-m depth below the ground surface level (**Figure 7.20b**).

The cracks passing through the house floor at 99 Ižišća Street (**Figure 7.21** and **Figure 7.22**) were aligned with the crack in the neighboring yards at 97 and 98 Ižišće Street. Ejecta at this property were also observed, as shown in Figure 7.23. The cracks were mapped across the different homes (**Figure 7.24**) and indicated this portion of the bank was moving towards the free face of the river.

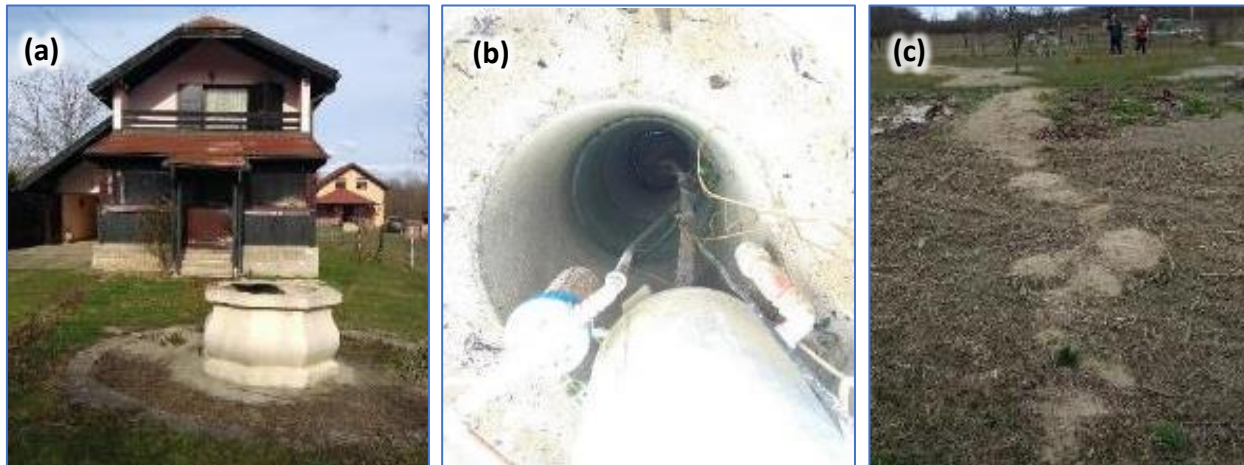


**Figure 7.20** (a) The southeastern view of the house at 99 Ižišća Street (45.480248N, 16.184285E) with the water well and sand ejected through the well and onto the ground during the Mw 6.4 earthquake and (b) the water well filled with sand to a depth of 6 m below the ground surface level. (c) Sand ejecta.



**Figure 7.21** (a) Northwestern side of the house at 99 Ižišća Street (45.480248N, 16.184285E) in Stari Brod, (b, c) the propagation of the crack through the western yards of the houses at 97 and 98 Ižišća Street marked (1) in Figure 7.23. Crack is deeper than 1m, with opening of around 10 cm and a vertical offset of 8cm.

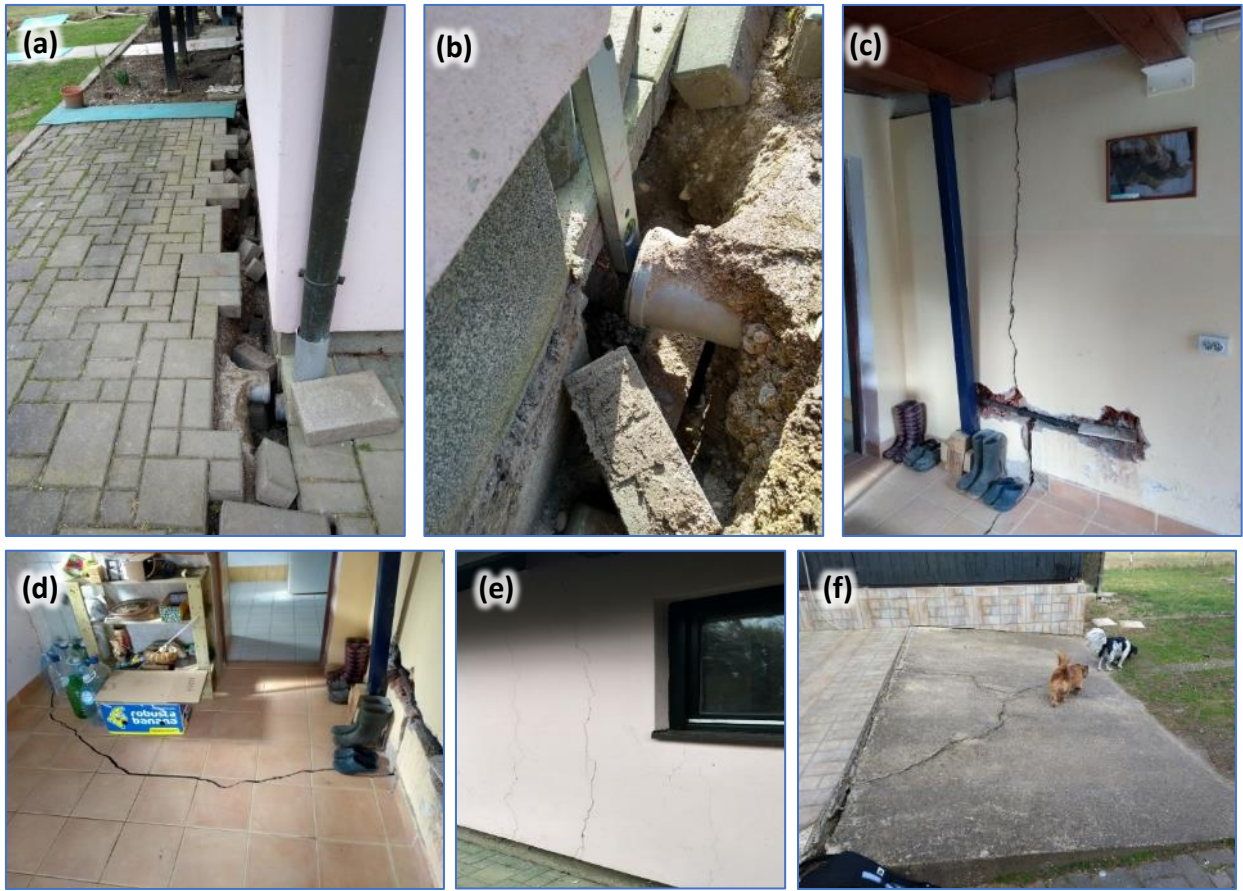


**Figure 7.22** (a, b) Western corner of the house at 99 Ižišća Street (45.480248N, 16.184285E) in Stari Brod with pavement heave of 8 cm and rupture of the roof drainage pipe, marked (2) in Figure 7.23. (c, d) Water pipe rupture caused by vertical crack in the wall and crack on the garage floor between the terrace and house foundation on the line marked (3) in Figure 7.23 and (e) corresponding crack on the outside. (f) Cracks on the pavement at the garage entrance marked (4) in Figure 7.23.

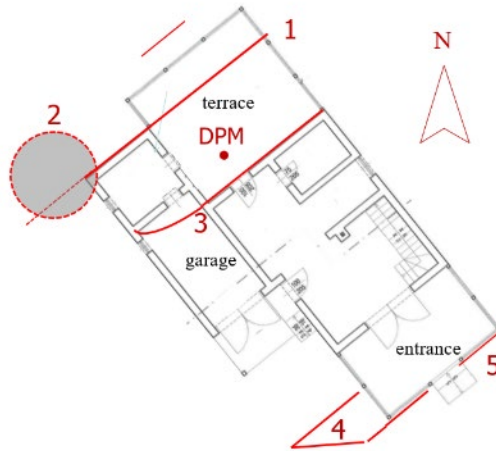


**Figure 7.23** Plan of house at 99 Ižišće Street (45.480248N, 16.184285E) in Stari Brod and cracks shown in red. Numbers indicate features of interest: (1) Crack shown in Figure 7.21; (2) Pavement deformation shown in Figure 7.22a-b; (3) Water pipe rupture caused shown in Figure 7.22c-d; (4) Cracks in the pavement as in Figure 7.22f; (5) Cracks along the south east wall, probably widening. Steps are moving away from the terrace. Red dot: DPM location.

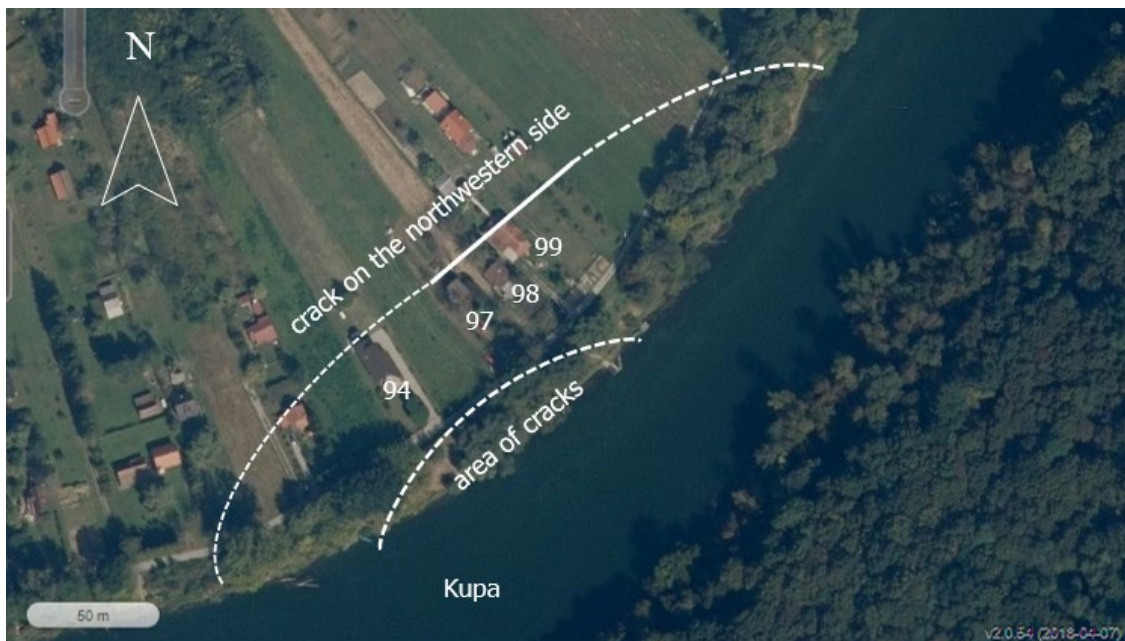


**Figure 7.24** Position of the cracks mapped at 97, 98, 99, 99 Ižišće Street in Stari Brod due to lateral spreading along the Kupa River (45.480N, 16.183E; Geoportal, <https://geoportal.dgu.hr/>).

Dynamic penetrometer (DPM 30) testing was performed near the foundations of the three aforementioned houses (97, 98, and 99 Ižišća Street). The test results are shown in **Figure 7.25**. The DPM 30 uses rods with a 20-mm diameter and the crown bottom that is 35.6 mm in diameter (i.e., its cross-sectional area is 10.00 cm<sup>2</sup>). A hammer with the mass of 30.0 kg is dropped from

the height of 20 cm and the number of blows required to drive the crown 10 cm into the soil is counted. The counted values are then converted into dynamic cone resistance. The test results indicate low penetration resistance in the upper 6 meters of the soil profiles.

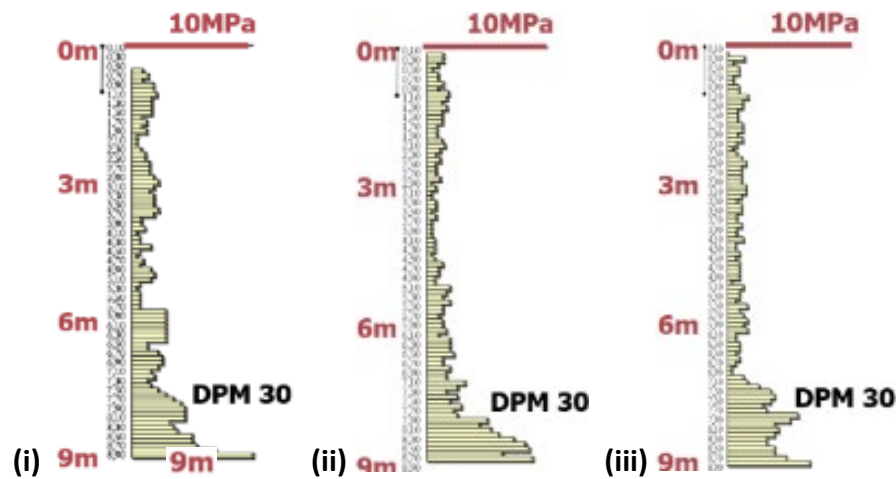


**Figure 7.25** The DPM 30 test results obtained at (i) 97 Ižišća St (45.480060N, 16.184103E), (ii) 98 Ižišća St (45.480158N, 16.184210E), and (iii) 99 Ižišća St (45.480229N, 16.18433E7) (Taus 2021e-g).

### 7.5.2 Effects of Liquefaction on Residential Structures

Many residential properties in Petrinja had sand ejecta in yards or around house foundations. **Figure 7.26** illustrates thin cracks above the foundation of a house in Petrinja. At the property across the street from this house, the sand ejecta were visible in the yard and along the fence foundation, and part of the yard heaved, all contributing to the formation of thin cracks in the house wall around the balcony near the single column, as shown in **Figure 7.27**.

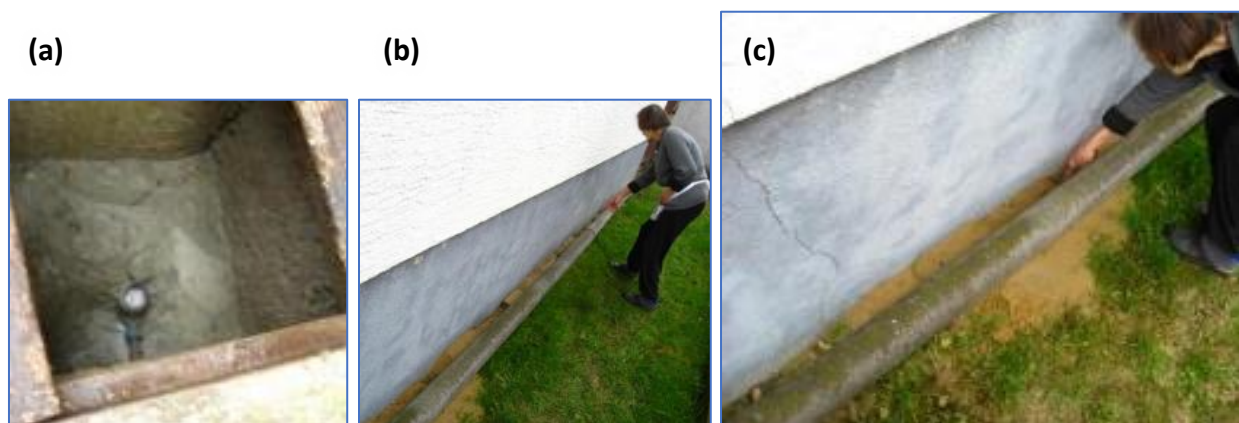


**Figure 7.26** (a) Sediment ejecta in the water meter shaft, (b) sand ejecta by the house, and (c) cracks above the foundation near the sand ejecta pointed at by the owner in Petrinja (45.4349N, 16.2683E).



**Figure 7.27** (a, b) During the main shock, sandy soil appeared along the fence foundation and the central part of the yard heaved. (c) Several thin cracks appeared in the house wall around the column and the balcony in Petrinja (45.43515N, 16.26844E).

Evidence of liquefaction was found at residential properties in Milana Makanca Street in Petrinja starting from the house number 1 all the way to the house number 44, with the volume of the ejecta around each house measuring typically up to  $1.5 \text{ m}^3$  (Gulam 2021). At 11 Milana Makanca Street, liquefaction induced flooding of the property by groundwater mixed with some soil sediments, as illustrated in **Figure 7.28**. The house itself was not damaged, but it was suggested that further investigations be undertaken. In accordance with that, a dynamic penetrometer (DPM 30) test was performed at the house corner (Taus 2021a). The test results provided in **Figure 7.29** show that the soil in the upper 3 m is very loose.

Many water wells in the area were filled with liquefied sandy soil. A well at 8 Milana Makanca Street in Petrinja was seen to eject sand some 150 cm above the ground level, as shown in **Figure 7.30**, causing cracks in the nearby house that was abandoned before the earthquake (also shown, in **Figure 7.30c**). The neighboring house at 10 Milana Makanca Street, also abandoned before the earthquake, had damage in the ceiling visible at **Figure 7.31**.



**Figure 7.28** (a) Flooding groundwater and sediment ejecta: (b) south corner, (c) northwest side around the house at 11 Milana Makanca Street, Petrinja (45.436061N, 16.262898E), recorded by the owner, Tomislav Zorčić, minutes after the Mw 6.4 earthquake.

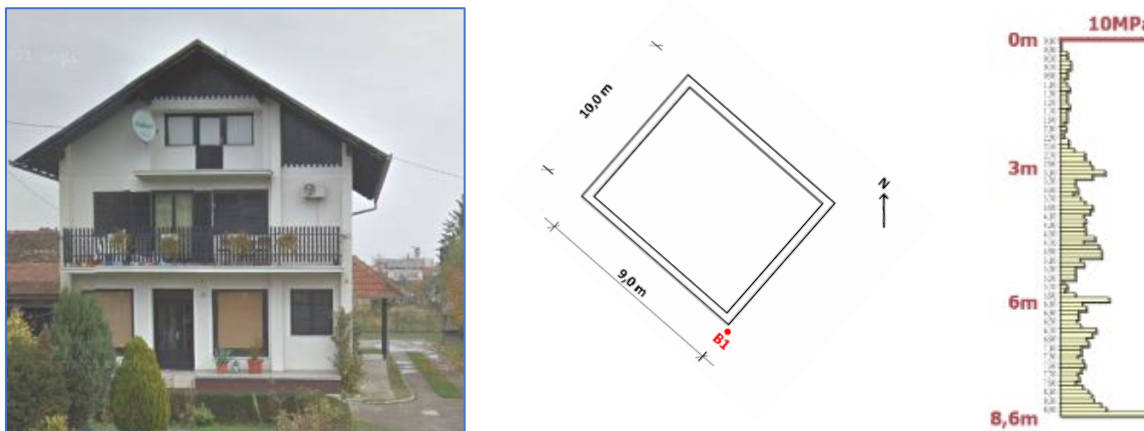


**Figure 7.29** The house at 11 Milana Makanca Street in Petrinja (45.436061N, 16.262898E), test location at the southern corner of house, and DMP 30 test results (Taus 2021a).

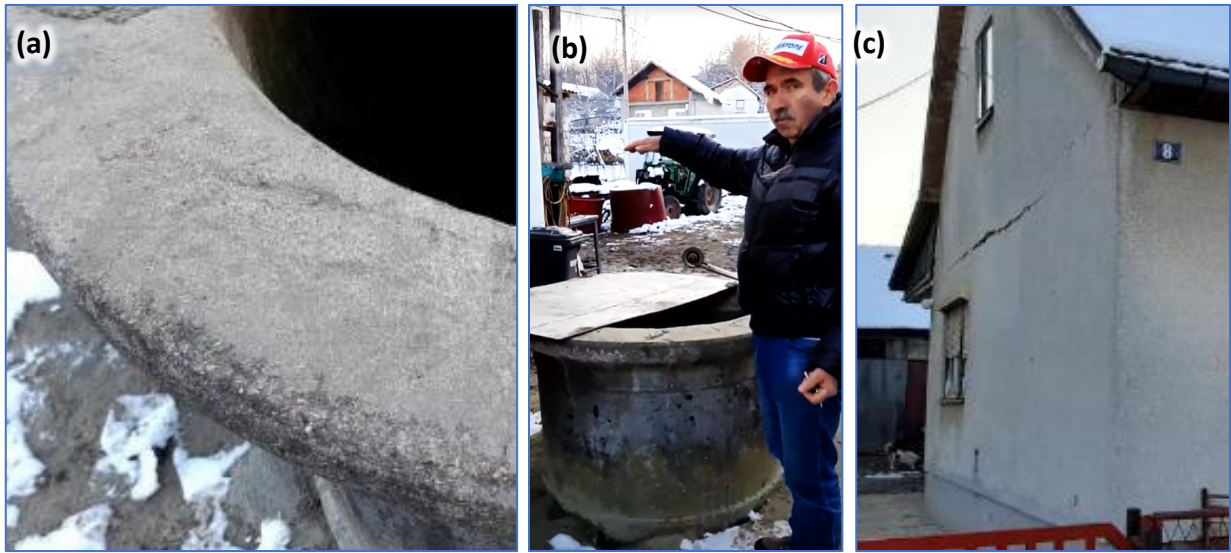


**Figure 7.30** (a) Rim of the water well at 8 Milana Makanca Street in Petrinja (45.4359N, 16.2627E) covered by the ejected sand. (b) A neighbor shows that during the earthquake sand and water were ejected upward from this well, around 150 cm above the ground level. (c) The abandoned house near the well.



**Figure 7.31** (a) Traces of sand ejecta and (b) the crack in the ceiling inside the house at 10 Milana Makanca Street in Petrinja (45.4358N, 16.2628E).

DPM 30 testing was also performed at several locations in Glina, approximately 12 km from the epicenter, to evaluate the subsurface conditions. Evidence of liquefaction was identified in the streets as well as at the properties. Liquefaction effects were especially notable in the streets along the former riverbed of the Maja River. DMP 30 testing was performed at one of these locations (20 6. kolovoza 1995. Street) with the results presented in **Figure 7.32**. The test results show that the soil in the upper 3 m of the profile (especially from the 1.5-m to 3-m depth) is extremely loose. Similar soil conditions were observed across the street (25 6. kolovoza 1995.

Street), as shown in **Figure 7.33**. Slightly stronger soils were found at the nearby location (35 6. kolovoza 1995. Street), as shown in **Figure 7.34**.



**Figure 7.32** The house at 20 6. kolovoza 1995. Street (45.3430N, 16.0911E), test location at the western corner, DMP 30 test results, and characteristic ejecta (Taus 2021b).

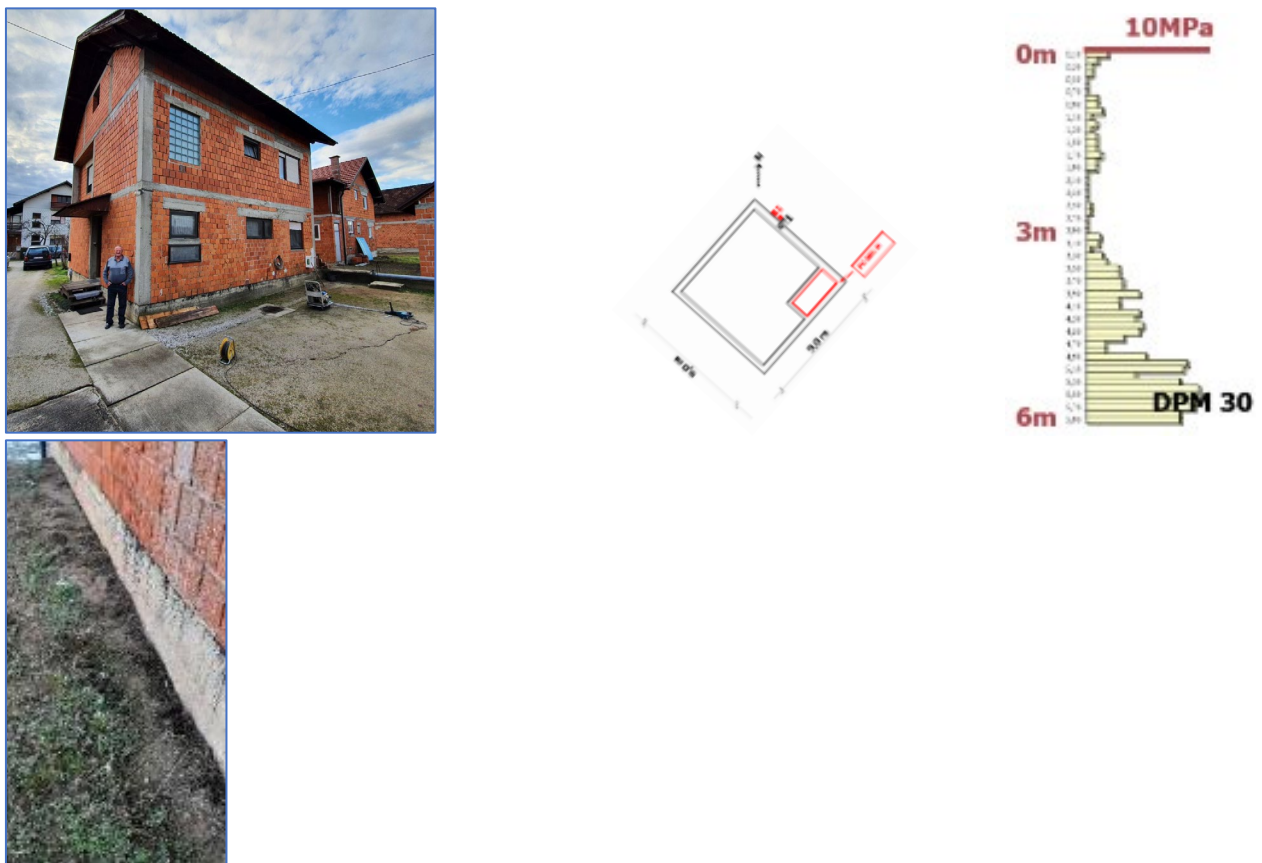


**Figure 7.33** The house at 25 6. kolovoza 1995. Street (45.3431N, 16.0911E), test location near the northern corner, DMP 30 test results, and characteristic ejecta (Taus 2021c).

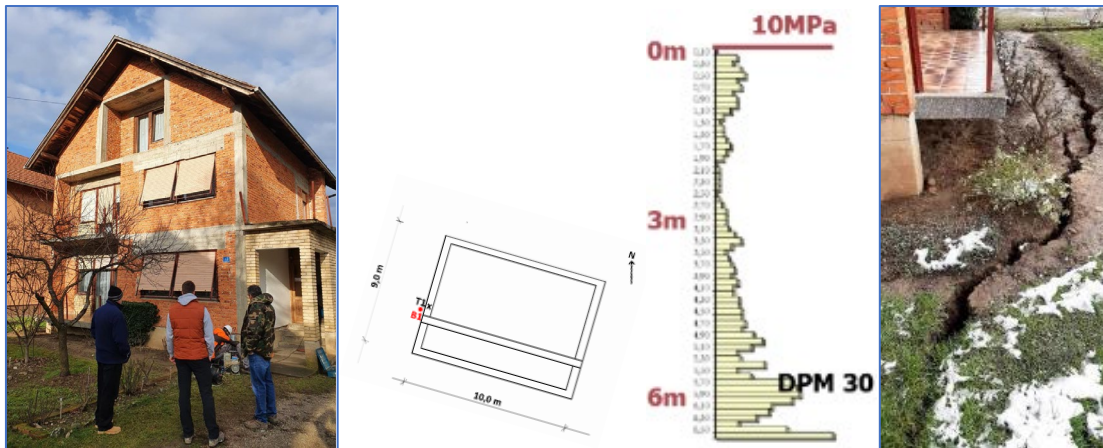


**Figure 7.34** The house at 35 6. kolovoza 1995. Street (45.3429N, 16.0920E), location of the testing near the eastern wall, DPM 30 test results, and characteristic crack (Taus 2021d).

## 7.6 Concluding Remarks

Extensive evidence of liquefaction was observed throughout the Kupa, Glina, and Sava river valleys. The field observations of liquefaction primarily occurred in areas mapped as either flood sediment or diluvium-proluvium on the geologic map by Pikija (1987). These Holocene units are described as primarily consisting of silts and sands. Liquefaction observations outside of these units primarily occurred near contact with one of these two units. All observations were within 17 km of the epicenter indicating that strong shaking was likely. Liquefaction within loose, saturated alluvial sediments near the epicenter has been widely observed in previous earthquakes and as such, these observations were expected.

## References

- Bostjančić, I. (2021). *Geološka prospekcija na području Starog Broda, općina Lekenik*. Croatian Geologic Survey, Zagreb
- Buljan, P. (2021). *Ekskluzivne snimke iz zraka: Ogromni rasjedi nastali nakon potresa uznemirili mjestane Budaseva kod Siska (Exclusive aerial video recordings: Huge cracks formed after the earthquake disturbed locals of Budasevo near Sisak)* [Online]. Dnevnik.hr. Available at: <https://dnevnik.hr/vijesti/potres/ogromni-rasjedi-uznemirili-mjestane-budaseva-kod-siska---639416.html> (Accessed: 15 February 2021)
- Gulam, V. (2021). *Posljedice "Petrijnskog" potresa od 29.12.2020. Geološka prospekcija Ulice Milana Makanca u Petrinji*. Zagreb: Hrvatski geološki institut / Croatian Geologic Survey.
- Herak, D., Herak, M. and Tomljenović, B., 2009. Seismicity and earthquake focal mechanisms in North-Western Croatia. *Tectonophysics*, 465(1-4), pp.212-220.
- Herak, D. and Herak, M. (2010). *The Kupa Valley (Croatia) Earthquake of 8 October 1909—100 Years Later*. *Seismological Research Letters* 81 (1), p30-36.

- Herak, M., Allegretti, I., Herak, D., Ivancic, I., Kuk, V., Maric, K., Markušić, S., Sovic, I. (2011) Republic of Croatia, Map of Seismic Areas (In Croatian). Available online: <http://seizkarta.gfz.hr>
- Jakubin, H. K. (2020, December 30). Zemlja u Palanjkju se doslovno otvorila: “Voda je ‘sikljala’ sva metra u zrak, to su bili gejziri!” [The ground in Palanjek literally opened up: “Water was being ‘spouted’ two meters in the air, those were geysers!"]. Jutarnji list. <https://www.jutarnji.hr/vijesti/hrvatska/zemlja-u-palanjku-se-doslovno-otvorila-voda-je-sikljala-dva-metra-u-zrak-to-su-bili-gejziri-15039756>
- Karakaš Jakubin, H. (2020). *Zemlja u Palanjkju se doslovno otvorila: “Voda je ‘sikljala’ sva metra u zrak, to su bili gejziri!” (The ground in Palanjek literally opened up: “Water was being ‘spouted’ two meters in the air, those were geysers!”)*. Jutarnji list, 30 December [Online]. Available at: <https://www.jutarnji.hr/vijesti/hrvatska/zemlja-u-palanjku-se-doslovno-otvorila-voda-je-sikljala-dva-metra-u-zrak-to-su-bili-gejziri-15039756> (Accessed: 15 February 2021)
- Kovač, M. J. (2021). *Timeline* [Facebook]. 1 January. Available at: <https://www.facebook.com/photo?fbid=4191104477583515&set=pcb.4191105817583381> (Accessed: 1 January 2021)
- Lai, C. G., Bozzoni, F., De Marco, M. C., Zuccolo, E., Bandera, S., and Mazzocchi, G. (2018). GIS database of the historical liquefaction occurrences in Europe and European empirical correlations to predict the liquefaction occurrence starting from the main seismological information. Report, LiquefACT Research Project, Deliverable D2.4, Version 1.0. <http://www.liquefact.eu/wp-content/uploads/2020/03/D2.4.pdf>
- Mikic, D. (2021). ‘Nevjerojatna snimka: Tlo nakon potresa potonulo za pola metra, a to nije i najveći problem stanovnika općine Martinska Ves (Unbelievable recording: Ground settled half a meter after the earthquake, but not even that is the main problem of Martinska Ves County residents)’ [Online]. Dnevnik.hr. Available at: <https://dnevnik.hr/vijesti/hrvatska/martinska-ves-stanovnici-u-problemima-zbog-mulja-i-pjeska-u-bunarima-te-rasjedima-na-pasnjacima---639759.html?fbclid=IwAR2p-wgf5lvZbH-yEhI-qU-vY8HT8e6C94ks4FZtFFAamMM5d9sEPy9yiH8>
- Milotić, I. & Uremović, K. (2021, January 4) *Topla voda je sikljala 2 metra u zrak! Bili su i geolozi, kazu da se s ovako necim nisu susreli (Warm water was spouted 2 meters in the air! There were geologists too, saying they had not encountered something like this)*. 24sata, 4 January [Online]. Available at: <https://www.24sata.hr/news/rupe-su-se-otvorile-voda-je-sikljala-2-metra-u-zrak-teren-je-nocas-potonuo-30-centimetara-737744> (Accessed: 15 February 2021)
- Pikija, M. 1987 *Osnovna geološka karta SFRJ 1:100.000, List Sisak L33–93*. – Geološki zavod, Zagreb (1975–1986); Savezni geološki institut, Beograd. Geologic map available on request at <https://www.hgi-cgs.hr/osnovna-geoloska-karta-republike-hrvatske-1100-000/>
- Smolar, J., Maček, M., and Petkovšek, A. (2019). *Liquefaction potential of sands at the Krško-Brežice field, Slovenia*. Geologia Croatica, Journal of the Croatian Geological Survey and the Croatian Geological Society, 72(2), p. 129–135.
- Šarčević, A. (2021) *Mjestani u strahu: Pojavio se veliki rasjed u selu kod Siska (Locals in fear: A big fault appeared in the village near Sisak)*. 24sata, 10 February [Online].

<https://www.24sata.hr/news/mjestani-u-strahu-pojavio-se-veliki-rasjed-u-selu-kod-siska-744827> (Accessed: 15 February 2021)

Šikić, K. (2014): Osnovna geološka karta SFRJ 1:100.000, List Bosanski Novi L33-105. – Fond stručne dokumentacije Instituta za geološka istraživanja, Zagreb. (manuskript) Available at request at <https://www.hgi-cgs.hr/osnovna-geoloska-karta-republike-hrvatske-1100-000/>

Veinović, Ž., Domitrović, D. & Lovrić, T. (2007): Pojava likvefakcije na području Zagreba u prošlosti i procjena mogućnosti ponovne pojave tijekom jačeg potresa.– Rud.-Geol.-Naft. Zb., 19, 111–120.

## 8 Earthen Levee Systems (Sonja Zlatović, Adda Athanasopoulos-Zekkos, Ingrid Tomac, Ivan Mihaljević)

### 8.1 Introduction and Background

The earthquake-affected area comprises mostly of flat valleys of the rivers Kupa and Sava, with tributaries. Both Kupa and Sava have been meandering and producing layers of soft sediments: layers of soft clays, silts, and sands. In the 1950s, the system of levees was constructed to protect the cities, villages, and agricultural fields from flooding. Understanding that climate changes increase the requirements on the levees, Croatian Waters (in Croatian: Hrvatske Vode), the institution in charge of water management in Croatia, started the process of acquiring the design of the improvements to the existing levee system. Therefore, the new geotechnical investigation was performed before the earthquake, and some of the obtained data are presented here. Immediately after the earthquake, the levees were inspected by the Croatian Waters and local GEER-team members. Different levels of damage and distress signs were noticed on seven levee sections as shown in **Figure 8.1** and **Figure 8.3**.

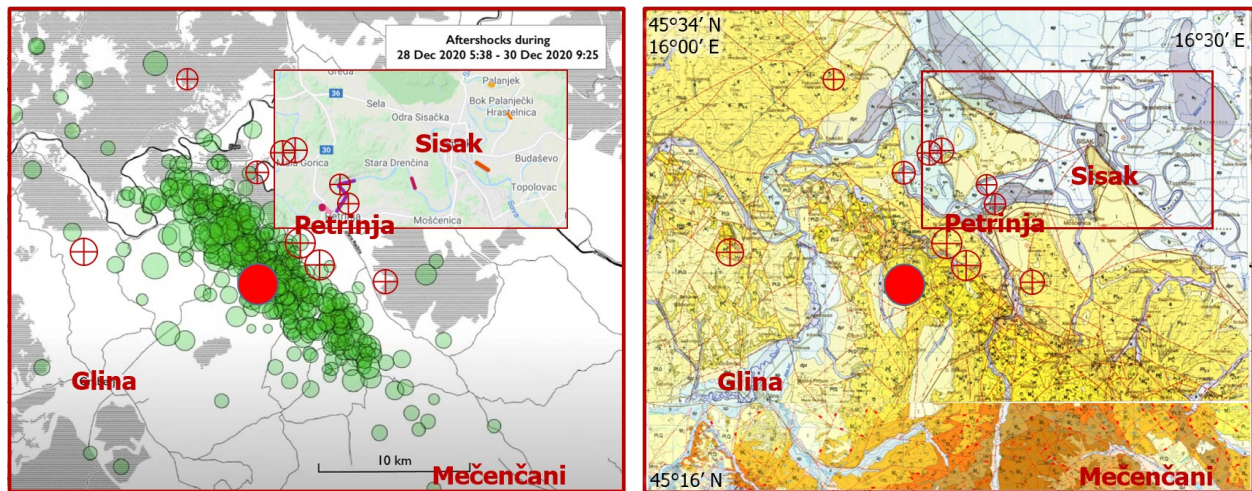


**Figure 8.1** (Left) Area damaged in the Petrinja earthquake. The full red circle shows the epicenter of the main shock, green circles show epicenters of earthquakes from 28 December to 30 December at 9:25 (Croatian Seismologic Survey 2020), and red circles with crosses show epicenters of earthquakes of magnitudes above M2.5 from December 2020 to April 2021 in the area. The inner frame shows the area of the damaged levees as given in detail in the next figure. (Right) Geologic maps of affected areas (Pikija 1987, Šikić 2014).

**Figure 8.2** shows a section of the geologic map (Pikija 1987) for the damaged areas and **Figure 8.3** is a closeup view of the geology map showing the area of the damaged levees. The upper layers – mostly around 6 to 8 m depth – of the inspected areas consist of clays serving as the foundation for the levees. The levees were built of local clays as well, in a trapezoidal shape. Levee maintenance consists of visual checks of the levees and nurturing the grass cover. Apart from occasional mole holes, no other problems could be noticed. Mostly agricultural fields cover the

dry side of the levees. Two days after the earthquake Croatian Waters started with urgent works on the levees at locations Galdovo and Palanjek. In 3 weeks, the secondary levees or repairs on the levees were finished on six seriously damaged levee sections. Box barriers were used to build secondary levees on Galdovo (740m), Palanjek (250m), Krnjica (530m), and Stara Drenčina (580m). Aftershocks caused deterioration of the damages resulting in the opening of 8 new locations until the middle of March.

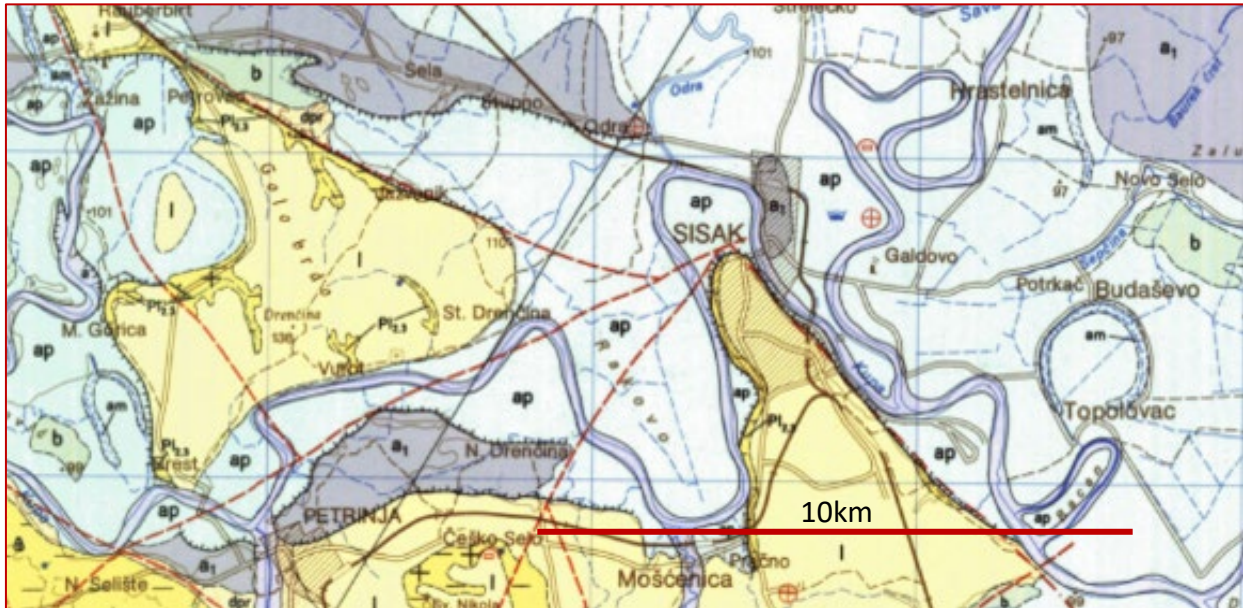


**Figure 8.2** Section of the geologic map near Sisak (Pikija 1987) as shown by frame in Figure 8.1.

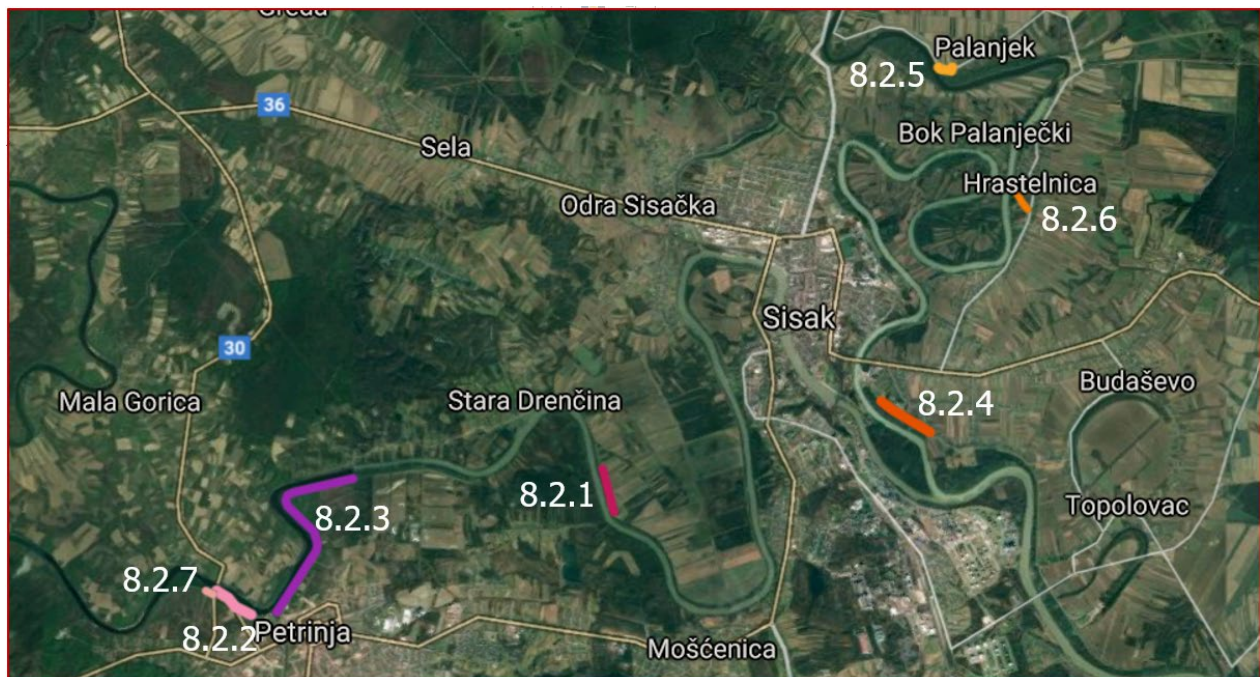


**Figure 8.3** Locations of damaged levees on the Google Map as shown by frame in Figure 8.1. Individual stretches of the levees are shown in the corresponding indicated subchapters.

## 8.2 Performance of Levees during Croatia M<sub>w</sub>6.4 earthquake

On six sections (**Figure 8.3**) longitudinal cracks appeared on the levees or near them. Near a few of the cracks, sand ejecta was visible, but around most of the damaged sections, ejecta was found on the distance of several meters or more. Damage was also observed on the connection of two perpendicular levees (Palanjek) and on the connection of a levee and a canal (near bridge Brest) where cracks perpendicular to the levee were seen. Typical damage is shown by location in the following sections with some additional details on the subsurface conditions where available.

### 8.2.1 Section of the levee south from Stara Drenčina, on the left bank of the Kupa river

The levee on the left bank i.e. eastern side of the Kupa river near Stara Drenčina exhibited a series of longitudinal cracks with some being near the levee on both sides throughout the 550m section. This levee was built around 30 m from the river, is 2 m in height with an approximately trapezoidal cross-section with side slopes of around 30°. This section is at a distance of 11 km from the epicenter.

The crack which spreads across the crest and continues down the slope of the levee extending for about 30 m along both sides of the levee is shown in **Figure 8.4** and **Figure 8.5** from above, in **Figure 8.7** on the field side, and **Figure 8.8** and **Figure 8.9** on the river side. Cracks are vertical in general but irregular in shape, so a maximum depth of 2 m was measured.

On both sides in the field irregular ejecta was found, the longest stretch being approximately 60 m long as seen in the air photo in **Figure 8.10**.

Information on the subsurface soil conditions through a borehole conducted by Geokon-Zagreb in 2015 (Geokon-Zagreb 2016) for the upgrade of the levee was available near the crack and is shown in **Figure 8.12**. The levee is underlain by 7 m of clays, which are underlain by a 0.50m clayey sand layer, and finally a mixture of poorly graded gravel and sand.



**Figure 8.4** Cracks across and along the levee (Photo documentation: Geokon – Zagreb LLD, January 7, 2021, 45.4614N, 16.3358E).



**Figure 8.5** Cracks across and along the levee (Photo documentation Geokon – Zagreb LLD, January 7, 2021, 45.4614N, 16.3358E).



**Figure 8.6** Crack across and along the levee (21.2.2021.; 45.46142N, 16.33580E). Secondary levee is visible in the distance.

In the first days after the earthquake, Croatian Waters started building a secondary levee far enough on the field side to prevent flooding. The cracks on the river side and the deformation of the slope towards the river make the riverbank unstable.



**Figure 8.7** Crack across and along the levee (21.2.2021.; 45.46130N, 16.33592E).



**Figure 8.8** At the river side of the levee crack is 2 m deep (21.2.2021.; 45.4612192N, 16.3358308E).



**Figure 8.9** At the river side of the levee (21.2.2021.; 45.4612015N, 16.3358606E).



**Figure 8.10** Ejecta in the field: length approximately 60m (Photodocumentation Geokon-Zagreb d.o.o.; January 7 2021; 45.46006N, 16.33759E).



**Figure 8.11** Ejecta in the field (21.2.2021.; 45.4611943N, 16.3358866E).

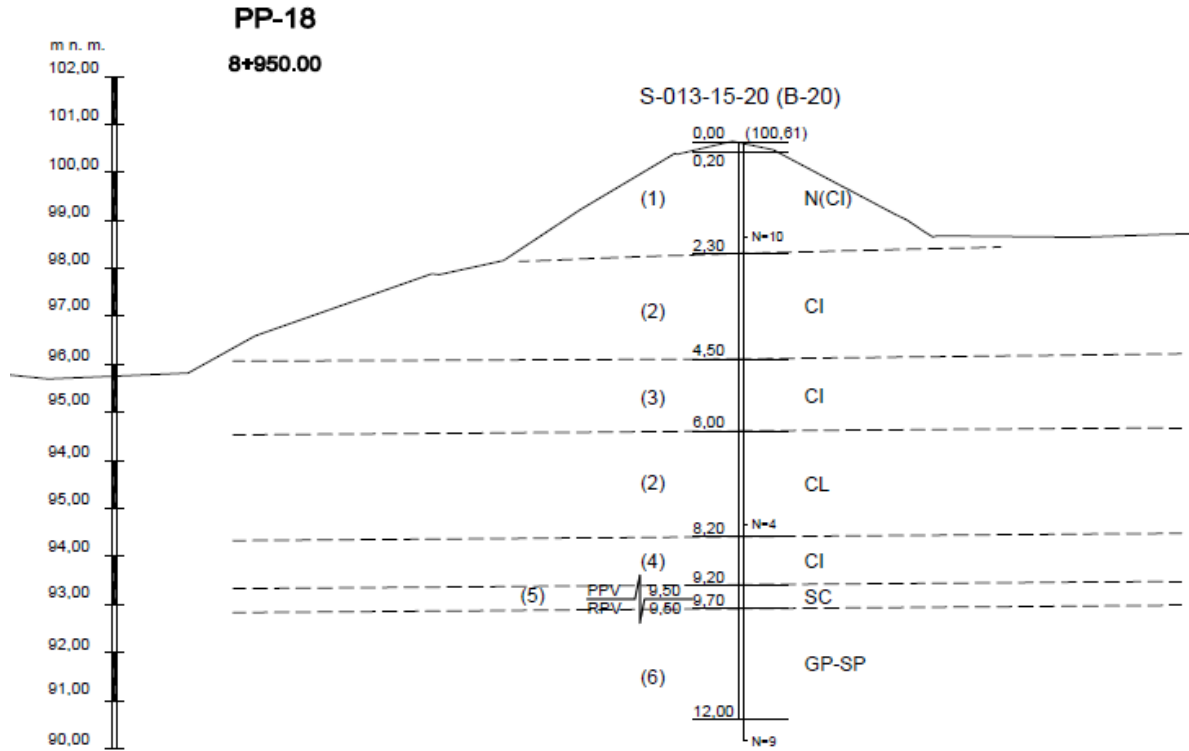


**Figure 8.12** Cross-section of the levee south from Stara Drenčina, on the left bank of the river Kupa at the position 45.46134N, 16.33583E (Geokon – Zagreb LLD 2016).

### 8.2.2 Section of the levee south near Petrinja, on the right bank of the Kupa river from the Bridge Brest to the Beach

Along the levee from Bridge Brest downstream to the Beach, on the right (southern) bank, cracks have been found along with the tow as shown in Figure at the distance of about 1m and width up to 7 cm. Liquefied sand was ejected on the other side of the levee, in the fields. Previous geotechnical investigation (Geokon-Zagreb LLD, 2021) shows the presence of silty sand from the depth of about 2 to 4m to about 5.5 to 5.8m.



**Figure 8.13** Typical cracks near the levee toe (6 February 6, 2021; 45.4450N, 16.2660E).



**Figure 8.14** Liquefied sand ejecta on the field side of the levee (45.4453N, 16.2649E).

### 8.2.3. Section of the levee south near Petrinja, on the right (southern) bank of the Kupa river from the Beach towards east

Along the levee from the Petrinja Beach, at a length of 4 km, cracks are visible on both sides the levees. Cracks are irregular in shape and the maximum measured depth is 2m. Typical cracks are shown in the **Figure 8.15-17**. In some locations, liquefied sand ejecta is found. **Figure 8-18** shows one of the cracks with liquefied sand. Croatian Waters in the first days after the earthquake started building secondary protection visible in **Figure 8-19**.



**Figure 8.15** One of the deep cracks in the levee north of Petrinja (February 19, 2021; 45.4593N, 16.2738E).



**Figure 8.16** Typical cracks on the river Kupa side of the levee north from Petrinja (19 February 2021; 45.4591N, 16.2739E)



**Figure 8.17** Typical cracks on the river Kupa side of the levee north from Petrinja (February 19, 2021; 45.4592N, 16.2740E).



**Figure 8.18** Typical crack on the field side of the levee north from Petrinja with liquefied sand ejecta (19 February 2021; 45.4613N, 16.2748E)



**Figure 8.19** Secondary levee built by Croatian Waters (19 February 2021; 45.46180N, 16.2775E).

#### 8.2.4 Section of the levee south in Galdovo, on the left (eastern) bank of the Sava river

The levee on the left bank i.e. the eastern side of the Sava river in Galdovo Bridge experienced a series of longitudinal cracks with some being near the levee on both sides of the 1000 m section. The levee is approximately 3 m in height with a trapezoidal cross-section, sitting 100 m to 140 m away from the river bank. This section is at a distance of 16 km from the earthquake epicenter. The liquefaction near the levee was most dramatic as seen in the video recorded about 100m from the levee on the protected side (Pavlič, 2020) – a snapshot is shown in **Figure 8.20**.



**Figure 8.20** A snapshot from the video made during the M6.4 earthquake near Galdovo levee (Udruga Kas, recorded by Daniel Pavlič (Pavlič, 2020) (45.4735, 16.3926)

The longitudinal cracks are up to 50 cm wide and there is also vertical displacement observed as can be seen in **Figure 8.21 a-c**. A nearby boring from the year 2013. (Geokon-Zagreb LLD 2021) shows the presence of medium density sand at 5 m depth as shown in **Figure 8.21d**. Regarding the widespread liquefaction in the area, this could suggest that liquefaction may have played a role in the deformation of the levee and surrounding ground. Croatian Waters built a secondary levee to protect 800m of the primary levee. The densest are the cracks around the discharge pipe through the levee - where Croatian Waters built separate protection as seen in **Figure 8.22**.

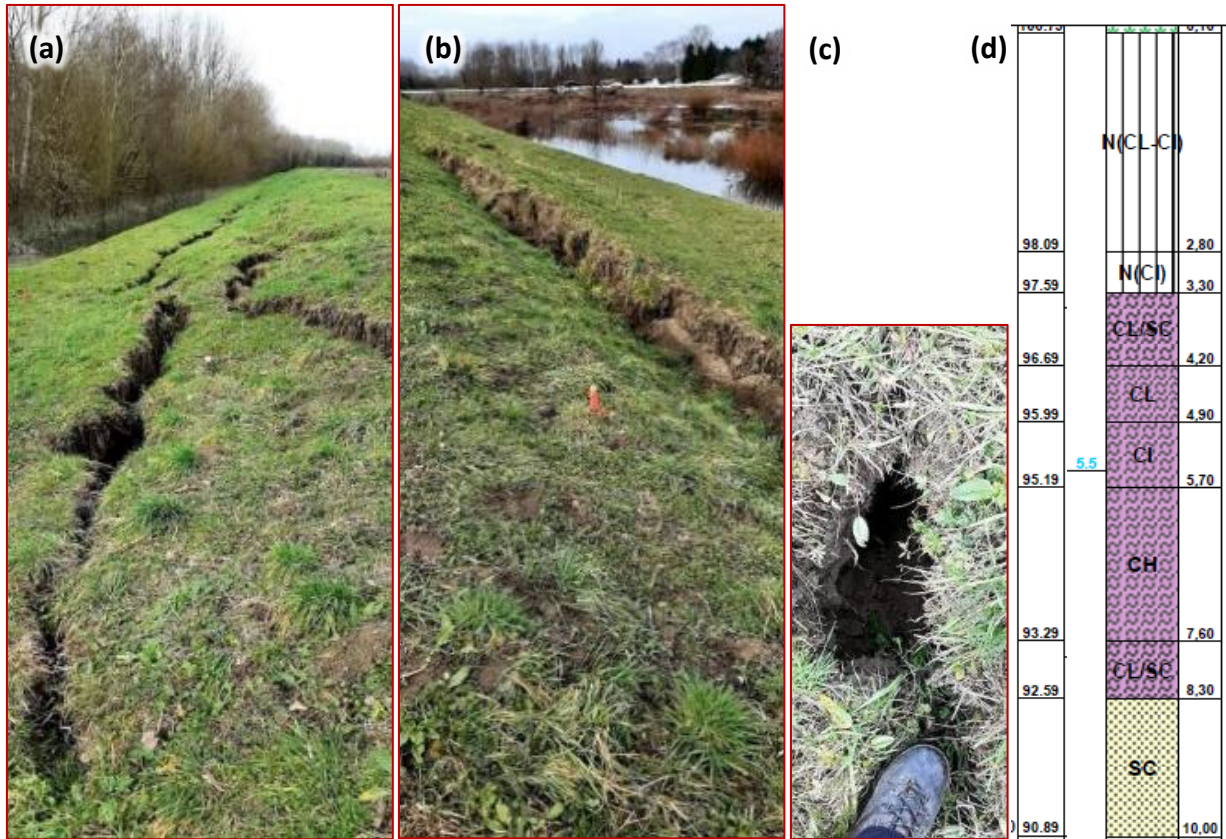


**Figure 8.21** (a) Some of the cracks at the river side of the levee (45.4704728N,16.3957025E), and (b) on the opposite side (45.47059N,16.3954E), (c) typical crack (45.4705N,16.3957E). (d) Borehole done in the year 2017 (Geokon-Zagreb LLD 2021) on a nearby location shows the presence of clayey sand at the depth of around 5 m below the ground surface – the upper 3.3 m represent the levee.

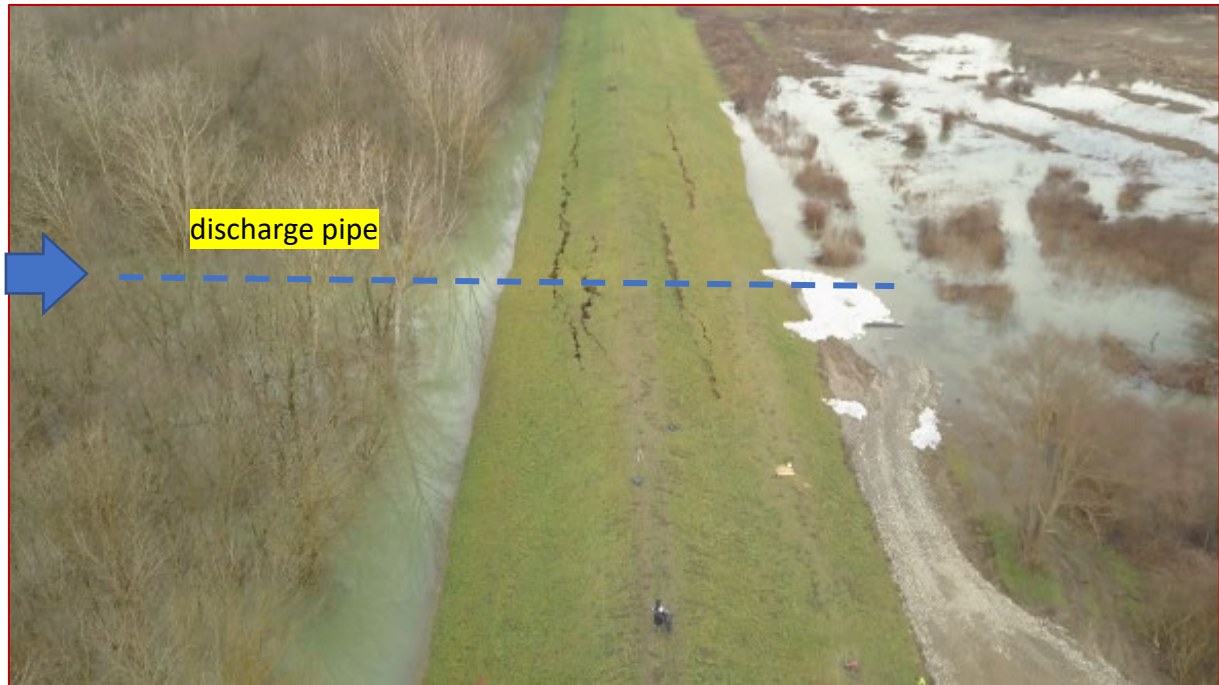


**Figure 8.22** Two air views of the southern part of the damaged levee with a high level of the Sava river. The white sandbags were installed right after the earthquake on the discharge pipe location, also the secondary levee was built. (Photo documentation of Geokon – Zagreb LLD, 45.4708 16.3952).

### 8.2.5 Section of the levee in Palanjek, on the left bank of the Sava river

At a distance of 19.5 km from the epicenter, the levee on the left bank of the Sava river was damaged over a length of approximately 250m in the area shown in **Figure 8.23**. Transverse cracks followed by vertical displacement of about 50 cm occurred near the location where two levees meet as shown in **Figure 8.24**. Longitudinal cracks along the road and the toe are shown in **Figure 8.25**, together with some ejecta on the river side. On the field side, more sand was ejected to the surface as seen in **Figure 8.26a**. A sand layer was found at a depth of about 5m as shown in **Figure 8.26b**.



**Figure 8.23** Map of the damaged section of the levee on the left bank of the Sava river near Palanjek.



**Figure 8.24** (a,b) Transverse cracks and settlement. (45.518732N, 16.4028826E), (c) longitudinal cracks along the levee toe on the eastern side.

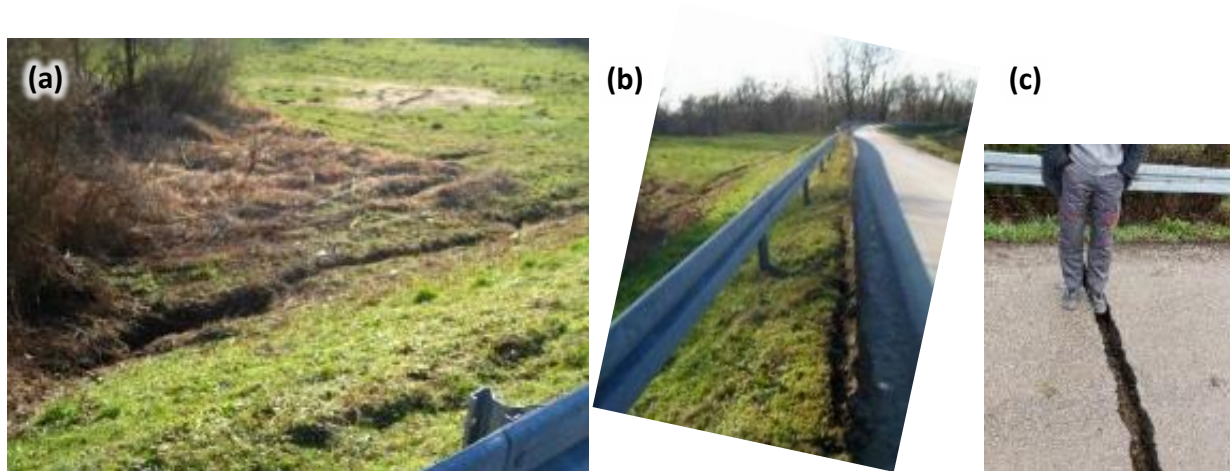


**Figure 8.25** (a) Sand ejecta in the field, longitudinal cracks along the levee along the toe and (b) along the crest and settlement. (45.51874, 16.402). (c) Transverse crack on the road on the levee crest (Photo documentation Geokon – Zagreb LLD).

(a)



(b)

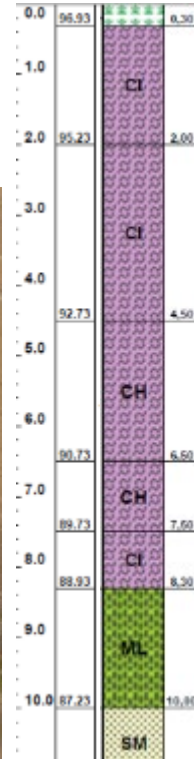


**Figure 8.26** (a) Aerial view of the liquefaction in the field near Palanjek. (45.520N, 16.402E, Photo documentation Geokon – Zagreb LLD. (b) Borehole from 2013 (Geokon-Zagreb LLD 2021) on a nearby location shows the presence of clayey sand at the depth of around 5 m below the ground surface.

### 8.2.6. Section of the levee in Hrastelnica, on the left bank of the Sava river

At a distance of 19km from the epicenter, along the section of the left bank of the Sava river, sand ejecta are visible on both sides of the levee, on the levee slopes, near the toe, and in the fields. In addition to some smaller areas, sand ejecta are visible on the river side in the field along the stretch of 40 m of the levee, and at a distance of 40 m or more as seen in **Figure 8.27**. A similar area is covered with sand on the opposite side as shown in **Figure 8.28**. A nearby borehole from 2017 (Geokon-Zagreb LLD 2021) shows the presence of a sand layer at a depth of 3 m (**Figure 8.28c**).



**Figure 8.27** (a, b) Liquefied sand on the river side of the levee near Hrastelnica from the levee toe to the distance of 40 m, and cracks on the levee (45.5007N, 16.4162E).



**Figure 8.28** Liquefied sand on the dry side of the levee near Hrastelnica (45.5015N, 16.4163E). Borehole from 2017 (Geokon-Zagreb 2021) on a nearby location shows the presence of clayey sand at the depth of around 5 m below the ground surface.

### 8.2.7. The section near the Brest Bridge in Brest Pokupski, near Petrinja (Ingrid Tomac)

A levee south of Brest Bridge along the Kupa river was damaged in two locations. The first location is at the contact of the levee and the bridge embankment and the second is where a water channel perpendicularly crosses the levee. **Figure 8.29** shows the plan view and **Figure 8.30** damaged concrete channel under the levee and remediation works that were performed immediately after the earthquake. The images were taken on March 22<sup>nd</sup>, 2021.



**Figure 8.29** Plan view of the Brest Bridge and levee damage in Brest Pokupski, near Petrinja (45.4476N, 16.259E) (source: Ingrid Tomac)



**Figure 8.30** Levee damage and remediation works on the south bank Kupa river levee near the Brest Bridge in Petrinja (45.4478N, 16.2583E; 45.4475N, 16.2595E) (source: Ingrid Tomac).

## References

- Geokon-Zagreb (2016). *Geotehnički istražni radovi za rekonstrukciju lijevog kupskog nasipa Staro Pračno—Stara Drenčina od km 0+000 do km 11+692 na području Grada Siska*. Geokon-Zagreb Ltd., Zagreb
- Geokon-Zagreb (2021). *Izvanredni pregled oštećenja lijevog savskog nasipa na dionicama u Palanjku, Hrastelnici i Galdovu uzrokovanih potresom od 29.12.2020*. Geokon-Zagreb Ltd., Zagreb
- Pavlić D. (2020). *Potres u Sisku, 29.12.2020, rascjepi zemlje – likvefakcija tla* [Online]. Available at: <https://youtu.be/hH3AhtYMEKE>. (Accessed: 15 April 2021)
- Pikija, M. (1987). Osnovna geološka karta SFRJ 1:100.000, List Sisak L33–93. – Geološki zavod, Zagreb (1975–1986); Savezni geološki institut, Beograd. Available at request at <https://www.hgi-cgs.hr/osnovna-geoloska-karta-republike-hrvatske-1100-000/>
- Šikić, K. (2014): Osnovna geološka karta SFRJ 1:100.000, List Bosanski Novi L33-105. – stručne dokumentacije Instituta za geološka istraživanja, Zagreb. (manuskript) Available at request at <https://www.hgi-cgs.hr/osnovna-geoloska-karta-republike-hrvatske-1100-000/>

## 9 Infrastructure Damage (Jelena Bleiziffer, Igor Gukov, Ingrid Tomac, Sonja Zlatović, Petar Krešimir Žderić, Zvonimir Vlahović)

Infrastructure damage in Sisak-Moslavina County due to earthquakes on December 28 and 29 2020 that was recorded by the reconnaissance team, media and Croatian Roads is shown in this chapter. According to the Croatian Roads report, significant damages occurred on roads and bridges in Sisak-Moslavina, Karlovac, and Zagreb Counties. **Figure 9.1** shows an overview of the damage locations and causes as reported by Croatian Roads (Hrvatske ceste 2021). Reported co-seismic effects include cracks on roads and subgrade, re-activation of existing landslides as well as bridge columns, abutments, and bearings damage. The GEER reconnaissance was performed on bridges Brest, Galdovo, and Gromovi and Old Bridge in Sisak, while the rest of this chapter documents road damage as reported by Croatian Roads and media.

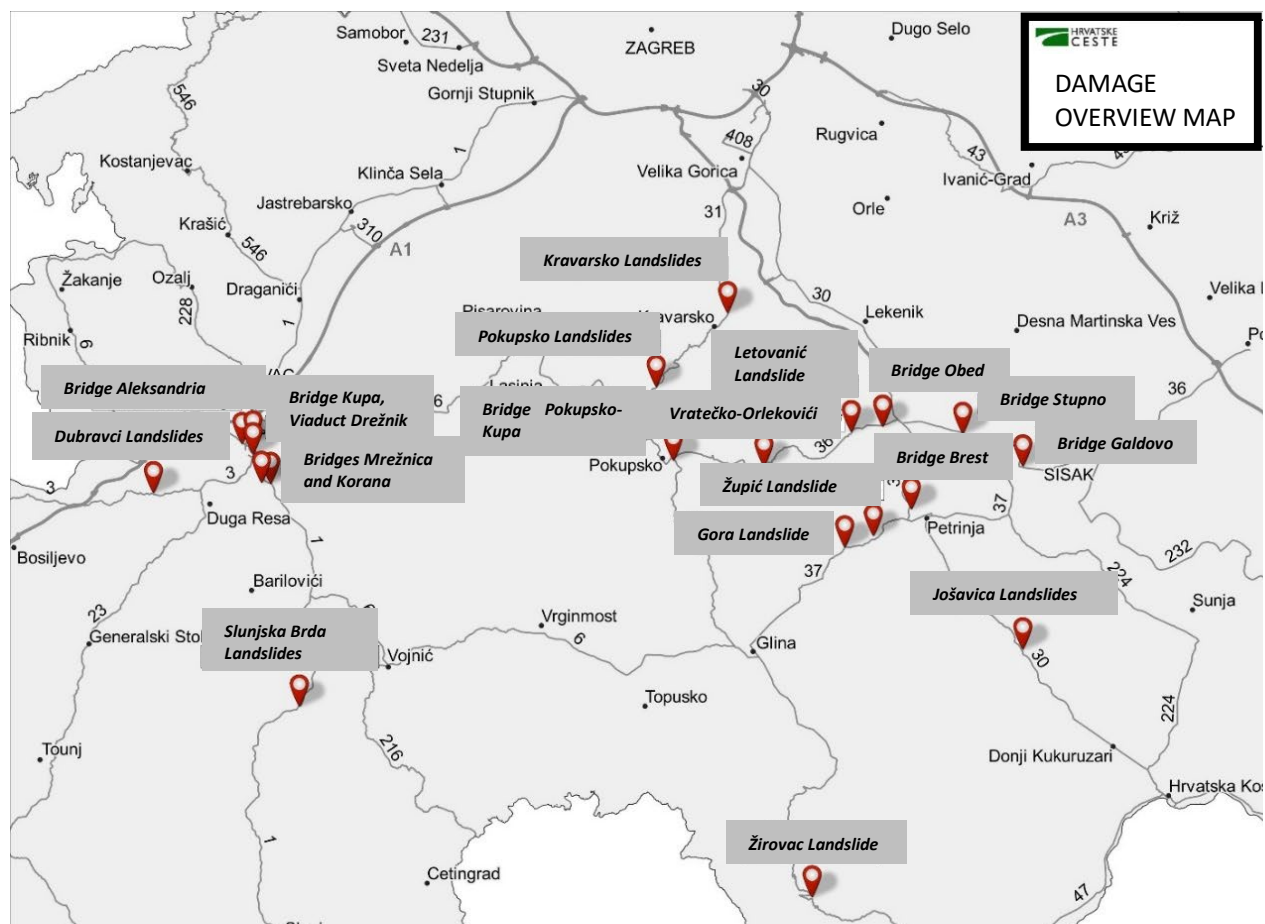


**Figure 9.1** A comprehensive infrastructure damage overview map in Sisak-Moslavina, Zagreb, and Karlovac Counties (source: Hrvatske Ceste - Croatian Roads).

## 9.1 Damage to Roads

The Sisak-Moslavina County roads include 11 state roads with a total of 413 km length, 84 county roads, and 170 local roads in the length of 1226.56 km total, where 647.09 km are county roads and 579.56 km are local roads, 1009.05 km are asphalt roads and 217.60 km is macadam. On top of that, there is 2000 km of uncategorized roads (Sisačko-moslavačka županija, n.d.; Županijska uprava za ceste Sisačko-moslavačke županije, n.d.). **Figure 9.2** shows specific locations of reported road damage.

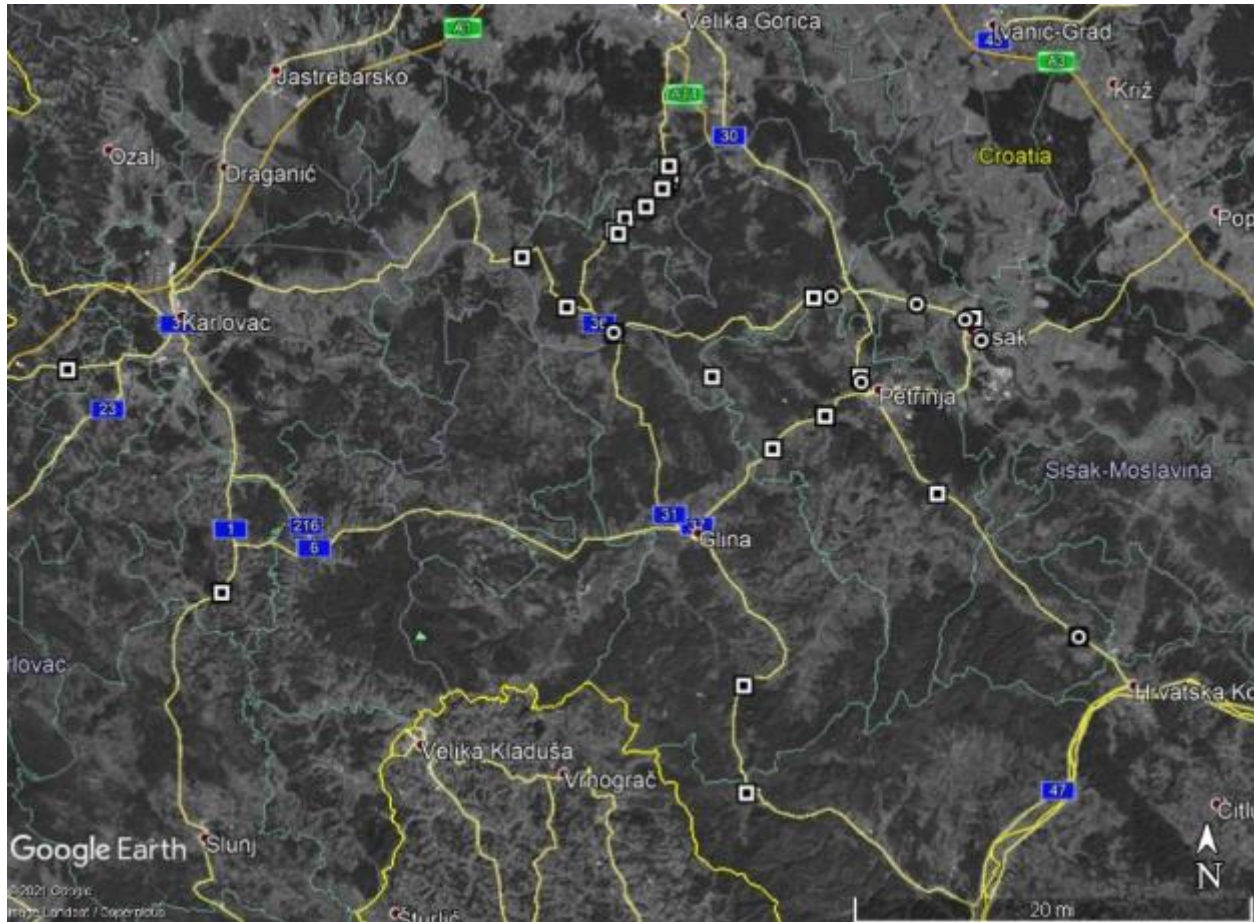


**Figure 9.2** Specific locations of road damage (squares) and damaged bridges (circle) (Justin Wong and Ingrid Tomac).

Asphalt and subgrade cracking occurred on roads from which roughly 95% are in Sisak-Moslavina County. Asphalt damage in perpendicular, parallel, or inclined direction from the road axes occurred as opening cracks and, in several instances, accompanied with vertical displacements, as shown in **Figure 9.3**.

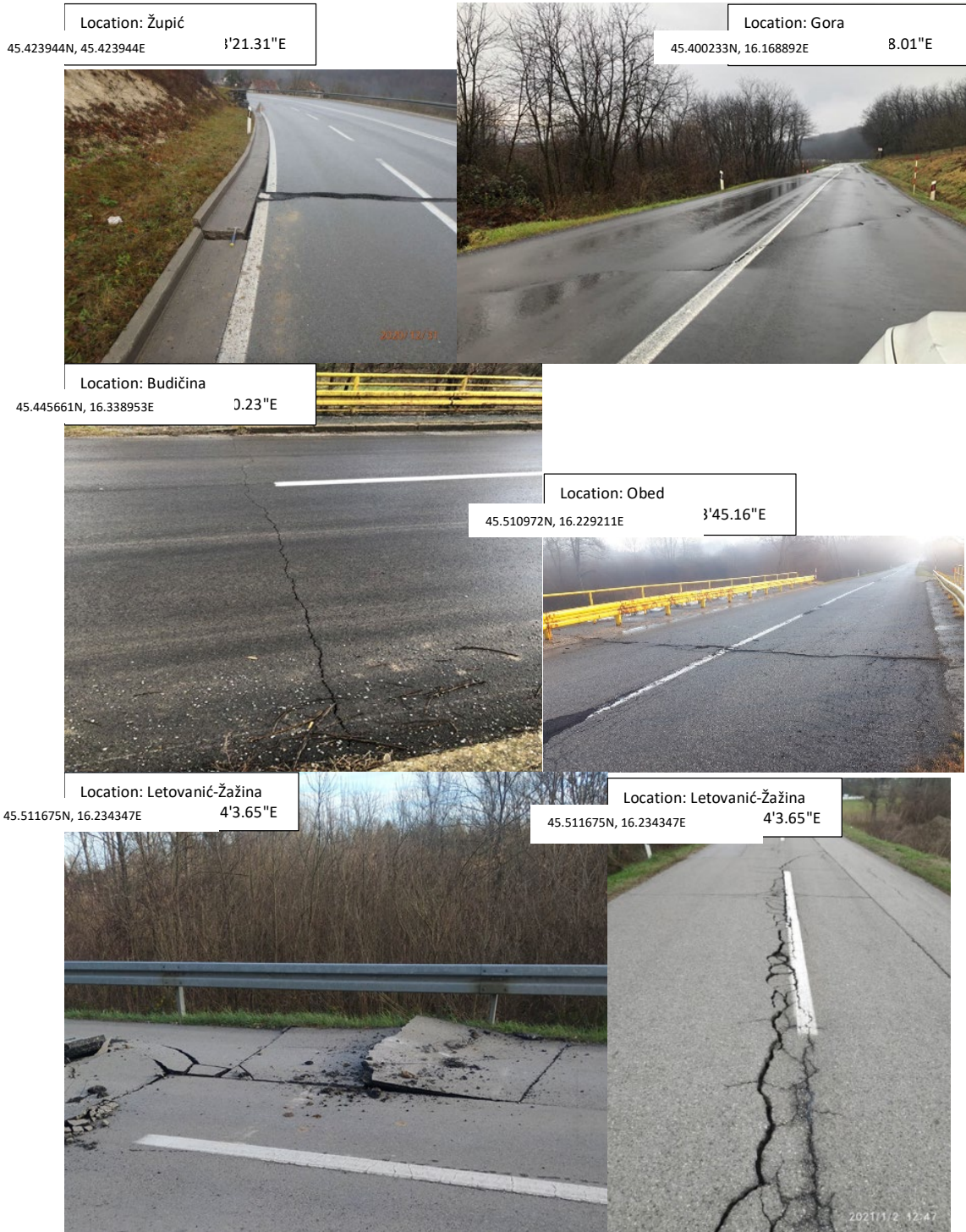


**Figure 9.3** Horizontal and vertical displacement cracks in asphalt perpendicular, parallel, or inclined towards the road axis in several locations (Source: Croatian Roads – Hrvatske ceste).

Road damage was associated with an adjacent slope stability failure, either as a road embankment loss of stability or as re-activation of previously known landslides. Croatian Roads report a series of reactivated landslides with referral to previous road repair works, pointing that

the slopes deformed additionally during the earthquake causing different levels of severity of road damage. Demonstrated effects span from thin asphalt cracks to cm-scale displacements, subgrade failure, and displacement and terrain slope displacement. Reported landslides are Landslide Župić, Landslide Gora, Landslide Jošavica, Landslide Vratečko-Orleković, Landslide Vratnik, Landslide Klasnić, Landslide Žirovac, 10 landslides on the state road DC31, landslide on the state road DC36, the state road DC1 near Brebornica, and the state road DC3 near Dubravci. **Figure 9.4** shows selected examples of a few severe sliding-related road damage as reported by Croatian Roads (2021).



**Figure 9.4** Road damage accompanied with adjacent slope instability.

## 9.2. Damage to Bridges

## ***Galdovo Bridge***

Galdovo Bridge is a bridge across the Sava river in the Sisak suburb of Galdovo. The current bridge was erected at the end of the 1980s, but it incorporates 3 columns from a previous bridge at the same location (Novak, 1984; Radić, Žderić & Puž, 2007). The previous, through steel truss bridge is estimated to date from 1895 (Novak, 1984). The bridge superstructure is a 4-span continuous half-through steel girder structure. Cross girders support a concrete roadway slab. Pedestrian and bicycle paths are provided on both sides (Radić, Žderić & Puž, 2007). The three columns are made of brick, with partial stone cladding. There is no information available on the foundation design (Novak, 1984). The inspection in the 1980s, before the decision of erecting the new bridge on the existing supports, revealed that columns are in good condition, with no noticeable damage, cracks, or deformations, except at the top, immediately below the bearings (Novak, 1984). New cap beams were erected on top of columns to support the new structure (Radić, Žderić & Puž, 2007; Urbane ideje, 2018), as well as new bridge abutments, at a different location than those of the previous bridge (Novak, 1984; Radić, Žderić & Puž, 2007; Urbane ideje, 2018). The bridge was hit by a missile during the war in the 1990s, causing a rupture in the web of the main girder. The damage was subsequently repaired (Radić, Žderić & Puž, 2007). The bridge was once again repaired in 2019/2020 (dpreradus, 2020; Marković, 2020). The repair works addressed RC slab and steel bridge structure, as well as asphalt layers on the bridge and on the approach roads (Sisačko-moslavačka županija, 2019; Urbane ideje, 2018).

**Figure 9.5** shows an aerial image of the Galdovo Bridge. Some liquefaction evidence in the proximity of the Galdovo bridge is shown in Chapter 7. Geotechnical soil reconnaissance revealed cracks in soil around the east abutment and the adjacent column on the left riverbank, while no visible soil surface damage was observed on the right riverbank near the bridge (**Figures 9.6 and 9.7**). It should be noted that there is a shaft in the area between the east abutment and the adjacent column to which some cracks in soil seem to be directed.



**Figure 9.5** Galdovo Bridge over the river Sava (source: Google Maps).



**Figure 9.6** Left Sava riverbank, east bridge abutment a) north face, upstream, b) north face, upstream and c) south face, downstream (45.4790N, 16.3854E).



**Figure 9.7** Left bank of Sava, soil cracks between the abutment and the adjacent column (45.4790N, 16.3854E).

Damage suggests that the roadway slab rotated clockwise, where the western bridge portion displaced towards the north and the east towards the south. This can particularly be observed at

the east abutment. Following are conclusions from the inspection carried out on February 6, 2021:

- There was a longitudinal displacement during the earthquake of at least 8 cm (**Figures 9.6 – 9.10**) – evidenced by pulling out of the railing at its expansion joint, and misalignment of the bridge finger expansion joint,
- There was a failure of transversally unmovable bridge bearing on the east abutment, and permanent 15-cm transverse displacement of the bridge (**Figures 9.6 and 9.9**). The bearings on the columns also suffered damage due to the bridge rotation.

In addition, concrete spalling was noticed on several joints of longitudinal steel girder-steel cross girder and concrete roadway slab.



**Figure 9.8** Galdovo Bridge, displacement of the bridge expansion joint on the east abutment (45.4790N, 16.3854E).



**Figure 9.9** Galdovo Bridge, 15-cm transverse displacement of the bridge railing (45.4790N, 16.3854E).



**Figure 9.10.** Galdovo Bridge, measuring longitudinal displacement on railing and expansion joint (45.4790N, 16.3854E).



**Figure 9.11** Galdovo Bridge, damaged bearing on the east abutment (45.4790N, 16.3854E).

**Figure 9.12** shows inclined trees on the riverbank, which typically indicate recent in inclined trees or historical in partially inclined trees slope instability. An absence of images and information before an earthquake makes it difficult to draw any conclusions about earthquake effects.



**Figure 9.12** Inclined trees on the left bank of Sava river, the eastern side of the bridge, view towards the south (45.479N,16.385E).

As a part of the reconnaissance effort, a Lidar scan of what was identified as the bridge span with the most obvious damage was carried out on March 27, 2021, i.e., the bridge span between the east abutment and the adjacent column. 25 setups (**Figure 9.13**) were linked with 28 links in a bundle with a bundle error of 5 mm (NHERI RAPID Facility, 2021). The point cloud data obtained has not yet been fully analyzed, but it might provide further data. An example of the point cloud obtained is shown in **Figure 9.14**.

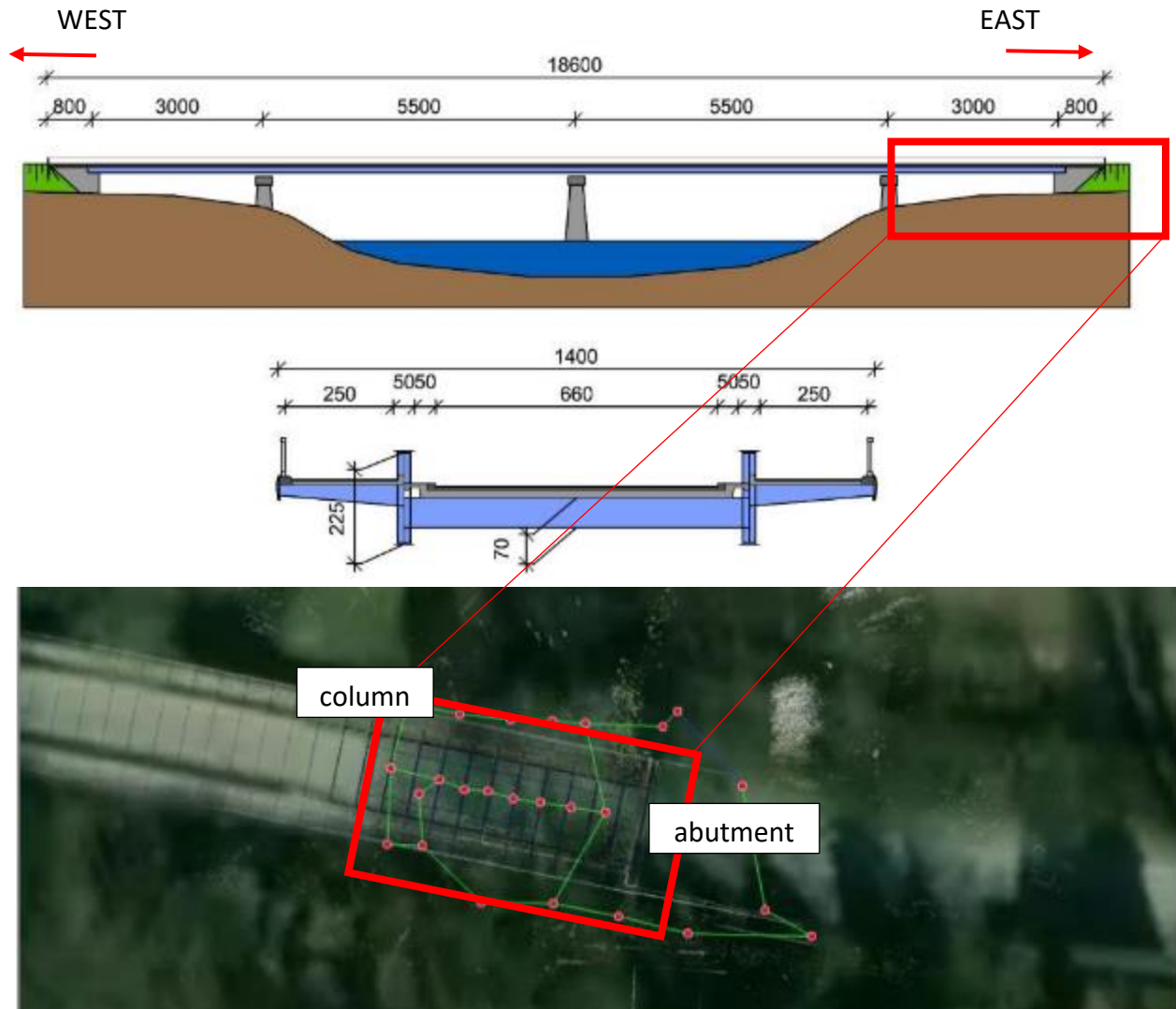


**Figure 9.13** Galdovo Bridge, Lidar setups (location indicated on longitudinal bridge section obtained from Radić, Žderić & Puž, 2007).



**Figure 9.14** Galdovo Bridge, Point cloud of the east abutment.

### ***Gromovi Bridge***

The original blueprint of the Gromovi Bridge dates from 1971, as shown in **Figure 9.15**. Gromovi Bridge is in Sisak and crosses river Kupa, with an axis oriented north-south. The bridge consists of a central 3-span structure, and approach viaducts at both sides. Bridge superstructures – in steel for the central portion of the bridge, and prestressed concrete for the approach viaducts, are supported by a series of 2-column piers consisting of 2 inclined columns and a cap beam with cantilevers on top. The piers of the approach viaducts are founded on shallow concrete spread footings, 4.5 x 4.5 m, 1.0 m deep embedded 2.5 m under the soil surface. Retrofit in 2019 focused on the steel structure of pedestrian passageways, the central bridge end columns, which provide a transition from concrete to steel superstructure and vice versa, and bearings on positions S13 and S16. The column S13 top portion, which had a crack, was strengthened with concrete anchors. Columns of the central steel bridge are founded on 100 cm in diameter reinforced concrete circular piles 10 m deep. There are 12 piles under each column. **Figure 9.15** shows the original bridge with the original foundation types.

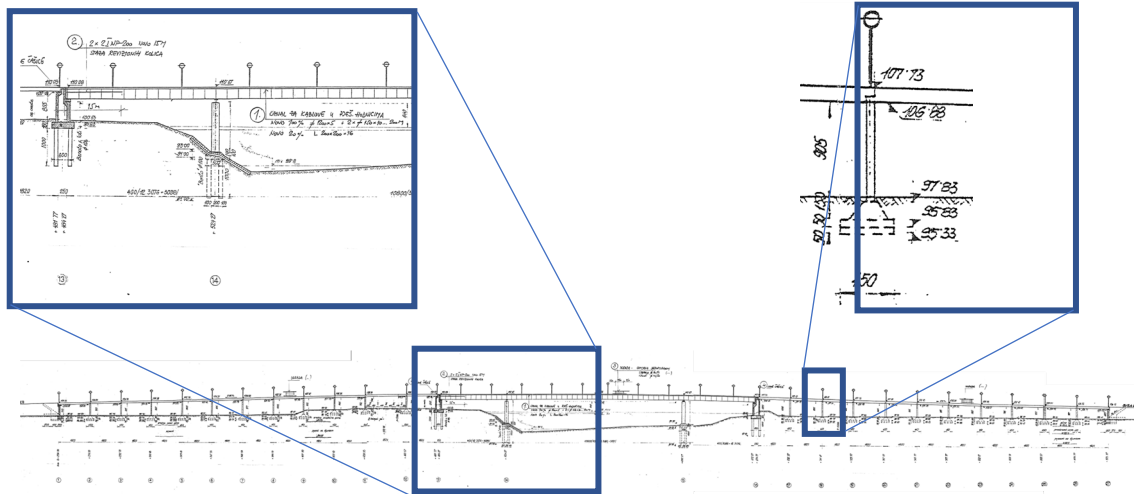


**Figure 9.15** An original blueprint of Gromovi Bridge from 1970 (ŽPB, 2002).

Damage was detected after the earthquake on columns S4, S7, and S20 at the column-cap beam joint. On S4 (**Figure 9.16a**), the west column has horizontal cracks on the side facing south. On S7 (**Figure 9.156b**) the east column also has horizontal cracks on the south-facing side. On S20 (**Figure 9.16c**), the east column, the eastern and southern face at the top of the column show surface cracks.

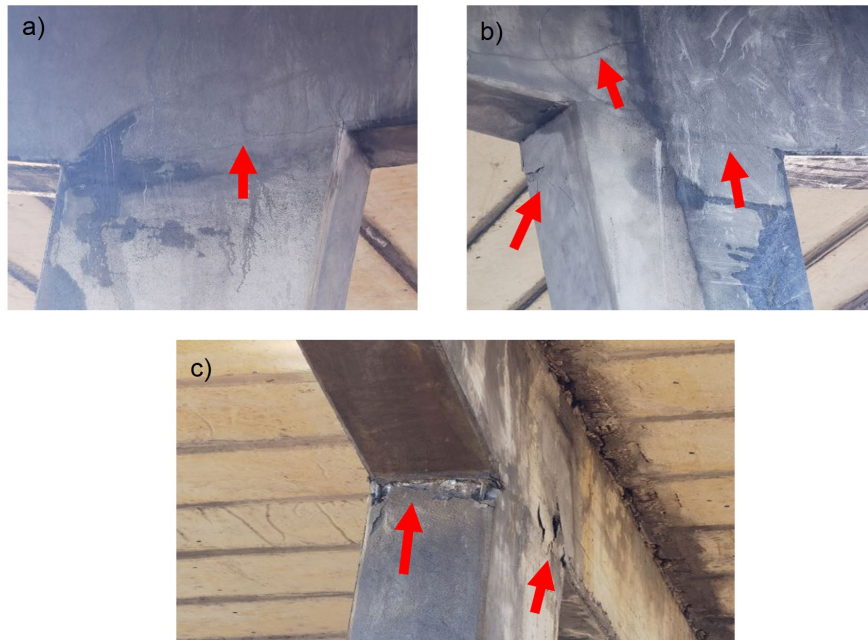


**Figure 9.16.** a) damage at S4, b) damage at S7 and c) damage at S20. (source: Earthquake Petrinja 29 12 2021 GP HC\_Road and bridge damage report", in Croatian).

Column at S13 is the edge column under the steel span on the northern side (**Figure 9.17**). Previously existing crack was repaired with concrete anchors during the retrofit in 2019. **Figure 9.17 b**) shows the side ramp as it was before the retrofit. The ramp is a reinforced concrete viaduct supported on elastomeric bearings, that suffered a visible crack on the asphalt along with the connection to the bridge and was sideways hitting the S13 column during the earthquake and caused local column damage, which is only superficial. **Figure 9.18** shows cracks on the soil surface between S4 and S5, which are in the east-west direction, perpendicular to the bridge longitudinal axis. To summarize, the damage on the Gromovi Bridge was detected on the columns and connections between columns and the roadway slab on the northern side of the Kupa river. The damage suggests a lateral spread of the northern embankment. It is interesting to note that most of the damage occurred on the parts of the bridge with shallow foundations, while the deep-founded bridge supports were not damaged. **Figure 9.19** links an aerial image obtained after the earthquake where liquefaction was detected on a wider area of the city of Sisak, including both sides of the Gromovi Bridge. The approximate position of identified damage is also shown.



**Figure 9.17** a) reinforced pre-existing crack and dilation above on the column S13 on the northern side of the Kupa river and b) side ramp. (Source: Metal Projekt Ltd).



**Figure 9.18** Cracks in soil between S4 and S5 (source: Hrvatske ceste 2021).



**Figure 9.19** Aerial view of the area with “Most Gromova” bridge after the earthquake.

### ***Brest Bridge***

Brest Bridge crosses Kupa river at Brest, near Petrinja. The current bridge was erected in 1998 (DDmontaza, 2016), as the superstructure of its predecessor was blown up in 1991, during the war (Radić et al., 2007). The bridge superstructure is a 2-span continuous half-through steel girder structure. Cross girders support a reinforced concrete roadway slab. Pedestrian and bicycle paths are provided on both sides (Radić et al., 2007). The superstructure was erected on supports of the previous bridge, which were strengthened by adding new reinforced concrete cap beams (Radić et al., 2007). It was decided to incorporate the supports of the earlier bridge (dating from 1898) on a basis of the following considerations (Lazić, 1998):

- detailed inspection and surveying carried out in 1996 revealed no settlement or inclination,
- a long period of consolidation (100 years),
- even though the new structure is much heavier (3x), this should not adversely affect the stress in the ground, as the weight of the foundation and the support is very large.

The column and abutments were constructed of cut stone filled with lean concrete and founded on 12-18 m deep caissons (Lazić, 1998). Fixed pot bearings (6000 kN) are installed on the central pier, while the pot bearings on the abutments (2000 kN) are movable in one direction (Lazić, 1998). Expansion joints KT-160 are installed at both abutments (Lazić, 1998). Damage observed includes settlement and damage to bridge embankment and asphalt layer just before the bridge, and damage to the bridge bearing and bearing pedestal on the column, as shown on **Figure 9.20**.

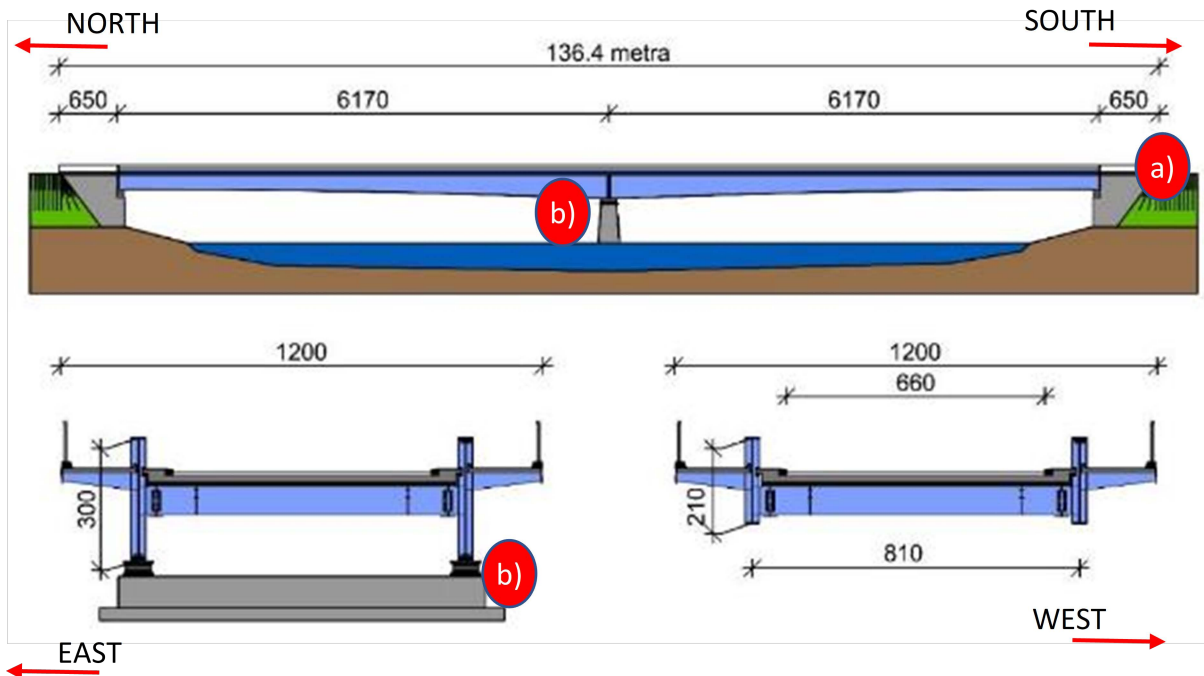


**Figure 9.20** Brest Bridge damage indicated in longitudinal and cross-section of the bridge (from Radić et al., 2007): a) settlement of the sidewalk before the abutment, b) damage to the bearing pedestal on the column (right).

### **Old Bridge in Sisak**

The Old Bridge in Sisak is an arch bridge across the Kupa river from 1934. A portion of its brick railing fell during the earthquake as illustrated in **Figure 9.21 (a&b)**. Some other railing portions were displaced (**Figure 9.21 c,d&e**), but according to an article (siscia.hr, 2018) they were damaged even before the earthquake. Some damage is visible in masonry above the arch, close to an abutment.



**Figure 9.21** Damage to the pedestrian railing of the Old Bridge in Sisak: a (45.483N, 16.371E), b (45.4829N, 16.3705E), c (45.4829N, 16.3707E), d (45.4829N, 16.3707E), e (45.4830N, 16.3707E), f (45.4825N, 16.3692E).

## References

- Hrvatske ceste d.o.o. – Croatian Roads Ltd. (2021). *Izveštće o štetama od potresa u Sisačko-moslavačkoj županiji koji su se dogodili 28. i 29.12.2020.* (in Croatian; *Earthquake Petrinja 29 12 2021 GP HC\_Road and bridge damage report*). Zagreb, Croatia.
- dpreradus (2020) 'Obilazak mosta u Galdovu', SISA.INFO, 17 May [online]. Available at: <https://www.sisak.info/2020/05/17/obilazak-mosta-u-galdovu/> (Accessed: 4 February 2021)
- Đuro Đaković Montaža (2020) *Reference - Mostovi*, Available at: [http://www.ddmontaza.hr/data/source/file/2017\\_10\\_16%20Reference%204\\_2016%20Mostovi.pdf](http://www.ddmontaza.hr/data/source/file/2017_10_16%20Reference%204_2016%20Mostovi.pdf) (Accessed 21 April 2021)
- Lazić, D. (1998) Obnova mosta preko Kupe kod Bresta, *Ceste i mostovi*, 44(1-6), p.41-44
- Marković, S. (2020) 'Završetak sanacije Galdovačkog mosta u Sisku', PORTAL53, 14 May [online]. Available at: <http://portal53.hr/zavrsetak-sanacije-galdovackog-mosta-u-sisku/> (Accessed: 4 February 2021)
- NHERI RAPID Facility (2021) GEER - Croatia, Galdovo Bridge Cyclone REGISTER 360 Registration Report
- Novak, J. (1984) Naši mostovi – Most preko Save kod Galdova, *Ceste i mostovi* 30 (8), p.339-341
- Radić, J., Žderić, Ž., Puž, G. (2007) *Vrijeme rušenja, vrijeme građenja*, Zagreb: Hrvatska sveučilišna naklada
- Sisačko-moslavačka županija (2019) *Obilazak mosta u Galdovu prije početka sanacije* [Online]. Available at: <https://www.smz.hr/6369-obilazak-mosta-u-galdovu-prije-pocetka-sanacije> (Accessed: 4 February 2021)
- Sisačko-moslavačka županija (n.d.). *Natječaji i javni pozivi/smz/O županiji/Infrastruktura* [Online]. Available at: <https://www.smz.hr/natj/javni/details/133-javni-poziv-potpورا-subvencija-za-organizirani-dolazak-turista> (Accessed: 15 February 2021)
- Urbane ideje d.o.o. (2018) *Dokumentacija za nadmetanje Most Galdovo na državnoj cesti DC36 (Izvedbeni projekt sanacije)*, Samobor: Urbane ideje Ltd.
- Županijska uprava za ceste Sisačko-moslavačke županije (n.d.). *Cestovna mreža Sisačko-moslavačke županije* [Online]. Available at: <https://www.zuc-sk.hr/index.php/ceste> (Accessed: 15 February 2021)
- Željeznički projektni biro Ltd. (ŽPB). (2002). *Sanacija cestovnog mosta preko rijeke Kupe u Sisku na D-37. Čelična konstrukcija i ograda. Izvedbeni projekt broj ev. 3088D/2002.* Zagreb: Željeznički projektni biro Ltd.

## 10 Complementary Geotechnical and Geophysical Investigation Works (Ingrid Tomac, Ivan Salković, Biljana Kovačević-Zelić, Dubravko Domitrović, Helena Vučenović, Petar Hrženjak)

This chapter summarizes the advanced survey, geophysical, and geotechnical testing methods performed within the scope of the GEER reconnaissance efforts between March 15 and 26, 2021 to complement field observations. Geotechnical investigation works were performed mostly around Mečenčani and Borojevići villages where a substantial number of sinkholes surfaced in the two months following the main shock, from January until mid-March 2021. Investigation works included 5 geotechnical boreholes, in-situ soil classification, and index tests, two Multichannel Analysis of Surface Waves (MASW) profiles in Mečenčani and Borojevići villages and two in Petrinja on-field liquefaction site and 65 Horizontal-to-vertical Spectral Ratio seismic method (HVSr) measurements, 61 HVSr in Mečenčani and Borojevići villages and 4 HVSr in Petrinja near MASW's. This chapter describes the methods and works, including detailed results that are used and embedded in different chapters of this report. It is noted that the NHERI-DesignSafe Data Depot is being utilized to disseminate data from this reconnaissance.

### 10.1. Horizontal-to-vertical Spectral Ratio (HVSr)

HVSr was performed as an attempt to characterize sediment and clay thicknesses that overlay karstic formation in the area where sinkholes appeared. Additional four measurements complemented MASW profiles in Petrinja. HVSr data was collected using two Nanometrics Trillium Compact broadband three-component seismometers, with a flat response from 100 Hz-20 s. Waveforms were recorded using a Nanometrics Centaur three-component digitizer, where the passive ambient noise was recorded for 25 minutes intervals at 8 locations around the largest sinkhole UVM001, and for 40-60 minutes in the remaining locations. A typical HVSr setup is shown in **Figure 10.1**, and consists of a seismometer, digitizer, a foldable plastic bucket that covers the seismometer to reduce the effects of wind and sun, the GPS sensor, and a battery.



**Figure 10.1** Nanometrics setup, with a seismometer aligned to the North.

HVSr analysis was performed using the HVSrweb application that utilizes *hvsrpy* (Vantassel 2020) to allow the processing of ambient noise data in the cloud. HVSrweb is hosted on computing

resources made available through the DesignSafe-CI (Rathje et al. 2017, Vantassel et al. 2018). **Figures 10.2 to 10.4** show spatial positions of 61 Nanometrics in the area.



**Figure 10.2** Spatial distribution of Nanometrics surrounding Borojevići and Mečenčani.



**Figure 10.3** Spatial distribution of Nanometrics around the largest sinkhole S001.



**Figure 10.4** Spatial distribution of Nanometrics in the liquefied field in Petrinja.

The time records were divided into 60 s block for processes. Time windows with excessive noise were rejected while the remaining time windows were used to create a spectral average representing the response of each array. The analysis used the time-averaged shear-wave velocity ( $V_S$ ) to a depth of 30 m,  $VS_{30}$  measured in the area. Seismometer recordings were processed immediately following the field reconnaissance using the HVSReb application (**Table 10.1**), as listed with positions in **Table 10.2** and all the analyses used the following setup:

1. Window Length (s): 60 s
2. Cosine Taper Width: 0.1
3. Butterworth Filter: No
4. Konno and Ohmachi Smoothing Coefficient: 40
5. Resampling:
  - a. Minimum Frequency (Hz): 3
  - b. Maximum Frequency (Hz): 50
  - c. Number of Frequency Points: 128
  - d. Type: Logarithmic
6. Define Horizontal Component with Multiple-Azimuths
7. Azimuth Interval: 15
8. Distribution of  $f_0$ : Lognormal

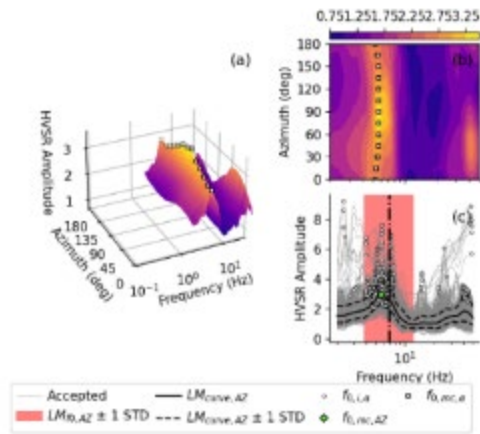
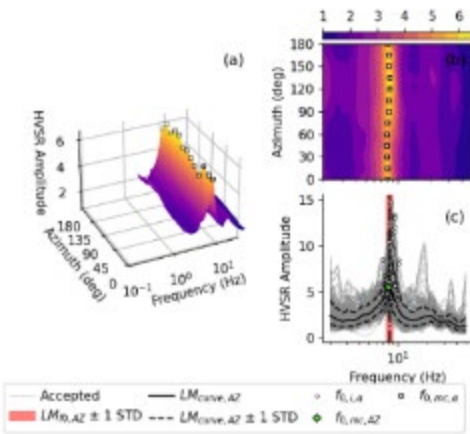
- 9. Distribution of Median Curve: Lognormal
- 10. Apply Frequency-Domain Window-Rejection? Yes
- 11. Number of Standard Deviations (n): 2
- 12. Maximum Number of Allowed Iterations: 50

**Table 10.1** shows only a smaller number of analyses of collected nanometric data. Weathered karst that contains an underground cavernous system yields a complex signal, which can be further analyzed to determine various horizons of contacts between cover clay soil, weathered karst, and competent karst at the bottom, as it is shown on one example of N-15 nanometric in **Table 10.1**. The rest of the data in **Table 10.1** correspond to selected analyses that yielded a clear peak at  $f_0$ . N-62, N-63, N-64, and N-65 show liquefaction field results.

**Table 10.1** HVSRweb analysis of ambient noise data.

N-1:  $f_0 = 8.06$

N-2:  $f_0 = 5.65$



N-3:  $f_0 = 4.17$

N-4:  $f_0 = 12.9$

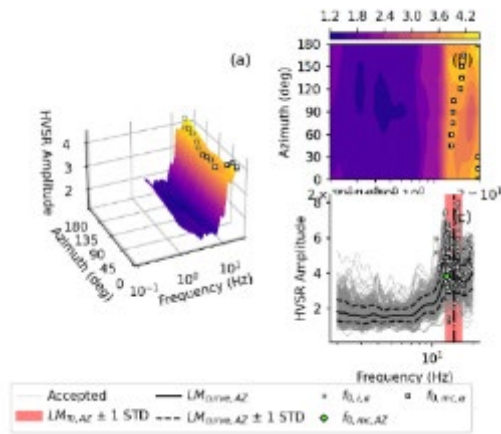
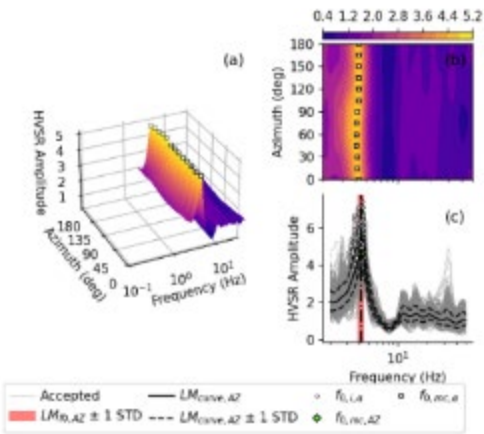
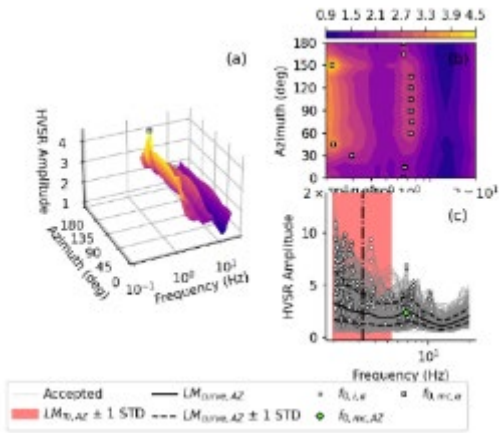
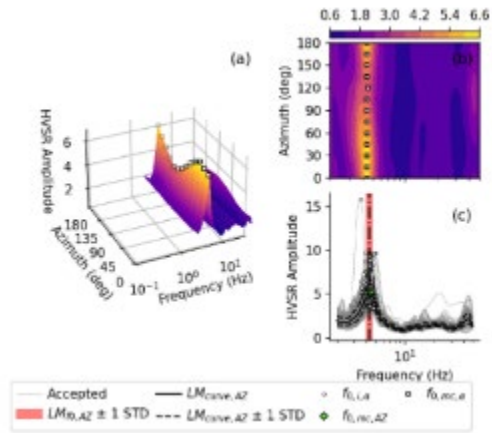


**Table 10.1 (cont.)** HVSRweb analysis of ambient noise data.

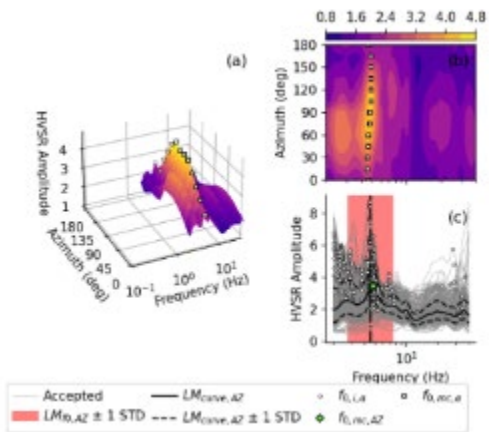
N-5:  $f_0 = 6.86$



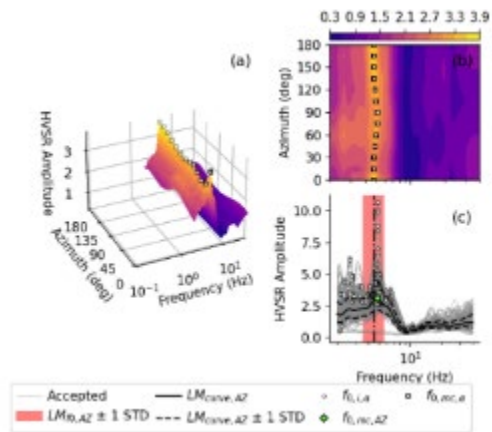
N-8:  $f_0 = 4.38$



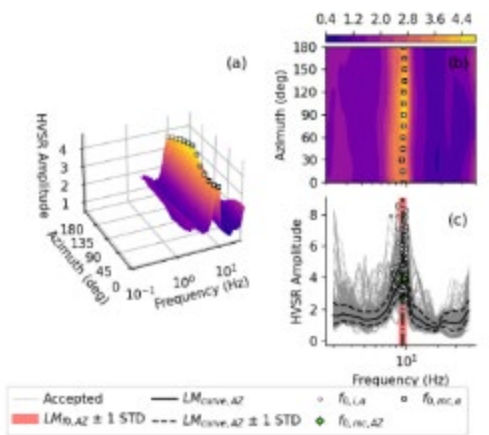
N-11:  $f_0 = 4.78$



N-13:  $f_0 = 4.90$



N-14:  $f_0 = 9.48$



N-15:  $f_0 = 4.06$

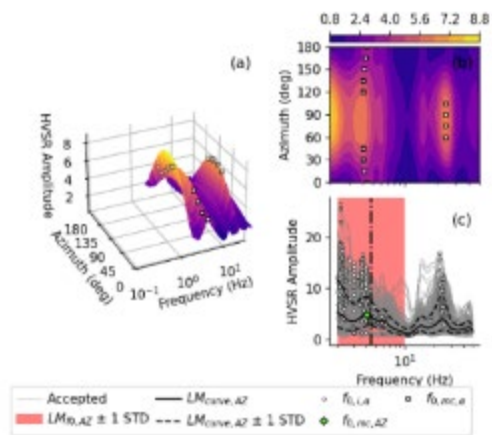
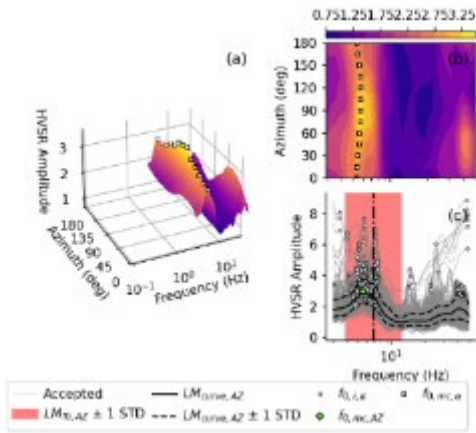
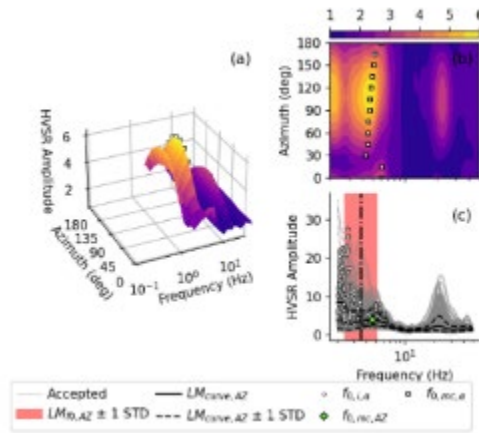


**Table 10.1 (cont.)** HVRSweb analysis of ambient noise data.

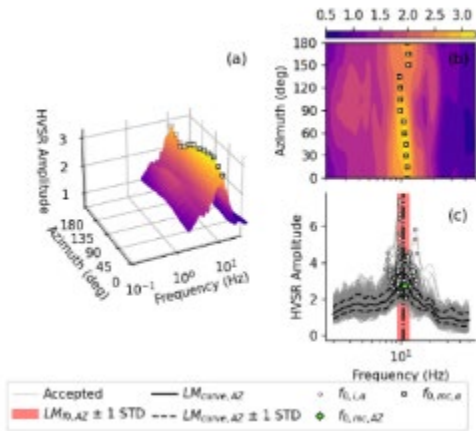
N-19:  $f_0 = 5.57$



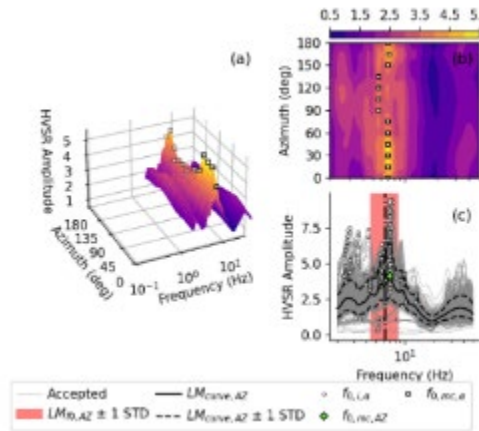
N-21:  $f_0 = 4.61$



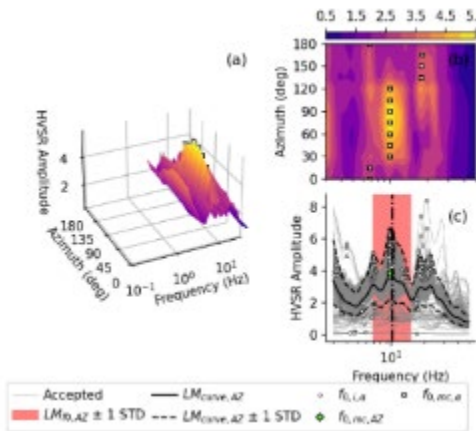
N-23:  $f_0 = 10.9$



N-25:  $f_0 = 6.92$



N-26:  $f_0 = 9.92$



N-62:  $f_0 = 26.9$  (Petrinja Liquefaction)

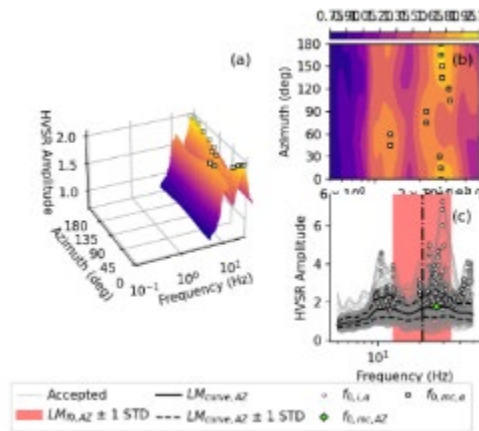
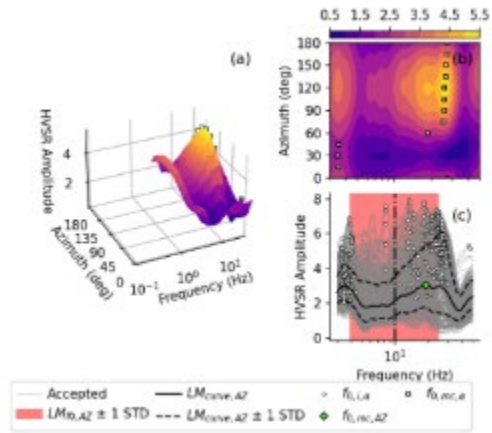
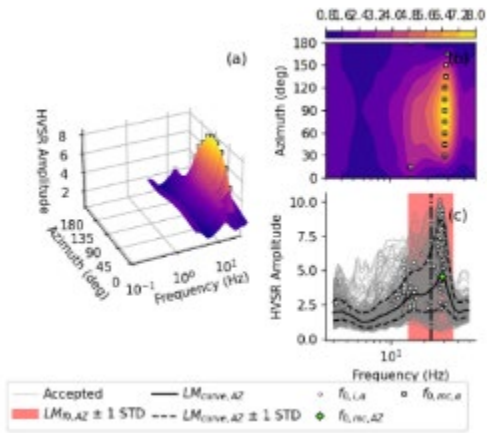


**Table 10.1 (cont.)** HVRSweb analysis of ambient noise data.

N-63:  $f_0 = 28.7$  (Petrinja Liquefaction)

N-64:  $f_0 = 18.8$  (Petrinja Liquefaction)



N-65:  $f_0 = 25.7$  (Petrinja Liquefaction)

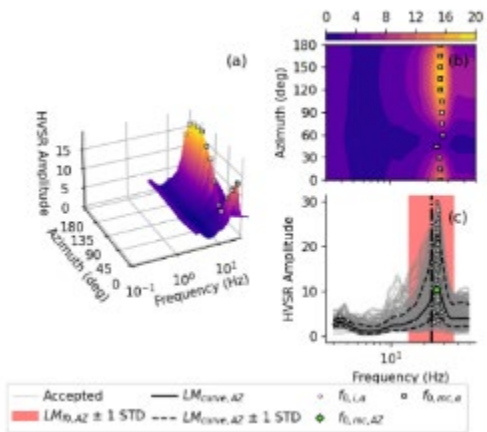


**Table 10.2** Geographical positions of all the Nanometrics analyses.

Name	Latitude (N)	Longitude (E)
N-1	45.299619	16.402617
N-2	45.300653	16.403486
N-3	45.296692	16.406081
N-4	45.300031	16.407336
N-5	45.298325	16.408683
N-6	45.297356	16.411283
N-7	45.296025	16.410425
N-8	45.295419	16.407100
N-9	45.293564	16.409775

N-10	45.294767	16.412025
N-11	45.296044	16.413425
N-12	45.296156	16.413769
N-13	45.296272	16.413708
N-14	45.297147	16.414508
N-15	45.290731	16.412222
N-16	45.293394	16.413853
N-17	45.294897	16.415822
N-18	45.296236	16.417139
N-19	45.291119	16.415125
N-20	45.292467	16.416731
N-21	45.294558	16.418317
N-22	45.288203	16.415844
N-23	45.290697	16.420042
N-24	45.292422	16.420061
N-25	45.292750	16.422119
N-26	45.293708	16.423089
N-27	45.285092	16.419381
N-28	45.287769	16.421892
N-29	45.289514	16.423169
N-30	45.290731	16.423447
N-31	45.291939	16.425236
N-32	45.283881	16.422106
N-33	45.285142	16.422933
N-34	45.286764	16.424575
N-35	45.287658	16.424372
N-36	45.285339	16.425444
N-37	45.286025	16.426192
N-38	45.281669	16.423294
N-39	45.283272	16.427617
N-40	45.281233	16.427764
N-41	45.282889	16.429358
N-42	45.284061	16.431828
N-43	45.281078	16.432081
N-44	45.283778	16.426000
N-45	45.283583	16.426292
N-46	45.283333	16.425139
N-47	45.283139	16.425361
N-48	45.282972	16.425722
N-49	45.282750	16.426028

N-50	45.283483	16.425558
N-51	45.283486	16.426136
N-52	45.283506	16.426058
N-53	45.283511	16.425931
N-54	45.283433	16.425825
N-55	45.283367	16.425775
N-56	45.283283	16.425794
N-57	45.283253	16.425881
N-58	45.283258	16.425992
N-59	45.282917	16.430008
N-60	45.282756	16.429886
N-61	45.282536	16.424969
N-62	45.448861	16.276967
N-63	45.447778	16.277125
N-64	45.446525	16.276614
N-65	45.445661	16.276119

## 10.2 Multichannel Analysis of Surface Waves (MASW)

The main objectives of the Multi-channel Analysis of Surface Waves (MASW) survey carried out was to delineate depth to bedrock, assess soil stiffness, and estimate average shear wave velocities down to 30 m depth. In addition, acquired shear-wave data can be subsequently used further for the analysis of the horizontal-to-vertical spectral ratio (HVSr) measurements conducted and NEHRP (National Earthquake Hazards Reduction Program) or Eurocode 8 site classification based on average shear-wave velocity values of 30 m depth ( $V_s 30$ ).

A total of four sites were selected for the survey. Two sites in the Mečenčani and Borojevići area (**Figures 10.6 to 10.8**) and two sites in Petrinja - one where clear evidence of liquefaction in form of sand boils was present (**Figure 10.9**) and a nearby site without sand boils present.



**Figure 10.6** Spatial distribution of MASW - Mečenčani and Borojevići.



**Figure 10.7** MASW spread near the largest sinkhole S001 in Mečenčani.



**Figure 10.8** MASW spread adjacent to three small sinkholes S023, S024, S025 in Borojevići.



**Figure 10.9** MASW in Petrinja on a site with sand boils.

Field data acquisition involved a 24-channel geophone array with 4.5 Hz vertical geophones spaced at 2 m intervals and a sledgehammer used as a shot source. A 24 channel Geometrics Geode seismograph was used to record the seismic data in a roll-along acquisition fashion, moving the array 10 m between shots. The total length of an array with 4 rolls was 86 m. For each position shots were conducted at -4.0 m, 0, 4 m, 8 m, 12 m. The same field setup (**Figure 10.10**) was used on all four sites.

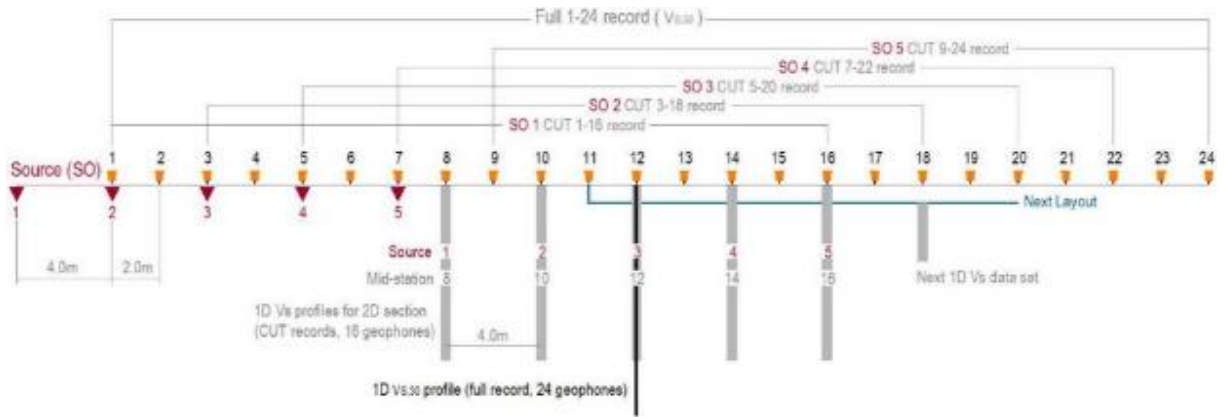


**Figure 10.10** Survey layout for 24 channel array.

Data reduction and analysis were performed using the SurfSeis software developed by the Kansas Geological Survey (KGS). Dispersion curves analysis was then performed for each shot gather in the multi-record file by examining the change in phase velocity vs. frequency using the fundamental mode component of the dispersion data. Non-linear inversion modeling of each dispersion curve was performed and resulted in a 1D mid-point representation of shear wave ( $V_s$ ) profile (**Figure 10.11** and **Figure 10.14**). Interpolation of the 1D data produced a 2D grid of the  $V_s$  data (**Figure 10.12**, **Figure 10.13**, and **Figure 10.15**). Color-filled contoured plots were then generated from the  $V_s$  grid.

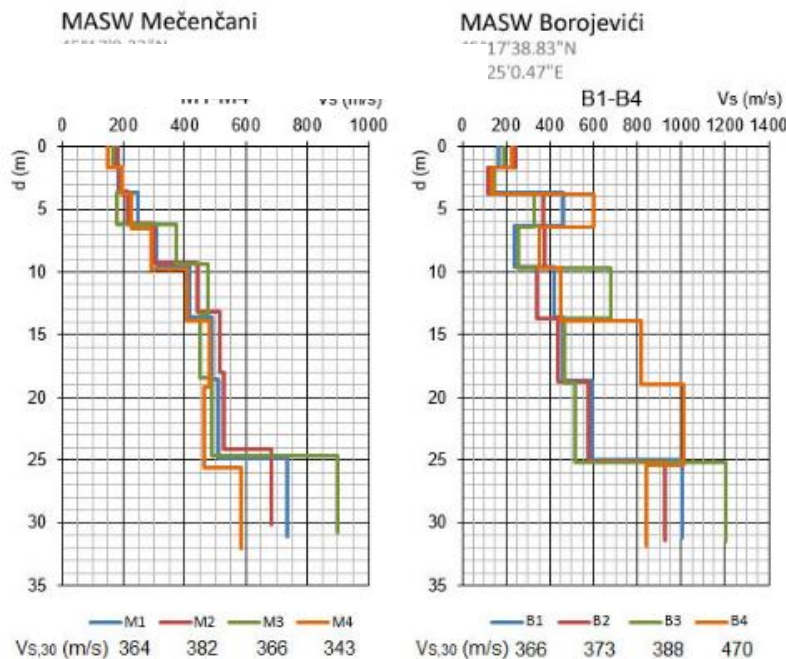


**Figure 10.11** 1D shear wave ( $V_s$ ) profiles with calculated average shear-wave velocity values of 30 m depth ( $V_{s30}$ ) in Mečenčani (45.283425N, 16.425781E) and Borojevići (45.294119N, 16.416797E).

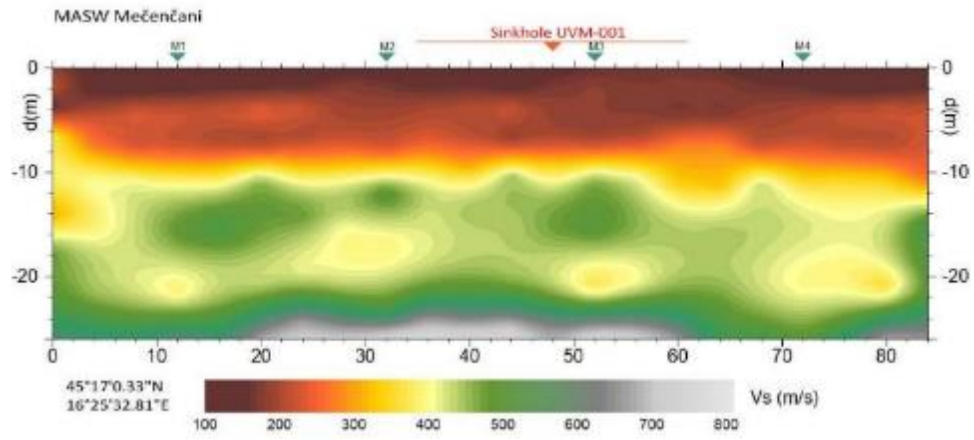


**Figure 10.12** 2D shear wave ( $V_s$ ) profile adjacent to the largest sinkhole in Mečenčani (45.283425N, 16.425781E).

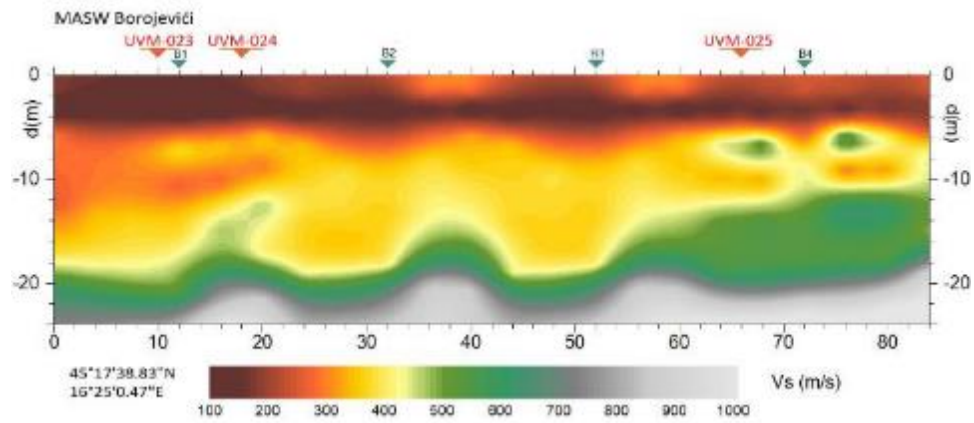


**Figure 10.13** 2D shear wave ( $V_s$ ) profile adjacent to three small sinkholes in Borojevići (45.294119N, 16.416797E).

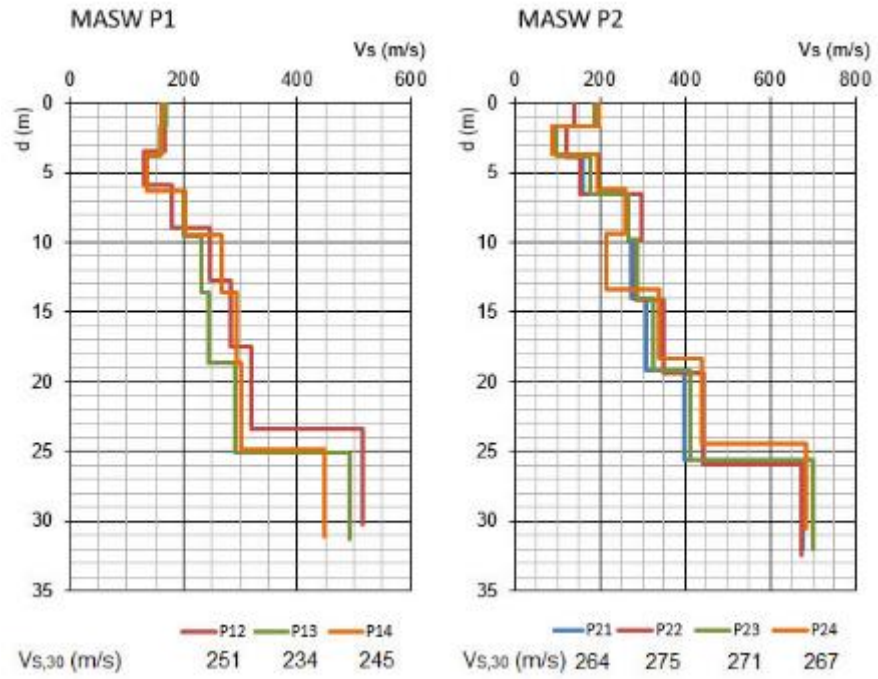


**Figure 10.14** 1D shear wave ( $V_s$ ) profiles with calculated average shear-wave velocity values of 30 m depth ( $V_{s,30}$ ) - MASW P1 and P2 in Petrinja (45.448303N, 16.276936E).

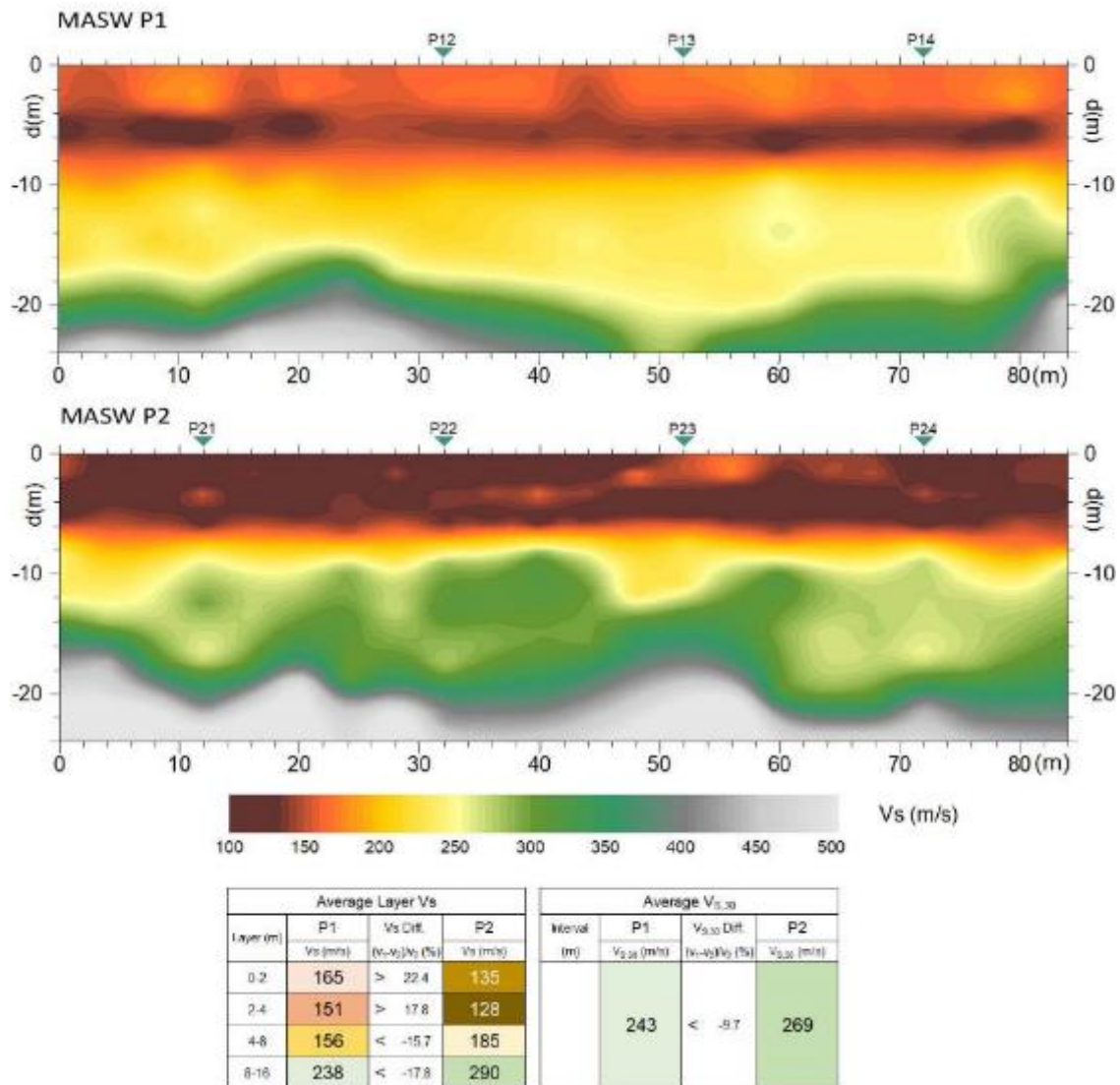


Figure 10.15 2D shear wave (Vs) profiles in Petrinja.

### 10.3 Geotechnical Investigation Works

Geotechnical site investigations and sampling was performed on 3 locations close to the cover collapse sinkholes No. S015 (location 1), S001 (location 2, boreholes B-1 and B-2) in Mečenčani (**Figure 10.16a**) and S009 (location 3, borehole B-3) and S040 (location 3, borehole B-4) in Borojevići (**Figure 10.16a**). Field work was performed at location 1 (S015) on February 23, 2021, at location 2 (S001) on March 23, 2021, and at location 3 (S009 and S040) on March 26, 2021.



a) Mečenčani

(**S001**: 45.283352N, 16.425852E; **S015**:  
45.282922N, 16.429898E)



b) Borojevići

(**S009**: 45.296609N, 16.415221E; **S040**:  
45.292921N, 16.422418E)

**Figure 10.16.** Map of field testing and soil sample locations (background image from Google Earth).

#### 10.3.1 Location 1 (S015)

At location 1 (**Figure 10.17**) the following equipment was used:

1. Eijkelkamp liner sampler, set for hard soils,  $\Phi$  50 mm, with plastic sample liners (<https://en.eijkelkamp.com/products/augering-soil-sampling-equipment/liner-sampler-set-sb-uk.html>)
2. Eijkelkamp field inspection vane tester, the standard set for measurements to 200 kPa (20 t/m<sup>2</sup>) and a depth of 3 m, standard vane 16 x 32 mm (<https://en.eijkelkamp.com/products/field-measurement-equipment/field-inspection-vane-tester.html>), and
3. DPL-dynamic penetrometer light (manually driven) SD-10 (ZNWIG) compatible with the Eurocode 7: Geotechnical design - Part 3: Design assisted by field testing.

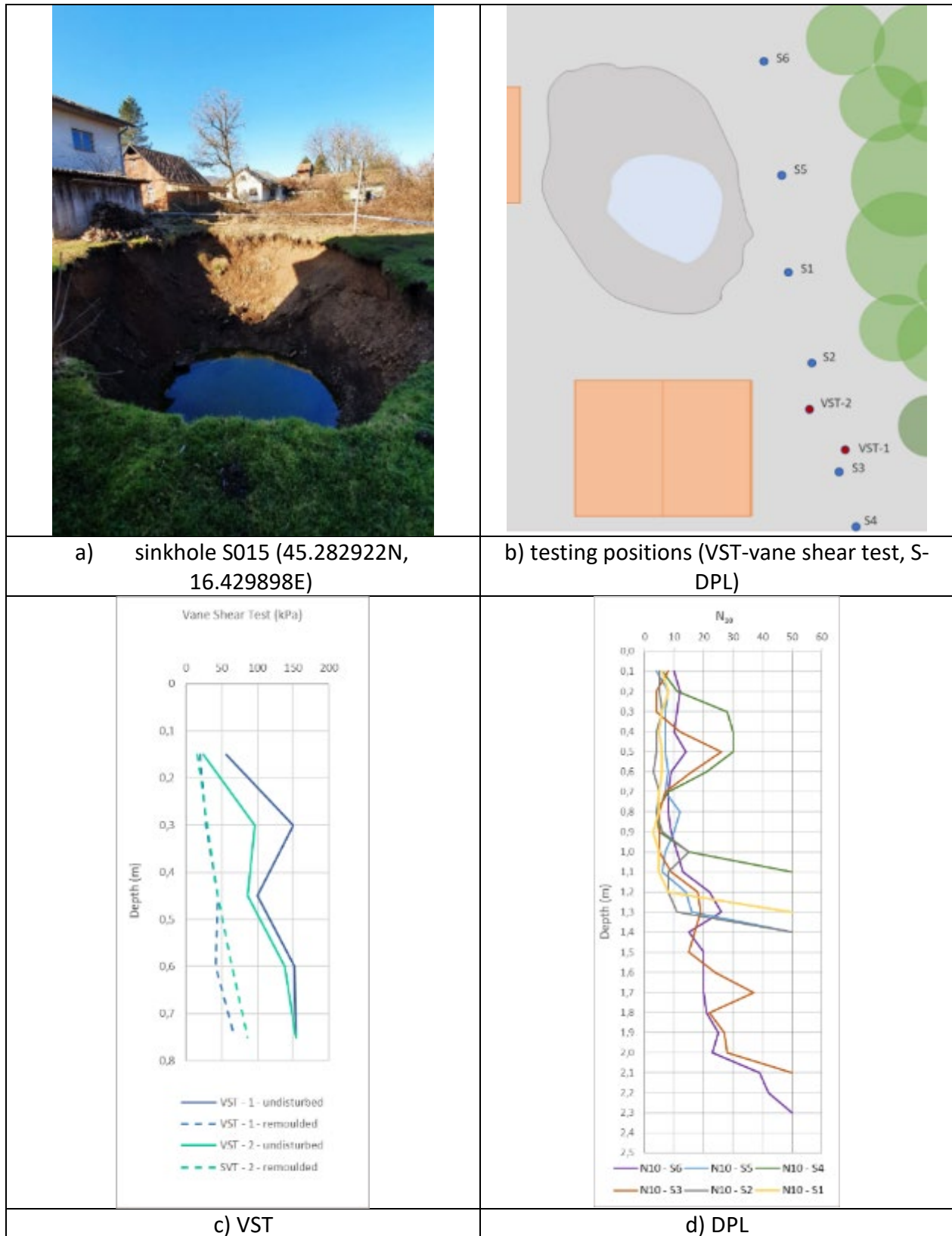


**Figure 10.17** Field work at location 1 (S015).

All the equipment was manually driven. Because of that fact together with the appearance of a shallow layer (depth of approximately 1.0 – 2.0 m) of coarse gravel with cobbles, field testing results are relevant only for a very shallow vertical profile (as shown in **Figure 10.17c** and **10.17d**). Two undisturbed samples were also taken (0.0 - 0.3 m; 0.3 - 0.6 m), preserved in the original plastic foil. Grain-size analyses and Atterberg limit test, which were performed in the Geotechnical laboratory at the Faculty of Mining, Geology and Petroleum Engineering University of Zagreb, showed that these samples belong to the group CL – sandy lean CLAY according to the ASTM classification (ASTM D 2487).

VST could be performed only to the depth of 0.75 m, showing the trend of undrained strength increase with depth, and 1.5 to 5.4 times smaller strength in remolded state comparing to the undisturbed strength. Six dynamic penetration tests were conducted at the site of the sinkhole S015. In all six probes, the test was terminated at depths of 1.1 m to 2.3 m because the probe penetrated negligible at 50 blows. The occurrence of water was observed at a depth of 1.7 m only at the DP03 probe. Based on the visible walls of the sinkhole and the number of blows per 10 cm of cone penetration,  $N_{10}$ , three units could be distinguished: a surface layer and lean clay with a low resistance to cone penetration ( $N_{10}$  3-15 blows); second unit where fine gravel is present ( $N_{10}$  15-42 blows), and bedrock or large cobbles with  $N > 50$ . When handling the probe, the friction of the metal against the gravel grains was felt in the second layer. With the appearance of coarse gravel (grains with a diameter of 20 cm were visible in the sinkhole), penetration was no longer possible. By visual inspection of the sinkhole and DPL results, up to the depth of 1-1.5 m, a yellowish-brown sandy lean clay can be seen. Below that depth, the content of coarse gravel and cobbles increases. The water level was pretty high, at the depth of approximately 2.0 m, and the soil was visible moist from the depth of 1.5 m.

### **10.3.2 Location 2 and 3 (S001, S009, S040)**

At the locations, 2 – Mečenčani (boreholes B-1 and B-2) and location 3 – Borojevići (boreholes B-3 and B-4) boring is performed by solid rod bottom auger without casing and without the use of drilling fluid (**Figure 10.18**). Besides, standard penetration test (SPT), DPL-dynamic penetrometer light (manually driven) SD-10 (ZNWIG), soil sampling and groundwater table measurements have been done. Disturbed samples were continuously taken (auger sampling) and undisturbed samples (drive sampling with split tube sampler  $\Phi$  85 mm) were taken at intervals of approximately 1 m followed by SPT (disturbed samples  $\Phi$  35 mm). DPL was performed close to boreholes B-1 and B-2 at location 2 and those results are presented in **Figure 10.18c**.

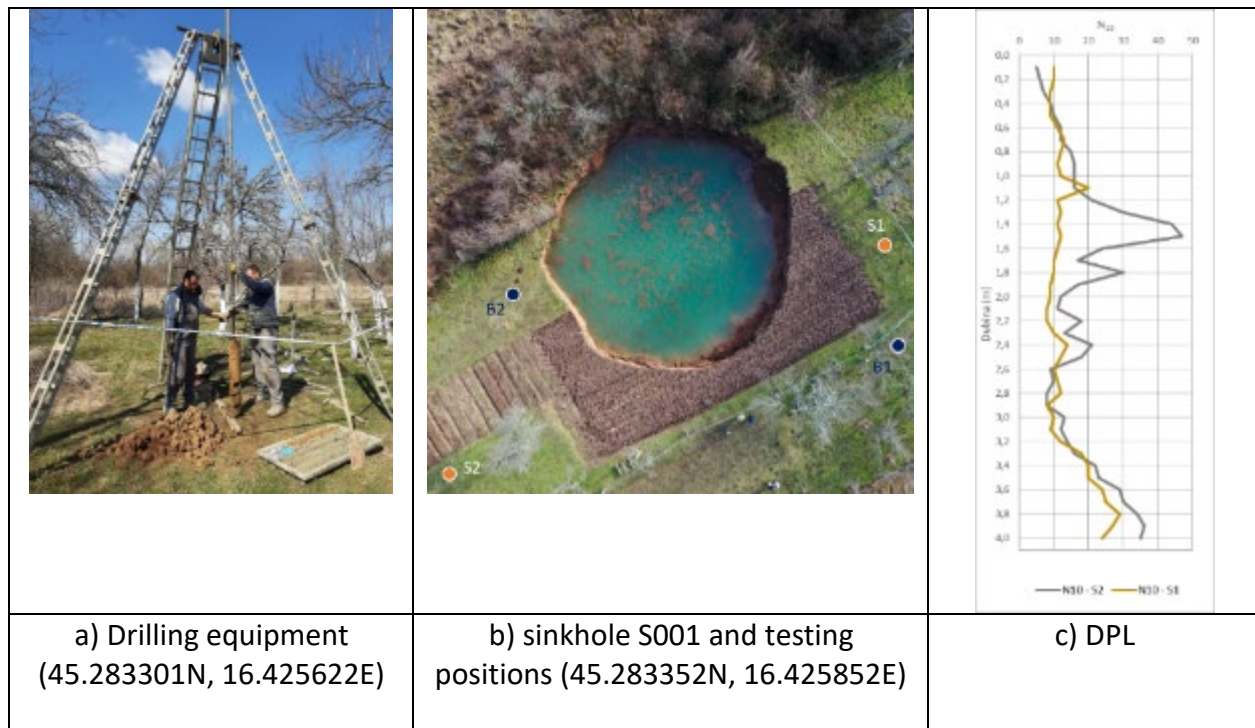


**Figure 10.18** Field work at location 2 (S001).

Two dynamic penetration tests were conducted at the site of the sinkhole S001. For both probes, the test was terminated at a depth of 4.0 m, as the declared maximum penetration depth for the equipment was reached. No occurrence of water was observed during testing. S2 probe (**Figure 10.18c**) showed small values of  $N_{10}$  to the depth of 3.2 m ( $N_{10}$  8-14 blows), only one reading showed a higher value (at 1.1 m,  $N_{10}$  was 20 blows). Below the depth of 3.3 m  $N_{10}$  was 18-29 blows. S1 probe showed significantly higher values of  $N_{10}$ . The maximum value ( $N_{10}$  47 blows) was measured at the depth of 1.5 m.

### 10.3.3 Laboratory Testing and Results

A laboratory testing program was undertaken at the Geotechnical laboratory of the Faculty of Mining, Geology and Petroleum Engineering University of Zagreb from February to March 2021. The following index tests were performed following applicable American Society for Testing and Materials (ASTM) standards:

1. Standard Test Methods for Particle-Size Distribution (Gradation) of Soils Using Sieve Analysis (ASTM 6913M)
2. Standard Test Method for Particle-Size Distribution (Gradation) of Fine-Grained Soils Using the Sedimentation (Hydrometer) Analysis (ASTM D7928)
3. Standard Test Methods for Liquid Limit, Plastic Limit, and Plasticity Index of Soils (ASTM D4318)
4. Standard Test Methods for Laboratory Determination of Water (Moisture) Content of Soil and Rock by Mass (ASTM D2216)

5. Standard Test Methods for Specific Gravity of Soil Solids by Water Pycnometer (ASTM D 854)
6. Geotechnical investigation and testing - Laboratory testing of soil - Part 2: Determination of bulk density (ISO 17892-2:2014; EN ISO 17892-2:2014)

Based on the field description and identification and laboratory results, each sample was classified according to ASTM D2487: Standard Practice for Classification of Soils for Engineering Purposes (Unified Soil Classification System) and ASTM D 2488: Standard Practice for Description and Identification of Soils (Visual-Manual Procedures).

Summary of laboratory test results for the boreholes B-1 and B-2 are presented in Tables 1, 2, and 3 (Appendix 1). The summary of grain-size distribution curves and plasticity charts are shown for the location 2 (UVM-01) boreholes B-1 and B-2 in **Figure 10.19**. and **Figure 10.20** respectively. For the location Borojevići, the same is presented in **Figure 10.21**.

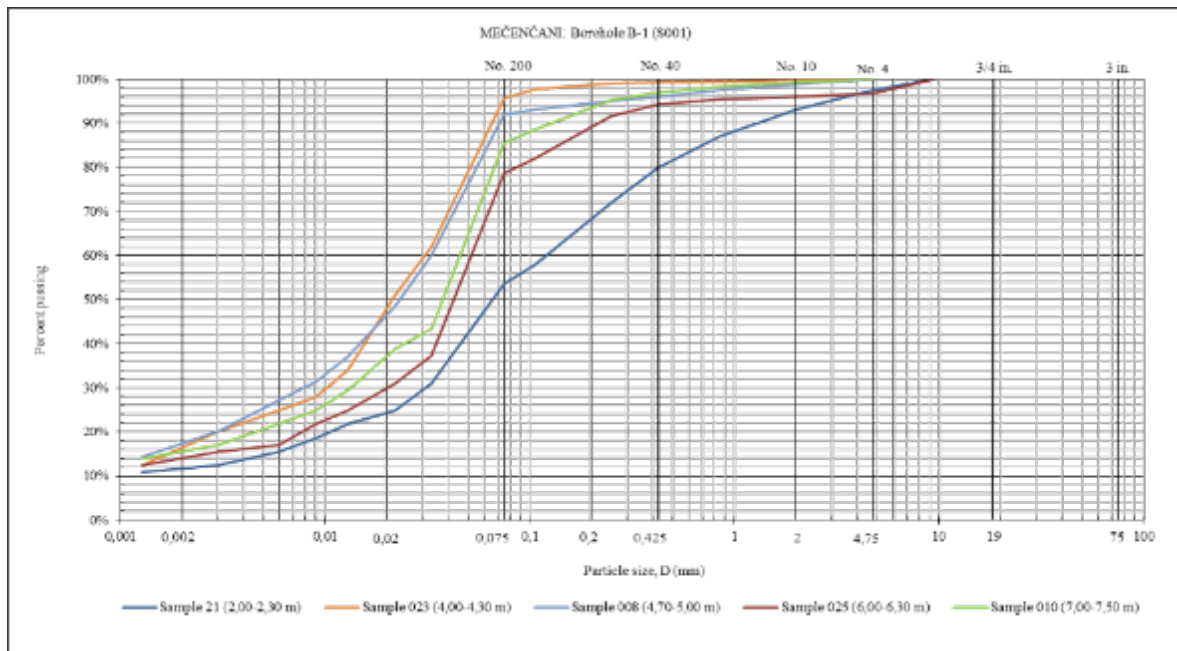


**Figure 10.19** Mečenčani: B-1 (S001).

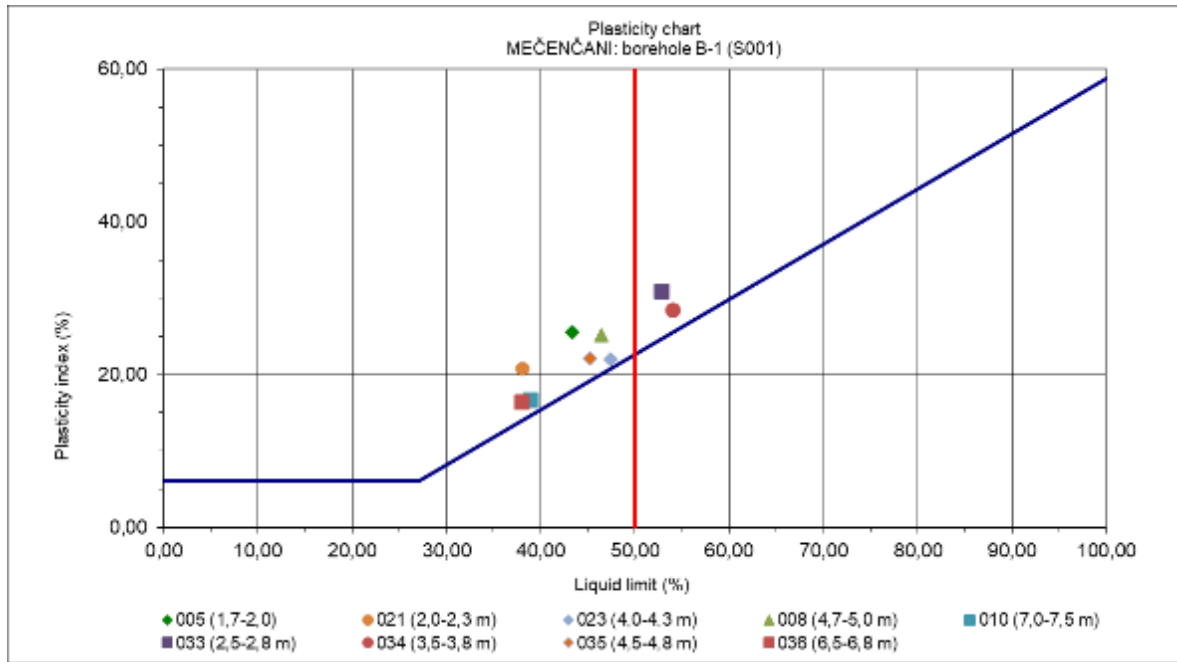


Figure 10.19 (cont.) Mečenčani: B-1 (S001).

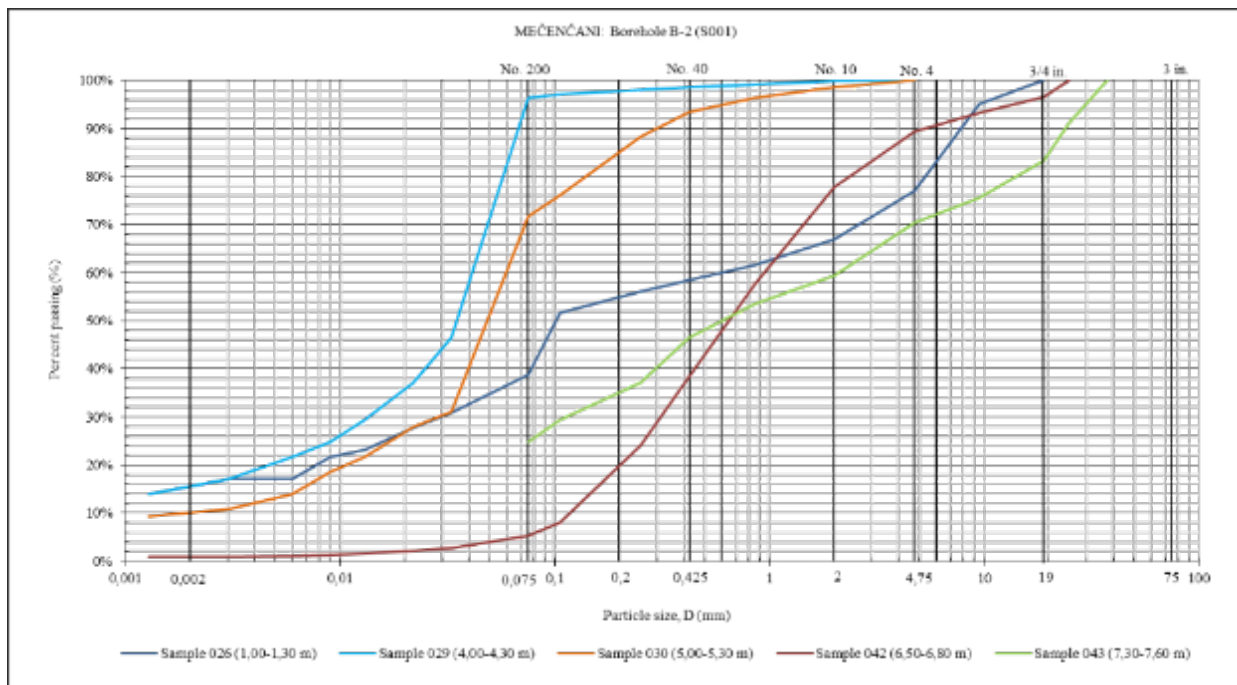


Figure 10.20 Mečenčani: B-2 (S001).

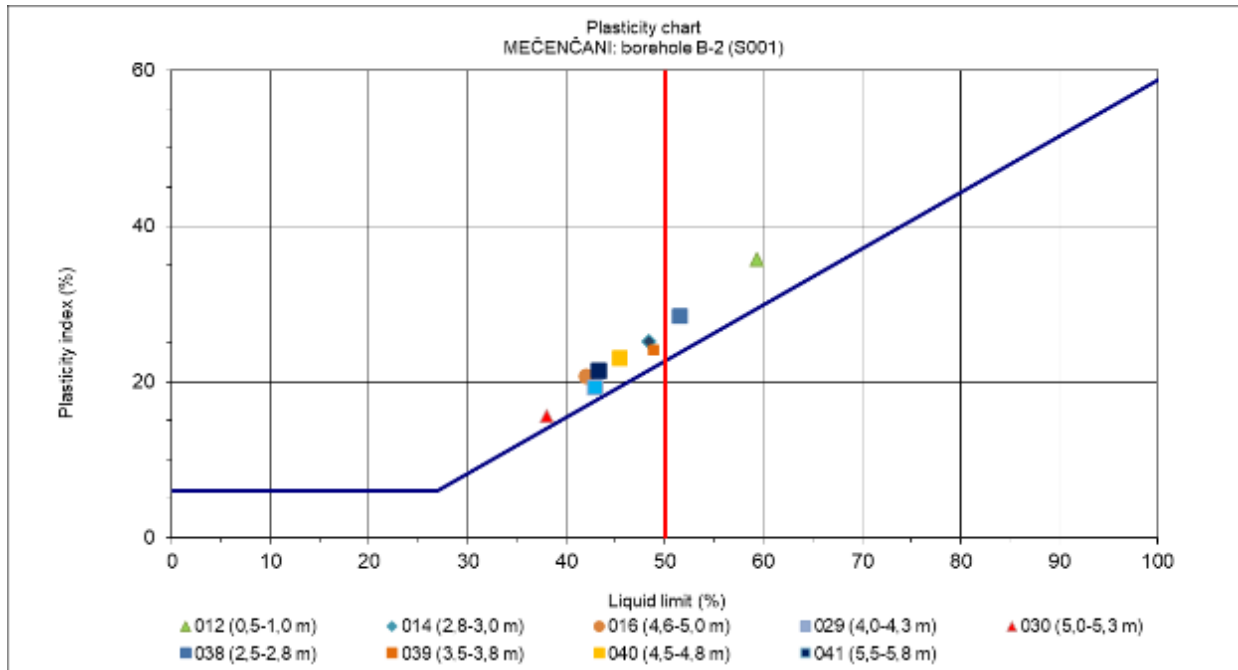


Figure 10.20 (cont.) Mečenčani: B-2 (S001).

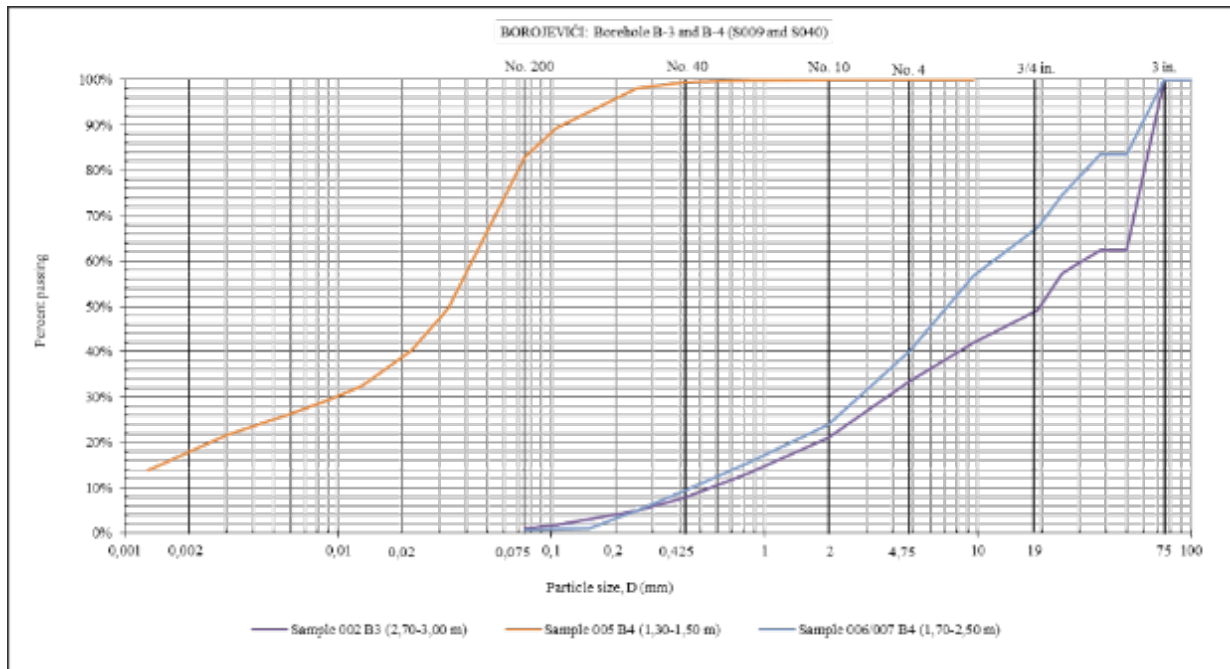
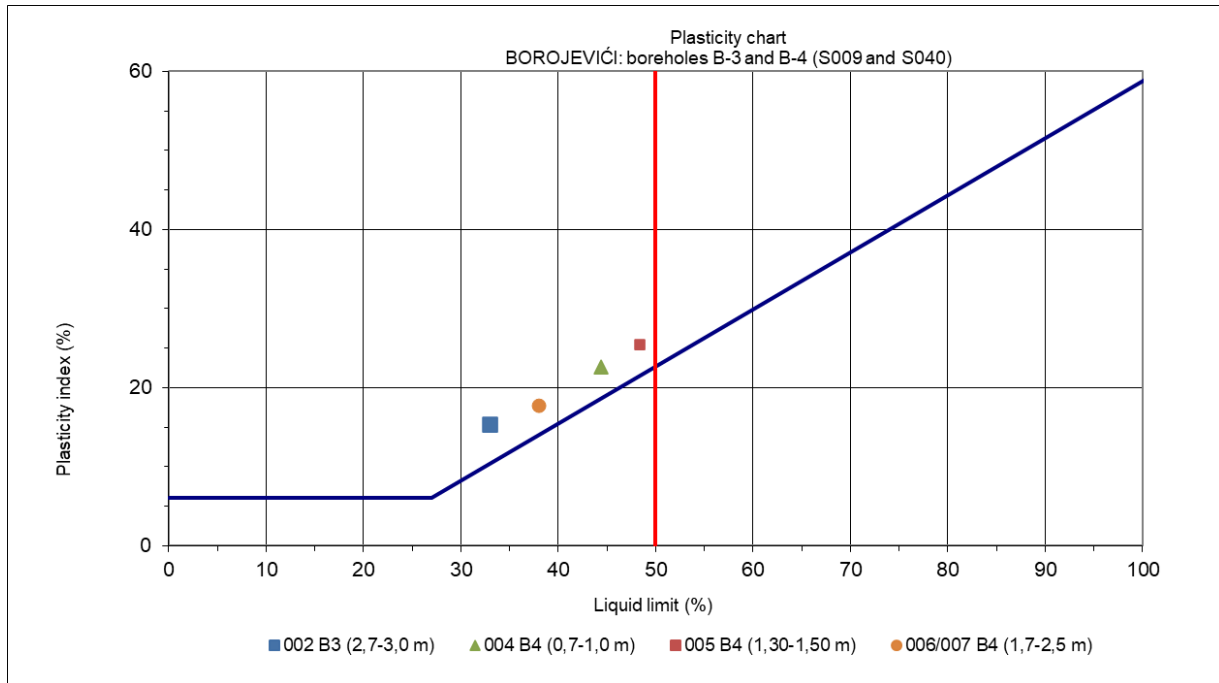


Figure 10.21 Borojevići: B-3 and B-4 (S009 and S040)



**Figure 10.21 (cont.)** Borojevići: B-3 and B-4 (S009 and S040)

Two samples of rock material were obtained from the borehole from the abandoned core previously drilled by Geotehnicki Studio L.L.D, in Borojevići 101 location near a private house. Later on, Geotehnicki Studio Ltd. kindly provided the borehole log for GEER. It was possible only to perform one point load strength index test per sample. The test is performed according to Suggested Method for Determining Point Load Strength of the International Society for Rock Mechanics (ISRM, 1985). The obtained values (**Figures 10.22** and **10.23**) for corrected Point Load Strength Index  $I_s(50)$  show that tested samples belong to weak rock (R2).

### Point Load Index Test Report

Work Item: 21-008 Received: 3/16/2021  
 Client: Geotechnical Extreme Events Reconnaissance  
 Project: GEER Petrinja 2021  
 Field Sampl.: Dr. sc. Ingrid Tomac Sampling Date.: 3/17/2021  
 Lab Prepar: E. Oršulić, dipl. ing. geot. Prepar. Date: 4/2/2021

Sample Handling: The sample was not protected from moisture changes.

Location: Borojevići  
 Litological Description: Limestone, calcarenite to calcrudite, composed of numerous bioclasts of red algae Lithotamnium and small bioclasts, peloids and intraclasts. Rock is characterized by significant intragranular porosity.  
 Lab. No: 21-008-001 Depth: between 6-12 m

Length l (mm)	Width W (mm)	Density (kg/m <sup>3</sup> )			
57,5	73,0	2062			



Strength Index $I_{s(50)}$	Effective Diameter $D_e$	Correction Factor F
1,33 MPa	73,1 mm	1,186

Method: ISRM Suggested method for determining point load strength, 1985

Comments:

Failure Validity: Correct Duration: 15 s  
 Equipment: Robertson Research Date: 4/7/2021

Responsible Person: <i>P. Hrženjak</i> Dr. sc. Petar Hrženjak	No. and Report Date: 21-008-001PLTR 9. 04. 2021.	Lab Director: <i>P. Hrženjak</i> Dr. sc. Petar Hrženjak
---	--	---

**Figure 10.22** Point load Index test – Borojevići.

### Point Load Index Test Report

Work Item: 21-008 Received: 26. 03. 2021.  
 Client: Geotechnical Extreme Events Reconnaissance  
 Project: GEER Petrinja 2021  
 Field Sampl.: Dr. sc. Ingrid Tomac Sampling Date.: 17. 03. 2021.  
 Lab Prepar: E. Oršulić, dipl. ing. geot. Prepar. Date: 2. 04. 2021.  
 Sample Handling: he sample was not protected from moisture changes.T

Location: Borojevići  
 Litological Description: Compact limestone composed of Lithotamnium bioclasts, gastropods and fine-grained bioclasts, intraclasts and peloids. Rock is characterized by visible intragranular porosity.  
 Lab. No: 21-008-002 Borehole: B-1 Depth: 6.15-6.25 m

Length l (mm)	Width W (mm)	Density (kg/m3)			
54,9	112,5	2290			



Strength Index $I_{S(50)}$	Effective Diameter $D_e$	Correction Factor F
1,66 MPa	88,0 mm	1,290

Method: ISRM Suggested method for determining point load strength, 1985

Comments:

Failure Validity: Correct Robertson Duration: 20 s  
 Equipment: Research Date: 4/7/2021

Responsible Person: <i>P. Hrženjak</i> Dr. sc. Petar Hrženjak	No. and Report Date: 21-008-002PLTR 9. 04. 2021.	Lab Director: <i>P. Hrženjak</i> Dr. sc. Petar Hrženjak
---	--	---

**Figure 10.23** Point Load Index test – Borojevići.

Representative borehole log profiles are presented in **Figures 10.24 to 10.27**.

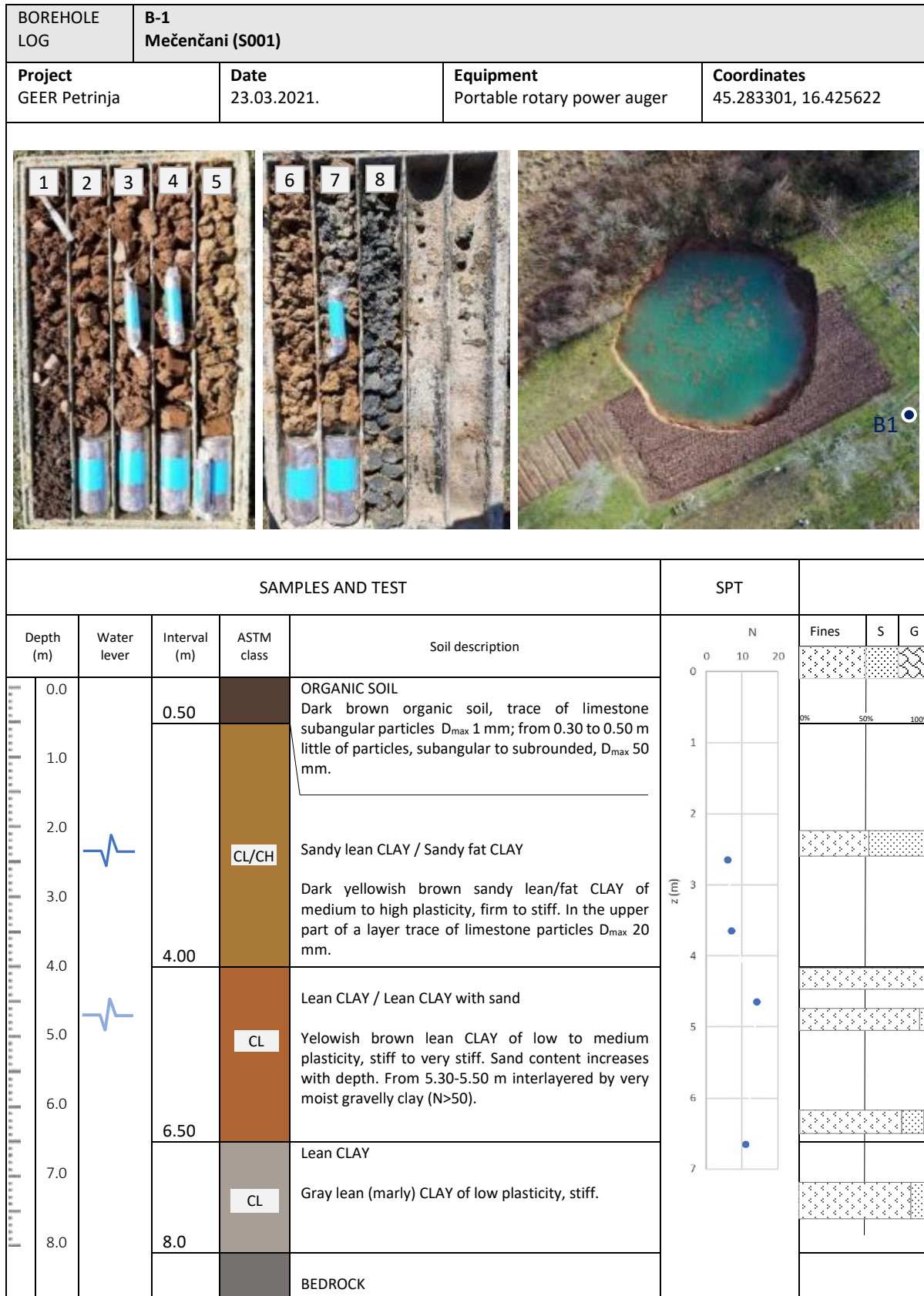


Figure 10.24: Borehole log B1

BOREHOLE LOG		B-2 Mečenčani (S001)		
Project GEER Petrinja		Date 23.03.2021.	Equipment Portable rotary power auger	Coordinates 45.283416, 16.426094

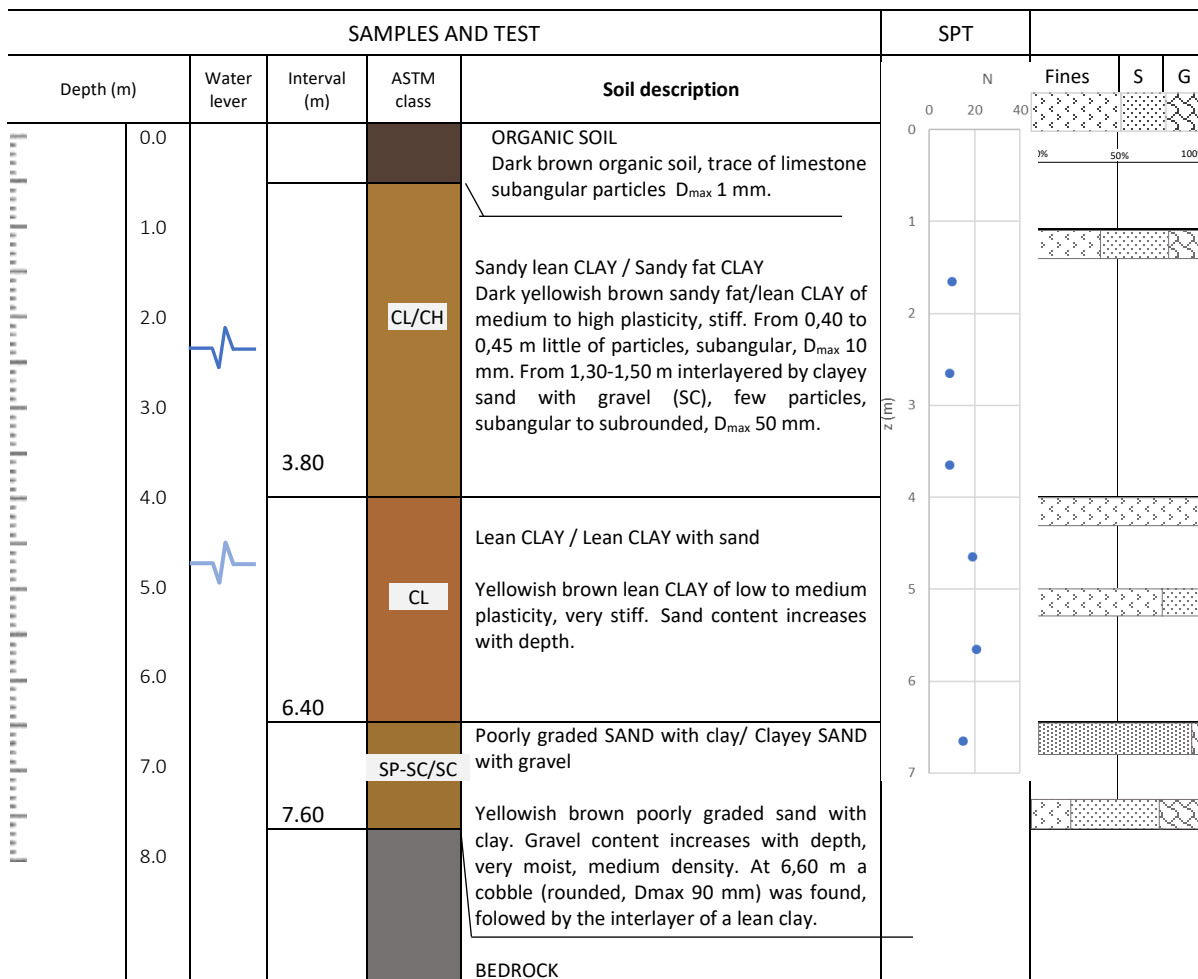


Figure 10.25: Borehole log B2

<b>BOREHOLE LOG</b>		<b>B-3</b>	
		<b>Borojevići (S009)</b>	
<b>Project</b>	<b>Date</b>	<b>Equipment</b>	<b>Coordinates</b>
GEER Petrinja	26.03.2021.	Portable rotary power auger	45.296609, 16.415221



SAMPLES AND TEST					SPT	Fines S G			
Depth (m)	Water lever	Interval (m)	ASTM class	Soil description	N	Fines S G			
						0	50	100	
0.0		0.30		ORGANIC SOIL, dark brown					
				Lean CLAY					
1.0		1.40	CL	Yellowish brown lean clay of medium plasticity, stiff. Limestone concretions in traces.					
2.0				Poorly graded GRAVEL with sand					
3.0				Yellowish brown coarse to fine poorly graded gravel with sand, soft, medium density. From 3,10 m very moist.					
4.0		4.00		COBBLES ?					
5.0									
6.0		5.80		BEDROCK					
7.0									

Figure 10.26: Borehole log B3

BOREHOLE LOG		B-4 Borojevići (S040)		
Project GEER Petrinja	Date 26.03.2021.	Equipment Portable rotary power auger	Coordinates 45.292921, 16.422418	

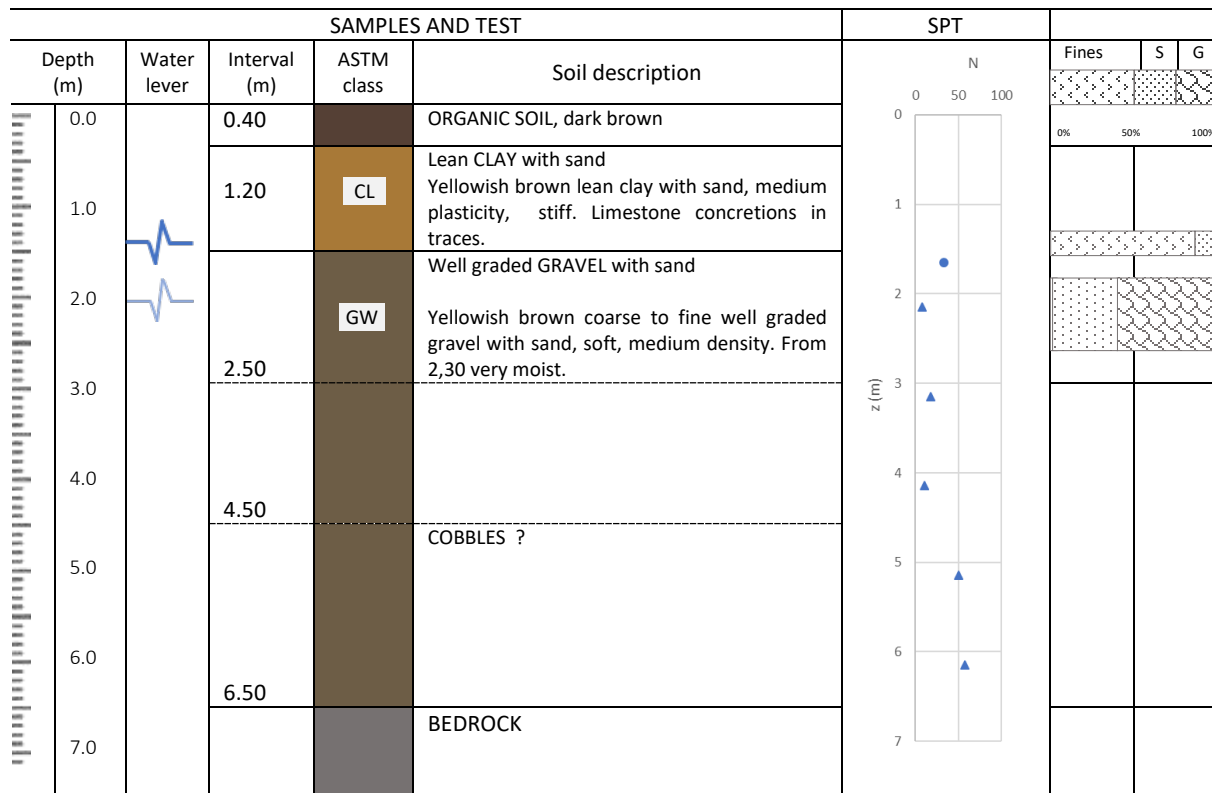


Figure 10.27: Borehole log B4

APPENDIX A

Table A.1: SUMMARY LABORATORY TEST REPORT – MEČENČANI; B-1 (S001)

APPENDIX 1  
Table 1: SUMMARY LABORATORY TEST REPORT – MEČENČANI; B-1 (S001)



University of Zagreb  
FACULTY OF MINING, GEOLOGY AND PETROLEUM ENGINEERING

Ordered by: **GEER**  
Address:

**GEER**

Project:  
Project designation:

GEER Petrinja Mečenčani, B  
21-005

**SUMMARY LABORATORY TEST REPORT**

Sample ID	Borehole log	Depth (m)	Sample type	Method	ASTM 6913M ASTM D7928		ASTM D 4318		EN ISO 17892-2:2014		Consistency index
					Type of testing	Symbol	Grain size analyses	Water content	Unit weight	Dry unit weight	
(-)	(-)	(m)	USCS/Unit	(%)	(%)	(%)	(%)	(%)	(%)	(%)	(-)
21-005-001	B-1	0.0-0.3	D-A	CL	26.8	26.8					
21-005-002	B-1	0.3-0.7	D-A	CL	17.3	17.3					
21-005-003	B-1	0.7-1.0	D-A	CL	25.3	25.3					
21-005-004	B-1	1.0-1.3	D-A	CL	15.7	15.7					
21-005-005	B-1	1.7-2.0	D-A	CL	23.7	23.7	43.4	17.9	25.5	0.77	
21-005-021	B-1	2.0-2.3	TKW	CL	23.2	23.2	38.0	17.2	20.8	0.71	
21-005-033	B-1	2.5-2.8	D-SPT	CH	29.1	29.1	52.8	21.9	30.9	0.77	
21-005-006	B-1	2.7-3.0	D-A	CH	29.9	29.9					
21-005-034	B-1	3.5-3.8	D-SPT	CH	30.1	30.1	54.0	25.5	28.5	0.84	
21-005-007	B-1	3.7-4.0	D-A	CL	27.9	27.9					
21-005-023	B-1	4.0-4.3	TKW	CL	32.2	32.2	47.4	25.4	22.0	0.69	
21-005-035	B-1	4.5-4.8	D-SPT	CL	24.5	24.5	45.2	23.1	22.1	0.94	
21-005-008	B-1	4.7-5.0	D-A	CL	30.7	30.7	46.4	21.2	25.2	0.62	
21-005-009	B-1	5.7-6.0	D-A	CL	32.4	32.4					
21-005-025	B-1	6.0-6.3	TKW	CL	22.1	22.1	41.2	23.1	18.1	1.06	
21-005-036	B-1	6.5-6.8	D-SPT	CL	24.9	24.9	38.0	21.5	16.5	0.79	
21-005-010	B-1	7.0-7.5	D-A	CL	28.8	28.8	38.9	22.2	16.7	0.60	



**Table A.2: SUMMARY LABORATORY TEST REPORT – MEČENČANI; B-2 (S001)**

Sample ID	Borehole log	Depth (m)	Sample type	Method	ASTM 6913M ASTM D7928			EN ISO 17892 – 2:2014			ASTM D 4318				
					Grain size analyses	Water content	Unit weight	Grain size analyses	Unit weight	Atterberg limits	Plasticity index	Consistency index			
(-)	(-)	(m)	USCS/Unit	Symbol	G (%)	S (%)	Fine S (%)	W (%)	γ Mg/m <sup>3</sup>	γ <sub>d</sub> Mg/m <sup>3</sup>	LL (%)	PL (%)	PI (%)	I <sub>c</sub> (-)	
21-005-011	B-2	0.0–0.15	D-A					26.5							
21-005-012	B-2	0.5–1.0	D-A	CH	22.9	38.3	38.8	20.1	1.99	1.66	55.8 / 59.3	22.7 / 23.6	36.2 / 35.7	0.96 / 1.00	
21-005-026	B-2	1.0–1.3	TKW					18.3							
21-005-037	B-2	1.5–1.8	D-SPT					24.6							
21-005-013	B-2	1.8–2.0	D-A					27.8			51.5	23.0	28.5	0.83	
21-005-038	B-2	2.5–2.8	D-SPT	CH				28.1			48.4	23.3	25.1	0.81	
21-005-014	B-2	2.8–3.0	D-A	CL											
21-005-028	B-2	3.0–3.3	TKW												
21-005-039	B-2	3.5–3.8	D-SPT	CL				28.9			48.9	24.8	24.1	0.83	
21-005-015	B-2	3.8–4.0	D-A					28.6							
21-005-029	B-2	4.0–4.3	TKW	CL	0.0	3.6	96.4	25.3	2.00	1.60	42.9	23.7	19.2	0.92	
21-005-040	B-2	4.5–4.8	D-SPT	CL				23.8			45.4	22.3	23.1	0.93	
21-005-016	B-2	4.6–5.0	D-A	CL				22.4			42.0	21.3	20.7	0.95	
21-005-030	B-2	5.0–5.3	TKW	CL	0.0	28.3	71.7	22.5	2.05	1.68	38.0	22.4	15.6	0.99	
21-005-041	B-2	5.5–5.8	D-SPT	CL				24.4			43.3	21.9	21.4	0.88	
21-005-017	B-2	5.8–6.0	D-A					22.5							
21-005-018	B-2	6.3–6.8	D-A					25.7							
21-005-042	B-2	6.5–6.8	D-SPT		10.5	84.1	5.4	23.5							
21-005-019	B-2	6.8–7.0	D-A					23.4							
21-005-043	B-2	7.3–7.6	D-SPT		29.5	45.7	24.8	9.3							



SUMMARY LABORATORY TEST REPORT

Sample ID	Borehole log	Depth (m)	Sample type	Method	ASTM 6913M ASTM D7928 Grain size analyses			ASTM D 2216 Water content	EN ISO 17892 - 2:2014		ASTM D 4318		
					G (%)	S (%)	Fine S (%)		Unit weight $\gamma$ Mg/m <sup>3</sup>	Dry unit weight $\gamma_d$ Mg/m <sup>3</sup>	LL (%)	PL (%)	PI (%)
(-)	(-)	(m)	USCS/Unit	Symbol	(%)	(%)	(%)	(%)	(%)	(%)	(%)	(%)	(-)
21-006-001	B - 3	0,50 - 1,00	D-A				24,3						
21-006-002	B - 3	2,70 - 3,00	D-A	CL	66.5	32.5	1.0	12,0	32,90	17,56	15,34	1,36	
21-006-003	B - 4	0,00 - 0,30	D-A				29,2						
21-006-004	B - 4	0,70 - 1,00	D-A	CL			26,3		44,40	21,70	22,65	0,80	
21-006-005	B - 4	1,30 - 1,50	D-A	CL	0.0	17.1	82.9	28,6	48,40	22,99	25,41	0,78	
21-006-006	B - 4	1,70 - 2,00	D-A				18,5						
21-006-006+7	B - 4	1,70 - 2,50	D-A	CL	59.9	39.1	1.0	20,9	38,00	20,22	17,78	0,96	
21-006-007	B - 4	2,00 - 2,50	D-A				23,2						

## 10.4 Terrestrial Surveys

Terrestrial surveys were performed during reconnaissance works between March 15 and March 26, 2021. Leica RTC360 lidar scanned about 60 sinkholes and Galдово Bridge, and the scans are deposited in DesignSafe Data Depot.

### References

- ASTM D2216-19 (2019). *Standard Test Methods for Laboratory Determination of Water (Moisture) Content of Soil and Rock by Mass*. Available at: [www.astm.org](http://www.astm.org). ASTM International, West Conshohocken, PA.
- ASTM D2487-17e1 (2017). *Standard Practice for Classification of Soils for Engineering Purposes (Unified Soil Classification System)*. Available at: [www.astm.org](http://www.astm.org). ASTM International, West Conshohocken, PA.
- ASTM D4318-17e1 (2017). *Standard Test Methods for Liquid Limit, Plastic Limit, and Plasticity Index of Soils*. Available at: [www.astm.org](http://www.astm.org). ASTM International, West Conshohocken, PA.
- ASTM D6913 / D6913M-17 (2017). *Standard Test Methods for Particle-Size Distribution (Gradation) of Soils Using Sieve Analysis*. Available at: [www.astm.org](http://www.astm.org). ASTM International, West Conshohocken, PA.
- ASTM D7928-17 (2017). *Standard Test Method for Particle-Size Distribution (Gradation) of Fine-Grained Soils Using the Sedimentation (Hydrometer) Analysis*. Available at: [www.astm.org](http://www.astm.org). ASTM International, West Conshohocken, PA.
- ASTM D854-14 (2014). *Standard Test Methods for Specific Gravity of Soil Solids by Water Pycnometer*. Available at: [www.astm.org](http://www.astm.org). ASTM International, West Conshohocken, PA.
- ISO 17892-2:2014 and EN ISO 17892-2:2014 (2014) *Geotechnical investigation and testing - Laboratory testing of soil - Part 2: Determination of bulk density*. Available at: <https://www.iso.org/standard/55244.html>. International Organization for Standardization.
- DD ENV 1997-3:2000 (2000) Eurocode 7: Geotechnical design - Part 3: Design assisted by field testing. Available at: <https://geotechnicaldesign.info/ec7p3.html>. European Committee for Standardization, Brussels, Belgium.
- Eijkelpamp Soil&Water. (2018). *Foil Sampler Set B Manual* Available at: <https://en.eijkelpamp.com/products/augering-soil-sampling-equipment/liner-sampler-set-sb-uk.html>. Eijkelpamp Soil and Water, Giesbeek, the Netherlands.
- Eijkelpamp Soil&Water. (2009). *Field Inspection Vane Tester Operating Instructions*. Available at: <https://en.eijkelpamp.com/products/field-measurement-equipment/field-inspection-vane-tester.html>. Eijkelpamp Soil and Water, Giesbeek, the Netherlands.
- Vantassel, J., Cox, B., Wotherspoon, L. and Stolte, A. (2018). *Mapping depth to bedrock, shear stiffness, and fundamental site period at Centreport, Wellington, using surface-wave methods: Implications for local seismic site amplification*. Bull. seism. Soc. Am., 108(3B), p1709–1721
- Rahtje E.M., Dawson C., Padgett J.E., Pinelli J-P., Stanzione D., Adair A., Arduino P., Brandenburg S.J., Cockerill T., Dey C., Esteva M., Haan F.L.Jr., Hanlon M., Kareem A., Lowes L., Mock S., Mosqueda G. (2017). *DesignSafe: New Cyberinfrastructure for Natural Hazards Engineering*. Nat. Hazards Rev. 18(3), p06017001.